Linear and Nonlinear Waves in Space Plasmas

By

Francois Nsengiyumva

Submitted in fulfilment of the academic requirements

for the degree of Doctor of Philosophy

in the School of Chemistry and Physics,

University of KwaZulu-Natal

Durban

March 2014

Preface

The work presented in this thesis was carried out in the School of Chemistry and Physics, University of KwaZulu-Natal, Durban, from September 2010 to January 2014, under the supervision of Prof. Manfred A. Hellberg and Prof. Richard L. Mace.

These studies represent original work by the author and have not otherwise been submitted in any form for any degree or diploma to any tertiary institution. Where use has been made of the work of others, it is duly acknowledged in the text.

Signed .....

Declaration 1 – Plagiarism

I, Francois Nsengiyumva, declare that

1. The research reported in this thesis, except where otherwise indicated, is my original research.
2. This thesis has not been submitted for any degree or examination at any other university.
3. This thesis does not contain other persons' data, pictures, graphs, or other information, unless specifically acknowledged as being sourced from other persons.
4. This thesis does not contain other persons' writing, unless specifically acknowledged as being sourced from other researchers. Where other written sources have been quoted, then:

a. Their words have been re-written, but the general information attributed to them has been referenced.

b. Where their exact words have been used, then their writing has been placed in italics and inside quotation marks, and referenced.

5. This thesis does not contain text, graphics, or tables copied and pasted from the Internet, unless specifically acknowledged, and the source being detailed in the thesis and in the References sections.

Signed: .....

Declaration 2 – Publications

Based on the research described in this thesis, one paper has been published to date, a further article is in draft form, and two others are in preparation.

1. Published paper:
Nsengiyumva F., Mace R. L., and Hellberg M. A. 2013, **"Ion Bernstein waves in a plasma with a kappa velocity distribution"**, **Physics of Plasmas, 20, 102107.** The supervisors devised and guided the research. The first author wrote the computer programs, carried out all calculations and wrote the first draft of the paper. The three authors were all deeply involved in the interpretation of the results and the final writing.

2. Paper in Draft, intended for publication in **Physics of Plasmas**:
"On the presence of stopbands in acoustic soliton existence domains", by **Nsengiyumva F., Hellberg M. A., Verheest F., and Mace R. L.** The calculations for this paper have been completed. The first author wrote all computer programs, found a novel phenomenon while working on section 3.5.4 of the thesis, explored it further, and, after discussion with the second author, drafted a manuscript. To date, the first two authors have both been deeply involved in developing and interpreting the results, as well as the drafting. The third author, an Honorary Professor in the School of Chemistry and Physics, has independently verified some of the fundamental calculations and commented on the draft manuscript. The fourth author has participated in some discussions, and will be involved in the final manuscript.

3. In preparation, intended for publication, **probably in Physics of Plasmas**: **"Thermal effects on solitary waves in plasmas with two adiabatic ion species, Part One: The slow mode",** by **Nsengiyumva F., Hellberg M. A., and Mace R. L.** The calculations and most of the interpretation of data have been completed. The first author was responsible for the mathematical and computational developments, under guidance, and carried out all the calculations. The work has been supervised mainly

by the second author, with participation by the third author.

4. In preparation, intended for publication, **probably in Physics of Plasmas**: **"Thermal effects on solitary waves in plasmas with two adiabatic ion species, Part Two: The fast mode",** by **Nsengiyumva F., Hellberg M. A., and Mace R. L**. The calculations and most of the interpretation of data have been completed. The first author was responsible for the mathematical and computational developments, under guidance, and carried out all the calculations. The work has been supervised mainly by the second author, with participation by the third author.

Signed .....

Acknowlegements

Many thanks to my supervisors, Prof. Manfred Hellberg and Prof. Richard Mace, for academic guidance and financial support.

This work was funded in part by the National Research Foundation (NRF) of South Africa through supervisors' nomination. Further financial support was provided by the supervisors using their research grants provided to them by the University of KwaZulu-Natal.

Thanks to Prof. Frank Verheest for the discussions that I had with him during his visits in Durban. These discussions improved the quality of the work involving solitons and double layers presented in this thesis.

Daily interaction with my office mates and fellow students, particularly Mr Reginald Abdul, had a positive impact on this work.

My M. Sc. and B. Sc. (Honours) studies were supervised and fully funded by the National Astrophysics and Space Science Programme (NASSP) of South Africa, hosted by the University of Cape Town. I am convinced that a strong momentum provided by NASSP had a positive impact on this work.

Last but not least, many thanks to my wife Mrs Clementine Niyibizi whose presence next to me is always an important support.

Abstract

The work presented in this thesis is about a study of some linear and nonlinear plasma waves.

Firstly, a kinetic-theoretical approach is used to study ion Bernstein waves in an electron-proton plasma with a kappa velocity distribution. The effects of the parameter kappa on the dispersion relation of ion Bernstein waves are discussed in detail, considering various values of the ratio of the ion plasma frequency to the ion cyclotron frequency, ω_{pi}/ω_{ci}, allowing application of the results to various space environments.

For a fixed value of $\omega_{pi}/\omega_{\rm ci}$, we have found that the dispersion relation depends significantly on the parameter kappa of the ions, κ_i, but is independent of the electron kappa. Over all cyclotron harmonics, the dispersion curves are shifted to higher wavenumbers (k) if κ_i is reduced. When the value of ω_{pi}/ω_{ci} is increased, the fall-off of the wave frequency, ω, at large k is smaller for lower κ_i, and curves are shifted towards larger wavenumbers.

For large values of ω_{pi}/ω_{ci}, the ion Bernstein wave dispersion curves within and above the lower hybrid frequency band exhibit coupling for the Maxwellian case, unlike the kappa case. We have suggested that this result may be a useful diagnostic for determining whether the ion velocity distribution possesses a power law tail.

Considering parameter values that have been observed in the Earth's plasma sheet boundary layer, and neighbouring environments, it has been found that the dispersion curves of ion Bernstein waves are typical of those obtained for the case of a high-density plasma immersed in a weak magnetic field.

Secondly, a fluid model is used to study linear and nonlinear ion acoustic waves supported by a two-adiabatic-ion plasma in which both ion species are positively and singly charged. This plasma model supports the propagation of two modes with different phase speeds. By normalising variables with respect to the characteristics of the hotter ion species, the thermal effects of the cooler ion species and the electrons on the two modes are discussed in detail.

The main thrust has been to study arbitrary amplitude ion acoustic solitons and double layers, using the fully nonlinear Sagdeev potential theory, but we have also considered linear theory and the KdV theory as a useful background.

The thermal effects of the cooler ion species and the electrons on the soliton existence domain and on the soliton/double layer speed, amplitude, and maximum profile steepness are discussed in detail. While some of the results are consistent with the results that are in the literature, there are many new results which have not been reported previously.

These include the existence of a novel stopband in the existence domain of fast solitons. By a stopband, we mean a range of Mach numbers between two passbands of an existence domain over which solitary wave propagation does not occur. The presence of a stopband is dependent on the ion-ion mass ratio and the hotter ion to electron temperature ratio, and it exists only when the thermal effects of the cooler ion species are small.

Contents

List of Figures

List of Tables

Chapter 1

General introduction

1.1 Plasma waves

Plasmas found in space are usually composed of electrons and one or more species of ions, as well as, sometimes, massive charged dust grains. They are immersed in a background magnetic field which is not uniformly distributed, and the plasma constituents often have different temperatures or may even best be represented by a combination of temperatures.

Perturbation of plasmas causes a great variety of waves to propagate. These include waves whose amplitudes are vanishingly small (i.e. linear waves) and waves with larger amplitudes (i.e. nonlinear waves). In this Introduction, we discuss the theory of these waves, in brief and with emphasis on the waves that we are interested in, leaving the details to the appropriate chapter.

In the theoretical study of linear plasma waves, variable quantities are written as a sum of two terms corresponding to the undisturbed and disturbed states of the plasma configuration under consideration. Substitution of the variable quantities, written in this way, in the basic equations yields the linear equations, when nonlinear terms are neglected. Then one looks for solutions of these linear equations in which all the perturbed quantities, assumed to undergo sinusoidal oscillations, are proportional to $\exp[i(\mathbf{k}.\mathbf{r}-\omega t)]$ where ω is the angular frequency of the wave, $\mathbf{k}$ is the wave vector, $\mathbf{r}$ is the position vector, and t is the time. After some algebra, one finds that ω and

the wave number k obey the relation

$$D(k, \omega) = 0, \tag{1.1}$$

known as the dispersion relation. For each real value of k, the allowed value of ω is obtained by solving the dispersion relation. The obtained solution is called a normal mode. The fact that the equations are linear allows one to construct a more general solution by adding the normal modes (see details, for example, in Infeld & Rowlands (1990), pp. $29 - 31$).

The linear theory of plasma waves is relevant only when the amplitude of the wave is small. To study larger amplitude plasma waves, nonlinearities in the system must be taken into account. Solitary waves and double layers are important nonlinear plasma waves that have been the subject of numerous investigations, as discussed below.

Early work on weakly nonlinear solitary waves on shallow water showed that they preserved their shape, as a result of the balance between the nonlinearities and dispersive effects, and that this was so even after their collisions (Korteweg & De Vries (1895); Zabusky & Kruskal (1965)). Because of their particle-like properties, solitary waves of this type have also been known as "solitons" (Zabusky & Kruskal, 1965).

A double layer is a structure in a plasma consisting of two adjacent layers, with equal and opposite electric charge, hence the name "double layer" (e.g. Block (1978); Raadu & Carlqvist (1981); Raadu & Rasmussen (1988); Hellberg et al. (1997)). The electric field is much stronger inside than outside the double layer and the potential drop (φ_{DL}) through the layer satisfies $\varphi_{DL} \gtrsim K_B T/e$ (Block (1978); Raadu & Carlqvist (1981)), where K_B is the Boltzmann constant, e is the electronic charge, and T is the temperature of the coldest plasma bordering the layer.

Researchers have attempted to distinguish strong or large amplitude double layers from weak or small amplitude double layers, depending on their potential strength compared to $K_B T/e$ (see details for example in Raadu & Carlqvist (1981); Hellberg et al. (1997)). Small amplitude double layers are commonly found in plasmas containing at least two species with different temperatures (e.g. Hellberg et al. (1997), p. 3).

Extensive theoretical investigation of solitons and/or double layers has been carried out in various plasma configurations (e.g. Zabusky & Kruskal

(1965); Washimi & Taniuti (1966); Sagdeev (1966); Tagare (1973); Tran (1974); Tagare (1986); Baboolal et al. (1988); Bhattacharyya & Roychoudhury (1988); Baboolal et al. (1989, 1990); Yadav & Sharma (1990); Mace et al. (1991); Bharuthram & Shukla (1992); Cairns et al. (1995); Ghosh et al. (1996); Mamun (1997); Mamun & Shukla (2002); Verheest et al. (2005); Hellberg et al. (2006); Verheest et al. (2008); Baluku & Hellberg (2008); Baluku et al. (2008); Hellberg & Verheest (2008); Mamun (2008); Saini et al. (2009); Yaroshenko et al. (2010); Verheest & Hellberg (2010b); Baluku et al. (2010b); Verheest & Hellberg (2010a); Verheest (2010); Verheest & Hellberg (2010a); Verheest et al. (2011); Baluku & Hellberg (2011); Roy et al. (2012); Maharaj et al. (2012); Baluku & Hellberg (2012); Verheest (2013); Saini et al. (2013)).

Until a few years ago, it was commonly believed that when double layers occur in a given plasma configuration, they constitute the upper limit in speeds for the existence of solitons of the same polarity (e.g. Verheest et al. (2008)). Recent studies (e.g. Verheest (2009); Baluku et al. (2010b)), however, have shown that, in some plasma models, solitons may occur at speeds greater than those of double layers. Solitons that occur at speeds greater than those of double layers are currently known as "supersolitons" (e.g. Dubinov & Kolotkov (2012); Verheest et al. (2013a,b,c); Maharaj et al. (2013)).

Theoretical studies of solitons and/or double layers are often carried out using dimensionless quantities because the analysis of equations becomes simpler. The quantities having the dimensions of a speed are often normalised with respect to an acoustic-type speed or a thermal speed. The resulting dimensionless speed is often referred to as the Mach number. However, as discussed in detail by, for example, Dubinov (2009), this may not be the true Mach number. The true Mach number is that obtained by normalising the speed of a soliton/double layer with respect to the acoustic speed of the linear waves for the plasma model under consideration (e.g. Dubinov (2009)). This should also be borne in mind when interpreting the results presented in this thesis.

Weakly nonlinear plasma waves are often studied using the reductive perturbation technique (e.g. Tagare (1973); Tran (1974); Verheest (2008)). Defining V as the acoustic speed of the linear waves for the plasma model under consideration, ε as a small, non-zero, parameter, x as the space coor-

dinate, and t as the time, the reductive perturbation technique relies on the stretched coordinates (e.g. Tagare (1973); Tran (1974); Verheest (2008))

$$\xi = \varepsilon^{1/2}(x - Vt), \tag{1.2}$$

$$\tau = \varepsilon^{3/2}t. \tag{1.3}$$

Using these stretched coordinates and the expansion of the dependent variables in powers of ε in the basic equations governing the dynamics of the plasma model under consideration one obtains, after some algebra, an equation of the form (e.g. Tagare (1973); Tran (1974); Verheest (2008))

$$\frac{\partial \varphi}{\partial \tau} + a\varphi\frac{\partial \varphi}{\partial \xi} + b\frac{\partial^3 \varphi}{\partial \xi^3} = 0. \tag{1.4}$$

This is known as the Korteweg-de Vries (KdV) equation, where in this work φ is the electrostatic potential, but may represent another variable quantity, e.g. the density (Tagare (1973); Tran (1974)), and a and b are real constants that depend on the plasma model under consideration. For a given plasma model, the problem is then to determine the coefficients a and b; once they are known, investigation of small amplitude solitons can proceed.

Equation (1.4) expresses the balance between slow time variations (first term), nonlinearities (second term), and dispersive effects (third term). In the wave frame, in which explicit time variations vanish, a soliton solution of the KdV equation is of the form (e.g. Zabusky & Kruskal (1965); Tagare (1973))

$$\varphi(\eta) = \varphi_m \mathrm{sech}^2\left(\frac{\eta}{\mathrm{w}}\right). \tag{1.5}$$

Here φ_m and w are, respectively, the soliton amplitude and width which depend on the plasma model under consideration, and $\eta = \xi - c\tau$, c being the soliton speed in a co-moving frame. One important feature of this solution is that it represents a hump- or dip-like structure travelling at a constant speed which is linearly proportional to the amplitude, with unchanged shape during propagation (Zabusky & Kruskal, 1965).

In plasma models where large amplitude plasma waves exist, the reductive perturbation technique is not appropriate. Plasma waves of arbitrary amplitude have been studied for several years using the Sagdeev potential approach (Sagdeev, 1966). This approach has been effective in studying the

electrostatic plasma waves of arbitrary amplitude in various plasma configurations (e.g. Bharuthram & Shukla (1992); Cairns et al. (1995); Verheest et al. (2008); Mamun (2008); Saini et al. (2009); Yaroshenko et al. (2010); Verheest & Hellberg (2010b); Verheest et al. (2011); Baluku & Hellberg (2011); Roy et al. (2012); Maharaj et al. (2012)).

In the Sagdeev potential approach, the first task is to obtain the plasma densities expressed in terms of the electrostatic potential, by eliminating the velocities between the continuity and momentum equations per species. Substitution of the densities into Poisson's equation yields, after some algebra, an equation analogous to an energy equation in classical mechanics for a particle with unit mass in a potential well. This equation is of the form (e.g. Sagdeev (1966); Verheest et al. (2008))

$$\frac{1}{2}\left(\frac{d\varphi}{dx}\right)^2 + S(\varphi) = 0, \tag{1.6}$$

where $S(\varphi)$ is a function of the electrostatic potential, commonly known as Sagdeev potential or pseudopotential (Sagdeev, 1966). For a given plasma model, a knowledge of the Sagdeev potential allows one to carry out further discussion of solitons and/or double layers of arbitrary amplitude.

Weakly nonlinear plasma waves can also be studied by Taylor expanding $S(\varphi)$ about the origin $\varphi = 0$ (e.g. Baluku & Hellberg (2008)). To third order, this process results in an equation of the form (e.g. Baluku & Hellberg (2008))

$$\frac{1}{2}\left(\frac{d\varphi}{dx}\right)^2 + A\varphi^2 + B\varphi^3 = 0, \tag{1.7}$$

where A and B are constants that must be determined. Equation (1.7) leads to the usual KdV-type solution.

Recently, McKenzie (2002a) introduced a fluid dynamic approach as an alternative viewpoint in the study of fully nonlinear plasma waves. The approach assumes an adiabatic flow of plasma species and is based on the conservation of the total momentum of the system which, together with a Bernoulli-type energy equation for each species, yields the structure equation for the stationary nonlinear wave. It highlights the crucial role played by the species' "sonic points" in determining the conditions for the existence of solitons.

A "sonic point" is defined as the point in space at which the species'

local flow speed is equal to the local acoustic speed (McKenzie, 2002a). At that point, the species' flow is choked, hence limiting the amplitude of the wave (McKenzie, 2002a). The "sonic points" will play an important role in the determination of the soliton existence domains discussed in chapters 3 and 4 of this thesis.

Following the work of McKenzie (2002a) which involved an electron-proton plasma model, the fluid dynamic approach has been used to study solitons in many other plasma configurations (e.g. McKenzie (2002b); McKenzie & Doyle (2003); McKenzie (2003); McKenzie et al. (2004); Verheest et al. (2004); McKenzie et al. (2005); Verheest et al. (2005); Hellberg et al. (2006); Hellberg & Verheest (2008); Baluku et al. (2008)). However, the McKenzie fluid dynamic approach has been found to be equivalent to the Sagdeev potential approach, the only difference being that it uses a different viewpoint. In this work, we will use the Sagdeev potential approach to study nonlinear plasma waves of arbitrary amplitude.

Verheest (2008) discussed, in detail, the above three methods that can be used to study nonlinear plasma waves by giving a general overview of the methodology, followed by a specific application in each case.

In this work, we study some linear and nonlinear plasma waves in the context of space plasmas. As mentioned in the beginning of this chapter, space plasmas are immersed in a non-uniform magnetic field. In regions where the magnetic field strength is very weak, plasmas are often treated as unmagnetised. When a plasma is immersed in a background magnetic field of significant strength, many interesting phenomena arise, as the magnetic field introduces a further restoring force to drive oscillations. In particular, there are important differences between propagation of plasma waves along and across the magnetic field.

Electron Bernstein waves (e.g. Mace (2003, 2004); Viñas et al. (2005); Henning et al. (2011)) are linear plasma waves that propagate perpendicularly to the ambient magnetic field at frequencies between harmonics of the electron cyclotron frequency. There are also ion Bernstein waves (e.g. Fredricks (1968a,b); Puri et al. (1973)), that is, ion waves that propagate perpendicularly to the ambient magnetic field at frequencies between harmonics of the ion cyclotron frequency. Similarly, dust Bernstein waves (e.g. Deeba et al. (2011)) propagate perpendicularly to the ambient magnetic field at frequencies between harmonics of the dust cyclotron frequency.

Using the common assumption of Maxwellian plasma species, Bernstein (1958) first demonstrated that such waves are not subject to Landau damping, an important phenomenon that is discussed in Sec. 1.3. Bernstein waves propagate in a hot magnetised plasma and are studied using kinetic theory. Kinetic theory requires a knowledge of the particle velocity distribution, unlike the fluid theory where all plasma particles of a given species are assumed to be moving with the same velocity.

In a fluid model, if the inertial effects of a given plasma species are negligible, the balance between the thermal and electrostatic forces in the corresponding momentum equation gives a typical density distribution of the form

$$n = n_0 \exp\left(\frac{-q\varphi}{K_B T}\right), \tag{1.8}$$

commonly known as a Boltzmann density distribution, where n is the number density, with equilibrium value n_0, q is the charge, K_B is the Boltzmann constant, and T is the temperature.

It is common practice in plasma physics to express the temperature in energy units. In that case, the energy corresponding to $K_B T$ is used to denote the temperature. In this work, temperatures will be expressed in energy units.

As mentioned previously, a knowledge of the particle velocity distribution is important in the study of many plasma waves, and in particular in the study of Bernstein waves. Therefore, in the next section, we discuss the plasma velocity distributions that will be useful in this work.

1.2 Kappa velocity distribution

Traditionally, a Maxwellian velocity distribution has been the basis of many studies of plasma waves. However, under some circumstances, a Maxwellian distribution may fail to model appropriately the velocities of the plasma particles (Vasyliunas, 1968). This author investigated the low-energy electron population in the terrestrial magnetosphere using the observational data obtained with the OGO 1 and OGO 3 satellites. During the analysis, he noticed that the observational data could, in general, not be fitted by a Maxwellian distribution, particularly at high energies of the electron velocity distribution where a non-Maxwellian "tail" was observed.

Consequently, a model distribution function that generalises the Maxwellian and approaches a power law at high energies was introduced. The distribution function was written as (Vasyliunas (1968), p. 2866)

$$f(v) = \frac{N}{w_0^3} \frac{\Gamma(\kappa+1)}{(\pi\kappa)^{3/2}\Gamma(\kappa-\frac{1}{2})} \frac{1}{(1+v^2/\kappa w_0^2)^{\kappa+1}}, \tag{1.9}$$

where N is the total number density, w_0 is the most probable speed, κ is the exponent of the differential flux at high energies, v is the particle speed, and Γ is the usual gamma function. It was noted that the Maxwellian distribution was included in the distribution function given by Eq. (1.9) as a special case when $\kappa \to \infty$.

Considering a plasma where the electron velocity distribution function is a superposition of a bi-kappa and a bi-Maxwellian, Leubner (1982) discussed the Jupiter's whistler hiss and chorus emission. Defining an effective temperature for each component, he introduced θ to represent the most probable speed appearing in Eq. (1.9) relating it to the usual thermal speed of a Maxwellian plasma (v_t) as

$$\theta = \left(\frac{\kappa - 3/2}{\kappa}\right)^{1/2} v_t, \tag{1.10}$$

where $v_t = (2K_BT/m)^{1/2}$.

The kappa velocity distribution has been used by many other researchers either to carry out a theoretical study of plasma waves (e.g. Summers & Thorne (1991); Mace & Hellberg (1995); Hellberg & Mace (2002)) or to analyse the observational data (e.g. Christon et al. (1988, 1989); Divine & Garrett (1983); Krimigis et al. (1983); Sittler et al. (1983); Schippers et al. (2008)).

Theoretical studies of linear plasma waves in hot plasmas have shown that the dispersion relation of such waves involves a complex-valued function of a complex variable, commonly known as the plasma dispersion function. In particular, if a Maxwellian is used as the equilibrium velocity distribution, the plasma dispersion function takes the form (Fried & Conte, 1961)

$$Z(\xi) = \frac{1}{\sqrt{\pi}} \int_{-\infty}^{+\infty} \frac{e^{-s^2}}{s-\xi} ds, \tag{1.11}$$

where $\xi = x + iy$, and $\mathrm{Im}(\xi) > 0$, with a possible extension for $\mathrm{Im}(\xi) \leq 0$ by analytic continuation.

The presence of a non-Maxwellian high-energy tail (Vasyliunas, 1968) observed in space plasmas motivated Summers & Thorne (1991) to seek a new form of the plasma dispersion function that is suitable for a plasma with a kappa velocity distribution. They wrote the isotropic three-dimensional kappa velocity distribution as

$$f_\kappa(v) = \frac{N}{\pi^{3/2}} \frac{1}{\theta^3} \frac{\Gamma(\kappa+1)}{\kappa^{3/2}\Gamma(\kappa-1/2)} \left(1 + \frac{v^2}{\kappa\theta^2}\right)^{-(\kappa+1)}, \tag{1.12}$$

in which

$$\theta = \left(\frac{2\kappa-3}{\kappa}\right)^{1/2} \left(\frac{T}{m}\right)^{1/2}, \tag{1.13}$$

provided $\kappa > 3/2$. We note that the expression for θ in Eq. (1.13) is the same as that in Eq. (1.10) if the temperatures are expressed in the same units.

The authors emphasised that the Maxwellian and kappa velocity distributions differ significantly for small values of κ (i.e. at the high-energy tail), but that the difference decreases with increasing value of κ, as shown in Fig. 1.1. Furthermore, they obtained the plasma dispersion function for a plasma with a kappa velocity distribution as

$$Z^*_\kappa(\xi) = \frac{1}{\sqrt{\pi}} \frac{\Gamma(\kappa+1)}{\kappa^{3/2}\Gamma(\kappa-1/2)} \times \int_{-\infty}^{+\infty} \frac{ds}{(s-\xi)(1+s^2/\kappa)^{\kappa+1}}, \tag{1.14}$$

which they named the modified plasma dispersion function.

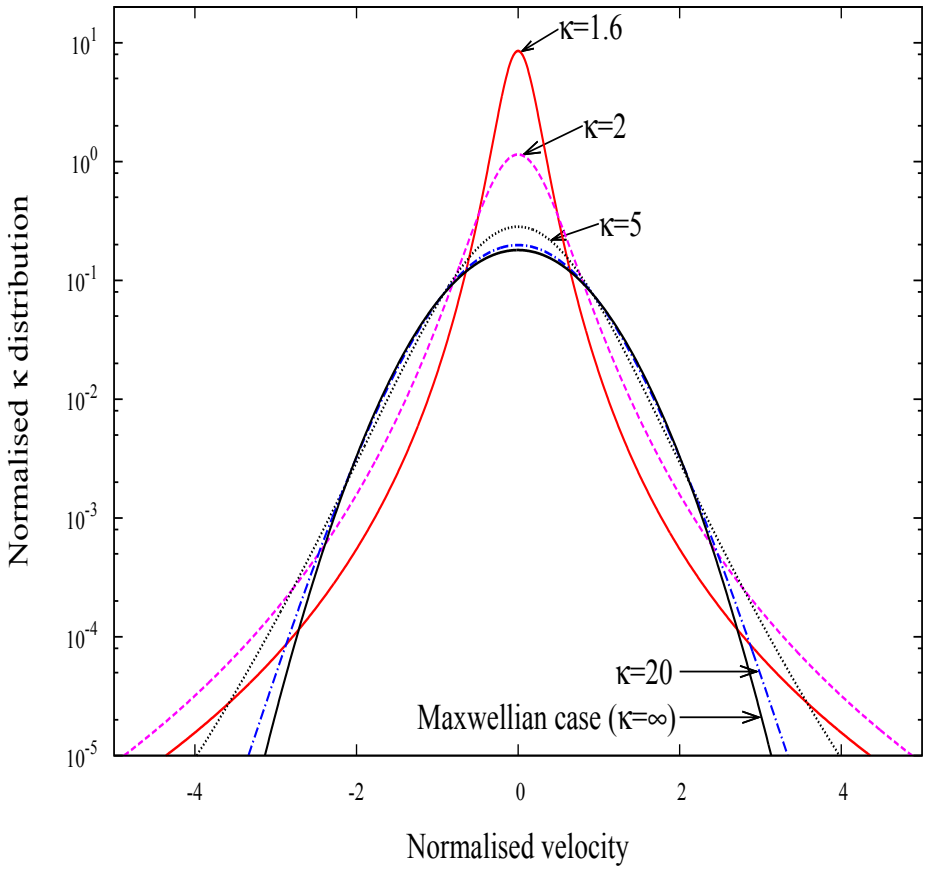

Figure 1.1: Kappa velocity distribution, plotted as $f(v)(2v_t^2)^{3/2}/N$ against $v/\sqrt{2}v_t$, for κ=1.6, 2, 5, 20, and ∞.

In deriving Eq. (1.14), Summers & Thorne (1991) restricted the parameter κ to strictly integral values. This point motivated Mace & Hellberg (1995) to seek another form of the plasma dispersion function that is appropriate for a kappa-distributed plasma for arbitrary real values of κ. They obtained the plasma dispersion function, which they expressed in closed form in terms of Gauss's hypergeometric function, ${}_2F_1$, as

$$Z_\kappa(\xi) = \frac{i(\kappa+\frac{1}{2})(\kappa-\frac{1}{2})}{\kappa^{3/2}(\kappa+1)} {}_2F_1\left[1, 2\kappa+2; \kappa+2; \frac{1}{2}\left(1-\frac{\xi}{i\sqrt{\kappa}}\right)\right], \qquad (1.15)$$

which they then applied to the study of the electron plasma waves in an unmagnetised kappa-distributed plasma.

Hellberg & Mace (2002) suggested that some plasmas may have anisotropic

power-law distributions. They proposed a velocity distribution that has a one-dimensional kappa distribution along a preferred direction in space, and a two-dimensional Maxwellian distribution in the plane perpendicular to it. They obtained the form of the distribution function as

$$f_{\kappa M}(v_{\parallel}, v_{\perp}) = \frac{1}{\pi^{3/2}\theta_{\perp}^2\theta_{\parallel}} \frac{\Gamma(\kappa+1)}{\kappa^{3/2}\Gamma(\kappa-\frac{1}{2})} \times \left(1+\frac{v_{\parallel}^2}{\kappa\theta_{\parallel}^2}\right)^{-\kappa} \exp\left\{-\left(\frac{v_{\perp}}{\theta_{\perp}}\right)^2\right\}, \tag{1.16}$$

which they named kappa-Maxwellian velocity distribution. Furthermore, the plasma dispersion function for such a distribution was obtained as

$$Z_{\kappa M}(\xi) = i\frac{\kappa-\frac{1}{2}}{\kappa^{3/2}} {}_2F_1\left[1, 2\kappa; \kappa+1; \frac{1}{2}\left(1-\frac{\xi}{i\sqrt{\kappa}}\right)\right], \tag{1.17}$$

which they then used to study the ion-acoustic and ion-cyclotron-sound waves propagating at an angle to the magnetic field.

Observations (e.g. Christon et al. (1988, 1989)) have shown that both ion and electron velocity distributions in the Earth's plasma sheet are non-thermal and that they can be accurately modelled by a kappa distribution. Assuming that all the observed ions were protons, and fitting a kappa distribution to the observed energy spectra of plasma sheet ions and electrons, Christon et al. (1988, 1989) reported best fits for κ values in the range $4-8$, with a most probable value between 5 and 6, for both ions and electrons.

Divine & Garrett (1983) showed that protons and electrons in the Jovian magnetosphere can be modelled by a kappa distribution. They produced detailed kappa contour maps of the Jovian magnetosphere, indicating the kappa values that best apply to a particular region of the magnetosphere, citing, inter alia, typical values of order $2-3$ for both κ_i and κ_e.

Assuming that all the ions in the Saturnian magnetosphere were protons, Krimigis et al. (1983) showed that a kappa distribution best fitted the observed ion distribution, with typical values of κ in the range $6-8$, whereas the electron spectrum was described by either a Maxwellian or a power-law fit. More recently, the coexistence of two nonthermal electron populations in the Saturnian magnetosphere has been reported (e.g. Sittler et al. (1983); Schippers et al. (2008)). Schippers et al. (2008) showed that the electron energy distribution is best fitted by a superposition of a hot and a cool component, each having its own low value of spectral index κ.

A more historical perspective of the kappa velocity distribution may be obtained from the paper by Hellberg et al. (2009) and references contained therein.

1.3 Landau damping of plasma waves

A plasma wave can be damped by converting its energy into heat as a result of collisions with plasma particles or can be amplified by some instability mechanism.

In the absence of collisions or instabilities, damping or amplification of a plasma wave is also possible if the wave interacts with plasma particles whose velocities are almost equal to the phase velocity of the wave (e.g. Sagdeev (1966); Chen (1984)). The particles are those, commonly known as resonant particles, which travel along with the wave and can exchange energy with the wave.

The average energy exchange between the wave and the particles whose velocities are equal to the phase velocity of the wave is zero (e.g. Chen (1984)). Those particles satisfy the resonance condition given by $\omega - kv \approx 0$ (e.g. Sagdeev (1966); Chen (1984)), where ω is the wave frequency, k is the wavenumber, and v is the particle speed.

The particles that play a role in the Landau damping process are those whose velocities are approximately equal to the wave phase velocity. Such particles can be divided into two groups: those whose velocities slightly exceed the phase velocity and those whose velocities are slightly slower than it. Whether a particle is accelerated or decelerated by the wave depends on its position relative to the wave phase, regardless of whether it is travelling faster or slower than the wave. However, those particles travelling slower than the wave which are accelerated are brought closer to resonance, whereas those that are decelerated are moved further from resonance. Conversely, those that are travelling faster than the wave which are accelerated are moved further from resonance, whereas those that are decelerated are brought closer to resonance. The net effect of this is that the most strongly interacting particles from the slower group are those that are accelerated by the wave, taking energy from it, and the most strongly interacting particles from the faster group are those that are decelerated by the wave, giving energy to it.

Consequently, if there are more slower particles than faster ones, the wave loses energy and decays, i.e. the wave is damped. This damping of the wave is known as Landau damping (e.g. Sagdeev (1966), Chen (1984)). Landau damping of plasma waves is one of the characteristics of collisionless plasmas. It is an effect that is predicted by kinetic theory.

In the case of Landau damping, the distribution function, $f(v)$, describing the velocities of the resonant particles has a negative slope (e.g. Sagdeev (1966), Chen (1984)), i.e. $df/dv < 0$ at $v = \omega/k$.

On the other hand, if there are more faster particles than slower ones, the wave gains energy and grows, i.e. the wave amplitude increases. In that case, the distribution function describing the velocities of the resonant particles has a positive slope (e.g. Sagdeev (1966), Chen (1984)), i.e. $df/dv > 0$ at $v = \omega/k$.

To minimise the number of resonant particles, and hence the Landau damping, one requires that the phase velocity of the wave be much greater or much smaller than the thermal velocity (e.g. Sagdeev (1966), Chen (1984)).

In the case of ion waves in the standard electron-ion plasma (e.g. Sagdeev (1966); Tagare (1973); Chen (1984)), Landau damping is negligible if $T_e \gg T_i$ and it is significant for $T_e \lesssim T_i$ (e.g. Chen (1984)), where T_e and T_i are, respectively, the electron and ion temperatures.

Collisionless damping of linear plasma waves was first reported by Landau (1946), but the author did not provide a physical explanation of the damping. It is an effect that was discovered purely mathematically, while analysing a contour integral. Brodin (1997) provided an alternative approach to linear Landau damping, mentioning advantages and drawbacks of the approaches used by Landau (1946) and Dawson (1961). Although the approaches of both Dawson (1961) and Brodin (1997) provide insight into the physical mechanism of Landau damping, the approach of Brodin (1997) uses a simpler mathematical technique.

A number of authors (e.g. Bandyopadhyay & Das (2002); Ghosh & Bharuthram (2011)) have discussed the effect of Landau damping on solitary waves, and it has been found that Landau damping causes the soliton amplitude to decay with time.

1.4 Outline of the thesis

In this work, we study some linear and nonlinear plasma waves in the context of space plasmas. The work involves a kinetic-theoretical study of ion Bernstein waves in an electron-proton plasma with a kappa velocity distribution and a study of linear and nonlinear ion acoustic waves in a two-adiabatic-ion plasma, using a fluid theory.

We, first, consider a kinetic-theoretical approach and investigate the effects of the parameter kappa on ion Bernstein waves, with an application of the results to the Earth's plasma sheet boundary layer.

A derivation of the dispersion relation of Bernstein waves in a plasma with a kappa velocity distribution was reported by Mace (2003), with an alternative derivation in Henning et al. (2011). While this dispersion relation was used to study electron Bernstein waves (e.g. Mace (2003); Henning et al. (2011)), in this work, we use it to study ion Bernstein waves, in Chap. 2.

Next, we consider, in Chap. 3, a plasma composed of two adiabatic, positively and singly charged, ion species and Boltzmann electrons, and use a fluid theory to investigate the effects of the ion and electron temperatures on linear and, particularly, nonlinear ion acoustic waves. It is well-known (e.g. Tran (1974); Tran & Coquerand (1976)) that two modes with different phase velocities are supported by such a plasma model. We study both the slow and the fast modes.

In Chap. 4, we consider a two-adiabatic-ion plasma studied in Chap. 3, but with kappa-distributed electrons rather than Boltzmann electrons, and investigate the effect of the parameter kappa on the existence domain of the fast mode ion acoustic solitons.

Finally, Chap. 5 provides the general summary and conclusions of the thesis.

Chapter 2

Ion Bernstein waves in a plasma with a kappa velocity distribution

This chapter is based essentially on a paper published as:
Nsengiyumva F., Mace R. L., and Hellberg M. A. 2013, "Ion Bernstein waves in a plasma with a kappa velocity distribution", Physics of Plasmas, 20, 102107.

2.1 Introduction

Waves propagating perpendicularly to the ambient magnetic field, $\mathbf{B}_0$, at frequencies between harmonics of the ion cyclotron frequency have been observed in various space environments (e.g. Russell et al. (1970); Perraut et al. (1982); Cattell et al. (2002); Broughton et al. (2008)).

From OGO 3 observations of ELF noise in the terrestrial magnetosphere, Russell et al. (1970) reported the existence of waves in the outer plasmasphere that propagated almost perpendicularly to the ambient magnetic field between about twice the proton cyclotron frequency (ω_{ci}) and half the lower hybrid frequency, which was found to occur near $43\omega_{ci}$. These waves were confined to a region within about 2° of the geomagnetic equator.

Perraut et al. (1982) investigated ULF waves observed by GEOS 1 and 2 in the vicinity of the geomagnetic equator (within $\pm 10°$) at L values between ~ 4 and ~ 8. Generally, their fundamental frequency was observed

to be of the order of the local proton gyrofrequency and they were accompanied by higher frequency waves. The latter had a well-defined harmonic structure with a high number of harmonics (up to 8 harmonics were seen), and propagated perpendicularly to $\mathbf{B}_0$.

Cattell et al. (2002) carried out a study of the waves associated with ion beams flowing downward along the Earth's magnetic field, as observed by the FAST satellite in the auroral zone. They observed that these waves were electrostatic, as a result of the lack of magnetic signatures, and that their intensity peaked at or near the lower hybrid (LH) frequency, $\omega_{\rm LH}$. In addition, they also observed that, above and/or below $\omega_{\rm LH}$, these waves had a harmonic structure associated with the proton gyrofrequency.

Using magnetic field data obtained by the Cluster spacecraft in the Earth's plasma sheet boundary layer, Broughton et al. (2008) reported observations of harmonically-related waves with the fundamental near the local proton cyclotron frequency. Their measurements of the wave vector, $\mathbf{k}$, using the wave telescope technique (Motschmann et al., 1996; Glassmeier et al., 2001) and of the angle between $\mathbf{k}$ and $\mathbf{B}_0$, showed that the waves propagated nearly perpendicularly to $\mathbf{B}_0$.

Several kinetic-theoretical investigations of electrostatic ion waves propagating perpendicularly to $\mathbf{B}_0$, commonly known as ion Bernstein waves (Bernstein, 1958), have been reported (e.g. Fredricks (1968a,b); Puri et al. (1973)). Ion Bernstein waves propagate at frequencies between the harmonics of the ion cyclotron frequency ($n\omega_{ci}$), and their dispersion behaviour depends on whether the wave frequency lies below, above, or within the LH frequency band. Here and in the remainder of this chapter, n denotes the harmonic number.

Adopting a Maxwellian velocity distribution function, Fredricks (1968a) investigated the structure of the dispersion curves of ion Bernstein waves for the case where $\omega_{\rm LH}$ lies in one of the high harmonic bands. In addition to confirming the well-known dispersion behaviour of ion Bernstein waves, Fredricks (1968a) showed that the modes propagating within the LH band and in a few frequency bands directly above it do not have a sharply-defined peak, but rather exhibit a fairly broad flat maximum. Thus, there is a finite range of values of the wavenumber, k, over which the group velocity, $d\omega/dk$, is vanishingly small.

Furthermore, it was found that for parameter values for which $\omega_{\rm LH} \gg$

ω_{ci}, propagation in these bands with $\omega \geq \omega_{\mathrm{LH}}$ was possible across the full intra-harmonic band. The close proximity of these frequency peaks to the next ion cyclotron harmonic produced a strong coupling between modes in adjacent bands, such that the lower hybrid branch appeared to cut across the harmonics, and thus propagation was possible over a continuous range of frequency covering numerous harmonics.

Fredricks (1968b) later extended his earlier work (Fredricks, 1968a) to allow for electromagnetic effects by removing the constraint $\mathbf{k} \times \mathbf{E} = 0$. The Bernstein waves that propagate under such conditions are often referred to as generalised ion Bernstein modes. He found that the full electromagnetic dispersion relation asymptotically approaches the electrostatic approximation at large values of k. Puri et al. (1973) obtained the dispersion curves for the generalised ion Bernstein modes in a Maxwellian plasma, and found that the modes are predominantly electrostatic and that they exhibit an electromagnetic character only where the phase velocity becomes superluminal, i.e., where $k \to 0$, in agreement with the earlier findings of Fredricks (1968b).

It is well-known that ion and electron Bernstein wave types have dispersion curves that are in principle similar in shape, but they obviously differ in both wavelength range (being characterised by ion and electron Larmor radii, respectively) and frequency range (ion versus electron cyclotron harmonics, centred on the lower and upper hybrid frequency, respectively). Physically, an important difference between the two types is that the ions are dynamically unimportant in the electron Bernstein case and can be neglected in the dispersion relation, whereas for the ion Bernstein waves, the electrons do not just form a charge neutralising background, but play a small but crucial shielding role, whose effects cannot be neglected.

Numerical studies of both the electron and ion Bernstein waves in Maxwellian plasmas have shown that the frequencies are real, i.e. the waves are stable (e.g. Fredricks (1968a,b); Puri et al. (1973)). However, this is not necessarily true if the plasma has a different velocity (energy) distribution. For instance, Tataronis & Crawford (1970) considered perpendicularly propagating electron cyclotron harmonic waves in a plasma whose electrons had, inter alia, a ring distribution, a spherical shell distribution and a mixed ring-Maxwellian distribution. They showed that these distributions may all lead to unstable waves for certain parameter values.

A key factor in considering stability is whether there is an available source of free energy to drive an instability. This may arise, for instance (Cottrell et al., 1993), due to non-monotonicity of $f(v_\perp)$, i.e., if the perpendicular velocity space derivative satisfies $\partial f/\partial v_\perp > 0$ for a range of $v_\perp$ (Hall et al., 1965; Cattell et al., 2002; Gary et al., 2010). Depending on the velocity distribution assumed, various authors have discussed ion cyclotron harmonic instability that can be generated by beams (e.g. Crary et al. (2001)), loss-cone (e.g. Harris (1970)) or subtracted Maxwellian distributions (e.g. Gary et al. (2010)), although it should be noted that in some cases, authors refer to the modes as being ion Bernstein waves, even though $k_\parallel/k_\perp$ is small but non-zero.

Following on the introduction of a generalisation (Summers & Thorne, 1991) of the standard plasma dispersion function (Fried & Conte, 1961), there have been numerous kinetic-theoretical studies of electrostatic waves in unmagnetised κ-distributed plasmas. These led to a representation of the dispersion function based on the Gauss hypergeometric function, ${}_2F_1(a, b; c; z)$ (e.g. Mace & Hellberg (1995); Hellberg & Mace (2002); Mace & Hellberg (2009)), which was applied to the study of, for instance, electron plasma waves, ion acoustic waves and electron acoustic waves (Baluku et al., 2011).

These ideas were extended to the study of waves in magnetised kappa plasmas. Using a Gordeyev integral approach, Mace (2003) derived the dispersion relation for electrostatic Bernstein waves in a multi-species kappa plasma, expressing it in a closed form in terms of generalised hypergeometric functions (${}_1F_2$ and ${}_2F_3$). He obtained a similar closed form for electrostatic Bernstein waves in a Maxwellian plasma in terms of ${}_2F_2$ functions. Neglecting the ion dynamics, he solved both dispersion relations numerically for electron Bernstein waves, considering various values of κ. He found significant κ dependence of ω over a wide range of wavenumber, the changes over the low range, satisfying $1.5 < \kappa < 5$, being as large as those for $5 < \kappa < \infty$ (Maxwellian). Recently, Henning et al. (2011) used the Lerche-Newberger sum rule for Bessel functions to provide an alternative derivation of the dispersion relations of Mace (2003). They then investigated the behaviour of electron Bernstein waves in plasmas whose electrons have two kappa distributions, applying the results to the Saturnian magnetosphere.

Mace (2004) generalised his earlier work (Mace, 2003), to incorporate electromagnetic effects, and observed that the modes are predominantly

electrostatic, regardless of κ value, with an electromagnetic character as $k \to 0$. It was found that electromagnetic effects couple the Bernstein mode in the vicinity of the upper hybrid frequency to the lower frequency Z-mode branch of the cold plasma extraordinary wave, as is the case for a Maxwellian plasma (Puri et al., 1973).

2.2 Motivation, aims, and methodology

There are two motivations to carry out the work presented in this chapter. Firstly, the investigation of the effect of the parameter kappa on ion Bernstein waves is an unsolved problem. Thus, using the dispersion relations of ion Bernstein waves derived by Mace (2003), with an alternative derivation in Henning et al. (2011), we carry out a comprehensive numerical investigation of the effect of the parameter kappa on ion Bernstein waves, considering a wide range of values of $\omega_{\rm pi}/\omega_{\rm ci}$ for a broader picture that permits application to various space environments. Here, ω_{pi}/ω_{ci} is the ratio of the ion plasma frequency to the ion cyclotron frequency. For completeness, we also discuss, briefly, the effect of varying the ion-to-electron temperature ratio.

Secondly, since the characteristics of Bernstein waves are often used to infer important space plasma parameters (e.g. Viñas et al. (2005); Benson et al. (2013)), it is imperative that the theory used matches as closely as possible the underlying plasma conditions.

Whereas the ion velocity distributions in the terrestrial central plasma sheet (CPS) have been shown to be consistent with the kappa distribution (e.g. Christon et al. (1988, 1989)), less appears to be known about their precise form in the plasma sheet boundary layer (PSBL). However, it is not inconceivable that their boundary may become blurred, allowing mixing of the plasmas from the two regions, during disturbed times. At their interface, then, one might expect the plasma velocity distribution to have some non-thermal features, like a power law tail (e.g. Sarris et al. (1981); Eastman et al. (1984); Christon et al. (1988, 1989)).

Thus, the idea that the PSBL plasma may have some of the non-thermal features of the CPS, in conjunction with the recent observations in this region of perpendicularly propagating waves at frequencies between harmonics of the ion cyclotron frequency (e.g. Broughton et al. (2008)), is another strong motivation to carry out a study of ion Bernstein waves using the

kappa velocity distribution (e.g. Vasyliunas (1968); Summers & Thorne (1991); Hellberg et al. (2009)) as equilibrium distribution for the ions.

After a parameter survey that presents a broad overview of the numerical solutions of the dispersion relations of ion Bernstein waves derived by Mace (2003), we consider an application of our results to the PSBL in which waves propagating perpendicularly to the ambient magnetic field at frequencies between harmonics of the ion cyclotron frequency are frequently observed.

The numerical solutions of the above-mentioned dispersion relations have been obtained using Mathematica programming language. All plots have been obtained using gnuplot.

For a fixed value of ω_{pi}/ω_{ci}, the dispersion relation is found to depend significantly on the parameter kappa of the ions, κ_i. Over all cyclotron harmonics, the typical Bernstein wave curves are shifted to higher wavenumbers (k) if κ_i is reduced. As the value of ω_{pi}/ω_{ci} is increased, the fall-off of ω at large k is smaller for lower κ_i, and curves are shifted towards larger wavenumbers. For large values of ω_{pi}/ω_{ci}, the ion Bernstein waves dispersion curves within and above the lower hybrid frequency band exhibit coupling for the Maxwellian case, unlike the kappa case.

Considering parameter values that have been observed in the PSBL, and neighbouring environments, we find that the derived value of ω_{pi}/ω_{ci} is very large, and that the corresponding lower hybrid frequency, $\omega_{pi}/\omega_{\mathrm{LH}}$, has a value that is close to the upper limit given by $\sqrt{1836}\omega_{ci} \approx 42.85\omega_{ci}$, for an electron-proton plasma model. The associated ion Bernstein wave dispersion curves are typical of those found for the case of a high-density plasma immersed in a weak magnetic field.

2.3 Model and dispersion relation

Following Mace (2003), we consider an infinite, uniform, collisionless, non-relativistic electron-proton plasma that is immersed in a steady and homogeneous ambient magnetic field. The equilibrium velocity distributions are given by the kappa distribution, see Eq. (1.12) and Fig. 1.1. The dispersion relation for perpendicularly propagating electrostatic waves, derived in

Mace (2003), with an alternative derivation in Henning et al. (2011), is

$$1+\sum_{\alpha=i,e}\frac{1}{k^2\lambda_{\kappa\alpha}^2}\Bigg\{1-{}_2F_3\left[1,\frac{1}{2};\frac{1}{2}-\kappa_\alpha,1+\frac{\omega}{\omega_{c\alpha}},1-\frac{\omega}{\omega_{c\alpha}};2\lambda_\alpha^{'}\right]+$$
$$\pi^{1/2}\frac{\omega}{\omega_{c\alpha}}\csc\left(\pi\frac{\omega}{\omega_{c\alpha}}\right)\frac{\Gamma(\kappa_\alpha+1)\Gamma(\frac{1}{2}-\kappa_\alpha)}{\Gamma(\kappa_\alpha+\frac{3}{2}+\omega/\omega_{c\alpha})\Gamma(\kappa_\alpha+\frac{3}{2}-\omega/\omega_{c\alpha})}\times$$
$$(2\lambda_\alpha^{'})^{\kappa_\alpha+1/2}{}_1F_2\left[\kappa_\alpha+1;\kappa_\alpha+\frac{3}{2}+\frac{\omega}{\omega_{c\alpha}},\kappa_\alpha+\frac{3}{2}-\frac{\omega}{\omega_{c\alpha}};2\lambda_\alpha^{'}\right]\Bigg\}=0, \quad (2.1)$$

where ${}_nF_m$ is the generalised hypergeometric function for positive integers n and m; $k=k_\perp$; and the Debye length for a kappa plasma is (e.g. Mace et al. (1998); Bryant (1996))

$$\lambda_{\kappa\alpha}^2=\lambda_{D\alpha}^2\left(\frac{\kappa_\alpha-\frac{3}{2}}{\kappa_\alpha-\frac{1}{2}}\right), \quad (2.2)$$

with $\lambda_{D\alpha}$ the usual Debye length for a Maxwellian plasma. An important variable is $\lambda_\alpha^{'}=(\kappa_\alpha-\frac{3}{2})k^2v_{t\alpha}^2/\omega_{c\alpha}^2$, with $v_{t\alpha}$ the usual thermal speed of species α. We see that $\lambda_\alpha^{'}$ is proportional to $k^2R_{L\alpha}^2$, where $R_{L\alpha}$ is the Larmor radius of a "typical particle" of species α, with perpendicular speed in the magnetic field equal to the usual thermal speed.

It is useful to re-write Eq. (2.1) in a more convenient form. We choose to write $\lambda_{\kappa\alpha}$ and $\lambda_\alpha^{'}$ in terms of the common variable $\lambda_\alpha=k^2v_{t\alpha}^2/\omega_{c\alpha}^2=k^2R_{L\alpha}^2$.

From the definitions, Eq. (2.2) can be written as

$$\lambda_{\kappa\alpha}^2=\frac{\omega_{c\alpha}^2}{\omega_{p\alpha}^2}\frac{v_{t\alpha}^2}{\omega_{c_\alpha}^2}\left(\frac{\kappa_\alpha-\frac{3}{2}}{\kappa_\alpha-\frac{1}{2}}\right). \quad (2.3)$$

The full dispersion relation for ion Bernstein waves in a proton-electron plasma composed of kappa-distributed species becomes

$$1+\sum_{\alpha=i,e}\left(\frac{\kappa_\alpha-\frac{1}{2}}{\kappa_\alpha-\frac{3}{2}}\right)\frac{\omega_{p_\alpha}^2}{\omega_{c_\alpha}^2}\frac{1}{\lambda_\alpha}\left\{1-{}_2F_3\left[1,\frac{1}{2};\frac{1}{2}-\kappa_\alpha,1+\frac{\omega}{\omega_{c\alpha}},1-\frac{\omega}{\omega_{c\alpha}};(2\kappa_\alpha-3)\lambda_\alpha\right]+\right.$$
$$\pi^{1/2}\frac{\omega}{\omega_{c\alpha}}\csc\left(\pi\frac{\omega}{\omega_{c\alpha}}\right)\frac{\Gamma(\kappa_\alpha+1)\Gamma(\frac{1}{2}-\kappa_\alpha)}{\Gamma(\kappa_\alpha+\frac{3}{2}+\omega/\omega_{c\alpha})\Gamma(\kappa_\alpha+\frac{3}{2}-\omega/\omega_{c\alpha})}\times$$
$$\left.\left[(2\kappa_\alpha-3)\lambda_\alpha\right]^{\kappa_\alpha+1/2}{}_1F_2\left[\kappa_\alpha+1;\kappa_\alpha+\frac{3}{2}+\frac{\omega}{\omega_{c\alpha}},\kappa_\alpha+\frac{3}{2}-\frac{\omega}{\omega_{c\alpha}};(2\kappa_\alpha-3)\lambda_\alpha\right]\right\}=0, \tag{2.4}$$

where $\lambda_\alpha = k^2 v_{t\alpha}^2/\omega_{c\alpha}^2$.

Similarly, the dispersion relation for ion Bernstein waves in a Maxwellian plasma can be written as (Mace, 2003)

$$1+\sum_{\alpha=i,e}\frac{\omega_{p\alpha}^2}{\omega_{c\alpha}^2}\frac{1}{\lambda_\alpha}\left\{1-{}_2F_2\left[\frac{1}{2},1;1+\frac{\omega}{\omega_{c\alpha}},1-\frac{\omega}{\omega_{c\alpha}};-2\lambda_\alpha\right]\right\}=0. \tag{2.5}$$

Eq. (2.5) will be used to provide solutions for comparison with the kappa case.

2.4 Numerical solutions of the dispersion relations

This section presents the numerical solutions of Eqs. (2.4) and (2.5), for the ion Bernstein waves. We shall use $T_i/T_e = 7$ as a typical value of the temperature ratio, based on data in the terrestrial plasma sheet (e.g. Baumjohann et al. (1989); Christon et al. (1989)). Varying the temperature ratio between 10^{-4} and 10^3 had no observable effect on the dispersion curves. Similarly, our preliminary investigations of the effects of changing κ_e produced no visible differences in the dispersion relation, to within graphical accuracy, over the range $1.6 \leq \kappa_e \leq 1000$. Hence, we arbitrarily set $\kappa_e = 2$, a value consistent with the electron velocity distribution in the inner magnetosphere. As we shall see below, for typical PSBL parameters, the value of ω_{pi}/ω_{ci} is found to be large. Nonetheless, we shall consider a wide range of values of ω_{pi}/ω_{ci} for a broader picture that permits application of our results to other space environments.

The ion plasma frequency is related to the lower hybrid frequency ($\omega_{\rm LH}$)

through (e.g. Stix (1992), p. 29)

$$\frac{1}{\omega_{\rm LH}^2} = \frac{1}{\omega_{ci}^2 + \omega_{pi}^2} + \frac{1}{|\omega_{ce}|\omega_{ci}}, \tag{2.6}$$

which can, alternatively, be written as

$$\frac{\omega_{\rm LH}^2}{\omega_{\rm ci}^2} = \frac{1}{[1/(1+\omega_{pi}^2/\omega_{ci}^2)] + m_e/m_i}, \tag{2.7}$$

where m_e/m_i is the electron-to-ion mass ratio. We note that

$$\omega_{pi}^2/\omega_{ci}^2 \propto n_{i0}/B_0^2, \tag{2.8}$$

and that, depending on the values of the equilibrium ion density, n_{i0}, and B_0, ω_{pi}/ω_{ci} can span a wide range of values. From Eq. (2.7), it is seen that the lower and upper limiting values of $\omega_{\rm LH}/\omega_{ci}$ are $\sqrt{1/(1+m_e/m_i)}$ and $\sqrt{m_i/m_e}$, respectively.

In what follows, we solve the full dispersion relation, Eq. (2.4), numerically, without approximation, for a fixed value of ω_{pi}/ω_{ci}, but allowing κ_i to run through a sequence of values depicting various degrees of hardness of the ion tail, as compared to the Maxwellian distribution as the standard benchmark. The dispersion curves are presented as plots of ω/ω_{ci} against $\lambda_i = k^2 v_{ti}^2/\omega_{ci}^2$. It is noted that the independent variable is thus the square of the wavenumber, k, normalised to the square of a fixed Larmor radius for a "typical" thermal ion.

2.4.1 General features

Before discussing individual figures, we make the general observation that in all our calculations, the numerically-determined frequency is found to be real, just as it is for the Maxwellian distribution, i.e., the presence of excess superthermal particles in the ion tail of the kappa distribution does not drive the ion Bernstein waves unstable. This is not unexpected, as the kappa distribution is monotonically decreasing in $v_\perp$, i.e., $\partial f/\partial v_\perp < 0$ for all v, and thus the waves should be stable in such a plasma (e.g. Harris (1953); Hall et al. (1965)).

To illustrate typical ion Bernstein wave behaviour we choose, in Fig. 2.1, parameter values such that $\omega_{pi}/\omega_{ci} = 6.5$, giving a lower hybrid frequency

$\omega_{\rm LH} = 6.5\omega_{ci}$. Although the ion Bernstein waves comprise a potentially infinite sequence of harmonics, we illustrate only those dispersion curves extending up to the first two frequency bands above $\omega_{\rm LH}$ for reasons of clarity.

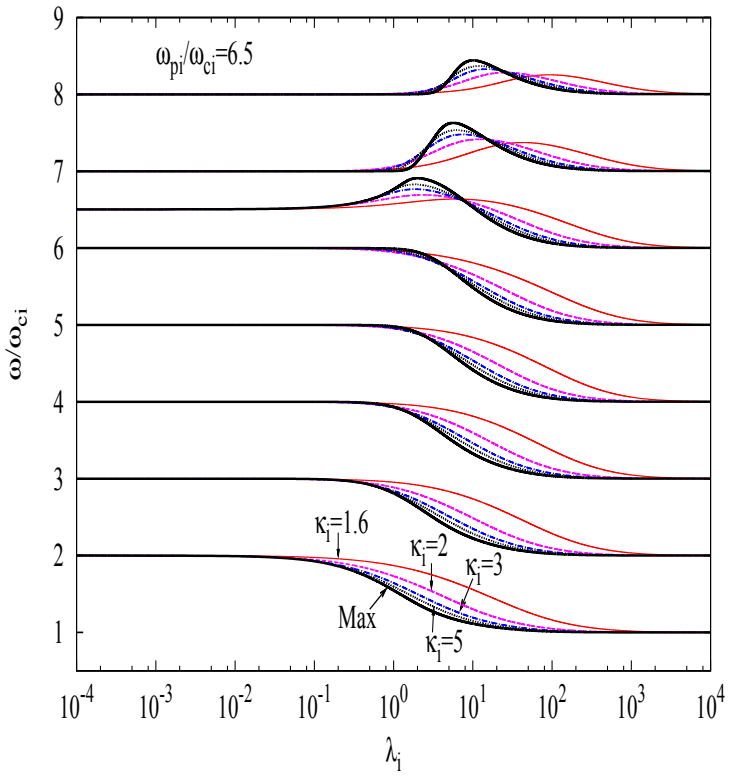

Figure 2.1: Dispersion curves of ion Bernstein waves in a plasma with a kappa velocity distribution presented as plots of ω/ω_{ci} against $\lambda_i = k^2 v_{ti}^2/\omega_{c_i}^2$, for $\omega_{pi}/\omega_{ci} = 6.5$. The lower hybrid frequency is at $6.5\omega_{ci}$. The Maxwellian curve is represented by the thick solid line, while the thin solid line denotes $\kappa_i = 1.6$, dashes indicate $\kappa_i = 2$, dot-dashes represent $\kappa_i = 3$, dots show $\kappa_i = 5$.

It is well-known that for Bernstein waves in a Maxwellian plasma, the dispersion curves below $\omega_{\rm LH}$ fall off from a value of $(n+1)\omega_{ci}$ for $\lambda_i \simeq 0$ to $n\omega_{ci}$ as $\lambda_i \to \infty$, where we recall that $\lambda_i \propto k^2$. This behaviour is unchanged for lower kappa values. The frequencies thus span the full range between harmonics. On the other hand, above the lower hybrid band the wave frequencies rise from a value $n\omega_{ci}$ for long wavelength to a peak, $\omega_{\rm peak}$, at a value of λ_i associated with a wavenumber, $k_{\rm peak}$, which is of order $kR_{Li} \sim 1$, and then fall back to the original cyclotron harmonic as $\lambda_i \to \infty$. In contrast to their counterparts below $\omega_{\rm LH}$, these waves all have frequencies that lie between successive cyclotron harmonics and do not span the full intra-harmonic range. As the frequency approaches its peak value, the group velocity, $d\omega/dk$, of the wave approaches zero. The electrostatic lower hybrid mode occurs at $\omega_{\rm LH}$ for vanishing and small wavenumber, but for $kR_{Li} \sim 1$ it rises, has a flat maximum below the next cyclotron harmonic, then drops, and finally tends to the harmonic below $\omega_{\rm LH}$ for short wavelengths.

Figure 2.1 shows that, in principle, all the dispersion curves have shapes that are similar to those found for the Maxwellian. However, there are very significant differences in detail between the Maxwellian curves and those for lower κ_i, particularly for the extreme values $\kappa_i = 1.6$ and 2, with quasi-Maxwellian behaviour being observed for $\kappa_i \geq 5$. Considering first the harmonics below $\omega_{\rm LH}$, the most notable feature is that, for lower κ_i, the fall-off from the upper to the lower cyclotron harmonic is displaced to considerably higher values of λ_i, i.e., to shorter wavelength. Whereas for the Maxwellian curve the steepest slope (largest $|d\omega/d(k^2)|$) occurs for $\lambda_i \sim 1$, the corresponding point is shifted to $\lambda_i \sim 10$ for $\kappa_i = 1.6$. In the lowest four frequency bands, it appears that at fixed λ_i, the frequency increases with decreasing κ_i for all λ_i.

However, in the band immediately below the LH band, the curves show clearly that, while at higher λ_i harder ion tails lead to an increase in frequency, the situation is reversed for lower values of wavenumber, where the curves show a decrease in frequency with decreasing κ_i. This difference in dependence of ω on κ_i in different ranges of wavenumber is even more clearly exhibited in the lower hybrid curves, as well as in the upper curves where $n\omega_{ci} > \omega_{\rm LH}$.

In Fig. 2.2, this behaviour is explored further. Here we have plotted, against λ_i, the difference between the frequency for a given value of κ_i and that found for the Maxwellian, $\Delta\omega = \omega_\kappa - \omega_M$. The three panels represent examples of frequencies that lie below, within and above the lower hybrid frequency band. From the shapes of the graphs, it is clear that increased excess superthermal ions have differing effects in the three cases. It is noted that, in general, the wavenumber at which $\Delta\omega$ changes sign varies with κ_i, but typically lies in the range $1 \lesssim \lambda_i \lesssim 20$.

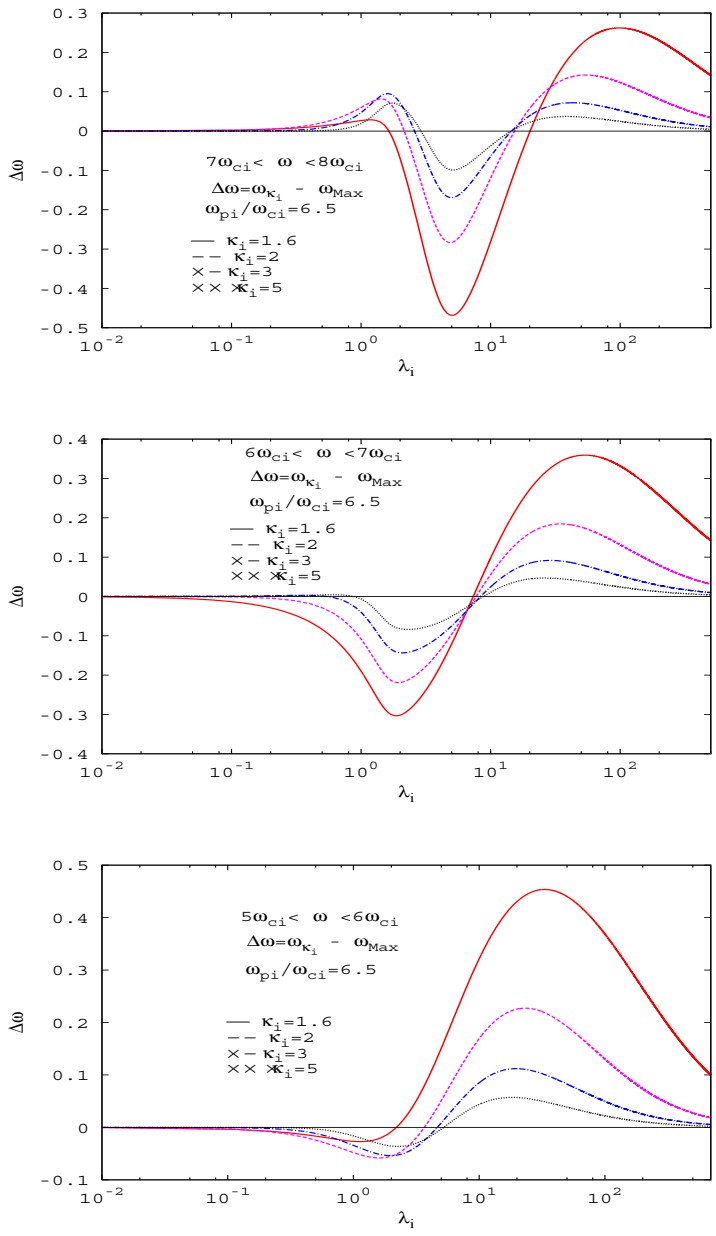

Figure 2.2: Differences between the frequency for a given value of κ_i and that for the Maxwellian plotted against λ_i. The three modes are (a) that below the lower hybrid frequency band (lower panel), (b) in the LH band (middle panel), and (c) in the band above the LH frequency (upper panel). Line types, for a given value of κ_i, and the expression for λ_i are as in Fig. 2.1.

We have previously alluded to an important characteristic of the waves that lie within and above the lower hybrid band, namely, that their dispersion curves exhibit a local maximum in frequency. In the case of electron Bernstein waves, the frequency maxima at which the group velocity vanishes are associated with the so-called Q_n resonances observed in magnetospheric sounding experiments (e.g. Viñas et al. (2005)). Viñas et al. (2005) have shown how the interpretation of these Q_n resonances in terms of electron Bernstein waves depends significantly on the underlying electron kinetic model. In particular, by analysing a variety of resonances observed by IMAGE, they were able to show, using both kappa and Maxwellian models for the electron Bernstein waves, that the electron velocity distribution of the inner magnetosphere was more consistent with a kappa distribution than with a Maxwellian. Viñas et al. (2005) proposed using the analysis of such resonances in terms of a general kappa-based wave model for Bernstein waves (with a priori unknown value of κ) as a useful reverse diagnostic to determine the kappa index for the electrons, and hence their type of velocity distribution. A similar concept had been applied by Hellberg et al. (2000). Very recently, Benson et al. (2013) extended the approach of Viñas et al. (2005), setting up a general tool to use the Q_n resonances of electron Bernstein waves as a diagnostic for the electron kappa values in space. Given the potential value of this kind of analysis, as explained by Viñas et al. (2005) and Benson et al. (2013), we now discuss the analogous situation for the ion Bernstein waves.

As κ_i is allowed to decrease from the Maxwellian case, two features related to these local peaks stand out: the "height" of the peak, ω_{peak}, is reduced and its wavenumber "position", $\lambda_{i,\text{peak}}$, is moved to higher values, that is, the peak wavenumber is shifted to higher values as the excess superthermal ion component is increased. This is illustrated in a more explicit manner in Fig. 2.3, for curves immediately above the lower hybrid frequency band. Whereas ω_{peak} increases continuously over the range of κ_i up to 5, the wavelength at which the frequency peak appears is strongly affected for $\kappa_i < 2.5$, but then exhibits a slow increase (decrease in λ_i) for increasing κ_i.

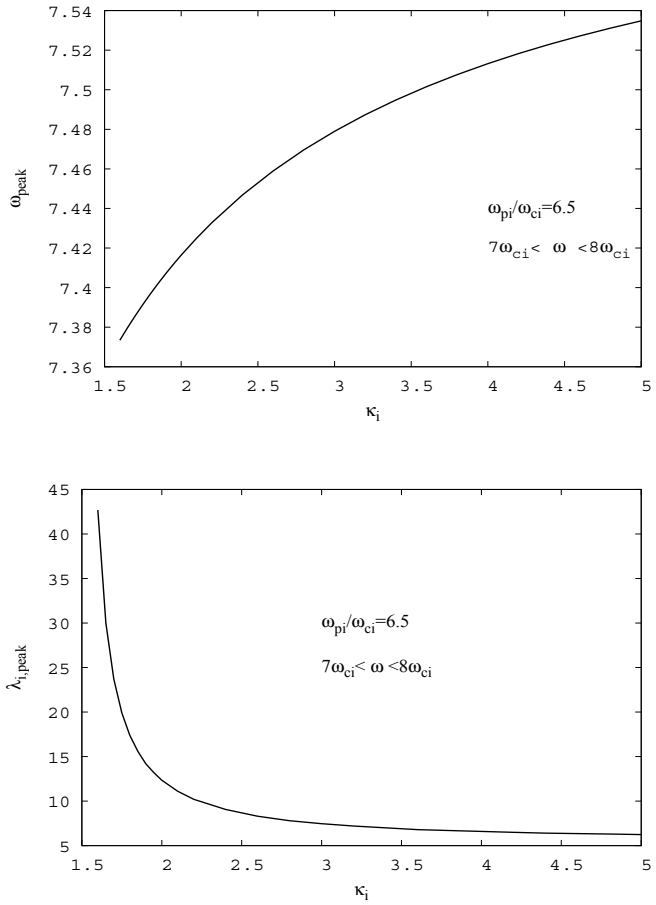

Figure 2.3: Peak frequencies, $\omega_{\rm peak}$ (upper panel), and the corresponding normalised wavenumber parameters, $\lambda_{i,\rm peak}$ (lower panel), plotted as functions of κ_i, for the mode immediately above the LH band.

Finally, it is observed that in the LH band, the dispersion curves exhibit a κ_i dependence with intermediate features between those of the curves below and above it.

One may wish to seek a simple explanation for the observed "shift" of the dispersion curves to higher wavenumber values as the ion tail is hardened through the choice of lower values of κ_i. The overall physics of Bernstein waves is affected by a number of characteristics. These include, for instance, scale lengths such as the Debye length, as the mode is inherently electrostatic and relies on local space charge effects, and the Larmor radius, as the magnetic field forces play a fundamental role. Both these length scales

appear in the dispersion relation, Eq. (2.1).

We have noted that in our figures we have chosen as the abscissa the variable $\lambda_i = k^2 R_{Li}^2$, where R_{Li} is the Larmor radius of a "typical" ion whose speed is given by the usual thermal speed, v_{ti}. However, it is well-known (e.g. Vasyliunas (1968); Summers & Thorne (1991); Hellberg et al. (2009)) that for a kappa distribution, the characteristic, most probable speed is given by $\theta = v_{ti}[(\kappa_i - 3/2)/\kappa_i]^{1/2}$. It may thus seem to be preferable to replace the standard expression for the Larmor radius by that of a typical particle in a kappa plasma, viz., $R_{Li} = (m_i v_{ti}/eB)[(\kappa_i - 3/2)/\kappa_i]^{1/2}$. That leads to a definition of an alternative independent variable that takes some account of the change in scale length when κ_i is varied, $\lambda_i' = \lambda_i(\kappa_i - 3/2)/\kappa_i$. Indeed, the arguments of the generalised hypergeometric function in Eq. (2.4) would appear to suggest such a replacement as natural.

If the sole effect of varying the ion spectral index were the change in the scale length of the magnetic force as discussed above, then simply re-plotting the curves relative to the corrected $\lambda_i^{'}$ should result in the curves for different κ_i values being shifted to lower wavenumbers, so that they are all superimposed on the Maxwellian curve. In fact the results are not that simple, as shown in Fig. 2.4. What we find is that the re-scaling leads to a significant shift of the curves with low κ_i to smaller wavenumbers, so that they actually overshoot the Maxwellian curve. Hence, for instance, the lower frequency curves reveal a reversed order with respect to wavenumber as κ_i is increased, as compared to what was observed in the original figure. However, it is noteworthy that the spread in wavenumber, at fixed ω, found over the range of κ_i from 1.6 to ∞ is reduced from that found in Fig. 2.1. Thus, we may conclude from Fig. 2.4 that the effect on the plotted dispersion curves of different values of κ_i is in part explained by the choice of independent variable (that is, of what is meant by a "typical" ion), but that the full story is a lot more complicated, as may be seen from the different mathematical structures in which κ_i appears in Eq. (2.4).

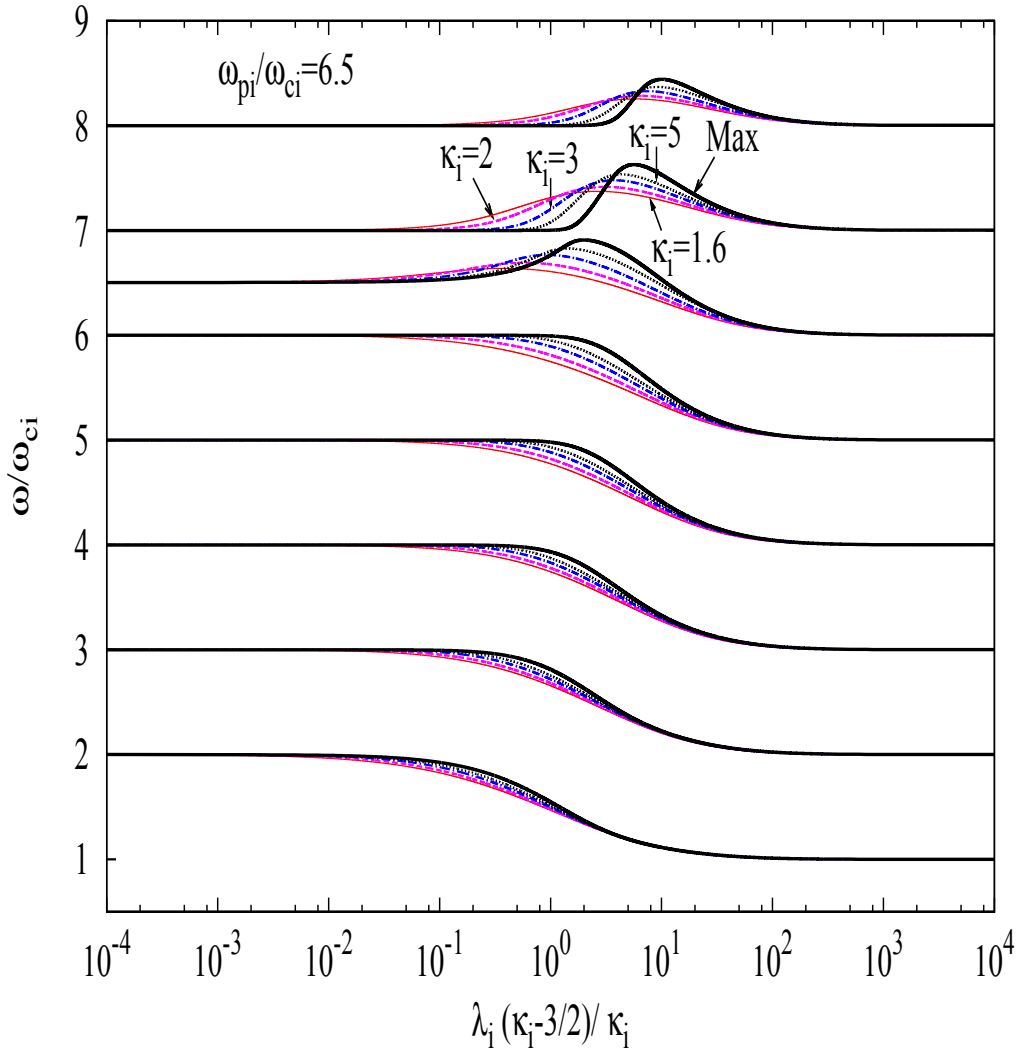

Figure 2.4: Dispersion curves of ion Bernstein waves in a plasma with a kappa velocity distribution for $\omega_{pi}/\omega_{ci} = 6.5$, showing the effect of rescaling the abscissa with $(\kappa_i - 3/2)/\kappa_i$. The expression for λ_i and line styles are as in Fig. 2.1.

A final comment on the behaviour of the wave frequencies for $\omega \geq \omega_{\rm LH}$ is appropriate. We have noted that in these frequency bands the curves span only a part of the space between the asymptotes, $n\omega_{ci}$ and $(n+1)\omega_{ci}$. In fact, for fixed n, the frequency range spanned by the waves is found to decrease with increasing excess of superthermal particles, i.e., decreasing value of κ_i. Although not shown in this figure, we find that the range spanned for fixed κ_i decreases with increasing n, while for sufficiently large values of n, the wave frequency asymptotically approaches $n\omega_{ci}$ over the whole range of the wavenumber, irrespective of the value of κ_i.

Having studied in some detail the dispersion curves and their dependence on κ_i for a standard value of $\omega_{\rm LH}/\omega_{ci}$, we turn next to a study of these curves as ω_{pi}/ω_{ci}, and hence $\omega_{\rm LH}/\omega_{ci}$, is varied. We consider first an increase to $\omega_{pi}/\omega_{ci} = 13$.

The dispersion curves for $\omega_{pi}/\omega_{ci} = 13$, corresponding to a lower hybrid frequency of $12.47\omega_{ci}$, are shown in Fig. 2.5. We show only a few curves below and above the LH band for reasons of clarity; the general trend of the curves in other frequency bands is as shown in Fig. 2.1. On comparison with the latter figure, it is observed that as ω_{pi}/ω_{ci} is increased from 6.5 to 13, for a fixed value of κ_i, the curves are shifted towards higher wavenumbers, relative to that case, and there is an increase in the frequency range spanned by the waves propagating in the LH band and the bands above it.

Perhaps more noteworthy in Fig. 2.5 is the tendency, seen explicitly in the vicinity of $\omega = 13\omega_{ci}$ with a hint of it near $14\omega_{ci}$, for ion Bernstein modes propagating in a Maxwellian plasma in adjacent harmonic bands to couple as ω_{pi}/ω_{ci} increases. This coupling, reported earlier by Fredricks (1968a), diminishes as the excess of superthermal ions is increased and is practically absent for $\kappa_i \leq 5$.

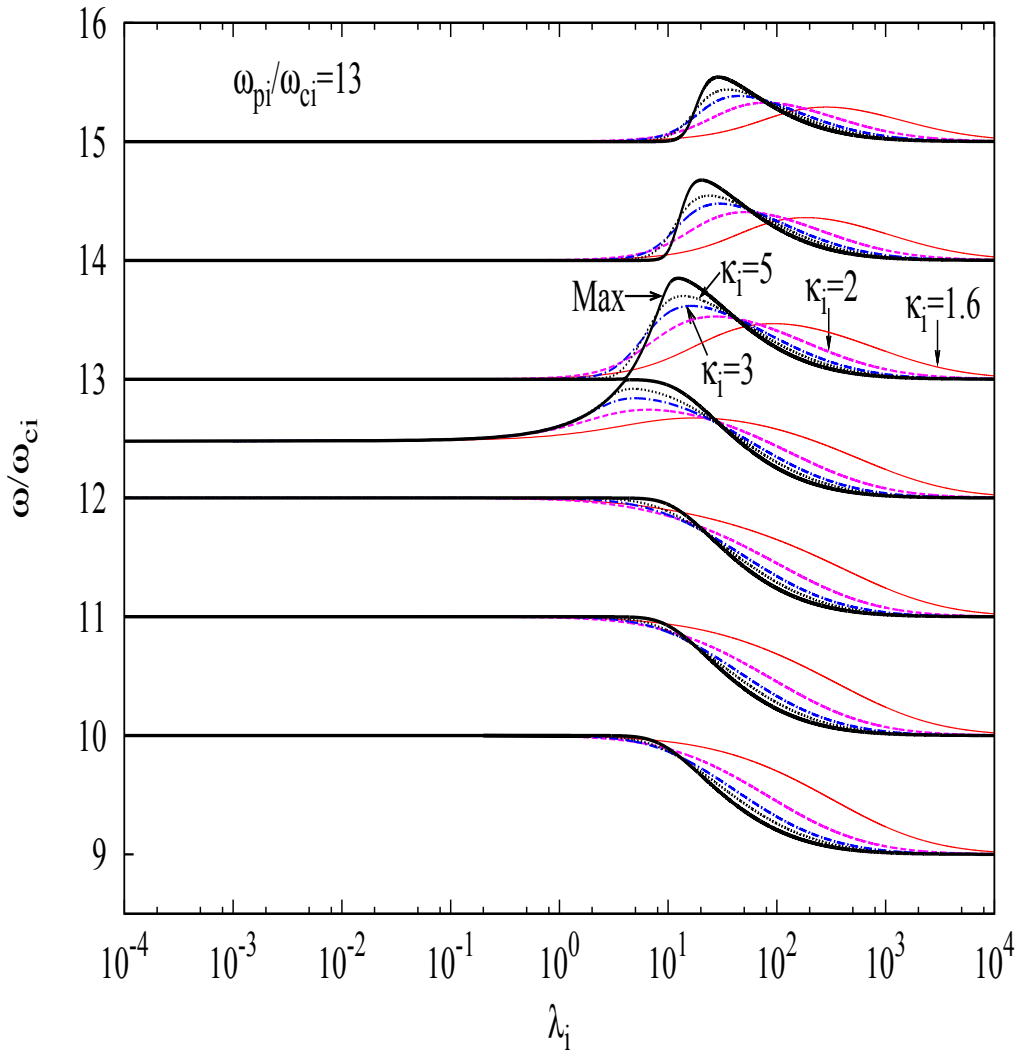

Figure 2.5: Dispersion curves of ion Bernstein waves in a plasma with a kappa velocity distribution for $\omega_{pi}/\omega_{ci} = 13$. The lower hybrid frequency is at $12.47\omega_{ci}$. The expression for λ_i and line styles are as in Fig. 2.1.

Figure 2.6 illustrates the dispersion curves for $\omega_{pi}/\omega_{ci} = 26$, for which $\omega_{\rm LH} = 22.24\omega_{ci}$. As ω_{pi}/ω_{ci} is increased from 13 to 26, the effects on the curves discussed previously become even more pronounced. Importantly, it is seen that in the LH band, the curve for the Maxwellian case does not reflect a clear peak, but rather has a finite range of λ_i (and hence of wavenumber) over which the frequency lies very close to the next higher harmonic, $(n+1)\omega_{ci}$, before decreasing and approaching $n\omega_{ci}$ for large λ_i. In that range of k values, the calculations required very high precision (10^3 digits) and a very small step size (10^{-6}), otherwise the root finder would jump to the next curve associated with the next band, giving the appearance (erroneously) that the curve crosses the asymptote $(n+1)\omega_{ci}$.

Thus, for the Maxwellian case, there is strong coupling between the modes propagating in the LH band and the band above, so that, in practice, observers would see a continuous passband beyond $\omega_{\rm LH}$, virtually up to $(n+2)\omega_{ci}$, where, in this case, n denotes the harmonic immediately below $\omega_{\rm LH}$, in a way similar to that discussed by Fredricks (1968a). It is noteworthy that this coupling between contiguous modes is limited to the Maxwellian case and possibly to high values of κ_i, as, certainly for the significantly nonthermal range $\kappa_i \leq 5$, there is a clear frequency gap between the curve in the LH band and that in the band above.

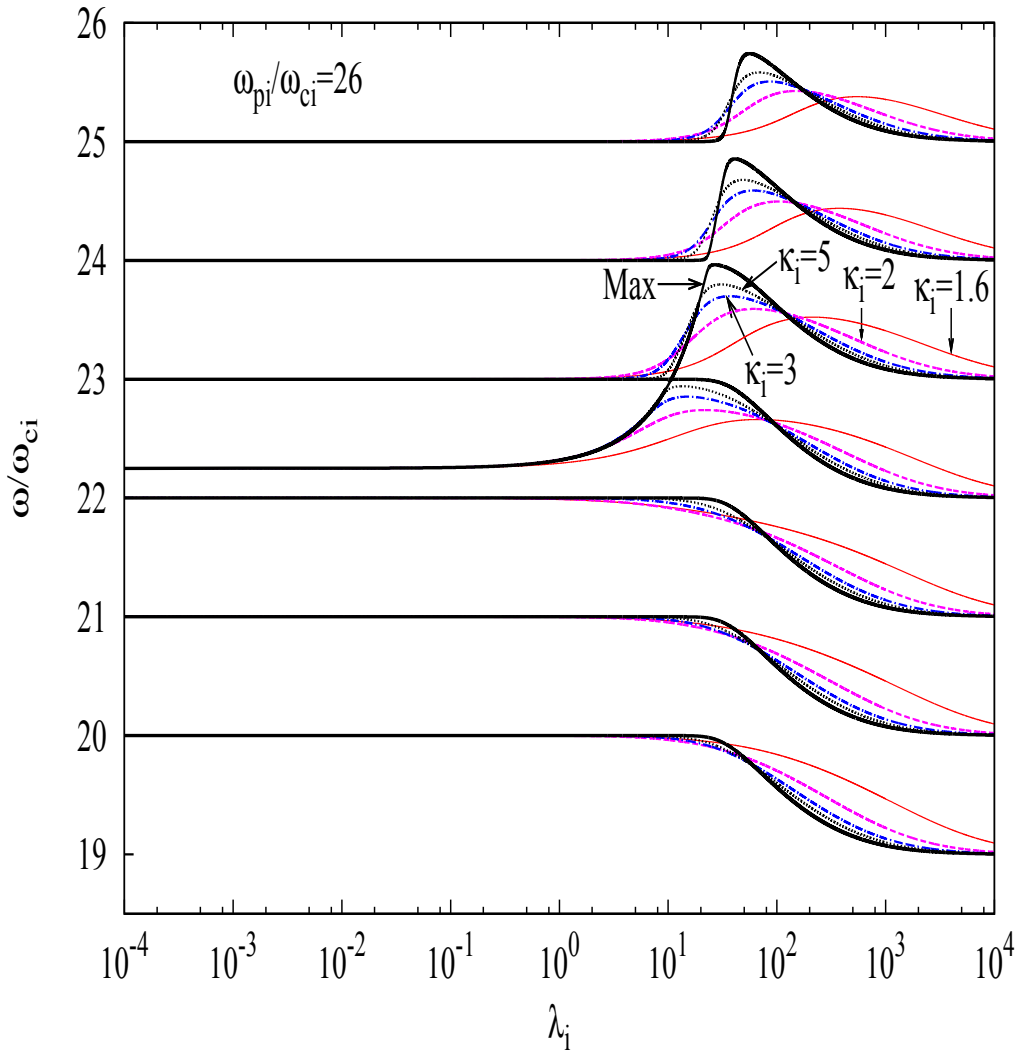

Figure 2.6: Dispersion curves of ion Bernstein waves in a plasma with a kappa velocity distribution for $\omega_{pi}/\omega_{ci} = 26$. The lower hybrid frequency is at $22.24\omega_{ci}$. The expression for λ_i and line styles are as in Fig. 2.1.

Finally, for completeness, we present a case in which $\omega_{\rm LH}$ is so low that there is only a single cyclotron harmonic curve below the lower hybrid frequency band. Figure 2.7 illustrates the results for ω_{pi}/ω_{ci}=2.5, for which $\omega_{\rm LH} = 2.69\omega_{ci}$. In this case, the effects of excess superthermal particles (low κ_i) are significant only for the lowest few harmonic curves, and may easily be understood on the basis of our earlier figures.

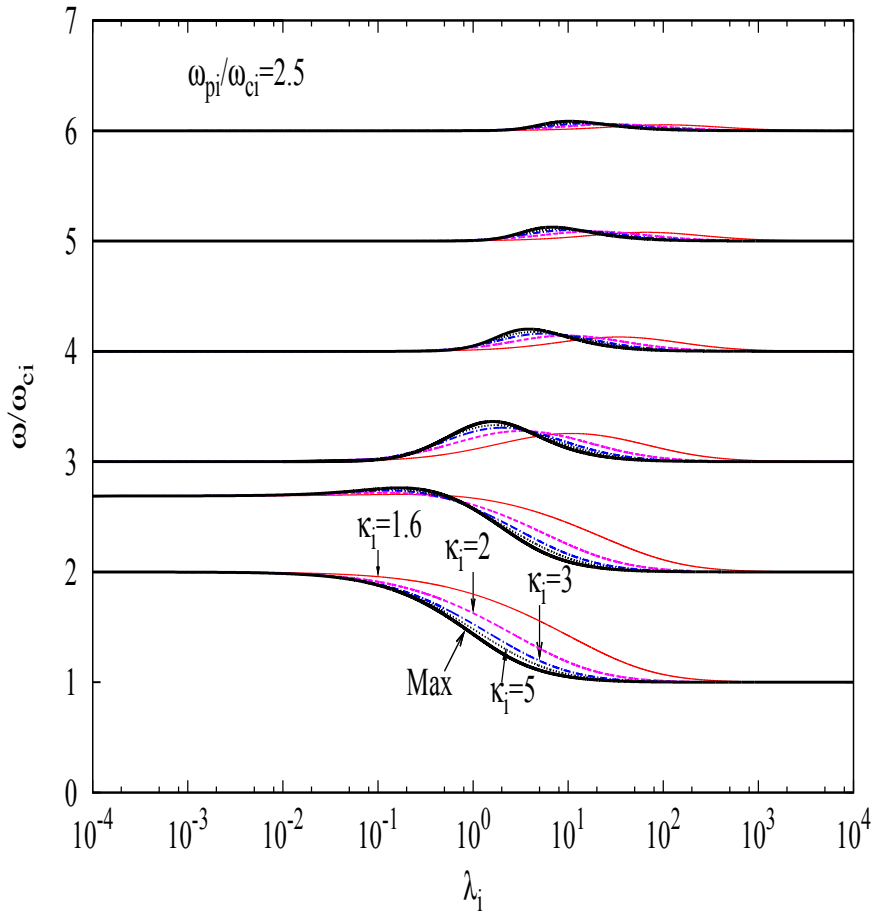

Figure 2.7: Dispersion curves of ion Bernstein waves in a plasma with a kappa velocity distribution for $\omega_{pi}/\omega_{ci} = 2.5$. The lower hybrid frequency is at $2.69\omega_{ci}$. The expression for λ_i and line styles are as in Fig. 2.1.

2.4.2 Application to the PSBL

The results presented above provide a broad overview, covering a large range of values of ω_{pi}/ω_{ci}. Motivated by observations in the PSBL of waves of the type discussed in Sec. I (e.g. Broughton et al. (2008)) and by the fact that the PSBL plasma may have some of the non-thermal features of the CPS, we shall now consider ion Bernstein waves for a value of ω_{pi}/ω_{ci} calculated from the values of n_{i0} and B_0 that have been observed in the PSBL. In Table 2.1 we present typical values of n_{i0} and B_0, together with the derived values of ω_{pi}/ω_{ci} and normalised $\omega_{\rm LH}$.

Table 2.1: Parameter values in the PSBL

$n_{i0} = 0.15$ cm^{-3} (e.g. Baumjohann et al. (1988); Engebretson et al. (2010))
B_0=32.8 nT (e.g. Denton et al. (2010))
ω_{pi}/ω_{ci}=162
ω_{LH}/ω_{ci}=41.4

Baumjohann et al. (1988) found a typical value of n_{i0}=0.1 cm^{-3}, while Engebretson et al. (2010) reported an average value of n_{i0}= 0.2 cm^{-3} ; in Table 2.1, we have used the average of the two. We note that the values of n_{i0} were obtained assuming that all ions were protons.

It is more instructive to know the order of magnitude of $\omega_{\rm pi}/\omega_{ci}$ and $\omega_{\rm LH}/\omega_{ci}$ for the regions neighbouring the PSBL, namely the CPS and the magnetotail lobe.

From data available in the literature (e.g. Eastman et al. (1984); Baumjohann et al. (1988, 1989)), the ion density in the CPS has a typical value of about 0.4 cm^{-3}, whereas a typical value of the ion density in the magnetotail lobe is about 0.01 cm^{-3} (e.g. Eastman et al. (1984); Mukai et al. (1994)), under the assumption that all the observed ions were protons. Indeed, it is well-known (e.g. Eastman et al. (1984)) that the plasma densities in the CPS are higher than those in the lobe regions, with intermediate densities in the PSBL. The magnetic field strength in the CPS is lower than that in the magnetotail lobe with, respectively, average values of $B_0 \approx$10 nT and $B_0 \approx$30 nT (Baumjohann & Treumann, 1997).

Assuming n_{i0}=0.4 cm^{-3} and B_0=10 nT, we find $\omega_{\rm pi}/\omega_{ci} = 869$ and $\omega_{\rm LH}/\omega_{ci} = 42.8$, for the CPS. For the magnetotail lobe, we find $\omega_{\rm pi}/\omega_{ci} = 46$ and $\omega_{\rm LH}/\omega_{ci} = 31$, on the assumption that n_{i0}=0.01 cm^{-3} and B_0=30 nT.

It is seen that in the PSBL and neighbouring environments, the ion plasma frequency has a large value. The resulting lower hybrid frequency has a value that is close to the upper limit given by $\sqrt{1836}\omega_{ci} \approx 42.85\omega_{ci}$, for an electron-proton plasma model, as discussed earlier in this section. This is consistent with $\omega_{\mathrm{LH}} \approx 43\omega_{ci}$, a value that has been observed in the outer plasmasphere by Russell et al. (1970).

The PSBL parameter values discussed above, with additional information from parameter values in the neighbouring environments, lead one to expect results that would be typical of those found for a high density, low magnetic field case, as illustrated in Fig. 2.6, but with an increase in the effects on wave propagation of the trend seen in Figs. 2.1, 2.5, 2.6. The dispersion curves for parameter values given in Table 2.1 are shown in Fig. 2.8. As expected, the curves are shifted towards even higher values of λ_i (i.e., wavenumber) than in Fig. 2.6.

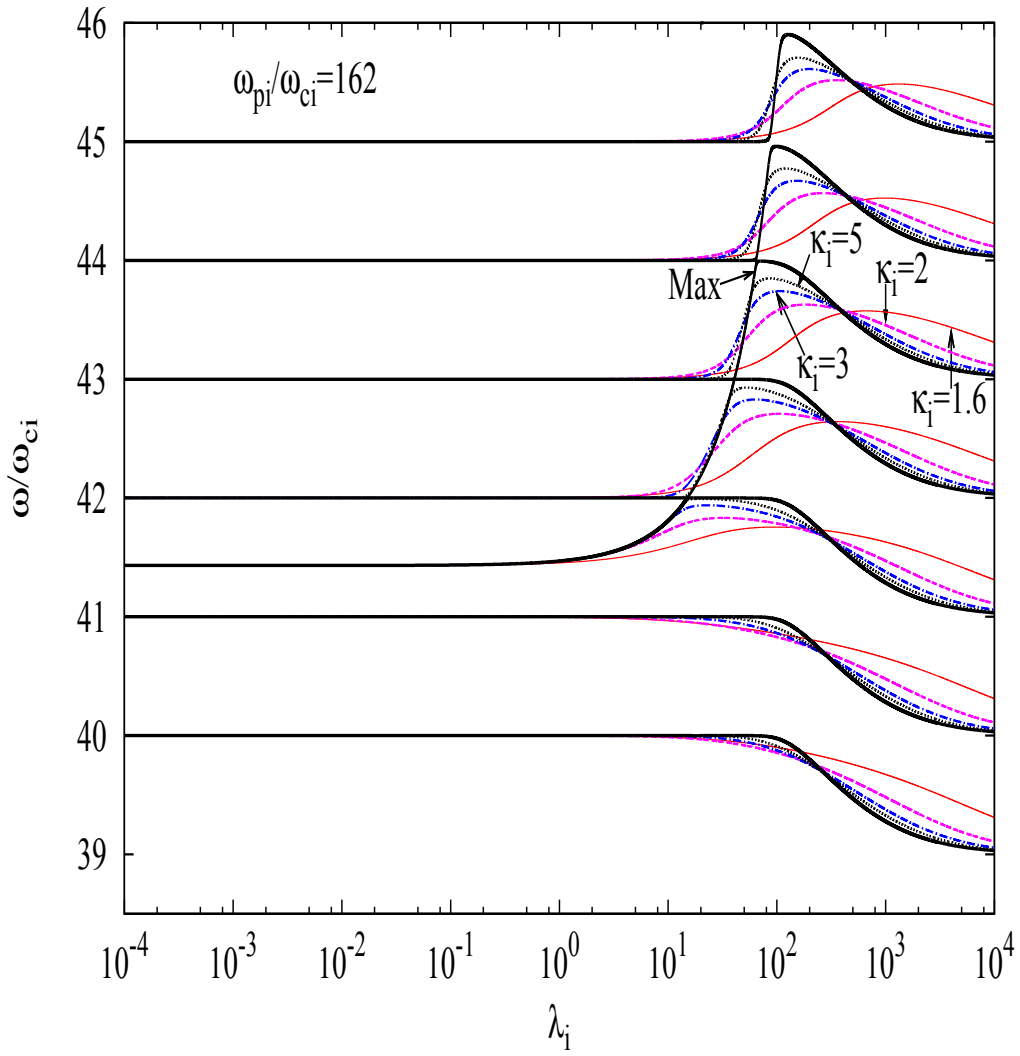

Figure 2.8: Dispersion curves of ion Bernstein waves in a plasma with a kappa velocity distribution for the PSBL ($\omega_{pi}/\omega_{ci} = 162$). The lower hybrid frequency is at $41.4\omega_{ci}$. The expression for λ_i and line styles are as in Fig. 2.1.

For the bands below $\omega_{\rm LH}$, the Maxwellian curves start dropping below $(n+1)\omega_{ci}$ at $\lambda_i \sim 10^2$, while for those above the LH band, maxima occur at around a similar normalised wavenumber (that is, $kR_{Li} \sim 10$). The low-κ_i curves are all shifted successively "to the right" (higher wavenumbers), and curves above the LH frequency peak at around $\lambda_i \sim 10^3$.

In the LH band and the next two bands above, the Maxwellian curves have broad flat maxima at $(n+1)\omega_{ci}$ for $\lambda_i \sim 10^2$, while low-κ_i curves have broad maxima well below $(n+1)\omega_{ci}$ around $\lambda_i \sim 10^3$. It is thus important to note that the propagation range does not span the entire intraharmonic space for low κ_i. In all frequency bands shown in Fig. 2.8, the curves, particulary for low κ_i, have not yet reached their asymptotic cyclotron harmonic values for $\lambda_i = 10^4$ (that is, $kR_{Li} = 10^2$), where the figure has been cut off.

Importantly, for the Maxwellian case the frequency behaviour in the LH band and the band above, observed in Fig. 2.6, now also extends to the next higher band. So, as a result of strong coupling between adjacent modes over a number of bands, the dispersion curve that begins at $\omega = \omega_{\rm LH}$ at vanishing λ_i appears to cross over the cyclotron harmonics. Thus, one sees that for a Maxwellian distribution, propagation is effectively possible over a continuous range of frequencies up to $\omega \simeq 45\omega_{ci}$. This effect of large ω_{pi}/ω_{ci} on the Maxwellian curves was reported earlier by Fredricks (1968a).

However, it is interesting to observe that, unlike the situation in Fig. 2.6, similar behaviour of the dispersion curves is now found for κ_i as low as 5, within the LH band. The curves for $\kappa_i \leq 3$ in the LH band, and for $\kappa_i \leq 5$ in the bands above do not exhibit this behaviour. That is, for plasmas that have a hard ion tail with a significant excess of superthermal ions, there are clear frequency gaps in which propagation does not occur, unlike the Maxwellian case.

It is worth noting that any larger value of ω_{pi}/ω_{ci} for such an electron-proton plasma model would have an effect on the dispersion curves similar to that illustrated in Fig. 2.8, since the resulting $\omega_{\rm LH}$ would be very close to the upper limit given by $\sqrt{1836} \approx 42.85\omega_{ci}$. However, it is likely that for such a case, the tendency for contiguous modes to couple, seen here in the lower hybrid band and its two neighbouring bands, would extend over even more upper bands, with the low-κ_i dispersion curves mimicking the behaviour of the Maxwellian curves in more bands.

The tendency for the ion Bernstein wave dispersion curves within and

above the lower hybrid band to couple in the Maxwellian case for large ω_{pi}/ω_{ci}, and those for low values of κ_i not to, provides a useful diagnostic for determining whether the ion velocity distribution possesses a power law tail. This applies particularly for values of ω_{pi}/ω_{ci} that are not too large. Thus, if observations of "banded" emissions in the PSBL indicate stopbands in the vicinity of the lower hybrid frequency and above it, this could be an indicator that the ions in this region of the magnetosphere have kappa velocity distributions with low values of κ_i.

Conversely, an apparently continuous lower hybrid mode would indicate ions having a velocity distribution more consistent with the Maxwellian. It should, however, be noted that this latter indicator is less strong, as its applicability would depend on the value of the key parameter, ω_{pi}/ω_{ci}.

The suggested indicator for the presence of excess superthermal ions is potentially important because, whereas the ion velocity distributions in the CPS have been shown to be consistent with the kappa distribution (e.g. Christon et al. (1988, 1989)), less appears to be known about their precise form in the PSBL.

2.5 Chapter summary and conclusions

In this chapter, we have investigated numerically the dispersion relation of ion Bernstein waves, using a Vlasov-Poisson model with ions and electrons that have a kappa velocity distribution. We recall that $\kappa \to \infty$ yields the Maxwellian distribution, while low κ implies a hard ion tail, that is, an excess of superthermal particles relative to the case of a Maxwellian distribution. In every case, the numerically-determined wave frequencies were real, that is, the nonthermal kappa distribution does not lead to unstable ion Bernstein waves. This is expected, as the kappa distribution satisfies $\partial f/\partial v_\perp < 0$ for all $v_\perp$, i.e., it is monotonic (e.g. Harris (1953); Hall et al. (1965)).

Having found that varying the electron spectral index, κ_e, and the temperature ratio, T_i/T_e, showed little effect on the dispersion curves, we have concentrated on the effects of the ion spectral index, κ_i, and the ratio that measures the relative strengths of the ion density and the magnetic field, ω_{pi}/ω_{ci}.

The dispersion curves are reminiscent of those found for electron Bernstein waves (e.g. Mace (2003, 2004)). Although for all κ_i they are, in prin-

ciple, similar to those found for a Maxwellian distribution, they are shifted to larger values of $\lambda_i = k^2 R_{Li}^2$ (higher wavenumber) for lower κ_i and for increasing ω_{pi}/ω_{ci}. This observation applies to all frequency bands.

In and above the LH band, the wave frequency in each band goes through a global maximum. In the case of the related electron Bernstein waves, the analogous maxima are believed to be responsible for the Q_n resonances observed in magnetospheric sounding experiments (e.g. Viñas et al. (2005)). It is found that, for decreasing values of κ_i and fixed harmonic number, n, the peak frequency, $\omega_{\rm peak}$, decreases, while the wavenumber at which the peak occurs, $k_{\rm peak}$, increases.

It is well-known for Bernstein waves in a Maxwellian plasma that, in these upper bands, the frequency spans only a part of the intraharmonic space, the range decreasing with increasing n. For ω_{pi}/ω_{ci} sufficiently large, the Maxwellian mode propagating in the LH band and in a few bands directly above it has a frequency which extends over the whole intraharmonic space, demonstrating coupling between adjacent modes. The maximum frequency is not a well-defined peak value, but rather a broad maximum that covers a finite range of λ_i, and whose value is indiscernible from the next cyclotron harmonic. It follows that, in practice, for large ω_{pi}/ω_{ci} ion Bernstein mode propagation is possible in a Maxwellian plasma over a continuous range of frequencies above ω_{LH}, covering one or more harmonic bands, the number of such bands increasing with ω_{pi}/ω_{ci}. Some of these results were reported earlier by Fredricks (1968a).

However, it is important to note that there is a significant difference between the curves obtained at small values of κ_i ($\kappa_i \leq 5$) and those for the Maxwellian. For low κ_i, the resonance peaks in the LH band and above are lower and do not coincide with the next cyclotron harmonic. Hence, unlike the Maxwellian case, propagation in a low-κ_i plasma at high ω_{pi}/ω_{ci} does not occur over a continuous range of frequencies, but instead the propagation band is separated into bands, with stopbands interspersed at the cyclotron harmonics. As ω_{pi}/ω_{ci} is increased, the intraharmonic range in frequency within each successive band increases, for fixed κ_i. Hence, these gaps in propagation (stopbands) then decrease in width.

By analogy with the work of Viñas et al. (2005) and Benson et al. (2013) for electron Bernstein waves, we have suggested that the strongly κ_i-dependent dispersion curves for ion Bernstein waves, especially in the

vicinity of the lower hybrid frequency and neighbouring bands, be used as a diagnostic for the presence of enhanced levels of superthermal ions.

As an application, we have considered ion Bernstein waves in a kappa-distributed plasma in the PSBL for which $\omega_{\rm LH} = 41.4\omega_{ci}$. An interesting point is that, for these very high values of ω_{pi}/ω_{ci}, the reduced coupling between adjacent modes is found only for $\kappa_i \leq 3$, as the behaviour at $\kappa_i = 5$ is very similar to that for the Maxwellian.

In order to have a broader picture of the order of magnitude of the lower hybrid frequency in the regions neighbouring the PSBL, we have considered parameter values from the CPS and magnetotail lobe and found $\omega_{\rm LH} = 42.8\omega_{ci}$ and $\omega_{\rm LH} = 31\omega_{ci}$, respectively. It is seen that in the PSBL and neighbouring environments, the lower hybrid frequency has a large value that is close to the upper limit (i.e. $\sqrt{1836} \approx 42.85\omega_{ci}$), for an electron-proton plasma model. This is consistent with $\omega_{\rm LH} \approx 43\omega_{ci}$, a value that has been observed in the outer plasmasphere by Russell et al. (1970).

The results presented in this chapter could be useful for the interpretation of observations of waves propagating perpendicularly to the ambient magnetic field at frequencies between harmonics of the ion cyclotron frequency, which are commonly observed in space environments, as discussed in Sec. 2.1.

Chapter 3

Linear and nonlinear ion acoustic waves in a plasma with two positive ion species and Boltzmann electrons

3.1 Introduction

A plasma composed of two positive ion species and Boltzmann electrons has been theoretically studied in the past (e.g. Tran & Hirt (1974); Tran (1974); Bhattacharyya & Roychoudhury (1988); Verheest et al. (2008, 2011)), and it has been found that if the temperature of one or both of the ion species is finite, two modes with different phase speeds propagate in such a plasma configuration.

Tran & Hirt (1974) studied a plasma made up of two cold ion species and Boltzmann electrons. They derived the linear dispersion relation and the KdV equation whose soliton solution was obtained. Their results show that only one mode propagates in such a plasma.

Tran (1974) generalised the work of Tran & Hirt (1974) by allowing the temperature of both ion species to be finite. The author derived the linear dispersion relation and clearly demonstrated that, as a result of a finite ion temperature, two modes with different phase speeds propagate. The phase speed of the slow mode lies between the thermal speeds of the two ion species, whereas that of the fast mode lies between the thermal speeds of

the light ions and the electrons. We note that, in the work of Tran (1974), the temperatures of the two ion species were assumed to be equal.

Tran (1974) also derived the KdV equation for the plasma model that he considered and obtained its soliton solution. He also investigated numerically the effects of the ion temperature on the amplitudes and widths of KdV solitons, for both the slow and the fast modes. The author presented the results as plots of normalised amplitudes/widths against normalised densities of the light ions for various values of the heavy-to-light ion mass ratio, for both the slow and the fast modes (see his Figs. $1-4$). As is well known (e.g. Mace et al. (1991)), and as shown by Tran (1974), the amplitude of a KdV soliton explicitly depends on the soliton speed. However, regarding the numerical work of Tran (1974), i.e. his Figs. $1-4$, it is not clear how the values of the soliton speed were chosen. Thus, we need no further discussion of his numerical results.

Using the Sagdeev potential approach, Bhattacharyya & Roychoudhury (1988) investigated the effects of the ion temperature on arbitrary amplitude ion acoustic solitons in an unmagnetised plasma composed of two positive ion species and Boltzmann electrons. The authors, first, assumed the temperatures of the two ion species to be finite, and different, and normalised them with respect to the electron temperature. Having obtained the expression for the Sagdeev potential in dimensionless form, further discussion of solitons was carried out assuming that the two ion temperatures are equal, for simplicity.

One point that we have noted from the work of Bhattacharyya & Roychoudhury (1988) is that they never mentioned the existence of two modes in an adiabatic-two-ion plasma that they considered. They appear to have studied the fast mode only. The main result of their investigation is that a finite ion temperature modifies the range in the allowed soliton Mach numbers.

Verheest et al. (2008) considered a plasma composed of cold and adiabatic dust, as well as Boltzmann electrons and ions, to study nonlinear acoustic waves of large amplitude, using the Sagdeev potential approach. The authors demonstrated that such a plasma supports the propagation of two modes with different phase speeds, but specialised their study to the slow mode. In their analysis, the authors found that their expression of the Sagdeev potential does not explicitly contain the density of the Boltzmann

ions, and thus suggested that their discussion would also apply to a three-component plasma composed of Boltzmann electrons, cold and adiabatic dust species, where at least one dust species must be positively charged.

To study solitary waves, Verheest et al. (2008) first considered a model involving negative cold and positive warm dust and later turned to a model in which both dust species are negatively charged. In the latter case, the authors reported soliton existence domains in which solitons are limited by, successively, the infinite cold dust compression, the occurrence of the warm dust sonic point, and the occurrence of double layers which, for smaller Mach numbers, have the same polarity (sign) as the dust, but switch to the opposite polarity at the high Mach number end. In the case where both dust species are positively charged, the authors mentioned that the polarity of solitons and double layers changes, but the soliton existence domains remain the same. Furthermore, since their analysis did not use an assumption that the dust is much more massive than the ions, it was suggested that one or both dust species could be replaced by positive and/or negative ions and the conclusions would still apply to that plasma model.

During their analysis, Verheest et al. (2008) normalised various quantities with respect to the characteristics of the adiabatic dust. The temperatures of the electrons and ions were assumed to be very high in comparison with that of the adiabatic dust so that $\tau_e = T_a/T_e \to 0$ and $\tau_i = T_a/T_i \to 0$ where T_e, T_i, and T_a are the temperatures of the electrons, ions, and adiabatic dust, respectively.

Considering a plasma made up of cold and adiabatic positive ion species and Boltzmann electrons, Verheest et al. (2011) pointed out that, as a result of a finite ion temperature, such a plasma supports the propagation of two modes with different phase speeds. They normalised various quantities with respect to the characteristics of the adiabatic ion species, except the densities which they normalised with respect to the undisturbed electron density. The authors expressed the electron temperature (T_e) through the ratio $\tau = T_a/T_e$, where T_a is the temperature of the adiabatic ions.

Specialising their study to the slow mode only and considering various values of the electron temperature, Verheest et al. (2011) reported, among others, a systematic determination of the soliton existence domain for which the upper limit in Mach number results, successively, from the occurrence of infinite cold ion compression, adiabatic ion sonic point, positive double

layers, negative double layers and, sometimes, depending on the choice of parameter values, positive double layers again.

That a two-ion plasma with finite temperature of one or both ion species supports the propagation of two modes has been confirmed not only in the case of Boltzmann electrons, as discussed above, but also in the case where the electron inertia is retained (e.g. Fried et al. (1971); Gledhill & Hellberg (1986); Verheest et al. (2007)).

Using a kinetic-theoretical approach and assuming the Maxwellian distributions as the equilibrium velocity distribution functions, Fried et al. (1971) considered a plasma consisting of electrons and two ion species and derived the dispersion relation of ion acoustic waves, retaining the inertia and the thermal effects of all species. Considering an argon-helium plasma to carry out the numerical work, they showed that such a plasma supports the propagation of two modes with different phase speeds. A similar conclusion was reached by Gledhill & Hellberg (1986), also using kinetic theory.

Verheest et al. (2007) discussed the necessary conditions for the generation of acoustic solitary waves in multi-species plasmas. Retaining the inertia and the thermal effects of all species and using the fluid dynamic approach (McKenzie, 2002a), they demonstrated that in a three-component plasma there are two acoustic existence ranges for solitary waves, one for the slow mode and another for the fast mode. They then specialised their study to the cases in which one or more ion species are hotter than some or all of the electron species, including the case of a two-ion plasma.

A two-ion plasma with finite ion temperature has also been investigated experimentally (e.g. Tran & Coquerand (1976); Nakamura et al. (1976)). Considering a helium-argon plasma, with finite and equal temperatures, Tran & Coquerand (1976) carried out an experimental investigation of linear ion acoustic waves and reported the existence of two acoustic modes in such a plasma, supporting the earlier theoretical results of Tran (1974). A similar experiment, together with modelling based on a two-ion plasma, was carried out by Nakamura et al. (1976).

In this work, we will refer to the two ion species as the "cooler" and the "hotter" ions. Following Verheest et al. (2007), the words "cooler" and "hotter" do not directly refer to the temperatures, but they are expressed in terms of the thermal speeds.

3.2 Motivation, aims, and methodology

Motivated by the work of Tran (1974) and Bhattacharyya & Roychoudhury (1988), with further information from the work of Verheest et al. (2008, 2011), we have noted that the effects of the ion and electron temperatures on linear and nonlinear ion acoustic waves in a plasma composed of two positive ion species and Boltzmann electrons are poorly understood. Thus, we revisit this plasma model to carry out a comprehensive investigation of the effects of the ion and electron temperatures on linear and nonlinear ion acoustic waves, considering both the slow and fast modes.

Both Tran (1974) and Bhattacharyya & Roychoudhury (1988) assumed that the temperatures of the two ion species are equal and the normalisation was with respect to the electron temperature. This is fine as long as one is interested in the effects of the ion temperature only. However, for the plasma model under consideration, it is possible to use a normalisation that can allow the investigation of the effects of both the ion and electron temperatures on the wave propagation characteristics, as in Verheest et al. (2008, 2011).

In this work, dimensionless quantities will be introduced following Verheest et al. (2008), allowing a comparison of our results, for the slow mode, with theirs when the thermal effects of the cooler ions are ignored. This means that the normalisation of various quantities will be with respect to the characteristics of the hotter ions, and then one can carry out a survey of various parameters characterising the cooler ions and the electrons. Throughout this chapter, the thermal effects of the cooler ions, expressed through the cooler-to-hotter ion temperature ratio, T_c/T_h, will often be referred to as "ion temperature", for simplicity.

We will use, mainly, the Sagdeev potential approach to investigate the effects of the ion and the electron temperatures on solitons and double layers supported by the plasma model under consideration. This approach is preferred because it allows one to study nonlinear waves of arbitrary amplitude, unlike the KdV approach which permits a study of weakly nonlinear waves only. However, we will also consider the KdV approach, as a useful background.

The numerical results have been obtained using Mathematica (mainly) and Python programming languages. The plots have been obtained using

gnuplot (mainly) and Mathematica.

It will be shown that there are a number of new results that have not been reported in the literature. These new results include the existence of a stopband in the existence domain of fast solitons, for some parameter values. By a stopband, we mean a range of Mach numbers between two passbands of an existence domain for which solitary wave propagation does not occur. The existence of a stopband in the soliton existence domain is a novel result as, to the best of our knowledge, it has not been reported in any previous soliton existence study.

3.3 Linear waves and dispersion relation

3.3.1 Basic model and equations

We consider a non-relativistic, unmagnetised, collisionless, plasma consisting of Boltzmann electrons and two adiabatic ion species that are singly and positively charged. The basic equations governing the dynamics of this plasma model are, respectively, the momentum and continuity equations for both ion species

$$m_j n_j \left(\frac{\partial v_j}{\partial t} + v_j \frac{\partial v_j}{\partial x} \right) = -e n_j \frac{\partial \varphi}{\partial x} - \frac{\partial p_j}{\partial x}, \tag{3.1}$$

$$\frac{\partial n_j}{\partial t} + \frac{\partial (n_j v_j)}{\partial x} = 0, \tag{3.2}$$

the density of the inertialess electrons

$$n_e = n_{e0} \exp\left(\frac{e\varphi}{T_e} \right), \tag{3.3}$$

and Poisson's equation

$$\epsilon_0 \frac{\partial^2 \varphi}{\partial x^2} = e \left(n_e - \sum_{j=c,h} n_j \right), \tag{3.4}$$

where we have assumed one dimensional motion of all species. Furthermore, in Eqs. (3.1−3.4), m_j, n_j, v_j and p_j are the mass, density, speed and pressure of the j ion species, e is the magnitude of the electronic charge, n_e is the density of the electrons, with equilibrium value n_{e0}, T_e is the electron temperature expressed in energy units, φ is the electrostatic potential, t is

the time, x is the space coordinate, and the symbols "c" and "h" refer to the cooler and the hotter ion species, respectively.

The above basic equations will be used to study linear waves, weakly nonlinear waves using the KdV approach, and fully nonlinear waves using the Sagdeev potential approach.

Based on the above governing equations, we shall use the adiabatic-pressure-density relation with polytropic index, $\gamma = 3$. A drawback of retaining the inertia and pressure of both ion species is that expressing their densities in terms of the electrostatic potential, as required in the Sagdeev potential theory, becomes analytically impossible, unless one uses the adiabatic-pressure-density relation with polytropic index $\gamma = 3$ (see e.g. Verheest et al. (2008); Verheest & Hellberg (2010b)), that is,

$$p_j n_j^{-3} = p_{j0} n_{j0}^{-3} = \text{constant}. \tag{3.5}$$

3.3.2 Linear dispersion relation

Assuming plane waves varying as $\exp[i(kx - \omega t)]$, where k and ω are the wavenumber and the angular wave frequency, respectively, and linearising the basic equations in the usual way, we obtain the following dispersion relation, the details of whose derivation are in Appendix A.

$$\epsilon_0 m_c m_h \left(k^2+\lambda_{De}^{-2}\right)\frac{\omega^4}{k^4} - \left[\epsilon_0\left(k^2+\lambda_{De}^{-2}\right)(m_h T_c + m_c T_h) + e^2(n_{h0}m_c + n_{c0}m_h)\right]\frac{\omega^2}{k^2} + \epsilon_0\left(k^2+\lambda_{De}^{-2}\right)T_h T_c + e^2(n_{h0}T_c + n_{c0}T_h) = 0, \tag{3.6}$$

where $\lambda_{De} = (\epsilon_0 T_e / e^2 n_{e0})^{1/2}$ is the electron Debye length. This is the linear dispersion relation for ion waves propagating in a plasma composed of two adiabatic ion species and Boltzmann electrons.

It can be seen from Eq. (3.6) that if the thermal effects of the two ion species were to be neglected, i.e. taking $T_c = T_h = 0$, one would obtain

$$\omega^2 = k^2\left[\frac{T_e}{m_c}\left(\frac{n_{c0}}{n_{e0}} + \frac{n_{h0}}{n_{e0}}\frac{m_c}{m_h}\right)\right]\left(1 + k^2\lambda_{De}^2\right)^{-1}. \tag{3.7}$$

Apart from a difference in notations and a difference in the definition of the temperature, recalling that in this work the temperatures are expressed in

energy units, Eq. (3.7) is the dispersion relation reported by Tran & Hirt (1974), for a plasma composed of two cold, positively charged, ion species and Boltzmann electrons.

In the long wavelength limit, i.e. $k \to 0$ so that $k^2\lambda_{De}^2 \ll 1$, one gets from Eq. (3.6)

$$m_c m_h n_{e0}\frac{\omega^4}{k^4} - \left(n_{e0}m_h T_c + n_{e0}m_c T_h + n_{h0}m_c T_e + n_{c0}m_h T_e\right)\frac{\omega^2}{k^2} + n_{e0}T_h T_c + n_{h0}T_c T_e + n_{c0}T_h T_e = 0. \quad (3.8)$$

Equation (3.8) is the dispersion relation that we would have obtained had we used the plasma approximation, i.e. $n_i = n_e$ (e.g. Chen (1984)), instead of Poisson's equation. It is a biquadratic equation in the phase speed, $v_{\rm ph} = \omega/k$, which yields two independent solutions, i.e. two wave modes, subject to constraints on the discriminant.

Following Verheest et al. (2008, 2011), we normalise various quantities appearing in Eq. (3.8) with respect to the characteristics of the hotter ions, as follows. The mass of the cooler ions is expressed through the ratio $\mu = m_h/m_c$; the temperature of the cooler ions $\tau_i = T_c/T_h$; the temperature of the electrons is expressed through the ratio $\tau_e = T_h/T_e$; the equilibrium density of the cooler ions $f = n_{c0}/n_{h0}$, so that for the electrons we have $n_{e0}/n_{h0} = 1 + f$; the dimensionless phase speed $M_s = v_{\rm ph}/v_{\rm th}$, where $v_{\rm th} = (T_h/m_h)^{1/2}$ is the thermal speed of the hotter ions.

With this normalisation, Eq. (3.8) becomes

$$\tau_e(1+f)M_s^4 - [1+\mu f+\tau_e(1+f)(1+\mu\tau_i)]M_s^2 + \mu\tau_i\tau_e(1+f)+\mu\tau_i+\mu f = 0. \quad (3.9)$$

Equation (3.9) is also obtained using the KdV approach, discussed in Sec. 3.4, and the Sagdeev potential approach, discussed in Sec. 3.5. The subscript "s" associated with M refers to "sound", to emphasise the fact that M_s is the acoustic speed for the plasma model under consideration.

Equation (3.9) is satisfied by

$$M_{s-}^2 = \frac{1}{2\tau_e(1+f)}\Big\{[1+\mu f+\tau_e(1+f)(1+\mu\tau_i)] \\ -\{[1+\mu f+\tau_e(1+f)(1+\mu\tau_i)]^2-4\mu\tau_e(1+f)[\tau_i\tau_e(1+f)+\tau_i+f]\}^{1/2}\Big\}, \tag{3.10}$$

and

$$M_{s+}^2 = \frac{1}{2\tau_e(1+f)}\Big\{[1+\mu f+\tau_e(1+f)(1+\mu\tau_i)] \\ +\{[1+\mu f+\tau_e(1+f)(1+\mu\tau_i)]^2-4\mu\tau_e(1+f)[\tau_i\tau_e(1+f)+\tau_i+f]\}^{1/2}\Big\}. \tag{3.11}$$

Equations (3.10) and (3.11) imply the existence of two modes with different phase speeds, consistent with earlier investigations (e.g. Fried et al. (1971); Tran (1974); Tran & Coquerand (1976); Verheest et al. (2007, 2008, 2011)).

If the cooler ions were not present, i.e. $f = \tau_i = \mu = 0$, Eq. (3.10) would be

$$M_{s-} = 0, \tag{3.12}$$

i.e. the acoustic speed of the slow mode would vanish, whereas Eq. (3.11) would be

$$M_{s+} = \left(\frac{1+\tau_e}{\tau_e}\right)^{1/2}. \tag{3.13}$$

In dimensional form, Eq. (3.13) is written as

$$\frac{\omega}{k} = \left(\frac{T_e+T_h}{m_h}\right)^{1/2}. \tag{3.14}$$

Apart from the apparently-missing polytropic index (γ) and Boltzmann constant resulting from a difference in the definition of the temperature (see Eq. (A.9)), Eq. (3.14) is the same as Eq. (4-41) of Chen (1984), which is the dispersion relation of ion acoustic waves in a plasma composed of Boltzmann electrons and one component of warm ions. This means that the fast mode is an extension of the well-known ion acoustic wave (e.g. Sagdeev (1966); Tagare (1973); Chen (1984)). However, through its inertia (μ), density (f), and thermal effects (τ_i), we show in this work that the second ion component

introduces new interesting features.

It is well-known (e.g. Tran (1974); Verheest et al. (2007)) that the phase speed of the slow mode ($v_{\rm ph-slow}$) lies between the thermal speeds (v_{tj}) of the two ion species, whereas that of the fast mode ($v_{\rm ph-fast}$) lies between the thermal speeds of the hotter ions and the electrons, so that one has the ordering

$$v_{\rm tc} < v_{\rm ph-slow} < v_{\rm th} < v_{\rm ph-fast} < v_{\rm te}, \tag{3.15}$$

which may be expressed in dimensionless form as

$$\mu\tau_i < M_{\rm slow}^2 < 1 < M_{\rm fast}^2 < \frac{v_{\rm te}}{v_{\rm th}}, \tag{3.16}$$

where we recall that the speeds are normalised with respect to the thermal speed of the hotter ions.

To avoid heavy Landau damping of a plasma wave, it is important that the phase speed is not of similar magnitude to that of the thermal speed. Thus, as can be seen from (3.15), we require a sufficiently large gap between the thermal speeds of the two ion species, in the case of the slow mode, and a sufficiently large gap between the thermal speeds of the hotter ions and the electrons, in the case of the fast mode.

In Eq. (3.16), we have introduced the notation $M_{\rm slow}$ and $M_{\rm fast}$ rather than M_{s-} and M_{s+}, respectively, that we used in (3.10) and (3.11), because the discussion associated with (3.16) applies also to the nonlinear waves (slow and fast) that will be discussed later.

We recall that when we refer to the cooler and the hotter ion species, the words "cooler" and "hotter" are expressed in terms of the ion thermal speeds, and not directly in terms of the temperatures (see also e.g. Verheest et al. (2007)). Thus, one could have $v_{tc} < v_{th}$ (i.e. $\mu\tau_i < 1$), but with $T_c \geq T_h$ (i.e. $\tau_i \geq 1$). Nevertheless, in this work, we restrict our discussion to the case $T_c < T_h$ (i.e. $\tau_i < 1$), but allowing m_c to be greater than m_h (i.e. $\mu < 1$), equal to m_h (i.e. $\mu = 1$), or less than m_h (i.e. $\mu > 1$).

In this section and in the remainder of this work, the values of μ and τ_i that are needed for the numerical evaluation will be chosen in such a way that

$$\mu\tau_i < 1, \tag{3.17}$$

for both the slow and the fast modes, so that the ordering (3.16) is always satisfied.

In order to carry out an analytical analysis of the acoustic speeds of both modes, we express (3.10) and (3.11) in the form

$$M_{s\pm}^2 = \beta[1 \pm (1+x)^\alpha], \tag{3.18}$$

where $\beta = [1 + \mu f + \tau_e(1+f)(1+\mu\tau_i)]/2\tau_e(1+f)$, $\alpha = 1/2$, and

$$x = -\frac{4\mu\tau_e(1+f)[\tau_i\tau_e(1+f)+\tau_i+f]}{[1+\mu f+\tau_e(1+f)(1+\mu\tau_i)]^2}. \tag{3.19}$$

It is easy to show, numerically, that $|x| < 1$, irrespective of the choice of the values of the parameters μ, τ_i, τ_e, and f, and therefore the binomial series

$$(1+x)^\alpha = 1 + \alpha x + \frac{\alpha(\alpha-1)}{2!}x^2 + ... \tag{3.20}$$

that appears in (3.18) converges absolutely and is always a real quantity. Using (3.19) and (3.20) in (3.18), we obtain the approximate expressions of the square of the acoustic speeds of the slow and the fast modes, respectively, as

$$M_{s-}^2 = \frac{\mu[\tau_i\tau_e(1+f)+\tau_i+f]}{\tau_e(1+f)(1+\mu\tau_i)+1+\mu f} + O(2), \tag{3.21}$$

and

$$M_{s+}^2 = 1 + \mu\tau_i + \frac{1+\mu f}{\tau_e(1+f)} - \frac{\mu[\tau_i\tau_e(1+f)+\tau_i+f]}{\tau_e(1+f)(1+\mu\tau_i)+1+\mu f} + O(2), \tag{3.22}$$

which, in the limit of vanishing τ_i (i.e. neglecting the thermal effects of the cooler ions), become

$$M_{s-}^2 \approx \frac{\mu f}{\tau_e(1+f)+1+\mu f} < 1, \tag{3.23}$$

and

$$M_{s+}^2 \approx 1 + \frac{1+\mu f}{\tau_e(1+f)} > 1. \tag{3.24}$$

It is seen that each of Eqs. $\{3.23, 3.24\}$ is identical to its counterpart in Eq. (18) of Verheest et al. (2008), if their Boltzmann ion term is neglected and one uses $\sigma_a = \sigma_c = +1$, $|q_a| = |q_c| = +e$, as is appropriate for the present

study involving two positive and singly charged ion species. Furthermore, we see from Eq. (3.24) that, for $\tau_e \to 0$, M_{s+} tends to infinity. Thus, to study the fast mode, such values of τ_e will be avoided.

Summary

Briefly, in this subsection, we derived the dispersion relation of ion acoustic waves in a plasma composed of Boltzmann electrons and two adiabatic, positively and singly charged, ion species. For the purpose of subsequent discussion, this dispersion relation has also been presented in dimensionless form. The normalisation has been introduced following Verheest et al. (2008), that is, various quantities have been normalised with respect to the characteristics of the hotter ion species. The advantage of this normalisation is that it allows the investigation of the thermal effects of both the cooler ion species and the electrons.

As is well-known (e.g. Tran (1974); Tran & Coquerand (1976); Verheest et al. (2008, 2011)), we showed that the plasma model under consideration supports the propagation of two modes with different phase speeds. The phase speed of the slow mode lies between the thermal speeds of the two ion species, whereas that of the fast mode lies between the thermal speeds of the hotter ion species and the electrons. We showed that the fast mode is an extension of the well-known ion acoustic wave in the standard electron-ion plasma (e.g. Chen (1984)).

Furthermore, it has been shown that our results reduce to those of Verheest et al. (2008), when the thermal effects of the cooler ions are neglected.

The analytical expressions of the phase speeds of the two modes have been reported by Tran (1974), using a different normalisation (see his Eqs. (9) and (10)). As mentioned earlier, in the introduction of this chapter, Tran (1974) assumed that the temperatures of the two ion species are equal, and the normalisation was with respect to the electron temperature.

Obviously such a normalisation of Tran (1974) does not allow one to investigate the effects of the electron temperature on the wave propagation characteristics. Furthermore, the author did not discuss the effects of the ion temperature on the phase speeds of the two modes. He only reported the equations (see his Eqs. (9) and (10)).

Thus, in what follows, we carry out a comprehensive investigation of the effects of the ion and electron temperatures on the acoustic speeds of the

two modes. Our discussion is carried out analytically and numerically.

Most importantly, we show that, for the fast mode, the values of the ion mass ratio μ slightly greater than 1 lead to interesting results, which will be highlighted throughout the rest of this work, as long as the fast mode is concerned.

3.3.3 Thermal effects on the slow mode ion acoustic waves

i. The effects of the ion temperature on the acoustic speed of the slow mode

Here, we investigate the thermal effects of the cooler ion species on the acoustic speed of the slow linear wave. In our discussion, we assume that the electrons are much hotter than the hotter ion species so that $\tau_e \to 0$. We will often refer to this assumption as the superhot approximation for the electrons. Treating the electrons in this way allows us to compare our results with those of Verheest et al. (2008) when the thermal effects of the cooler ion species are negligible.

Assuming that the electrons are superhot, we obtain from Eq. (3.21)

$$M_{s-}^2 \approx \frac{\mu(\tau_i + f)}{1 + \mu f}. \tag{3.25}$$

It is seen from Eq. (3.25) that the acoustic speed of the slow linear wave increases with increasing temperature of the cooler ions. The value of M_{s-} tends to $\sqrt{\mu\tau_i}$ as f approaches 0, whereas M_{s-} approaches 1 at sufficiently large values of f. We recall that the case $f = 0$ must be avoided, as it would mean that the cooler ions do not exist, and therefore the slow wave would not exist in that case.

Differentiating M_{s-}, given by (3.25), with respect to f, we obtain

$$\frac{\partial M_{s-}}{\partial f} = \frac{\mu(1 - \mu\tau_i)}{2(1 + \mu f)^2\sqrt{\frac{\mu(\tau_i+f)}{1+\mu f}}}. \tag{3.26}$$

Since $\mu\tau_i < 1$, see (3.16), it follows that, for given values of μ and τ_i, the curve $M_{s-}(f)$ has a positive slope, and hence the acoustic speed of the slow wave increases with increasing density of the cooler ions. It is also seen that this slope decreases as the value of $\mu\tau_i$ is increased so that for values of $\mu\tau_i$ close to 1, the phase speed of the slow wave has almost a constant value,

regardless of the value of f. However, as discussed earlier, the values of $\mu\tau_i$ that are close to 1 must be avoided, because in that case there is a small gap between the thermal speeds of the two ion species, indicating that the phase speed of the slow wave is close to the thermal speeds of the two ion species, see (3.15) and (3.16), and therefore the wave is subject to strong Landau damping.

Although the effect of the ion temperature expressed through τ_i on M_{s-} is clear from Eq. (3.25), it is only qualitative, as Eq. (3.25) contains errors that result from various approximations. To get a more quantitative picture, the full expression of M_{s-} (f) given by Eq. (3.10) has been considered in the numerical evaluation.

Figure 3.1 illustrates M_{s-} plotted against f, for μ=0.1 (upper panel), μ=1 (middle panel), and $\mu = 10$ (lower panel). These values of μ represent cases in which the mass of the hotter ions is less than, equal to, and greater than that of the cooler ions, respectively. The value of $\tau_e = 0.0001$ has been chosen to represent a case in which the electrons are much hotter than the hotter ion species. The thermal effects of the cooler ions on the acoustic speed of the slow wave are investigated by increasing the value of τ_i from 0.0001 to a higher value shown in each panel. For each value of μ, the values of τ_i are chosen in such a way that $\mu\tau_i < 1$ (see Eq. (3.16)).

When the cooler ions are effectively cold ($\tau_i = 0.0001$), it is seen that, for a fixed value of μ, M_{s-} has a vanishing value at $f \sim 0$ and then increases with increasing f. At sufficiently large values of f, M_{s-} approaches 1.

As the value of τ_i is increased, for fixed value of μ, M_{s-} increases for all f. However, for large values of f, and particularly for large values of μ, M_{s-} is close to 1, regardless of the value of τ_i. That is, for large values of f, the acoustic speed of the slow mode is close to the thermal speed of the hotter ion species, implying that the wave is subject to Landau damping, and this effect is more marked as the value of μ is increased.

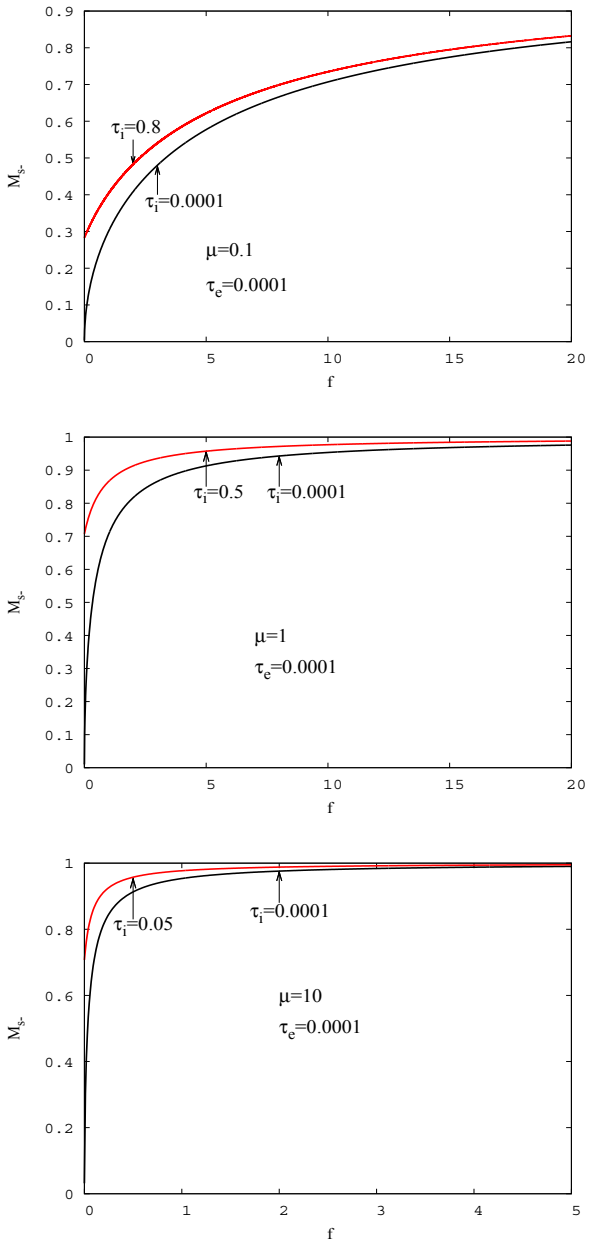

Figure 3.1: The normalised acoustic speed of the slow wave plotted against the normalised density of the cooler ions for $\mu = 0.1$ (upper panel), $\mu = 1$ (middle panel), and $\mu = 10$ (lower panel). For each value of μ, the effect of the temperature of the cooler ions on the acoustic speed of the slow wave is shown by increasing τ_i from 0.0001 to a higher value.

ii. The effects of the electron temperature on the acoustic speed of the slow mode

Here, we neglect the thermal effects of the cooler ions, i.e. we assume cold ions, and investigate the effects of the electron temperature on the acoustic speed of the slow wave. In this case, we recall from Eq. (3.23) that the acoustic speed of the slow wave is given by

$$M_{s-}^2 \approx \frac{\mu f}{\tau_e(1+f)+1+\mu f}. \tag{3.27}$$

When the electrons are much hotter than the hotter ion species, so that $\tau_e \to 0$, Eq. (3.27) reduces to Eq. (20) of Verheest et al. (2008), that is,

$$M_{s-}^2 \approx \frac{\mu f}{1+\mu f}. \tag{3.28}$$

Furthermore, Eq. (3.27) suggests that reducing the electron temperature leads to a decrease in the acoustic speed of the slow wave. We recall that $\tau_e = T_h/T_e$ so that increasing τ_e means decreasing the electron temperature (T_e).

Figure 3.2 shows M_{s-} plotted as a function of f, for $\mu = 0.1$ (upper panel), $\mu = 1$ (middle panel), and $\mu = 10$ (lower panel). The full expression for M_{s-} (f), given by Eq. (3.10), has been considered in the numerical evaluation.

It is observed that increasing τ_e (i.e. decreasing the electron temperature), for a fixed value of μ, leads to a decrease in the acoustic speed of the slow wave. This effect of the electron temperature on the acoustic speed of the slow wave is observed to be more significant for small values of the ion mass ratio μ, typically $\mu \lesssim 1$. Furthermore, it is observed that, for given values of μ and τ_e, M_{s-} approaches 1 for large values of f, and this effect is more marked as the value of μ is increased. That is, for these large values of f, particularly for large values of μ, the phase speed of the slow wave is of the order of the thermal speed of the hotter ion species, implying that the wave is subject to Landau damping.

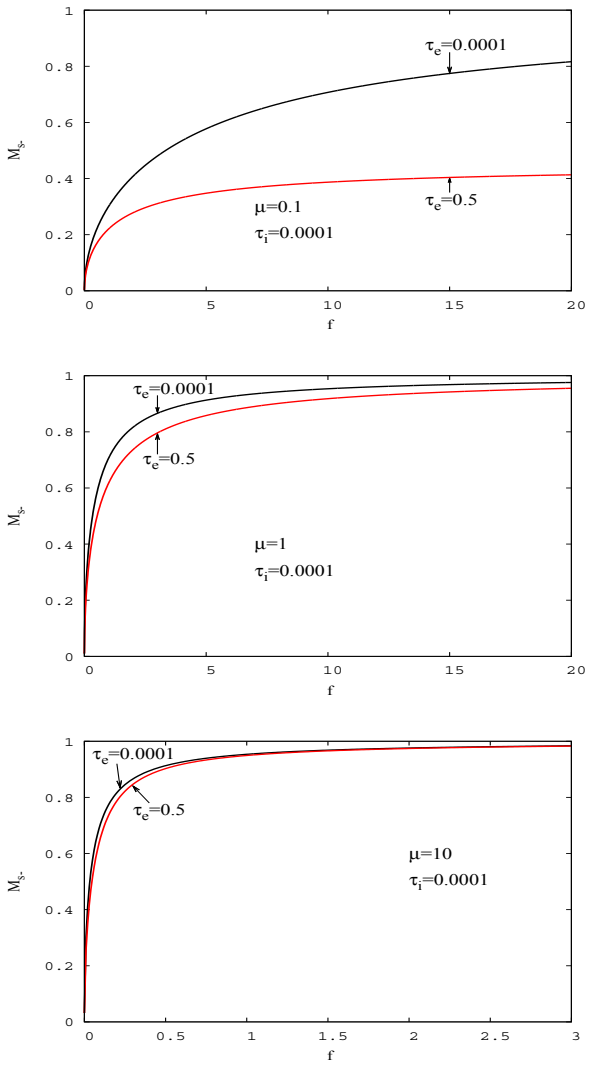

Figure 3.2: The normalised acoustic speed of the slow wave plotted against the normalised density of the cooler ions for $\mu = 0.1$ (upper panel), $\mu = 1$ (middle panel), and $\mu = 10$ (lower panel). For each value of μ, the effect of the electron temperature on the acoustic speed of the slow wave is shown by increasing τ_e from 0.0001 to 0.5 (i.e. decreasing the electron temperature from $10000T_h$ to $2T_h$). The value of $\tau_i = 0.0001$ means that the cooler ions are cold.

Summary

Briefly, in this subsection, we have investigated the thermal effects of the cooler ions, expressed through τ_i, and those of the electrons, expressed through τ_e, on the acoustic speed of the slow mode. The investigation was carried out analytically and numerically.

Our numerical work was carried out without any approximation, using Eq. (3.10), and the results have been presented as plots of the normalised acoustic speed, M_{s-}, against the normalised density of the cooler ions, f.

The thermal effects of the cooler ions on the acoustic speed of the slow mode have been investigated assuming that the electrons are superhot, i.e. $\tau_e \to 0$. We have found that the acoustic speed of the slow mode increases as the value of τ_i is increased.

The thermal effects of the electrons have been investigated assuming that the cooler ions are cold, i.e. $\tau_i \to 0$. We have found that the acoustic speed of the slow mode decreases as the value of the electron temperature is decreased.

For large values of f, the acoustic speed of the slow mode is close to the thermal speed of the hotter ion species, particularly for large values of the ion mass ratio μ, implying that, in that case, the wave is subject to Landau damping.

3.3.4 Thermal effects on the fast mode ion acoustic waves

i. The effects of the electron temperature on the acoustic speed of the fast mode

To investigate the effects of the electron temperature on the acoustic speed of the fast mode, we proceed as was for the case of the slow mode, that is, we assume that the cooler ions are cold so that $\tau_i \to 0$. On this assumption, we recall from our earlier discussion that the approximate and simplified expression of the acoustic speed of the fast mode is (see Eq. (3.24))

$$M_{s+}^2 \approx 1 + \frac{1 + \mu f}{\tau_e (1 + f)}. \tag{3.29}$$

We see, from (3.29), that M_{s+} decreases with increasing τ_e. Recalling that the electron temperature has been normalised with respect to the temperature of the hotter ions as $\tau_e = T_h/T_e$, this conclusion is equivalent to

saying that the acoustic speed of the fast mode decreases with decreasing temperature of the electrons.

In this work, we assume that the electrons are hotter than the hotter ion species, i.e. $\tau_e < 1$, but that the temperature difference is not very high, to avoid the case $\tau_e \to 0$, for which $M_{s+} \to \infty$. In some cases, however, we include $\tau_e = 1$ (i.e. $T_e = T_h$) for illustration, when necessary. For the standard electron-ion plasma (e.g. Sagdeev (1966); Tagare (1973); Chen (1984)), the ion waves are Landau-damped when $T_e \lesssim T_i$ (see e.g. Chen (1984), p. 267). This may not be applicable to a plasma composed of more than one ion species, as considered in this work. Clearly, we see from our Eq. (3.11) or the approximate and simplified form of it given by Eq. (3.29) that if $\tau_e = 1$, the phase speed of the fast wave may be much greater than the thermal speed of the hotter ions, depending on the choice of the values of other parameters.

Thus, in all our subsequent discussions of the fast mode, we shall consider values of τ_e in the range

$$0.1 \leq \tau_e \leq 1, \tag{3.30}$$

or equivalently $T_h \leq T_e \leq 10T_h$.

It is more instructive to know how the acoustic speed of the fast mode varies as the relative density f is varied. Differentiating M_{s+}, given by Eq. (3.29), with respect to f, we obtain

$$\frac{\partial M_{s+}}{\partial f} = \frac{(\mu - 1)\tau_e}{2[\tau_e(1+f)]^2\left[1 + \frac{1+\mu f}{\tau_e(1+f)}\right]^{1/2}}. \tag{3.31}$$

From Eq. (3.31), we see that the variation of M_{s+} with f depends, strongly, on the value of μ. For $\mu < 1$, the slope of the curve $M(f)$ is negative, i.e. M_{s+} decreases with increasing f. However, for $\mu > 1$, the curve $M(f)$ has a positive slope, implying that M_{s+} increases with increasing f. In principle, Eq. (3.31) suggests that M_{s+} does not vary with f for $\mu = 1$, as the slope of the curve $M(f)$ is zero in that case, but we note that Eq. (3.31) is only an approximate expression for M_{s+} (f). It will be shown numerically by considering the full expression of M_{s+} (f) given by Eq. (3.11) that for $\mu \sim 1$, the curve M_{s+} (f) may have a negative, zero, or positive slope, depending on the value of τ_e.

It should be noted that a strong dependence of the variation of M_{s+} with f on μ, as predicted by Eq. (3.31), is an important result, particularly for the study of the existence domain of fast solitons that will be discussed later, since the acoustic speed determines the lower limit in Mach numbers for the existence of solitons. Indeed, it will be shown that the variation of the maximum Mach number for the existence of fast solitons with f also depends on μ, with a trend similar to that predicted by Eq. (3.31). This point will be useful for the understanding of a stopband that we have observed in the existence domain of fast solitons, to be discussed later.

Up to this stage, Eqs. (3.29) and (3.31) permit us to understand the qualitative dependence of M_{s+} on τ_e and f, for a given value of μ. In what follows, we discuss the numerical results obtained considering the full expression of M_{s+} (f) given by Eq. (3.11). In our numerical evaluation, we considered values of μ in various ranges, namely, $0 < \mu < 1$, $\mu \sim 1$, and $\mu \gg 1$, for a broad picture.

Figure 3.3 illustrates the acoustic speed of the fast mode plotted against the normalised density of the cooler ions for $\mu = 0.5$ (upper left panel), $\mu = 1$ (upper right panel), $\mu = 1.5$ (lower left panel), and $\mu = 10$ (lower right panel), showing the effect of increasing the value of τ_e from 0.1 to higher values shown in each panel. The dependence of the slope of the curve M_{s+} (f) on μ discussed above based on the approximate expression given by Eq. (3.31) is now clearly observed. For each value of μ shown in the figure, M_{s+} decreases as the value of τ_e is increased. That is, the acoustic speed of the fast mode decreases as the electron temperature is decreased, and this effect is independent of the value of the mass ratio μ.

For $\mu = 0.5$, and for a fixed value of τ_e, it is observed that M_{s+} has its highest value at $f \sim 0$, from which it falls off as f increases. This dependence of M_{s+} on f is qualitatively unchanged for $\mu = 1$, regardless of the value of τ_e. However, the slope of a curve M_{s+} (f) obtained for a given value of τ_e is smaller for $\mu = 1$ than for $\mu = 0.5$, as expected in the light of Eq. (3.31).

For the cases where $\mu \gg 1$, represented by $\mu = 10$, the variation of M_{s+} with f is significantly different from that observed for the case $\mu \leq 1$. It is observed that, for $\mu = 10$, M_{s+} has its lowest value at $f \sim 0$ from which it increases with increasing f, as expected in the light of Eq. (3.31).

For values of μ slightly greater than 1, the variation of M_{s+} with f exhibits intermediate features between those for the cases $\mu \leq 1$ and $\mu \gg 1$,

depending on the value of τ_e. For this range of μ values, we present the results obtained for $\mu = 1.5$ (lower left panel of Fig. 3.3). We see that the dependence of M_{s+} on f is qualitatively similar to that observed for the case $\mu \leq 1$, for $0.5 \lesssim \tau_e \leq 1$. For $\tau_e = 0.5$, the slope of the curve M_{s+} (f) is zero. Below this value of τ_e, the variation of M_{s+} with f is observed to be qualitatively similar to that for the case $\mu \gg 1$.

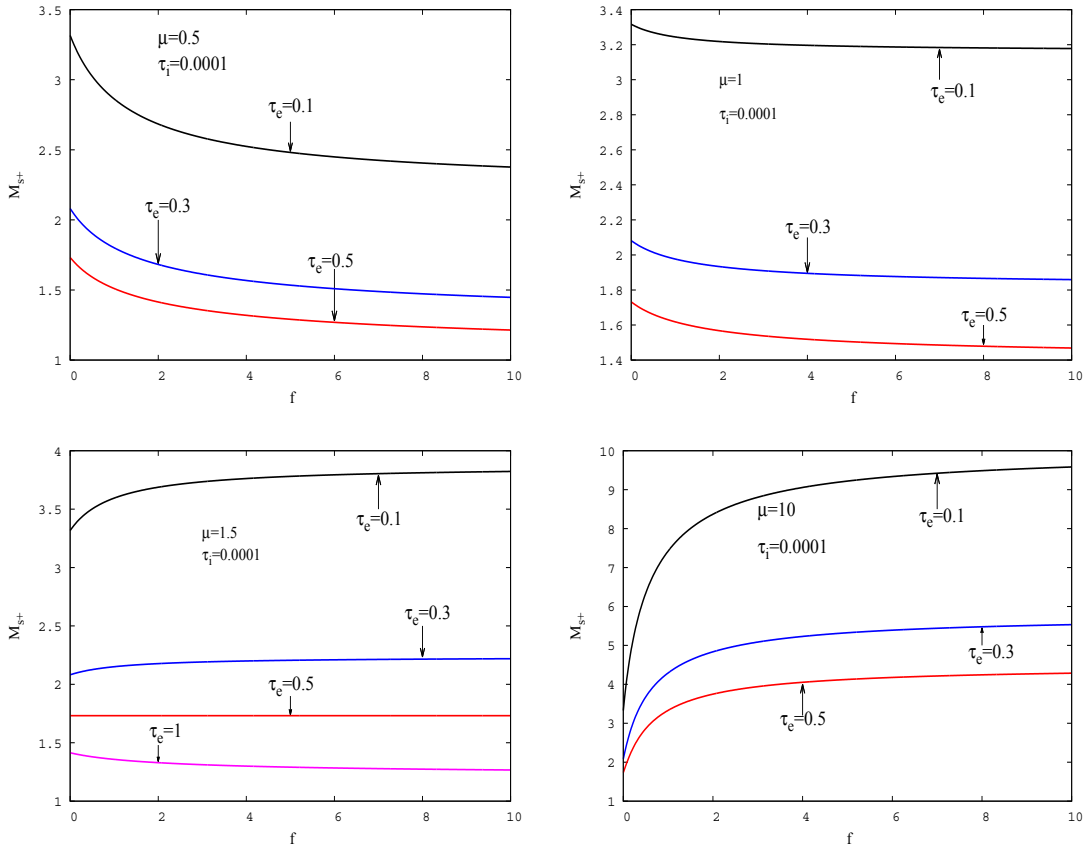

Figure 3.3: The normalised acoustic speed of the fast mode plotted against the normalised density of the cooler ions for $\mu = 0.5$ (upper left panel), $\mu = 1$ (upper right panel), $\mu = 1.5$ (lower left panel), and $\mu = 10$ (lower right panel), showing the effect of increasing the value of τ_e from 0.1 to higher values shown in each panel. The value of $\tau_i = 0.0001$ means that the cooler ions are cold.

ii. The effects of the ion temperature on the acoustic speed of the fast mode

To carry out an analytical investigation of the effects of the ion temperature on the acoustic speed of the fast mode, we use Eq. (3.22). However, we consider a further approximation to this equation in order to make the analysis simpler.

The last (fourth and negative) term on the RHS of Eq. (3.22) is negligible in comparison with the first three (positive) terms taken together. We prove this, assuming that the cooler ions are cold, i.e. $\tau_i = 0$, for simplicity, but the conclusion still holds, irrespective of the value of τ_i (we have checked this numerically!). For $\tau_i = 0$, the absolute value of the last (fourth and negative) term on the RHS of Eq. (3.22) is $\mu f/[\tau_e(1+f)+1+\mu f]$. Clearly, this is even smaller than the third term alone, i.e. it is smaller than $(1+\mu f)/[\tau_e(1+f)]$, and its value is clearly smaller than 1.

Thus, Eq. (3.22) can be further approximated as

$$M_{s+}^2 \approx 1 + \mu\tau_i + \frac{1+\mu f}{\tau_e(1+f)}. \tag{3.32}$$

From Eq. (3.32), we see that for given values of μ, τ_e, and f, M_{s+} increases with increasing τ_i. That is, the acoustic speed of the fast mode increases with increasing temperature of the cooler ions.

Based on Eq. (3.11), Fig. 3.4 illustrates the acoustic speed of the fast mode plotted as a function of the normalised density of the cooler ions, for $\mu = 0.5$ (upper left panel), $\mu = 1$ (upper right panel), $\mu = 1.1$ (lower left panel), and $\mu = 2$ (lower right panel), showing the effect of increasing the value of τ_i from 0.0001 to higher values chosen in such a way that $\mu\tau_i < 1$, for a fixed value of τ_e.

For all values of μ considered in Fig. 3.4, we see that the acoustic speed of the fast mode increases as the value of τ_i is increased, and this is so regardless of f. For all cases presented in the figure, the value of $\tau_e = 0.3$ has been used in our numerical evaluation. However, it should be noted that the effect of τ_i on M_{s+}, as shown in the figure, would be qualitatively similar had we used any other value of τ_e in the range given by (3.30).

For a given value of τ_i, the dependence of the slope of the curve M_{s+} (f) on μ discussed earlier (see the discussion associated with Eq. (3.31)) is observed. In particular, for values of μ slightly greater than 1 represented by $\mu = 1.1$, in the present discussion, M_{s+} has a constant value for $\tau_i = 0.6$, irrespective of f. Indeed, we will show later, in the study of fast solitons, that the values of μ in the approximate range $1 \lesssim \mu \lesssim 3$ are of special interest.

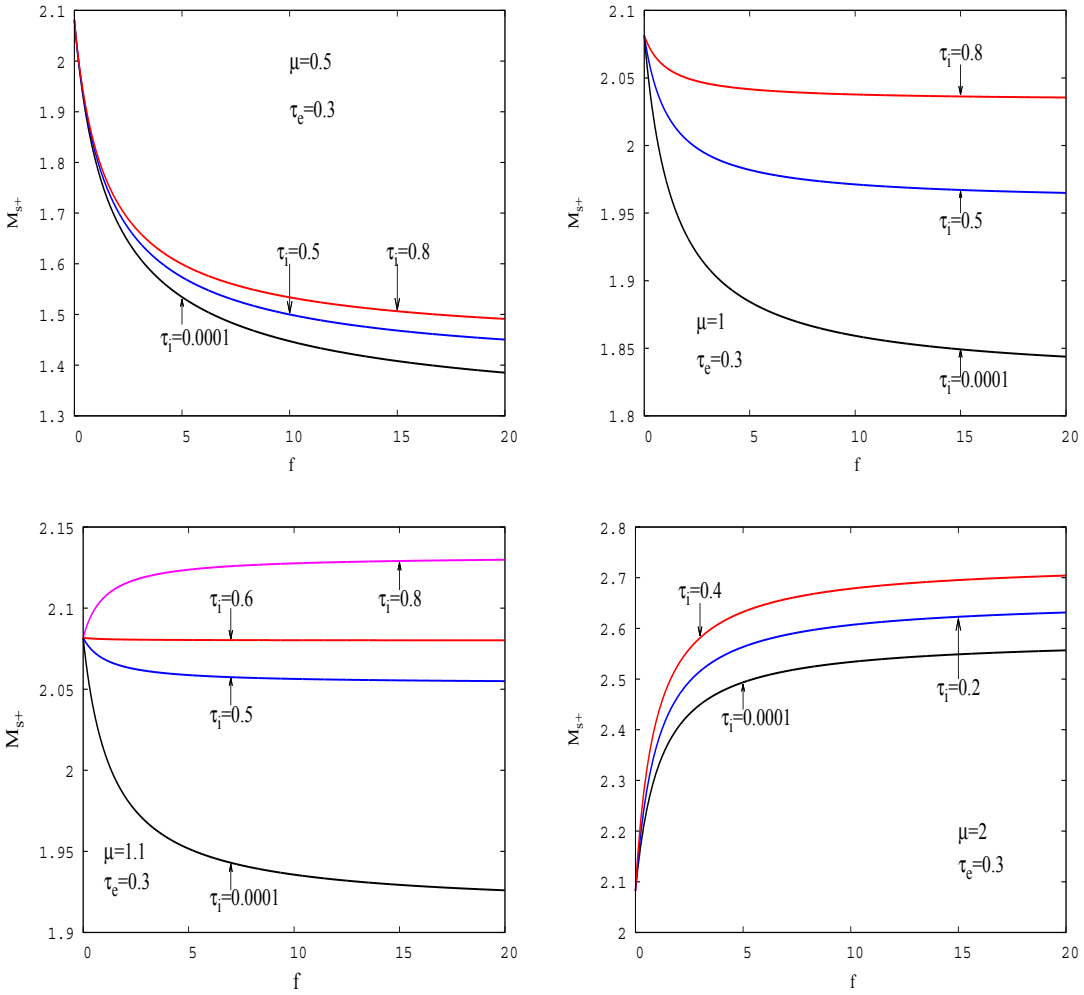

Figure 3.4: The normalised acoustic speed of the fast mode plotted against the normalised density of the cooler ions for $\mu = 0.5$ (upper left panel), $\mu = 1$ (upper right panel), $\mu = 1.1$ (lower left panel), and $\mu = 2$ (lower right panel), showing the effect of increasing the value of τ_i from 0.0001 to higher values chosen in such a way that $\mu\tau_i < 1$. The value of $\tau_e = 0.3$ has been used for all cases shown in the figure.

Summary

Briefly, in this subsection, we have investigated the thermal effects of the electrons and the cooler ions on the acoustic speed of the fast mode. The investigation was carried out analytically and numerically. We assumed that the electrons are hotter than the hotter ion species, but included also the case $T_e = T_h$ for illustration when it was necessary.

Our numerical results were based on the full expression of $M_{s+}(f)$, given by Eq. (3.11), and have been presented as plots of the normalised acoustic speed against the normalised density of the cooler ions (f).

Assuming that the cooler ions are cold, it has been found that the acoustic speed of the fast mode decreases as the value of the electron temperature is decreased. Furthermore, for a fixed value of the electron temperature, we have found that the acoustic speed of the fast mode increases as the temperature of the cooler ions is increased. These conclusions, which hold irrespective of the values of the ion-mass ratio μ and the ion-density ratio f, have been reached both analytically and numerically.

Most importantly, we have found that the variation of the acoustic speed of the fast mode with f depends strongly on μ. For some values of μ slightly greater than 1, there exist values of τ_i and τ_e for which the acoustic speed of the fast mode is constant, irrespective of f.

3.4 Small amplitude ion acoustic solitons: KdV approach

3.4.1 The KdV equation

In this section, we study small amplitude solitons using the Korteweg-de Vries (KdV) approach (e.g. Tagare (1973); Tran (1974); Verheest (2008)). We first derive the KdV equation for the plasma model under consideration, discussing the results in this section and presenting the details of the derivation in Appendix B. Having derived the KdV equation, we then discuss its soliton solution.

The KdV equation and its soliton solution for a related plasma model, in which the two ion species have equal temperatures, were also obtained by Tran (1974) (see his Eq. (16) and Sec. (4) of his paper).

Our present work may be regarded as an extension of the work of Tran (1974), as we provide more useful details. It serves, mainly, as a useful background for our discussion of arbitrary amplitude solitons/double layers presented in Sec. 3.5.

We consider the basic equations and the adiabatic-pressure-density relation given in Sec. 3.3, i.e. Eqs. (3.1)−(3.4) and Eq. (3.5), respectively. Using the adiabatic-pressure-density relation, we can express the pressure gradient of the j^{th} adiabatic species in terms of the density gradient as

$$\frac{\partial p_j}{\partial x} = \frac{T_j n_j^2}{n_{j0}^2}\frac{\partial n_j}{\partial x}, \tag{3.33}$$

and hence re-write the momentum equation, i.e. Eq. (3.1), as

$$m_j n_j\left(\frac{\partial v_j}{\partial t} + v_j\frac{\partial v_j}{\partial x}\right) = -en_j\frac{\partial \varphi}{\partial x} - \frac{T_j n_j^2}{n_{j0}^2}\frac{\partial n_j}{\partial x}, \tag{3.34}$$

where we have defined the undisturbed pressure of the j^{th} adiabatic species as $p_{j0} = n_{j0}T_j/3$ (e.g. Verheest & Hellberg (2010b), p. 279).

By normalising various quantities with respect to the characteristics of the hotter ion species, dimensionless quantities, denoted by primes, are introduced as follows. The electrostatic potential: $\varphi^{'} = e\varphi/T_h$; the time: $t^{'} = t\omega_{ph}$, where $\omega_{ph} = (n_{h0}e^2/\epsilon_0 m_h)^{1/2}$ is the plasma frequency for the hotter ion species; the space coordinate: $x^{'} = x/\lambda_{Dh}$, where $\lambda_{Dh} = (\epsilon_0 T_h/n_{h0}e^2)^{1/2}$ is the Debye length for the hotter ion species; the densities of the j^{th} adiabatic ion species and electrons (e): $n_{j,e}^{'} = n_{j,e}/n_{h0}$, where n_{h0} is the equilibrium density of the hotter ion species; the flow speed of the j^{th} adiabatic ion species: $v_j^{'} = v_j/v_{th}$, recalling that v_{th} is the thermal speed of the hotter ion species. Furthermore, the parameters μ, τ_i, τ_e, and f will be introduced as defined in Sec. 3.3, that is, $\mu = m_h/m_c$, $\tau_i = T_c/T_h$, $\tau_e = T_h/T_e$, and $f = n_{c0}/n_{h0}$.

With the above normalisation, and omitting primes for convenience, we can express the basic equations in dimensionless form as

$$n_c\left(\frac{\partial v_c}{\partial t} + v_c\frac{\partial v_c}{\partial x}\right) = -\mu n_c\frac{\partial \varphi}{\partial x} - \frac{\mu\tau_i}{f^2}n_c^2\frac{\partial n_c}{\partial x}, \tag{3.35}$$

$$n_h\left(\frac{\partial v_h}{\partial t} + v_h\frac{\partial v_h}{\partial x}\right) = -n_h\frac{\partial \varphi}{\partial x} - n_h^2\frac{\partial n_h}{\partial x}, \tag{3.36}$$

$$\frac{\partial n_j}{\partial t} + \frac{\partial (n_j v_j)}{\partial x} = 0, \tag{3.37}$$

$$n_e = g \exp(\tau_e \varphi), \tag{3.38}$$

and

$$\frac{\partial^2 \varphi}{\partial x^2} = n_e - n_h - n_c, \tag{3.39}$$

where $g = 1 + f$.

To obtain the KdV equation (e.g. Tagare (1973)), we use the usual reductive perturbation technique (e.g. Tagare (1973)). From the stretched coordinates (e.g. Tagare (1973))

$$\left.\begin{aligned} \xi &= \varepsilon^{1/2}(x - M_s t) \\ \tau &= \varepsilon^{3/2} t \end{aligned}\right\}, \tag{3.40}$$

one obtains

$$\left.\begin{aligned} \frac{\partial}{\partial x} &= \varepsilon^{1/2} \frac{\partial}{\partial \xi} \\ \frac{\partial}{\partial t} &= \varepsilon^{3/2} \frac{\partial}{\partial \tau} - \varepsilon^{1/2} M_s \frac{\partial}{\partial \xi} \end{aligned}\right\}, \tag{3.41}$$

where ε is a small, non-zero, expansion parameter and M_s is the normalised phase speed of the ion acoustic waves for the plasma model under consideration.

We consider the perturbation of variable quantities as follows.

$$n_c = f + \varepsilon n_c^{(1)} + \varepsilon^2 n_c^{(2)} + \varepsilon^3 n_c^{(3)} + ..., \tag{3.42}$$

$$n_h = 1 + \varepsilon n_h^{(1)} + \varepsilon^2 n_h^{(2)} + \varepsilon^3 n_h^{(3)} + ..., \tag{3.43}$$

$$v_c = \varepsilon v_c^{(1)} + \varepsilon^2 v_c^{(2)} + \varepsilon^3 v_c^{(3)} + ..., \tag{3.44}$$

$$v_h = \varepsilon v_h^{(1)} + \varepsilon^2 v_h^{(2)} + \varepsilon^3 v_h^{(3)} + ..., \tag{3.45}$$

$$\varphi = \varepsilon \varphi^{(1)} + \varepsilon^2 \varphi^{(2)} + \varepsilon^3 \varphi^{(3)} + ..., \tag{3.46}$$

and

$$\begin{aligned} n_e = g + \varepsilon g \tau_e \varphi^{(1)} + \varepsilon^2 [g \tau_e \varphi^{(2)} + \frac{1}{2} g \tau_e^2 (\varphi^{(1)})^2] + \\ \varepsilon^3 [g \tau_e \varphi^{(3)} + g \tau_e^2 \varphi^{(1)} \varphi^{(2)} + \frac{1}{6} g \tau_e^3 (\varphi^{(1)})^3] + ... \end{aligned} \tag{3.47}$$

The expression for the electron density, n_e, given by Eq. (3.47) results from the Taylor expansion of its form given by Eq. (3.38), in conjuction with Eq. (3.46).

Using (3.41)−(3.47), we can express the normalised basic equations in terms of the expansion parameter ε and consider their solutions at various orders of ε (see details in Appendix B).

At the zeroth order of ε, we obtain

$$g - f - 1 = 0, \tag{3.48}$$

which is the equilibrium charge neutrality condition.

At the first non-zero order of ε, we get

$$g\tau_e - \frac{1}{M_s^2 - 1} - \frac{\mu f}{M_s^2 - \mu\tau_i} = 0, \tag{3.49}$$

or equivalently

$$g\tau_e M_s^4 - [1 + \mu f + g\tau_e(1 + \mu\tau_i)]M_s^2 + \mu\tau_i g\tau_e + \mu\tau_i + \mu f = 0. \tag{3.50}$$

Recalling that $g = 1 + f$, it can be seen that Eq. (3.50) is the normalised dispersion relation of the ion acoustic waves discussed in detail in Sec. 3.3, i.e. Eq. (3.9), as expected (e.g. Verheest (2008)).

At the second non-zero order of ε, we find

$$\frac{\partial\varphi^{(1)}}{\partial\tau} + a\varphi^{(1)}\frac{\partial\varphi^{(1)}}{\partial\xi} + b\frac{\partial^3\varphi^{(1)}}{\partial\xi^3} = 0, \tag{3.51}$$

where

$$a = \frac{A}{B}, \tag{3.52}$$

$$b = \frac{1}{B}, \tag{3.53}$$

$$A = \frac{\mu^2 f(3M_s^2 + \mu\tau_i)}{(M_s^2 - \mu\tau_i)^3} + \frac{3M_s^2 + 1}{(M_s^2 - 1)^3} - (1 + f)\tau_e^2, \tag{3.54}$$

and

$$B = \frac{2M_s}{(M_s^2 - 1)^2} + \frac{2\mu f M_s}{(M_s^2 - \mu\tau_i)^2}. \tag{3.55}$$

Equation (3.51), written in terms of the first order electrostatic potential

and with the coefficients a and b given by Eqs. (3.52) and (3.53), is the desired KdV equation (Korteweg & De Vries, 1895) for weakly nonlinear solitary waves supported by a plasma composed of Boltzmann electrons and two adiabatic, positively and singly charged, ion species. The first term of the KdV equation shows the variation on a slow timescale, the second term describes the contribution of the nonlinearity, whereas the third term describes the contribution of the dispersion. This means that the KdV equation expresses a balance between the slow time variation, nonlinearities, and dispersive effects (see also e.g. Verheest (2008)).

It is seen that the RHS of Eq. (3.55) is a sum of two positive terms associated with the two ion species. This means that the coefficient b of the term describing the contribution of the dispersion in the KdV equation is always positive. Indeed, Verheest (2008) pointed out that this is always the case for plasmas without beam effects.

On the other hand, the RHS of Eq. (3.54) is composed of three terms associated with the three species involved in the plasma model under consideration. It is observed that the sum of these terms, and hence the coefficient a of the term describing the contribution of the nonlinearities in the KdV equation, can be negative, zero, or positive, depending on the choice of parameter values.

The vanishing of the coefficient a results in an imbalance between the nonlinearities and dispersive effects. In that case, i.e. when $a = 0$, the modified Korteweg-de Vries (mKdV) equation applies (e.g. Baboolal et al. (1988)). In our discussion, we consider parameter values for which $a \neq 0$.

3.4.2 Soliton solution of the KdV equation

The KdV equation has a well-known "sech^2"-type soliton solution (see e.g. Zabusky & Kruskal (1965); Tagare (1973); Tran (1974); Mace et al. (1991)). To obtain a soliton solution of the KdV equation, one seeks a stationary solution by using the transformation

$$\eta = \xi - M_0\tau, \tag{3.56}$$

where M_0 is the normalised soliton speed in the co-moving frame.

Using this transformation, and the boundary conditions

$$\eta \to \pm\infty, \varphi^{(1)} \to 0, \frac{d\varphi^{(1)}}{d\eta} \to 0, \frac{d^2\varphi^{(1)}}{d\eta^2} \to 0, \tag{3.57}$$

one finds that the KdV equation is satisfied by (see the details in Appendix B)

$$\varphi^{(1)} = \frac{3M_0}{a}\text{sech}^2\left(\sqrt{\frac{M_0}{4b}}\eta\right). \tag{3.58}$$

Transforming to the laboratory frame, following Mace et al. (1991), one gets (see the details in Appendix B)

$$\varphi(x,t) = \frac{3\delta M}{a}\text{sech}^2\left[\sqrt{\frac{\delta M}{4b}}(x - Mt)\right], \tag{3.59}$$

where $\delta M = \varepsilon M_0$ is a small parameter and $M = M_s + \delta M$ is the speed, in the laboratory frame, of a soliton whose amplitude (φ_m) and width (w) are, respectively,

$$\varphi_m = \frac{3\delta M}{a}, \tag{3.60}$$

and

$$\text{w} = \sqrt{\frac{4b}{\delta M}}. \tag{3.61}$$

Equation (3.59) will be used to compare the results obtained from the KdV theory with those obtained from the fully nonlinear Sagdeev potential theory. As discussed in various papers in the literature (e.g. Hellberg et al. (2010)), we note from (3.60) and (3.61) the following important aspects of the KdV theory.

The polarity (sign) of a KdV soliton, i.e. a soliton whose amplitude is so

small that it can be described by the KdV theory, depends on the sign of the coefficient a, suggesting that for a specific choice of parameter values, only either negative or positive KdV solitons can exist. Thus, the KdV theory fails to explain situations in which a given plasma configuration can support solitons of both polarities ("coexistence"), for a specific choice of parameter values (e.g. Baluku et al. (2010b)).

Furthermore, there is a linear relationship between the amplitude and the speed of a KdV soliton, Eq. (3.60). At the acoustic speed, M_s, the amplitude of a KdV soliton vanishes whereas its width is infinite. The words "KdV-like" and "nonKdV-like" have, recently, been introduced (e.g. Hellberg et al. (2010)) to distinguish solitons that obey the KdV theory from those that have finite amplitudes at the acoustic speed, reported in recent papers (e.g. Baluku et al. (2010a,b); Verheest & Hellberg (2010c); Verheest (2010)).

We recall that the purpose of this chapter is to investigate the effects of the ion and electron temperatures on linear ion acoustic waves and ion acoustic solitons supported by the plasma model under consideration. The effects of the ion and electron temperatures on linear ion acoustic waves have been discussed in detail in Sec. 3.3.

Initially, our intention was to investigate the effects of the ion and electron temperatures on ion acoustic solitons, using the fully nonlinear Sagdeev potential theory, discussed in Sec. 3.5, as this permits a study of all solitons (and double layers for cases where they occur), irrespective of their amplitudes, based on a well-determined soliton existence domain. Nevertheless, we have also considered the KdV approach, for completeness, as it also gives us a useful background for our discussion of the arbitrary amplitude solitons/double layers.

Figure 3.5 shows the normalised amplitudes of slow KdV solitons plotted against the true Mach numbers, M/M_s, for $\mu = 10$ and $\tau_e = 0.0001$. It should be noted that what we call a "Mach number", M, in this work, is not a true Mach number. A true soliton Mach number is obtained when the soliton speed is normalised with respect to the acoustic speed of the plasma model under consideration (e.g. Baluku & Hellberg (2008); Dubinov (2009)).

In the upper panel, we show the results obtained for $f = 0.07$, the middle panel is for $f = 0.21$, and the lower panel is for $f = 0.5$. In each case, we

show the effect of increasing the value of τ_i from 0.0001 to higher values chosen in such a way that $\mu\tau_i < 1$.

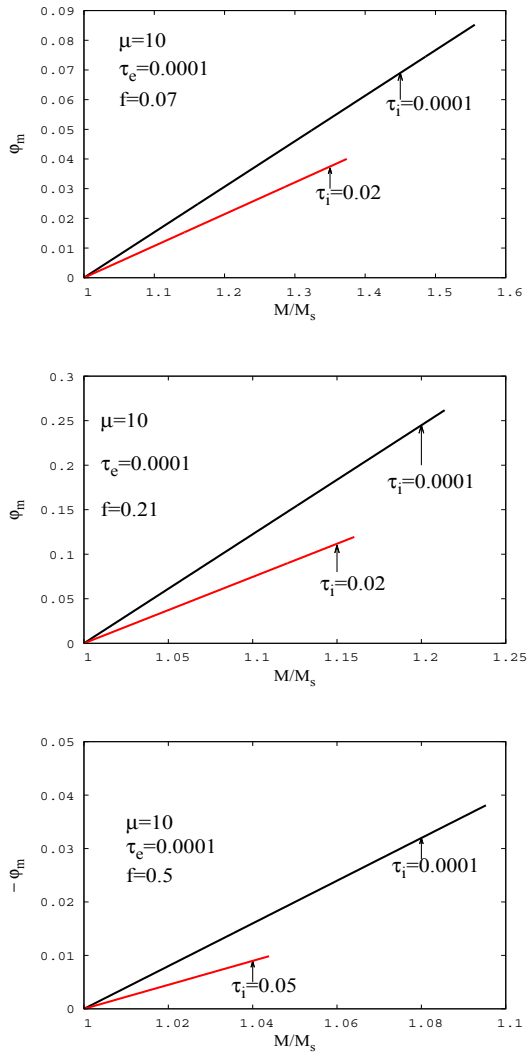

Figure 3.5: The normalised amplitudes of the slow mode KdV solitons plotted against the true Mach numbers for $\mu = 10$ and $\tau_e = 0.0001$. The upper panel is for $f = 0.07$, the middle panel is for $f = 0.21$, and the lower panel is for $f = 0.5$. The effect of increasing the value of τ_i from 0.0001 to higher values, chosen in such a way that $\mu\tau_i < 1$, is shown in the figure. The value of $\tau_e = 0.0001$ means that the electrons are superhot, compared to the hotter ion species.

The choice of the parameter values used in Fig. 3.5, and described above, allows a comparison of the results obtained from both the KdV and Sagdeev potential approaches. We will return to this point in Sec. 3.5.

One drawback of the KdV theory is that the maximum Mach number for the existence of KdV solitons is not precise, unlike the fully nonlinear Sagdeev potential theory where the range in Mach numbers over which solitons exist can be exactly determined. For given values of μ, f, τ_e, and τ_i, the soliton amplitudes shown in Fig. 3.5 have been calculated using Eq. (3.60) for Mach numbers ranging from the acoustic speed of the slow mode given by Eq. (3.10), until the limit of the model $M = 1$ is reached, see the ordering (3.16). In Sec. 3.5, we will show that this range includes Mach numbers beyond the soliton existence domain, as could be expected.

For each case shown in the figure, the value of $\tau_i = 0.0001$ means that the cooler ions are effectively cold. For this value of τ_i, the amplitude of a KdV soliton has a vanishing value at the acoustic speed, from which it increases linearly with increasing soliton speed, as expected. When the value of τ_i is increased, the obtained line has a similar trend, but with a reduced slope. This trend is unchanged when the value of f is increased. However, whereas for $f = 0.07$ and $f = 0.21$ there are positive solitons, negative solitons occur for $f = 0.5$. This point will be discussed in greater detail in Sec. 3.5.

3.5 Arbitrary amplitude ion acoustic solitons/double layers: Sagdeev potential approach

3.5.1 Introduction

In this section, we use the Sagdeev potential approach (Sagdeev, 1966) to study electrostatic ion acoustic solitons/double layers of arbitrary amplitude, for both the slow and the fast modes. The Sagdeev potential approach has been used by many authors to study solitons and/or double layers of large or arbitrary amplitude (e.g. Bhattacharyya & Roychoudhury (1988); Baboolal et al. (1988); Mace et al. (1991); Bharuthram & Shukla (1992); Cairns et al. (1995); Ghosh et al. (1996); Verheest et al. (2008); Mamun (2008); Baluku & Hellberg (2008); Mamun et al. (2008); Verheest & Hellberg (2010b); Baluku et al. (2010a); Verheest et al. (2011); Maharaj et al. (2012); Roy et al. (2012); Saini et al. (2013)).

This approach requires a knowledge of the densities (expressed in terms of the electrostatic potential) of the plasma species for the plasma model under consideration. In a frame co-moving with a solitary wave, the plasma species densities can be obtained by integrating the fluid equations of motion and continuity, and by using the boundary conditions far away from the solitary wave.

For electrostatic waves, substitution of the densities into Poisson's equation yields, after some algebra, the so-called energy equation involving a function of the electrostatic potential, commonly known as the Sagdeev potential/pseudopotential, which is discussed in terms of the classical mechanical analogy.

3.5.2 Plasma densities and Sagdeev potential

The adiabatic-pressure-density relation, i.e. Eq. (3.5), plays an important role in determining the plasma densities of the adiabatic species. Integrating the fluid momentum and continuity equations, with appropriate undisturbed boundary conditions far away from the solitary wave, and using the adiabatic-pressure-density relation with $\gamma = 3$, Verheest et al. (2008) have shown, following the ideas of Ghosh et al. (1996), that in a frame where the nonlinear structure is stationary, the density, n_j, with equilibrium value n_{j0}, of the j^{th} adiabatic species can be written as (see also Verheest & Hellberg

(2010b))

$$n_j = \frac{n_{j0}}{2v_{tj}}\left[\sqrt{\left(v_{tj}+V\right)^2 - \frac{2e\varphi}{m_j}} \pm \sqrt{\left(v_{tj}-V\right)^2 - \frac{2e\varphi}{m_j}}\right]. \tag{3.62}$$

In Eq. (3.62), V represents the plasma speeds far away from the solitary wave, as viewed in the wave frame, and we recall from Sec. 3.3 that e is the electronic charge, φ is the electrostatic potential, v_{tj} and m_j are, respectively, the thermal speed and mass of the j^{th} adiabatic species.

As discussed by Verheest et al. (2008), in Eq. (3.62) the upper sign has to be used for a subsonic species ($V < v_{tj}$) and the lower sign for a supersonic one ($V > v_{tj}$) in order to obtain the correct limit, n_{j0}, far away from the solitary wave, where the plasma is in equilibrium ($\varphi = 0$). This reasoning is based on the fact that $\sqrt{(v_{tj}-V)^2} = |v_{tj}-V| = v_{tj}-V$, if $V < v_{tj}$, but becomes $V - v_{tj}$, if $V > v_{tj}$ (Verheest et al., 2008). By analogy with Verheest et al. (2008), in this work, the upper sign refers to a subsonic species and the lower sign to a supersonic one.

It is well-known from fluid dynamic considerations (e.g. Verheest et al. (2004)) that in order for solitons to exist, there must be at least one supersonic and at least one subsonic species. Based on the ordering (3.15), it follows that, for both modes, the electrons are subsonic and the cooler ions are supersonic. However, the hotter ions are treated as subsonic when we study the slow mode, and supersonic for the fast mode.

The density of Boltzmann electrons, given by Eq. (3.3), and the ion densities are related by Poisson's equation as

$$\epsilon_0 \frac{d^2\varphi}{dx^2} + en_c + en_h - en_e = 0. \tag{3.63}$$

Following Verheest et al. (2008, 2011), we normalise various quantities with respect to the characteristics of the hotter ions, as in sections 3.3 and 3.4, using a prime to denote a dimensionless quantity, where necessary. That is, the dimensionless electrostatic potential $\varphi' = e\varphi/T_h$; the dimensionless space coordinate $x' = \sqrt{n_{h0}e^2/\epsilon_0 T_h}\,x$; the mass of the cooler ions is expressed through the ratio $\mu = m_h/m_c$; the temperature of the cooler ions $\tau_i = T_c/T_h$; the temperature of the electrons is expressed through the ratio $\tau_e = T_h/T_e$; the equilibrium density of the cooler ions $f = n_{c0}/n_{h0}$, so that for the

electrons we have $n_{e0}/n_{h0} = 1 + f$.

With the above normalisation, we obtain from Eqs. (3.3) and (3.62) the dimensionless expressions of the densities of the electrons, the hotter and the cooler ion species, respectively, as

$$n_e^{'} \equiv \frac{n_e}{n_{h0}} = (1+f)\exp(\tau_e \varphi^{'}), \tag{3.64}$$

$$n_h^{'} \equiv \frac{n_h}{n_{h0}} = \frac{1}{2}\left[\sqrt{(1+M)^2 - 2\varphi^{'}} \pm \sqrt{(1-M)^2 - 2\varphi^{'}}\right], \tag{3.65}$$

and

$$n_c^{'} \equiv \frac{n_c}{n_{h0}} = \frac{1}{2\sqrt{\tau_i}}\left[\sqrt{\left(M/\sqrt{\mu} + \sqrt{\tau_i}\right)^2 - 2\varphi^{'}} - \sqrt{\left(M/\sqrt{\mu} - \sqrt{\tau_i}\right)^2 - 2\varphi^{'}}\right], \tag{3.66}$$

where $M = V/\sqrt{T_h/m_h}$ is a "Mach number" of the nonlinear structure, the speed of which is normalised to the hotter ion thermal speed. We recall from Sec. 3.4 that M is not a true Mach number.

Using the above expressions for the dimensionless electrostatic potential, space coordinate, and densities, and omitting the primes for convenience, the dimensionless Poisson's equation is obtained as

$$\begin{aligned}\frac{d^2\varphi}{dx^2} - (1+f)\exp(\tau_e\varphi) + \frac{1}{2}\left[\sqrt{(1+M)^2 - 2\varphi} \pm \sqrt{(1-M)^2 - 2\varphi}\right] \\ + \frac{f}{2\sqrt{\tau_i}}\left[\sqrt{\left(M/\sqrt{\mu} + \sqrt{\tau_i}\right)^2 - 2\varphi} - \sqrt{\left(M/\sqrt{\mu} - \sqrt{\tau_i}\right)^2 - 2\varphi}\right] = 0.\end{aligned} \tag{3.67}$$

Multiplying Eq. (3.67) by $d\varphi/dx$ and integrating, with the boundary condition $\varphi = 0$ far away from the solitary wave, we obtain

$$\frac{1}{2}\left(\frac{d\varphi}{dx}\right)^2 + S(\varphi)_{\mp} = 0, \tag{3.68}$$

where

$$S(\varphi)_{\mp} = \frac{1+f}{\tau_e}[1-\exp(\tau_e\varphi)]+\frac{f}{6\sqrt{\tau_i}}\left\{2\tau_i\sqrt{\tau_i}+\frac{6M^2\sqrt{\tau_i}}{\mu}-\left[\left(\frac{M}{\sqrt{\mu}}+\sqrt{\tau_i}\right)^2-2\varphi\right]^{3/2}\right.$$
$$\left.+\left[\left(\frac{M}{\sqrt{\mu}}-\sqrt{\tau_i}\right)^2-2\varphi\right]^{3/2}\right\}+\frac{1}{6}\{2+6M^2-[(1+M)^2-2\varphi]^{3/2}$$
$$\mp[(1-M)^2-2\varphi]^{3/2}\}. \quad (3.69)$$

Eq. (3.68) looks like an energy equation in classical mechanics for a particle with unit mass in a potential well, with φ playing the role of the particle coordinate, x playing the role of the time, and $\mathrm{S}(\varphi)_{\mp}$ being the potential energy, known as the Sagdeev potential or pseudopotential (Sagdeev, 1966).

We recall from Eq. (3.65) that, in Eq. (3.69), the upper sign has to be used for a subsonic species ($M < 1$) and the lower sign for a supersonic species ($M > 1$) in order to obtain the correct undisturbed density far away from the solitary wave where $\varphi = 0$ (Verheest et al., 2008). It should be noted that the "$\pm$" appearing in Eq. (3.65) becomes "$\mp$" after integration of Poisson's equation. Thus, in Eq. (3.69) the upper sign ($-$) will be used when studying the slow mode and the lower sign ($+$) for the fast mode. It is important to bear in mind that the last term in Eq. (3.69) becomes $[(M-1)^2-2\varphi]^{3/2}$ when the lower sign is considered (i.e. in the case of the fast mode).

Our expression for the Sagdeev potential, Eq. (3.69), can be compared with that reported by Verheest et al. (2008), under appropriate constraints on μ, τ_i, and τ_e. We recall that Verheest et al. (2008) considered a plasma model composed of cold and adiabatic dust species as well as Boltzmann electrons and ions to study large amplitude acoustic solitary waves. As the authors pointed out, and as can be seen from their Eq. (19), their expression of the Sagdeev potential does not explicitly involve the density of the Boltzmann ions, and therefore their results could be applied to the case in which the density of the Boltzmann ions vanishes. Furthermore, their study did not assume the dust to be much more massive than the ions, suggesting a possibility of reproducing their results by replacing the cold and adiabatic dust species by cold and adiabatic ion species.

Thus, if we neglect the thermal effects of the cooler ions (i.e. $\tau_i \to 0$) and assume that the electrons are much hotter than the hotter ion species so that

$\tau_e \to 0$, as assumed by Verheest et al. (2008), our expression of the Sagdeev potential reduces to that reported by Verheest et al. (2008), provided in their work one uses $\sigma_a = \sigma_c = +1$ and $|q_a| = |q_c| = +e$. These values of σ_a, σ_c, q_a, and q_c are appropriate for our plasma model that involves positively and singly charged ion species.

In Fig. 3.6, we compare the Sagdeev potential of the slow mode obtained in this work (upper panel) with that of Verheest et al. (2008) (lower panel). The Sagdeev potential shown in the upper panel corresponds to $S(\varphi)_-$ given by Eq. (3.69) for parameter values shown in the figure, whereas that presented in the lower panel is Fig. 6 of Verheest et al. (2008). The values of μ, f, and M are as used by Verheest et al. (2008), in their Fig. 6. We have used the value of $\tau_i = 0.0001$ to represent the fact that the thermal effects of the cooler ions are negligibly small. One can see from Eq. (3.69) that for $\tau_i = 0$, the term corresponding to the density of the cooler ions, i.e. the second term, is of the form 0/0 which can be dealt with using the usual limiting techniques to obtain $(fM^2/\mu)\left(1-\sqrt{1-2\mu\varphi/M^2}\right)$ (Verheest et al. (2008), second term of their Eq. 19). Therefore, setting $\tau_i = 0$ has been avoided in the numerical evaluation. For reasons of consistency, the value of $\tau_i = 0.0001$ has been used in all our numerical results presented in chapters 3 and 4 to represent the fact that the thermal effects of the cooler ions are negligibly small. The value of $\tau_e = 0.0001$ represents a case in which the electrons are much hotter than the hotter ion species (i.e. $T_e \gg T_h$). This is equivalent to the superhot approximation for the electrons used by Verheest et al. (2008).

We recall that the results of Verheest et al. (2008) were obtained assuming that the two dust species are negatively charged, and therefore the polarity of solitary waves discussed in their work is opposite to that of solitary waves discussed in this work. Thus, the Sagdeev potential obtained in this work, upper panel of Fig. 3.6, has been plotted against "$-\varphi$" for ease of comparison. It is seen from Fig. 3.6 that we obtain the Sagdeev potential reported by Verheest et al. (2008), in their Fig. 6.

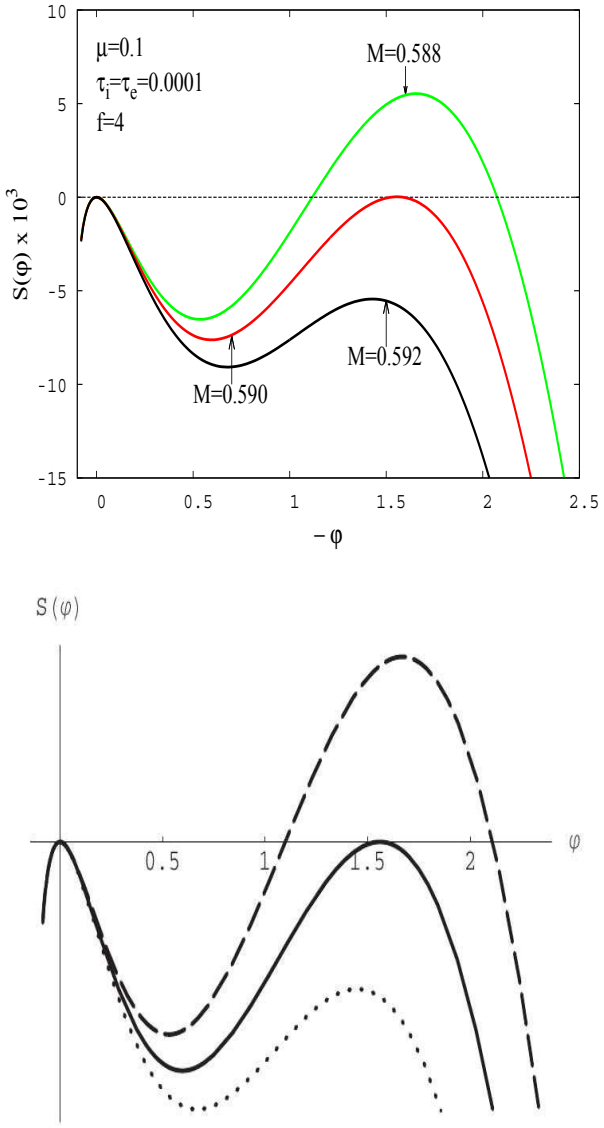

Figure 3.6: Comparison of the Sagdeev potential obtained in this work (upper panel) with that of Verheest et al. (2008) (lower panel). The Sagdeev potential presented in the upper panel corresponds to $S(\varphi)_-$ given by Eq. (3.69) for parameter values shown in the figure, whereas that presented in the lower panel is Fig. 6 of Verheest et al. (2008). The values of μ, f, and M are as used by Verheest et al. (2008), in their Fig. 6.

Calculating the first and the second derivatives of $S(\varphi)_\mp$ we obtain,

respectively,

$$S^{'}(\varphi)_{\pm} = -(1+f)\exp(\tau_e\varphi) + \frac{f}{2\sqrt{\tau_i}}\Bigg\{\Bigg[\left(\frac{M}{\sqrt{\mu}}+\sqrt{\tau_i}\right)^2 - 2\varphi\Bigg]^{1/2}$$
$$-\Bigg[\left(\frac{M}{\sqrt{\mu}}-\sqrt{\tau_i}\right)^2 - 2\varphi\Bigg]^{1/2}\Bigg\} + \frac{1}{2}\Bigg\{\Bigg[(1+M)^2-2\varphi\Bigg]^{1/2} \pm \Bigg[(1-M)^2-2\varphi\Bigg]^{1/2}\Bigg\}, \tag{3.70}$$

and

$$S^{''}(\varphi)_{\mp} = -\tau_e(1+f)\exp(\tau_e\varphi) + \frac{f}{2\sqrt{\tau_i}}\Bigg\{\Bigg[\left(\frac{M}{\sqrt{\mu}}-\sqrt{\tau_i}\right)^2 - 2\varphi\Bigg]^{-1/2}$$
$$-\Bigg[\left(\frac{M}{\sqrt{\mu}}+\sqrt{\tau_i}\right)^2 - 2\varphi\Bigg]^{-1/2}\Bigg\} + \frac{1}{2}\Bigg\{-\Bigg[(1+M)^2-2\varphi\Bigg]^{-1/2} \mp \Bigg[(1-M)^2-2\varphi\Bigg]^{-1/2}\Bigg\}. \tag{3.71}$$

From (3.69) and (3.70), we find that for both the slow and the fast modes $S(0) = S^{'}(0) = 0$, as required by Sagdeev potential theory (e.g. Verheest et al. (2008); Verheest & Hellberg (2010b); Verheest et al. (2011)). Here, a prime denotes the derivative of $S(\varphi)$ with respect to φ.

The standard approach to Sagdeev theory (e.g. Verheest et al. (2008); Verheest & Hellberg (2010b); Verheest et al. (2011)) states that, if parameter values are obtained from a correct soliton existence domain, the Sagdeev potential represents a soliton or a double layer only if $S(\varphi)$ has a local maximum at the origin, $\varphi = 0$, and hence

$$S^{''}(0) < 0. \tag{3.72}$$

It is well-known (e.g. Verheest et al. (2008); Hellberg et al. (2010); Verheest & Hellberg (2010b); Verheest et al. (2011)) that the true acoustic speed $M = M_s$ can be obtained from the second derivative of the Sagdeev potential evaluated at $\varphi = 0$, that is,

$$S^{''}(0) = 0. \tag{3.73}$$

In some plasma models, recent studies (e.g. Baluku et al. (2010a,b); Verheest & Hellberg (2010c); Verheest (2010)) have shown that solitons with finite amplitudes may exist at the acoustic speed, contrary to the KdV

theory and the Sagdeev two-fluid model, which allow only strictly super-acoustic solitons. Thus, this led to a more general representation of the soliton condition given by (3.72) as (Hellberg et al., 2010)

$$S^{''}(0) \leq 0. \tag{3.74}$$

Equation (3.74) means that the origin, i.e. the point ($\varphi = 0, S(0) = 0$), is either a local maximum or a point of inflexion.

The condition (3.73), together with (3.69) and (3.71), yields

$$-(1+f)\tau_e \mp \frac{1}{1-M_s^2} + \frac{\mu f}{M_s^2 - \tau_i \mu} = 0. \tag{3.75}$$

We note that, in Eq. (3.75), the denominator of the second term is $1 - M_s^2$ if the upper sign $(-)$ is considered, but becomes $M_s^2 - 1$ if the lower sign $(+)$ is used. However, whether the lower or the upper sign is considered, Eq. (3.75) is equivalent to

$$\tau_e(1+f)M_s^4 - [1+\mu f+\tau_e(1+f)(1+\mu\tau_i)]M_s^2 + \mu\tau_i\tau_e(1+f)+\mu\tau_i+\mu f = 0. \tag{3.76}$$

It is seen that Eq. (3.76) is exactly the same as Eq. (3.9), i.e. the normalised linear dispersion relation of ion acoustic waves discussed in detail in Sec. 3.3. It has also been obtained using the KdV approach (see Eq. (3.50)). Indeed, it is well-known that, for a given plasma model, the acoustic speed can be obtained from linear theory, KdV theory, or Sagdeev potential theory (e.g. Verheest (2008); Verheest et al. (2008)). The fact that the three different approaches led to exactly the same result gives us more confidence that our results are correct.

3.5.3 Thermal effects on ion acoustic solitons and double layers: The slow mode

a. General features of the slow mode ion acoustic solitons and double layers

As discussed in Sec. 3.3 for the case of the slow linear wave, this mode has a phase speed that lies between the thermal speeds of the two ion species

so that the Mach number of a slow soliton/double layer lies in the range

$$\sqrt{\mu\tau_i} < M < 1. \tag{3.77}$$

The Sagdeev potential for this mode is given by $S(\varphi)_-$, in (3.69). It is seen that there are critical values of the electrostatic potential (φ_l) beyond which $S(\varphi)_-$ becomes complex. They are

$$\varphi_{lh-} = \frac{1}{2}\left(1 - M_l\right)^2, \tag{3.78}$$

and

$$\varphi_{lc} = \frac{1}{2}\left(\frac{M_l}{\sqrt{\mu}} - \sqrt{\tau_i}\right)^2. \tag{3.79}$$

In these equations, the subscript l associated with the potential φ and the Mach number M refers to "limit", to emphasise the fact that φ_l and M_l are, respectively, the limiting potential and Mach number. As usual the subscripts "h" and "c" stand for "hotter" and "cooler", as the densities of the hotter and the cooler ion species become complex beyond those limiting potentials. The minus sign associated with φ_h, in Eq. (3.78), emphasises the fact that, in this case, the hotter ions are treated as subsonic (see the discussion associated with Eq. (3.69)). Throughout this subsection, the "$-$" sign associated with various quantities refers to the slow mode. This notation should be borne in mind, as it will appear many times in our subsequent discussions.

It is well-known (e.g. Verheest et al. (2008)) that the above limiting potentials occur when the flow of the adiabatic species reaches a sonic point, yielding a so-called choked flow (McKenzie, 2002a). We recall that a sonic point has been discussed in Sec. 1.1. For the plasma model considered in this work, there are two ion sonic points, namely, the hotter and the cooler ion sonic points. In the subsequent discussion, solitons whose limiting potentials are given by Eqs. (3.78) and (3.79) will be referred to as "solitons limited by the hotter ion sonic point" and "solitons limited by the cooler ion sonic point", respectively.

Analysis of the relative positions of the curves φ_{lh-} (M_l) and φ_{lc} (M_l) provides useful information for the study of the soliton existence domain.

The slopes of these curves are given by

$$\frac{d\varphi_{lh-}}{dM_l} = M_l - 1, \tag{3.80}$$

and

$$\frac{d\varphi_{lc}}{dM_l} = \frac{1}{\mu}(M_l - \sqrt{\mu\tau_i}), \tag{3.81}$$

respectively. Since, for the slow mode, we require that $\sqrt{\mu\tau_i} < M < 1$, see (3.16), it follows that the curve φ_{lh-} (M_l) has a negative slope, whereas the slope of the curve φ_{lc} (M_l) is positive, suggesting a definite crossover (co) from one limiting potential to the other. This occurs when φ_{lc} $(M_l) = \varphi_{lh-}$ (M_l) at a value of $M_l = M_{co-}$ given by

$$M_{co-} = \frac{(1+\sqrt{\tau_i})\sqrt{\mu}}{1+\sqrt{\mu}}. \tag{3.82}$$

It is seen that Eq. (3.82) reduces to Eq. (31) of Verheest et al. (2008) in the limit of vanishing τ_i. Furthermore, we see that, for a fixed value of μ, an increase in τ_i leads to an increase in M_{co-}. It will be shown later that this result has a significant impact on the maximum Mach numbers.

When $\varphi_{lc} < \varphi_{lh-}$ or equivalently

$$0 < M_l < M_{co-}, \tag{3.83}$$

the limitation on the soliton existence is due to the occurrence of the cooler ion sonic point. From Eq. (3.83), and with information about the effect of τ_i on M_{co-} that we have from Eq. (3.82), we already see that an increase in the value of τ_i leads to a larger range in M over which soliton Mach numbers are limited by the cooler ion sonic point.

On the other hand, the soliton limitation is due to the occurrence of the hotter ion sonic point if $\varphi_{lh-} < \varphi_{lc}$ or equivalently

$$M_l > M_{co-}. \tag{3.84}$$

However, as shown by Verheest et al. (2008, 2011) for the case $\tau_i = 0$, and as we will show later considering arbitrary values of τ_i, the plasma model considered in this work supports double layers (dl) with Mach numbers in the range

$$M_{co-} < M_{dl} < 1. \tag{3.85}$$

Hence, for this range, the maximum Mach numbers result from the occurrence of either the hotter ion sonic point or double layers. It will be shown, later, that this is so depending on the value of f (the normalised density of the cooler ions).

In the study of solitons, the determination of soliton existence domain is important because when the domain of existence is clarified, further investigation of solitons can readily be carried out by taking parameter values from a well-defined parameter space (e.g. Verheest et al. (2008); Verheest & Hellberg (2010b); Verheest et al. (2011)). In this context, the lower limit in Mach numbers for the existence of solitons is given by the acoustic speed, whereas the upper limit results from various limitations on the soliton speed (e.g. Verheest et al. (2008); Verheest & Hellberg (2010b); Verheest et al. (2011)). For the plasma model under consideration, in particular, the upper limit in Mach numbers, i.e. maximum soliton speeds, is obtained either when the densities of the adiabatic species become complex or when double layers occur. As mentioned earlier, the former case corresponds to positions in space where the flow of the adiabatic species reaches a sonic point (e.g. Verheest et al. (2008)).

In order to allow a comparison of our results with those of Verheest et al. (2008) when the thermal effects of the cooler ions are negligible, we present the soliton existence domains in $\{f, M\}$ parameter space, following Verheest et al. (2008), where we recall that f is the density of the cooler ion species normalised with respect to the density of the hotter ion species.

To find a relation between f and the maximum Mach numbers due to the occurrence of the sonic points, we have to solve (e.g. Verheest et al. (2008); Verheest & Hellberg (2010b); Verheest et al. (2011))

$$\left.\begin{aligned} S(\varphi_{lc})_- &= 0 \\ S(\varphi_{lh-})_- &= 0 \end{aligned}\right\}. \tag{3.86}$$

Each of the relations (3.86) results from the fact that, for the allowed Mach numbers, the Sagdeev potential represents a soliton only if $S(\varphi) \leq 0$ for the electrostatic potential in the range $0 \leq \varphi \leq \varphi_m$, where φ_m is the soliton amplitude (e.g. Mace et al. (1991)). It is well-known (e.g. Mace

et al. (1991)) that at $\varphi = 0$ and $\varphi = \varphi_m$, the Sagdeev potential representing a soliton must vanish. Thus, at the limiting potentials given by Eqs. (3.78) and (3.79), the Sagdeev potential vanishes and it no longer represents a soliton beyond those limiting potentials.

Therefore, Eq. (3.69) allows us to obtain from the condition $S(\varphi_{lc})_- = 0$ an implicit relation between the plasma composition parameter f and the maximum soliton speed M_l allowed by the cooler ion sonic point as

$$\alpha_{c-} f + \beta_{c-} = 0, \tag{3.87}$$

where

$$\alpha_{c-} = \frac{1}{\tau_e}\left\{1 - \exp\left[\frac{\tau_e}{2}\left(\frac{M_l}{\sqrt{\mu}} - \sqrt{\tau_i}\right)^2\right]\right\} + \frac{1}{6\sqrt{\tau_i}}\left\{2\tau_i\sqrt{\tau_i} + \frac{6M_l^2\sqrt{\tau_i}}{\mu} - \left[\left(\frac{M_l}{\sqrt{\mu}} + \sqrt{\tau_i}\right)^2 - \left(\frac{M_l}{\sqrt{\mu}} - \sqrt{\tau_i}\right)^2\right]^{3/2}\right\}, \tag{3.88}$$

and

$$\beta_{c-} = \frac{1}{\tau_e}\left\{1-\exp\left[\frac{\tau_e}{2}\left(\frac{M_l}{\sqrt{\mu}}-\sqrt{\tau_i}\right)^2\right]\right\}+\frac{1}{6}\left\{2+6M_l^2-\left[(1+M_l)^2-\left(\frac{M_l}{\sqrt{\mu}}-\sqrt{\tau_i}\right)^2\right]^{3/2} - \left[(1-M_l)^2 - \left(\frac{M_l}{\sqrt{\mu}} - \sqrt{\tau_i}\right)^2\right]^{3/2}\right\}, \tag{3.89}$$

provided $(1 - M_l)^2 - \left(M_l/\sqrt{\mu} - \sqrt{\tau_i}\right)^2 \geq 0$ or simply $0 < M_l \leq M_{co-}$, recalling that M_{co-} is given by Eq. (3.82). Neglecting the thermal effects of the cooler ions (i.e. $\tau_i \to 0$) and assuming that the electrons are much hotter than the hotter ions (i.e. $\tau_e \to 0$), we find that Eq. (3.87) reduces to Eq. (32) of Verheest et al. (2008). Here, in comparing our results with those of Verheest et al. (2008), it should be noted that we have preferred to associate a subscript l with M, to emphasise the fact that the Mach number that we are referring to is the limiting/maximum Mach number, unlike Verheest et al. (2008) who use just M.

Similarly, from Eq. (3.69) and the condition $S(\varphi_{lh-})_- = 0$, we obtain an implicit relation between the plasma composition parameter f and the

maximum soliton speed M_l allowed by the hotter ion sonic point as

$$\alpha_{h-} f + \beta_{h-} = 0, \tag{3.90}$$

where

$$\alpha_{h-} = \frac{1}{\tau_e}\left\{1 - \exp\left[\frac{\tau_e}{2}\left(1 - M_l\right)^2\right]\right\} + \frac{1}{6\sqrt{\tau_i}}\left\{2\tau_i\sqrt{\tau_i} + \frac{6M_l^2\sqrt{\tau_i}}{\mu}\right.$$
$$\left. - \left[\left(\frac{M_l}{\sqrt{\mu}} + \sqrt{\tau_i}\right)^2 - (1 - M_l)^2\right]^{3/2} + \left[\left(\frac{M_l}{\sqrt{\mu}} - \sqrt{\tau_i}\right)^2 - (1 - M_l)^2\right]^{3/2}\right\}, \tag{3.91}$$

and

$$\beta_{h-} = \frac{1}{\tau_e}\left\{1-\exp\left[\frac{\tau_e}{2}\left(1-M_l\right)^2\right]\right\}+\frac{1}{6}\left\{2+6M_l^2-\left[\left(1+M_l\right)^2-\left(1-M_l\right)^2\right]^{3/2}\right\}, \tag{3.92}$$

provided $\left(M_l/\sqrt{\mu} - \sqrt{\tau_i}\right)^2 - (1 - M_l)^2 \geq 0$ or simply $M_l \geq M_{co-}$. It is found that in the limit of vanishing τ_i and τ_e, Eq. (3.90) reduces to Eq. (33) of Verheest et al. (2008).

As mentioned briefly earlier, it is well-known (e.g. Verheest et al. (2008, 2011)) that, in a certain range of parameter values, the plasma model under consideration supports double layers of both polarities (negative and positive) and that the double layer Mach numbers determine the maximum Mach numbers for solitons of a given polarity.

The conditions for the occurrence of double layers are (e.g. Baboolal et al. (1988); Raadu & Rasmussen (1988); Verheest et al. (2008))

$$\left.\begin{aligned} S(\varphi_{dl}, M_{dl}) &= 0 \\ S^{'}(\varphi_{dl}, M_{dl}) &= 0 \end{aligned}\right\}, \tag{3.93}$$

where the prime denotes the derivative with respect to φ, $|\varphi_{dl}|$ and M_{dl} are, respectively, the double layer amplitude and the corresponding Mach number. In addition, acceptable M_{dl} values must satisfy the conditions $S^{''}(0, M_{dl}) < 0$ and $S^{''}(\varphi_{dl}, M_{dl}) < 0$, i.e. the Sagdeev potential has a local maximum at both the origin and the root (amplitude of the double layer). Furthermore, for the slow mode, $M_{s-} < M_{dl} < 1$.

Having discussed the general features of the slow mode ion acoustic solitons, we now consider the point of the work presented in this subsection, i.e. the thermal effects of the cooler ion species on solitons and double layers. In our discussion, we assume that the electrons are much hotter than the hotter ion species, so that $\tau_e \to 0$. This assumption allows us to compare some of our results with those of Verheest et al. (2008) when the thermal effects of the cooler ion species are omitted.

While Verheest et al. (2008) considered the above approximation for the electrons (i.e. $\tau_e \to 0$), Verheest et al. (2011) investigated the effects of the electron temperature on slow solitons and double layers by varying τ_e from 0.1 to 1 (i.e. by reducing the electron temperature from $10T_h$ to T_h). We recall that the results of Verheest et al. (2008) and Verheest et al. (2011) have been discussed in detail in Sec. 3.1. Thus, the effects of the electron temperature on slow solitons and double layers are not considered in this work.

b. The effects of the ion temperature on the existence domain of the slow mode ion acoustic solitons

The thermal effects of the cooler ion species on the existence domain of the slow mode ion acoustic solitons are investigated numerically.

We have shown in Sec. 3.3 (see Fig. 3.1) that the acoustic speed increases as the ion temperature is increased. This is already a first effect of the ion temperature on the soliton existence domain, since the acoustic speed determines the lower limit for the existence of solitons.

The next step is to investigate how the upper limits are affected by the ion temperature. For given values of μ, τ_i, and τ_e, we consider Eqs. (3.87) and (3.90) to obtain the values of f and the maximum Mach numbers due to the occurrence of the cooler and the hotter ion sonic points, respectively. Furthermore, considering the expression of the Sagdeev potential given by Eq. (3.69), and for given f, μ, τ_i, and τ_e, we solve simultaneously Eqs. (3.93) to obtain the double layer amplitudes and the corresponding Mach numbers which may determine the maximum Mach numbers for solitons of a given polarity.

For fixed values of μ and τ_e, we present the existence domain in $\{f, M\}$ parameter space, showing the effect of increasing the ion temperature, ex-

pressed through τ_i. We follow Verheest et al. (2008) and consider the cases μ=0.1, 1, and 10 (see Fig. 4 of Verheest et al. (2008) for the case τ_i=0). For reasons of graphical clarity, we discuss, for each value of μ, the effect of the ion temperature on the existence domain by varying τ_i from 0.0001 to one higher value. In Appendix C, we present the existence domains for other values of τ_i that will be useful for further study of solitons.

Figure 3.7 shows the results obtained for μ=0.1. Let us first consider the existence domain obtained for $\tau_i = 0.0001$. The lower curve indicated by the red solid line represents the lower limit for the existence of solitons and corresponds to the acoustic speed, i.e. Eq. (3.10), whereas the upper limit results from various physical limitations on the soliton speed, as explained below.

At vanishing f, the upper limit in Mach number indicated by the blue dashes is due to the occurrence of the cooler ion sonic point. It is seen that the maximum Mach number increases with increasing f up to a value given by M_{co-} (see Eq. (3.82)) beyond which the limitation is due to the hotter ion sonic point.

The latter limit is shown by the thick pink solid line. Again, the maximum Mach number is seen to increase with increasing f until a value of f is reached, beyond which the Mach number is limited by the occurrence of positive double layers.

The limit due to positive double layers is shown by the black thin solid line. It is observed that the positive double layer Mach number increases with increasing f, and that there exists a value of f at which the polarity changes from positive to negative. In the vicinity of the value of f at which there is a polarity switch, the double layer Mach number is very close to the acoustic speed. We will return to this point later, in this subsection, where we will also show that, in the vicinity of the polarity switch, the double layer amplitude is vanishingly small.

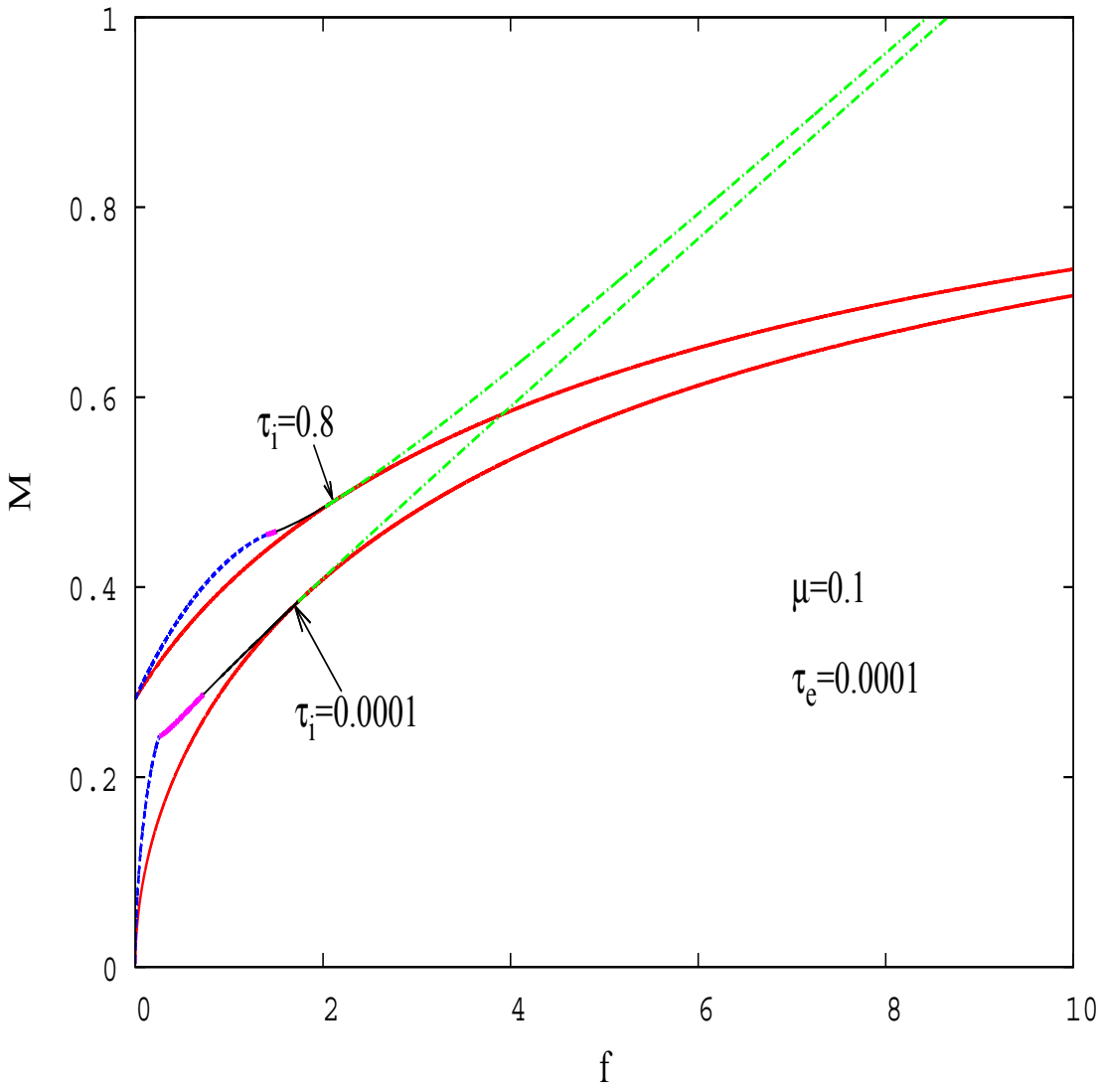

Figure 3.7: The existence domain of the slow mode ion acoustic solitons for μ=0.1 and τ_e=0.0001, showing the effect of increasing τ_i from 0.0001 to 0.8. The lower solid line represents the lower limit in Mach numbers for the existence of solitons and corresponds to the acoustic speed (see Eq. (3.10)), whereas the upper limit results from the occurrence of the cooler ion sonic point (blue dashed line), the hotter ion sonic point (thick pink solid line), positive double layers (thin black solid line), and negative double layers (green dot-dashed line). The cutoff observed for $M = 1$ is imposed by the model (see the ordering (3.16)).

Unlike the other physical limitations on the Mach number, negative double layers, shown by the green dot-dashed line, occur over a relatively large range in f. They have a Mach number that increases with increasing f until the restriction on M (i.e. $M = 1$), imposed by the model, is reached.

An important point to note is that, for a fixed value of f, allowed soliton Mach numbers lie between the acoustic speed and the maximum Mach number, as shown in Fig. 3.7, and this should be borne in mind when interpreting all our $\{f, M\}$ soliton existence domains.

We now consider the effect of increasing the ion temperature. We show in Fig. 3.7 the effect of increasing τ_i from 0.0001 to 0.8. It is seen that this large increase in τ_i leads to an increase in both the minimum and the maximum Mach numbers, irrespective of the value of f. Importantly, it is observed that the effect of the ion temperature on the maximum Mach number depends on the nature of the physical limitation on a soliton.

As a result of an increase in τ_i, the range in f over which soliton amplitudes are limited by the cooler ion sonic point increases significantly, whereas that for solitons limited by the hotter ion sonic point decreases. For the case that is analogous to the work of Verheest et al. (2008), i.e. $\tau_i = 0.0001$, the range in f for a limitation by the cooler ion sonic point is $0 \lesssim f \lesssim 0.25$, whereas the hotter ion sonic point limits solitons over $0.25 \lesssim f \lesssim 0.72$. Increasing τ_i to 0.8 causes these ranges to become $0 \lesssim f \lesssim 1.4$ and $1.4 \lesssim f \lesssim 1.5$, respectively.

As can be seen from Fig. 3.7, the range in f over which double layers occur also decreases due to an increase in τ_i, an effect which is more pronounced for the case of positive double layers. For the "cold" case, $\tau_i = 0.0001$, positive double layers occur within $0.7 \lesssim f \lesssim 1.7$, whereas negative double layers occur over the range $1.7 \lesssim f \lesssim 8.6$. When we increase τ_i to 0.8, we find that these ranges become, respectively, $1.5 \lesssim f \lesssim 2$ and $2 \lesssim f \lesssim 8.4$.

The above effects of τ_i on the maximum Mach numbers could be predicted from Eqs. (3.82), (3.83), (3.84), and (3.85), where it was shown that the Mach number at which the limiting potentials due to the occurrence of the cooler and the hotter ion sonic points cross over, i.e. M_{co-}, increases due to an increase in τ_i.

Having discussed in detail the existence domain, and the effect of the ion temperature on it, for a case where the cooler ions are heavier than the hotter ones, we now consider a case in which the two ion species have equal

mass, showing the results in Fig. 3.8. The structure of the existence domain obtained for $\tau_i = 0.0001$ is qualitatively similar to its counterpart in the case μ=0.1, discussed above, but it is useful to note that as a result of an increase in μ, the range in f over which the sonic points and double layers occur decreases (see also Fig. 4 of Verheest et al. (2008)). Here we only emphasise the effect of increasing the ion temperature.

If τ_i is increased from 0.0001 to 0.4, the existence domain is shifted to much higher Mach numbers than observed in the case $\mu = 0.1$ illustrated in Fig. 3.7, for all values of f, and positive solitons are limited mostly by the cooler ion sonic point and negative solitons by negative double layers. It is seen that, for $\tau_i = 0.4$, the limitations of positive solitons by the hotter ion sonic point and by double layers are found only within very narrow ranges of f, being respectively, $0.75 \lesssim f \lesssim 0.77$ and $0.77 \lesssim f \lesssim 0.9$.

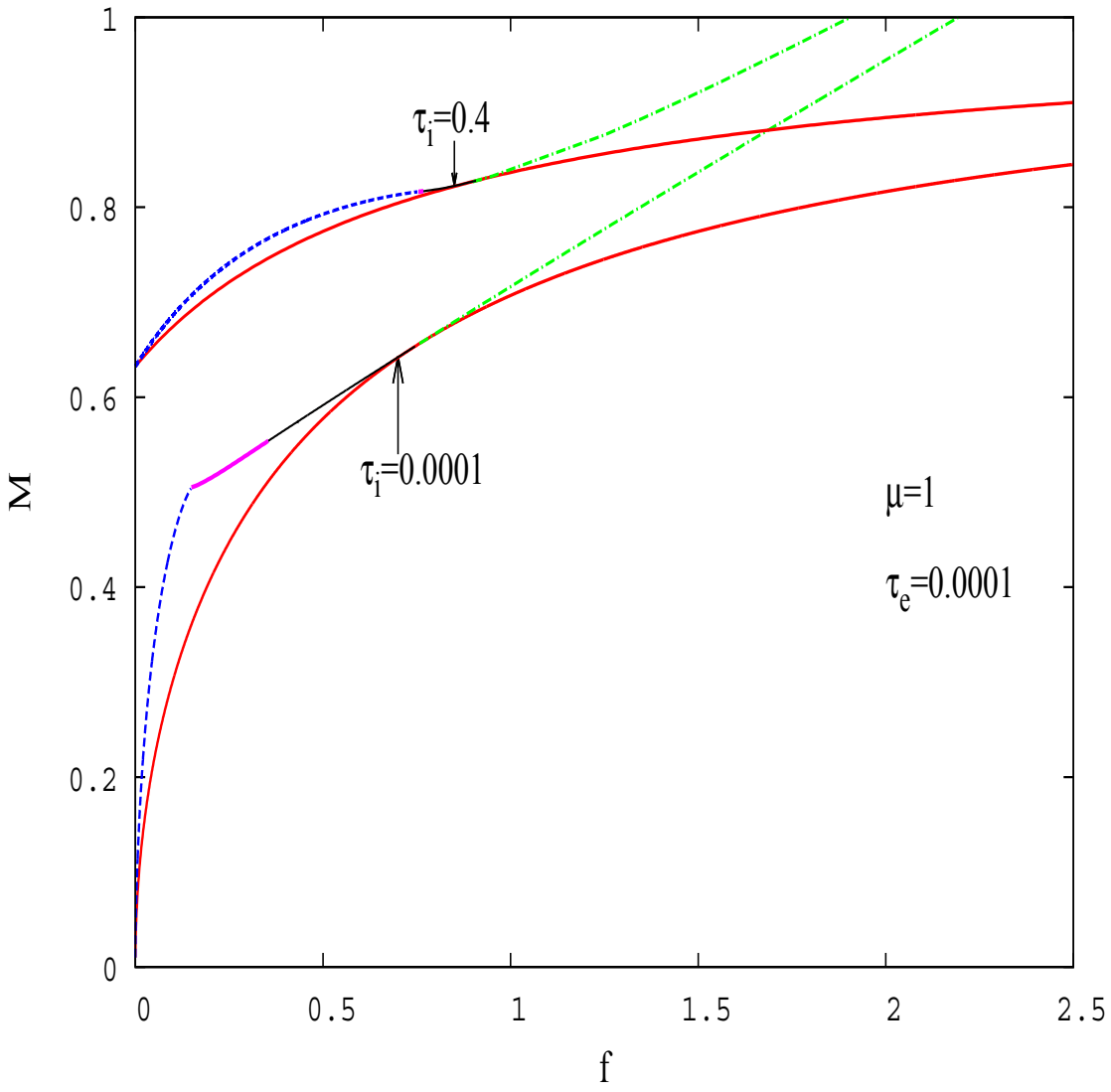

Figure 3.8: The existence domain of the slow mode ion acoustic solitons for $\mu = 1$ and $\tau_e = 0.0001$, showing the effect of increasing τ_i from 0.0001 to 0.4. The line styles are as in Fig. 3.7. The cutoff observed for $M = 1$ is imposed by the model (see the ordering (3.16)).

The above effects of τ_i on the existence domain of the slow mode ion acoustic solitons are even more pronounced for higher values of μ. We consider the case $\mu = 10$ and show the results in Fig. 3.9. We recall that the values of μ and τ_i must be chosen in such a way that $\mu\tau_i < 1$, and therefore in the case $\mu = 10$, the allowed values of τ_i must be less than 0.1. The effects of τ_i on the existence domain that we observed in the case $\mu = 1$ (see Fig. 3.8) are also observed here even for the values of τ_i as small as 0.05. The results obtained for higher values of τ_i (not shown here, but could be predicted from Fig. 3.9) show that the allowed Mach numbers are shifted to values very close to 1 over the whole range of f.

As mentioned earlier, the existence domains obtained for other values of τ_i that will be needed for further investigation of solitons are presented in Appendix C.

Summary

From the results discussed above for various values of μ and τ_i, and considering the existence domains presented in Appendix C, for other values of τ_i, our findings can be summarised as follows.

As the ion temperature is increased, both the acoustic speed and the maximum soliton speed are shifted to higher values, over the whole range of f, and this effect is enhanced as the value of μ is increased.

The effect of the ion temperature on the maximum Mach number depends on the nature of the physical limitation on a soliton. As a result of an increase in the ion temperature, the range in f over which soliton amplitudes are limited by the cooler ion sonic point increases, whereas that for other physical limitations decreases. The latter decrease in the range in f is more pronounced for the limitation by the hotter ion sonic point and positive double layers than for negative double layers.

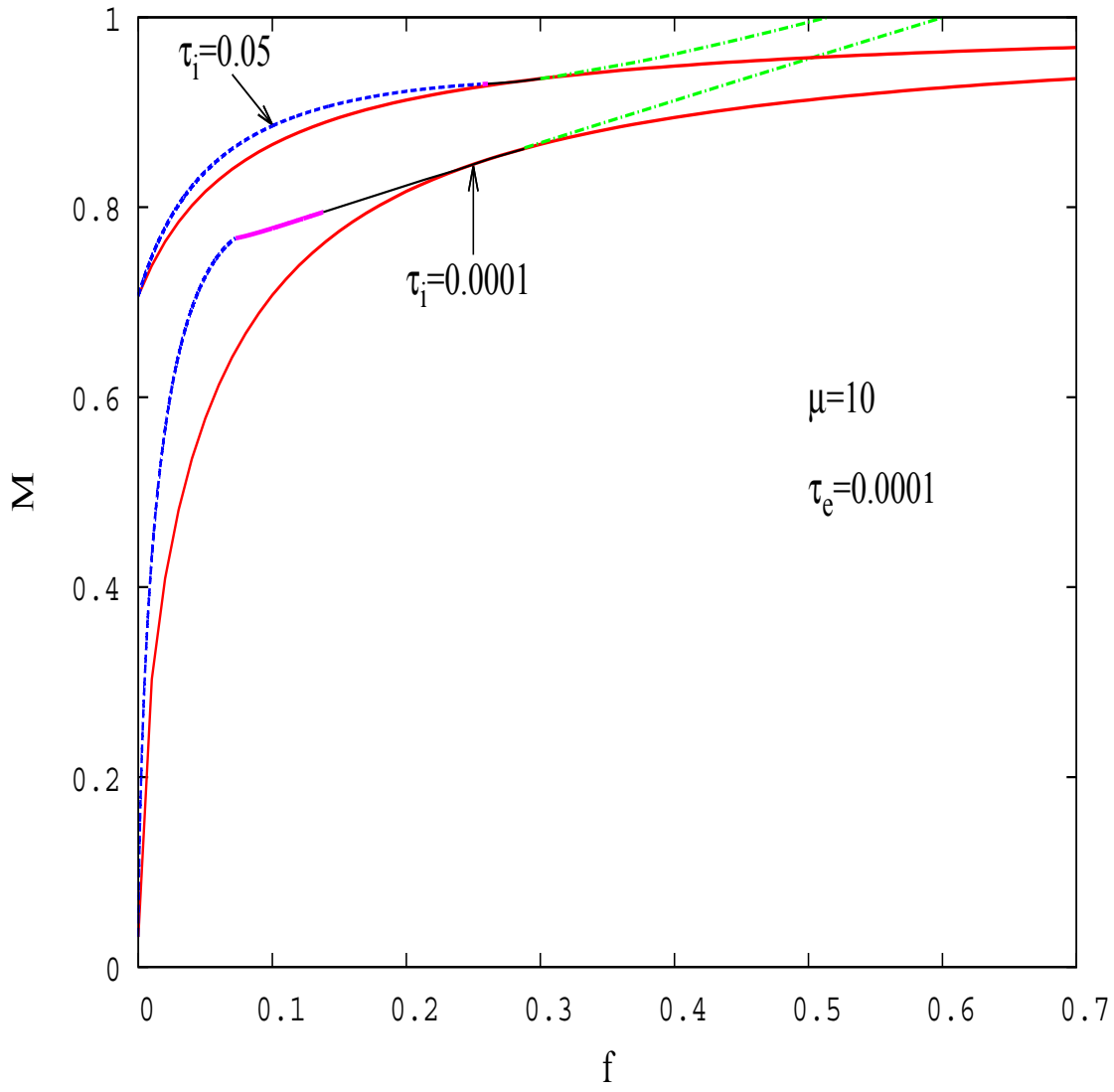

Figure 3.9: The existence domain of the slow mode ion acoustic solitons for $\mu = 10$ and $\tau_e = 0.0001$, showing the effect of increasing τ_i from 0.0001 to 0.05. The line styles are as in Fig. 3.7. The cutoff observed for $M = 1$ is imposed by the model (see the ordering (3.16)).

c. The effects of the ion temperature on the amplitudes and peak profile steepness of the slow mode ion acoustic solitons and double layers

Having established the $\{f, M\}$ soliton existence domains for various values of τ_i, clearly showing that, for a given value of f, the soliton speeds increase as the value of τ_i is increased, we now investigate the effects of the ion temperature on the amplitudes and profile steepness of the slow mode ion acoustic solitons and double layers.

We have shown, in this subsection, that the maximal Mach numbers, i.e. the Mach numbers beyond which solitons do not exist, result from various physical limitations, namely, the occurrence of the cooler ion sonic point, the hotter ion sonic point, positive double layers, and negative double layers.

Considering each of the above physical limitations on the soliton Mach number/speed, we discuss the effect of τ_i on the maximal/extreme amplitudes, for a given value of f. As in all other discussions of the slow mode solitons/double layers, we assume that the electrons are much hotter than the hotter ion species, and use $\tau_e = 0.0001$. A similar analysis was carried out by Verheest et al. (2008) (see their Fig. 5), but for only the case $\mu = 1$ and $\tau_i = 0$. Here, we consider the cases $\mu = 0.1$, $\mu = 1$, $\mu = 10$, and show the effect of increasing the value of τ_i from 0.0001 to a higher value, for each of these values of μ.

For the ease of comparison of our results with those of Verheest et al. (2008)), we present the results as plots of "$-$Extreme φ_m" against f. Usually, the symbol φ_m is used to denote the arbitrary amplitude of a soliton. For our plots, we preferred to use the notation "Extreme φ_m" to make it clear that we are referring to the extreme/maximal amplitudes. Furthermore, the polarity (sign) of solitons discussed by Verheest et al. (2008)) is opposite to that of solitons discussed in this work. Thus, presenting our results as plots of "$-$Extreme φ_m" against f makes it easier for us to compare our results with those of Verheest et al. (2008)).

Figure 3.10 illustrates the results obtained for $\mu = 0.1$, showing the effect of increasing the value of τ_i from 0.0001 to 0.4. The maximal amplitudes due to the cooler ion sonic point are shown by the blue dashes, the thick pink solid lines represent the maximal amplitudes due to the hotter ion sonic point, the thin black solid lines show positive double layer amplitudes, the green dot-dashes indicate negative double layer amplitudes, whereas the dots represent the maximal amplitudes obtained when the constraint $M < 1$, imposed by the model, is reached (see Eq. (3.16) and Fig. 3.7).

It is seen from Fig. 3.10 that, as a result of increasing the value of τ_i from 0.0001 to 0.4, the curves obtained for these two values of τ_i cross over at $f \sim 1.2$ and $|\varphi_m| \sim 0.18$. Consequently, this increase in τ_i leads to a decrease or an increase in the magnitude of the extreme amplitudes, i.e. Extreme $|\varphi_m|$, depending on the value of f.

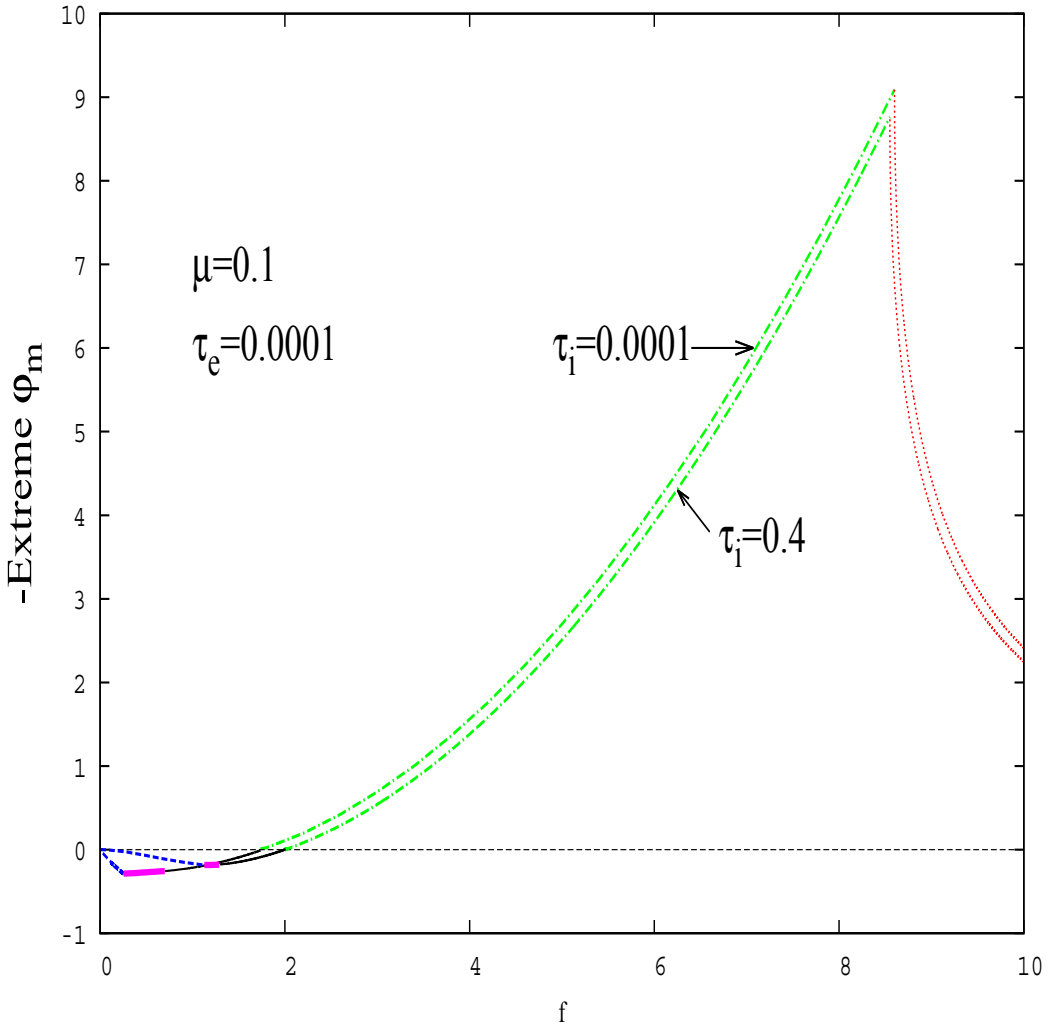

Figure 3.10: The normalised extreme amplitudes plotted against the normalised densities of the cooler ions for $\mu = 0.1$ and $\tau_e = 0.0001$, showing the effect of increasing the value of τ_i from 0.0001 to 0.4. The maximal amplitudes due to the cooler ion sonic point are shown by the blue dashes, the thick pink solid lines represent the maximal amplitudes due to the hotter ion sonic point, the thin black solid lines show the positive double layer amplitudes, the green dot-dashes indicate the negative double layer amplitudes, whereas the dots represent the maximal amplitudes obtained when the constraint $M = 1$ is reached (see the ordering (3.16)). The curves obtained for the two values of τ_i cross over at $f \sim 1.2$ and $|\varphi_m| \sim 0.18$.

As an illustration, let us consider typical values of f. For $f \sim 0.2$, the extreme amplitudes occur at the cooler ion sonic point. Clearly, for this value of f, the magnitude of the extreme amplitude decreases as a result of increasing the value of τ_i. For $f \sim 6$, there are negative double layers. It is, clearly, seen that, for this value of f, the magnitude of the negative double layer amplitude decreases as the value of τ_i is increased. It should be noted that, whereas for $f \sim 0.2$ increasing the value of τ_i from 0.0001 to 0.4 causes the extreme soliton amplitude to almost vanish, for $f \sim 6$, the same increase in τ_i has a little effect on the magnitude of the negative double layer amplitude. For $f \sim 1.6$, which supports positive double layers, the increment in τ_i, shown in the figure, leads to an increase in the magnitude of the positive double layer amplitude.

In our discussion of the soliton existence domain (see e.g. Fig. 3.7), we reached a conclusion that, as a result of an increase in τ_i, the range in f over which solitons are limited by the cooler ion sonic point increases, whereas that for solitons associated with other physical limitations decreases. Figure 3.10 provides an alternative illustration of this conclusion.

From the results illustrated by the dotted lines of Fig. 3.10, we see that, for a given value of τ_i, the maximal amplitudes obtained when the constraint $M = 1$ is reached (see the ordering (3.16)) decrease with increasing f. This is due to the fact that the acoustic speed tends to 1 as f increases (see Fig. 3.7), and therefore, at large values of f, the maximal Mach numbers are close to the acoustic speed, implying that, in this case, solitons have, in principle, small amplitudes. In fact, for such large values of f, solitons may not exist, as the linear waves would be subject to hotter ion Landau damping, since their phase speeds are very close to the thermal speeds of the hotter ions, and hence solitons are less likely to be sustainable.

In Fig. 3.11, we show the normalised extreme amplitudes plotted against the normalised densities of the cooler ions, but for $\mu = 1$, showing the effect of increasing τ_i from 0.0001 to 0.1. A similar plot has been reported by Verheest et al. (2008), but for the case $\tau_i = 0$ (see their Fig. 5). It is seen that the results obtained for $\tau_i = 0.0001$ are reminiscent of those of Verheest et al. (2008). An increase in τ_i shown in the figure has an effect on the magnitude of the extreme amplitudes that is, qualitatively, similar to that discussed for the case $\mu = 0.1$, presented in Fig. 3.10. However, there are quantitative differences. It is observed that, as a result of increasing μ, for a fixed value of τ_i, the maximal amplitudes decrease significantly. Also, as mentioned in our earlier discussion associated with Figs. 3.7, 3.8, and 3.9, the range in f over which solitons and double layers occur is reduced.

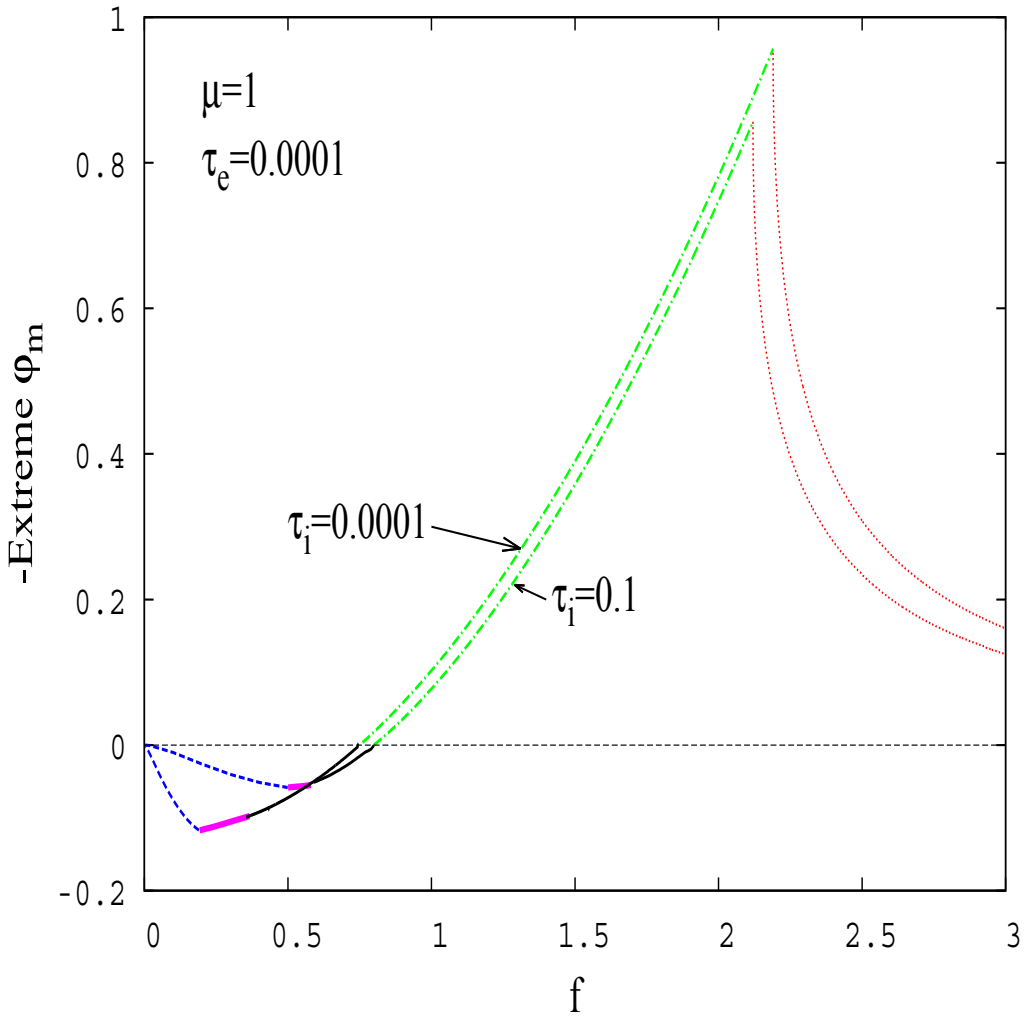

Figure 3.11: The normalised extreme amplitudes plotted against the normalised densities of the cooler ions for $\mu = 1$ and $\tau_e = 0.0001$, showing the effect of increasing τ_i from 0.0001 to 0.1. The curves obtained for the two values of τ_i cross over at $f \sim 0.6$ and $|\varphi_m| \sim 0.05$. The line styles are as in Fig. 3.10.

Figure 3.12 illustrates the results obtained for $\mu = 10$, and we show the effect of increasing the value of τ_i from 0.0001 to 0.02. We recall that the values of μ and τ_i must be chosen in such a way that $\mu\tau_i < 1$. This means that, for $\mu = 10$, all and only values of $\tau_i < 0.1$ are, in principle, allowed. However, we recall from our earlier discussion of the existence domain (see Figs. 3.7, 3.8, and 3.9) that the range in f over which solitons are limited by the hotter ion sonic point and by positive double layers significantly decreases and is shifted to higher values, as a result of increasing the value of τ_i. This can also be seen from Fig. 3.12. Thus, to study the effect of τ_i on the maximal amplitudes of these solitons and on positive double layer amplitudes, for a fixed value of f, one has to consider a small increment in τ_i, such as that considered in Fig. 3.12.

In this figure, positive double layers are found within the range $0.16 \lesssim f \lesssim 0.26$ for $\tau_i = 0.0001$, but this range is reduced to $0.21 \lesssim f \lesssim 0.28$ when the value of τ_i is increased to 0.02. The curves obtained for the two values of τ_i are found to cross over at $f \sim 0.23$, so that the magnitude of the positive double layer amplitudes is reduced within the range $0.21 \lesssim f \lesssim 0.23$, but increased within the range $0.23 \lesssim f \lesssim 0.26$, as a result of that increase in τ_i.

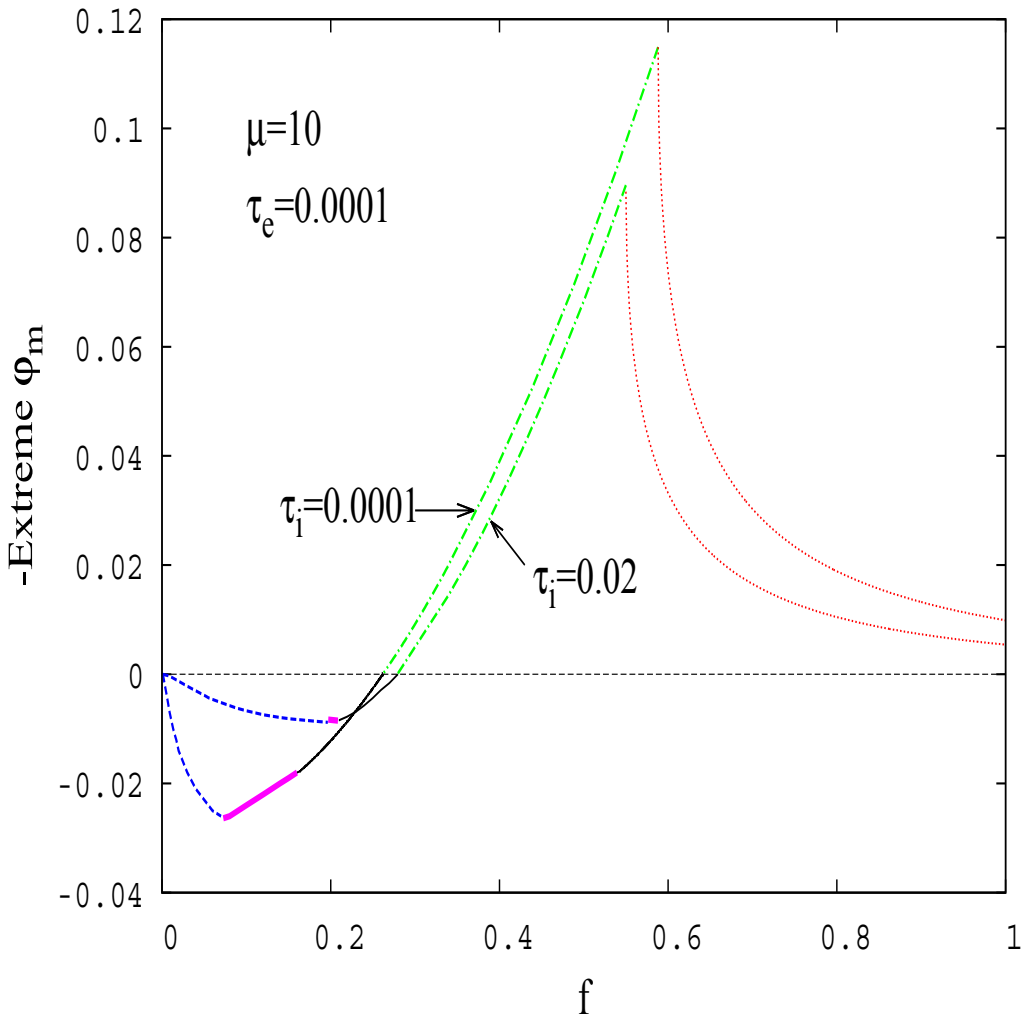

Figure 3.12: The normalised extreme amplitudes plotted against the normalised densities of the cooler ions for $\mu = 10$ and $\tau_e = 0.0001$, showing the effect of increasing τ_i from 0.0001 to 0.02. The curves obtained for the two values of τ_i cross over at $f \sim 0.23$ and $|\varphi_m| \sim 0.007$. The line styles are as in Fig. 3.10.

A further illustration of the effect of τ_i on the magnitude of the positive double layer amplitude is shown in Fig. 3.13. This figure shows plots of the Sagdeev potentials generating positive double layers for $\mu = 10$, and $f = 0.21$ (upper panel), $f = 0.25$ (lower panel), when the value of τ_i is increased from 0.0001 (black) to 0.02 (red). It is clear that due to this increase in τ_i, the magnitude of the positive double layer amplitude decreases for $f = 0.21$, but increases for $f = 0.25$.

However, as shown earlier (see Figs. C.7 and 3.9), the Mach numbers of these positive double layers increase as the value of τ_i is increased, irrespective of the value of f. For $f = 0.21$, the double layer Mach numbers are $M_{dl} = 0.827$ and $M_{dl} = 0.869$ for $\tau_i = 0.0001$ and $\tau_i = 0.02$, respectively. For $f = 0.25$, the double layer Mach numbers are $M_{dl} = 0.845$ and $M_{dl} = 0.879$ for $\tau_i = 0.0001$ and $\tau_i = 0.02$, respectively.

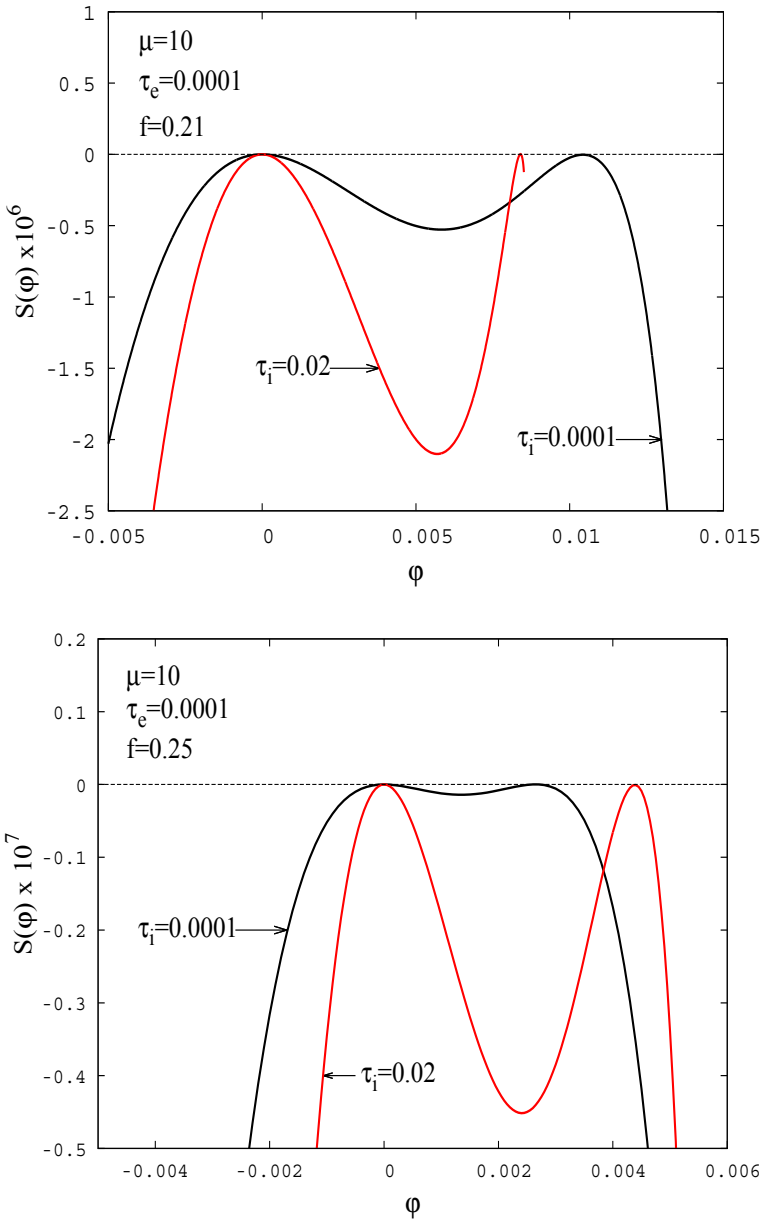

Figure 3.13: Positive double layers for $\mu = 10$, and $f = 0.21$ (upper panel), $f = 0.25$ (lower panel), showing the effect of increasing τ_i from 0.0001 (black curves) to 0.02 (red curves). For $f = 0.21$, the double layer Mach numbers are $M_{dl} = 0.827$ and $M_{dl} = 0.869$ for $\tau_i = 0.0001$ and $\tau_i = 0.02$, respectively. For $f = 0.25$, the double layer Mach numbers are $M_{dl} = 0.845$ and $M_{dl} = 0.879$ for $\tau_i = 0.0001$ and $\tau_i = 0.02$, respectively.

It is well-known from both the KdV and Sagdeev potential theories that, within a given soliton existence domain, the soliton amplitude increases with increasing soliton Mach number/speed (see e.g. Verheest & Hellberg (2010b) and Sec. 3.4 of this work). The KdV theory (see e.g. Sec. 3.4 of this work) predicts a linear relationship between the soliton amplitudes and speeds, and that the soliton amplitude vanishes at the acoustic speed. However, in the case of the arbitrary amplitude solitons, this relationship between the soliton amplitudes and speeds may not necessarily be linear, and for some plasma configurations solitons with finite amplitudes may exist at the acoustic speed (see e.g. Baluku et al. (2010a)).

Here, we study this relationship between the soliton amplitudes and speeds, considering various values of μ, τ_i, and f. In this regard, we calculated the amplitudes for Mach numbers ranging from the maximum value to the acoustic speed, for given values of μ, τ_i, f, and τ_e, and our results are presented in Fig. 3.14 for a series of parameter values.

In this figure, the soliton/double layer amplitudes have been plotted against their true Mach numbers given by M/M_s. It should be noted that we have inverted the sense of $-\varphi_m$ in lower panels, which show results for negative potential solitons, for ease of comparison. For a given value of μ, our analysis is carried out considering various ranges of f (see e.g. Figs. 3.7, 3.8, and 3.9). In this way, we have a broad picture of the effects of the ion temperature on solitons/double layers supported by the plasma model under consideration.

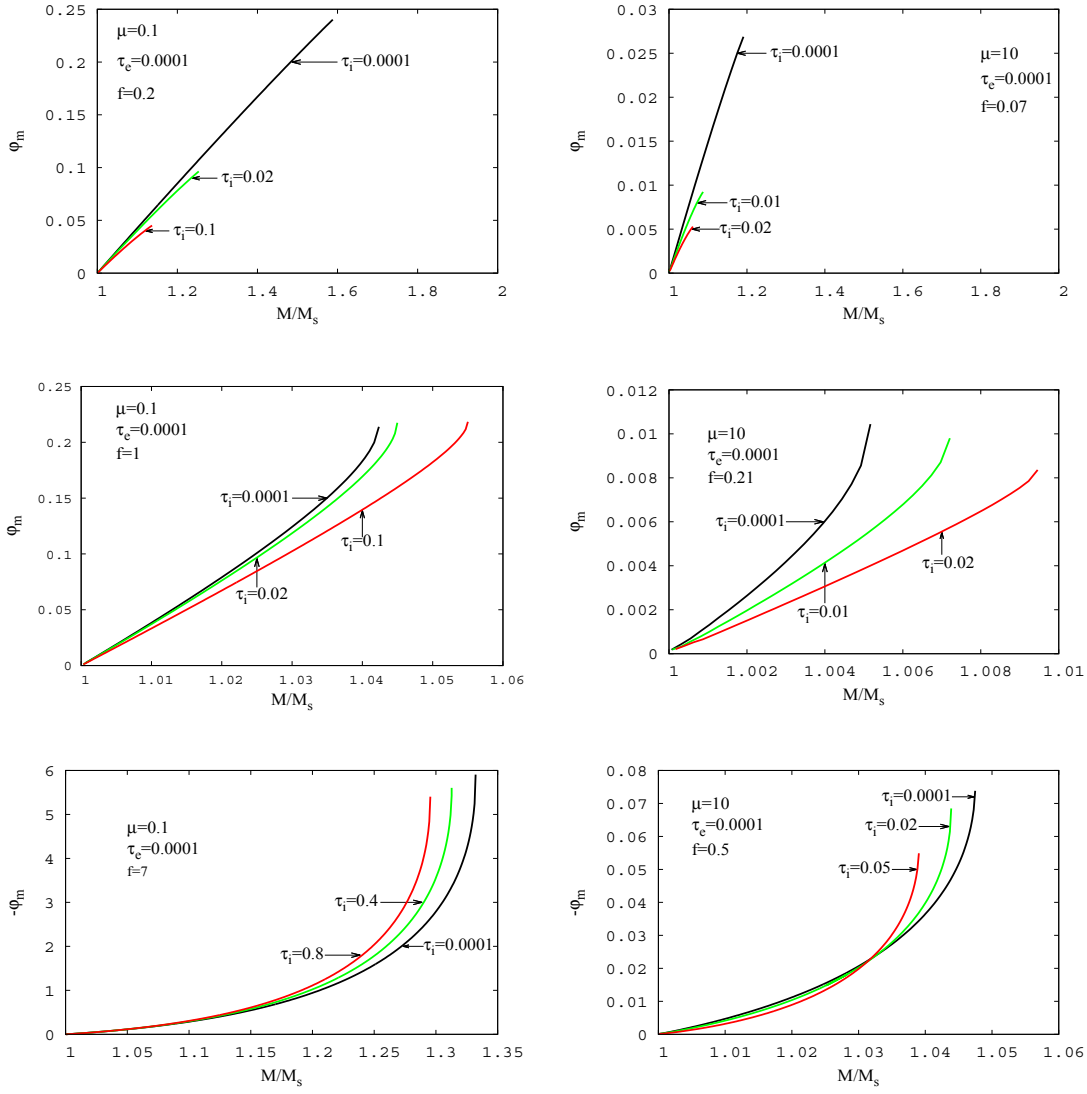

Figure 3.14: The normalised arbitrary amplitudes of the slow mode ion acoustic solitons/double layers plotted against the true Mach numbers, showing the effect of increasing the ion temperature, for $\mu = 0.1$ (left panels) and $\mu = 10$ (right panels). Various values of f that are appropriate for each value of μ are considered. In the left panels, we show the results obtained for $f = 0.2$ (upper left panel), $f = 1$ (middle left panel), and $f = 7$ (lower left panel). In the right panels, we show the results for $f = 0.07$ (upper right panel), $f = 0.21$ (middle right panel), and $f = 0.5$ (lower right panel).

In the left panels of Fig. 3.14, we present the results obtained for $\mu = 0.1$. In this case, the upper left panel shows the results obtained for $f = 0.2$, the middle left panel is for $f = 1$, and the lower left panel is for $f = 7$. For these values of f, the maximal amplitudes are, respectively, due to the occurrence of the cooler ion sonic point, positive double layers, and negative double layers.

In the right panels of Fig. 3.14, we present the results obtained for $\mu = 10$. We recall, once again, from our discussion of the existence domain (see Figs. 3.7, 3.8, and 3.9) that the range in f over which slow solitons/double layers exist is reduced as the value of μ is increased. Thus, the values of f that are appropriate for $\mu = 10$ have been considered. The upper right panel shows the results obtained for $f = 0.07$, the middle right panel is for $f = 0.21$, and the lower right panel is for $f = 0.5$. For these values of f, the maximal amplitudes are, respectively, due to the occurrence of the cooler ion sonic point, positive double layers, and negative double layers.

In our discussion, we consider the results obtained for a given value of μ and study the relationship between the soliton/double layer amplitudes and speeds as we vary f and τ_i. We start from the case $\mu = 0.1$ presented in the left panels of Fig. 3.14.

The results presented in the upper left panel, for $f = 0.2$, show that for a given value of τ_i, the relationship between the soliton amplitudes and speeds is reminiscent of that predicted by the KdV theory. That is, for a given value of τ_i, the soliton amplitude increases almost linearly with increasing soliton speed, and vanishes at the acoustic speed. Furthermore, it is observed that both the maximum amplitude and the ratio of the maximum Mach number to the acoustic speed ($M_{\max}/M_s$) decrease significantly as the value of τ_i is increased, and this is so even for a small increment in τ_i. This means that at high values of τ_i, the amplitudes of these solitons are small and their speeds are of the order of the acoustic speed.

Increasing f to 1, as shown in the middle left panel of Fig. 3.14, we see a different dependence of the maximum amplitude and the ratio $M_{\max}/M_s$ on τ_i. In this case, it is seen that increasing τ_i results in an increase in the maximum amplitude and the ratio $M_{\max}/M_s$. For a given value of τ_i, the soliton amplitude vanishes at the acoustic speed, as observed in the case $f = 0.2$, presented in the upper left panel and discussed above. However, we see that, close to the extreme amplitude values, the relation between the

amplitudes and the speeds is no longer linear.

This nonlinear effect is enhanced for the case $f = 7$, shown in the lower left panel. In this case, we recall that there are negative solitons limited by negative double layers. It is observed that, for a fixed value of M/M_s, the soliton amplitude is larger for a larger value of τ_i, unlike for the cases of positive solitons presented in the upper and middle left panels. An increase in τ_i decreases both the maximum amplitude and the ratio $M_{\max}/M_s$. However, this decrease is so small that the maximum amplitude and the ratio $M_{\max}/M_s$ are still very large even for values of τ_i as large as 0.8. Thus, for $\mu = 0.1$ and $f = 7$, the use of the KdV theory to study these negative solitons and double layers would be inappropriate.

Let us now see what the results look like when we increase μ to 10. In this case, the general and major observation from the results presented in the three right panels is that, for a given value of τ_i, the maximum amplitudes are relatively small and the maximum Mach numbers are closer to the acoustic speed. Thus, the value of $\mu = 10$ has been used to study small amplitude solitons using the KdV approach (see Fig. 3.5).

The results presented in the upper right panel of Fig. 3.14 for $\mu = 10$ and $f = 0.07$ are, qualitatively, similar to those we obtained for $\mu = 0.1$ and $f = 0.2$ (see upper left panel). We note that the value of $f = 0.07$ used to obtain these results is really small. Indeed, for $\mu = 10$ and $\tau_i = 0.0001$, solitons limited by the cooler ion sonic point are found within the range $0 \lesssim f \lesssim 0.07$ (see Fig. 3.9). This range becomes $0 \lesssim f \lesssim 0.2$ for $\tau_i = 0.02$ (see Fig. C.7). Recalling that $f = n_{c0}/n_{h0}$, this means that, in this case, the hotter ions are predominant.

In our earlier discussion related to Figs. 3.10, 3.11, 3.12, and 3.13, we showed that the effect of τ_i on the magnitude of the positive double layer amplitude depends on the value of f. In particular, for $\mu = 10$ and $f = 0.21$ (see upper panel of Fig. 3.13), we showed that an increase in τ_i leads to a decrease in the magnitude of the positive double layer amplitude. This effect of τ_i on the positive double layer amplitude can, alternatively, be seen from the results presented in the middle right panel of Fig. 3.14 (see the highest amplitude for each value of τ_i). Furthermore, it is seen from this figure that whereas the magnitude of the positive double layer amplitude decreases as the value of τ_i is increased, the ratio M_{dl}/M_s increases. However, for the case $\mu = 10$ and $f = 0.25$ (see lower panel of Fig. 3.13), we showed that

increasing the value of τ_i leads to an increase in the magnitude of the positive double layer amplitude, and we will show later, in this subsection, that the same increase in τ_i results in an increase in the ratio M_{dl}/M_s. Thus, had we considered the case $\mu = 10$ and $f = 0.25$ instead of $\mu = 10$ and $f = 0.21$, in the middle right panel of Fig. 3.14, we would have obtained the curves whose trend is, qualitatively, similar to that of the curves presented in the middle left panel of Fig. 3.14, for the case $\mu = 0.1$ and $f = 1$.

From the results shown in the lower right panel of Fig. 3.14, for the case $\mu = 10$ and $f = 0.5$, we see that increasing τ_i has an effect on the magnitude of the negative double layer amplitude (see the highest amplitude in magnitude for each value of τ_i) that is, qualitatively, similar to that observed for the case $\mu = 0.1$ and $f = 7$, presented in the lower left panel. This is in agreement with the results presented in Figs. 3.10, 3.11, and 3.12, where we showed that an increase in τ_i results in a decrease in the magnitude of the negative double layer amplitude for all values of μ that we considered, and for all values of f that support negative double layers. Furthermore, there is a clear crossover of the curves obtained for different values of τ_i at $M \approx 1.033 M_s$, suggesting important nonlinear effects.

From the results presented in all panels of Fig. 3.14, it is clearly observed that there are no solitons with finite amplitudes at the acoustic speed, and this is so irrespective of the values of μ, f, and τ_i that we considered. All solitons are "KdV-like", that is, their amplitudes tend to zero as their speeds approach the acoustic speed. This conclusion was reached by Verheest et al. (2011) who also studied the slow mode solitons and double layers supported by the plasma model under study in this work, but considering only the case $\tau_i = 0$, that is, in their study the cooler ions were treated as cold.

A comparative illustration of the results obtained from the KdV and Sagdeev potential approaches is presented in Fig. 3.15 for $\mu = 10$ and $\tau_e = 0.0001$. We remind the reader that the lower panels, corresponding to negative potential solitons, have potentials inverted for ease of comparison. The upper panel is for $f = 0.07$ and $\tau_i = 0.02$, the middle panel is for $f = 0.21$ and $\tau_i = 0.02$, and the lower panel is for $f = 0.5$ and $\tau_i = 0.05$.

We recall from the soliton existence domain presented in Fig. 3.9 that for $f = 0.07$ there are positive solitons limited by the cooler ion sonic point, for $f = 0.21$ solitons are limited by positive double layers, and for $f = 0.5$ there are negative solitons limited by negative double layers.

We also recall that, for the KdV theory discussed in Sec. 3.4, a plot of the amplitudes of the slow mode solitons against the true Mach numbers has been presented in Fig. 3.5. The amplitudes of the slow mode KdV solitons have been calculated for Mach numbers ranging from the acoustic speed of the slow mode, i.e. Eq. (3.10), to the highest Mach number allowed by the model, i.e. $M = 1$ (see the ordering (3.16)), and we pointed out that this range of Mach numbers may include values that are out of the soliton existence domain. The calculation was carried out in this way, since for the KdV theory one can not find a maximum Mach number beyond which solitons do not exist, unlike the Sagdeev potential theory where the range in the allowed Mach numbers is well-defined. We recall that, for the Sagdeev potential approach, the soliton amplitudes have been calculated for Mach numbers ranging from the maximum value to the acoustic speed, for given values of other parameters.

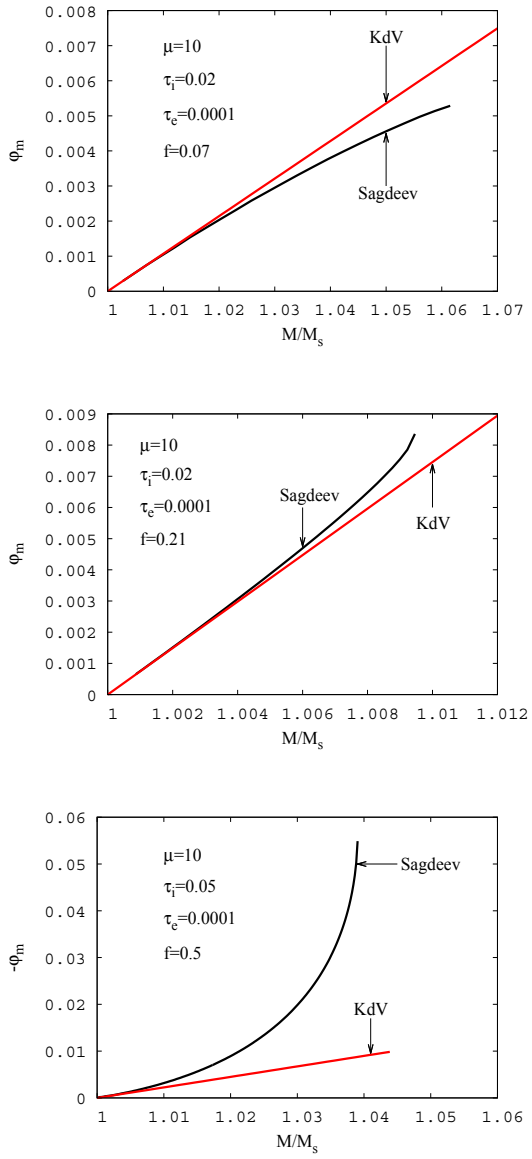

Figure 3.15: Comparison of the results obtained from the KdV and Sagdeev potential theories for $\mu = 10$ and $\tau_e = 0.0001$. The upper panel is for $f = 0.07$ and $\tau_i = 0.02$, the middle panel is for $f = 0.21$ and $\tau_i = 0.02$, and the lower panel is for $f = 0.5$ and $\tau_i = 0.05$.

We see that for $f = 0.07$ and $\tau_i = 0.02$ as well as $f = 0.21$ and $\tau_i = 0.02$, the results obtained using the Sagdeev potential and KdV approaches are in reasonable agreement for all Mach numbers that are within the soliton existence domain. This is consistent with the results presented in the upper and middle right panels of Fig. 3.14, from which it can be seen that, for $\tau_i = 0.02$, all soliton amplitudes are small and all soliton Mach numbers are close to the acoustic speed.

However, for the case $f = 0.5$ and $\tau_i = 0.05$, the results obtained using the Sagdeev potential and KdV approaches are only in reasonable agreement for Mach numbers ranging from M_s to $M \approx 1.01M_s$. This is consistent with the results presented in the lower right panel of Fig. 3.14, from which it can be seen that the curves obtained for different values of τ_i cross over at $M \approx 1.033M_s$, suggesting important nonlinear effects.

Up to this stage, we have sufficient information about the effects of τ_i on the extreme amplitudes, but do not have information about the effects of τ_i on the profile steepness/widths of a soliton with a maximal amplitude and of a double layer. We also have sufficient information about the relationship between the soliton amplitudes and the soliton speeds. In particular, for the parameter values that we have considered, we know that all solitons have vanishing amplitudes as their speeds approach the acoustic speed.

However, if we consider a soliton with an arbitrary speed between the acoustic speed (M_s) and the maximum speed ($M_{\max}$), for given values of μ and f, up to this stage, we do not have information about the effects of τ_i on its amplitude and profile steepness/width. Our subsequent discussion will address this point. In order to make our discussion simpler, we will consider a soliton with a speed/Mach number given by

$$M_{\text{ave}} = \frac{M_s + M_{\max}}{2}, \tag{3.94}$$

for given values of μ, τ_i, and f. We will often refer to the soliton speed/Mach number given by Eq. (3.94) as "average" speed or "average" Mach number.

This investigation will be carried out by analysing the Sagdeev potential plots. The effects of τ_i on the arbitrary amplitudes of solitons can be automatically observed by simply plotting the Sagdeev potentials for various values of τ_i. However, to get information about the effects of τ_i on the soliton profile steepness from a Sagdeev potential plot, one needs to remember

the following. From the so-called energy equation, see Eq. (3.68), we have

$$\left|\frac{d\varphi}{dx}\right| = \sqrt{-2S(\varphi)}, \tag{3.95}$$

implying that the deeper the Sagdeev potential well the greater the maximum steepness of the soliton profile and the smaller the soliton width. Since the necessary information will be obtained from the magnitude of the Sagdeev potential well, our discussion will be in terms of $|d\varphi/dx|$ and $\sqrt{2|S(\varphi)|}$. We note that the maximum profile steepness is, of course, the maximum electric field strength in the soliton.

We consider the cases $\mu = 0.1$ and $f = 0.2, 1, 7$ as well as $\mu = 10$ and $f = 0.07, 0.25, 0.5$. For these cases, the parameter values that are needed to obtain the Sagdeev potential plots are presented in Table 3.1. For given values of μ, τ_i, and f, Table 3.1 contains the acoustic speeds, the maximum speeds, and the "average" speeds calculated using Eq. (3.94). We have also included the ratios $M_{\rm ave}/M_s$ and $M_{\rm max}/M_s$, since they provide useful information about the order of magnitude of the "average" and maximum speeds compared to the acoustic speed, for given values of μ, τ_i, and f. We recall that, in the study of the slow mode throughout this chapter, we assume that the electrons are much hotter than the hotter ion species, and this has been expressed through $\tau_e \equiv T_h/T_e = 0.0001$.

From the parameter values presented in Table 3.1, we see that the values of the ratios $M_{\rm ave}/M_s$ and $M_{\rm max}/M_s$ are very close to unity for the cases where solitons are limited by positive double layers, namely, $\mu = 0.1$ and $f = 1$; $\mu = 10$ and $f = 0.25$. This means that, for these cases, the Mach numbers of solitons and positive double layers are very close to the acoustic speed. In particular, for the case $\mu = 10$ and $f = 0.25$, a plot of positive double layers has been presented in the lower panel of Fig. 3.13, and, indeed, it can be seen that these double layers have very small amplitudes, and could well be described by KdV theory.

$\mu = 0.1$, $\tau_i = 0.0001$		
$f = 0.2$	$f = 1$	$f = 7$
$M_s = 0.140$	$M_s = 0.302$	$M_s = 0.642$
$M_{\rm ave} = 0.182$	$M_{\rm ave} = 0.308$	$M_{\rm ave} = 0.748$
$M_{\rm max} = 0.223$	$M_{\rm max} = 0.314$	$M_{\rm max} = 0.855$
$M_{\rm ave}/M_s = 1.300$	$M_{\rm ave}/M_s = 1.020$	$M_{\rm ave}/M_s = 1.165$
$M_{\rm max}/M_s = 1.593$	$M_{\rm max}/M_s = 1.040$	$M_{\rm max}/M_s = 1.332$

$\mu = 0.1$		
$f = 0.2$, $\tau_i = 0.02$	$f = 1, \tau_i = 0.1$	$f = 7, \tau_i = 0.8$
$M_s = 0.147$	$M_s = 0.316$	$M_s = 0.677$
$M_{\rm ave} = 0.166$	$M_{\rm ave} = 0.325$	$M_{\rm ave} = 0.777$
$M_{\rm max} = 0.185$	$M_{\rm max} = 0.333$	$M_{\rm max} = 0.877$
$M_{\rm ave}/M_s = 1.130$	$M_{\rm ave}/M_s = 1.028$	$M_{\rm ave}/M_s = 1.148$
$M_{\rm max}/M_s = 1.260$	$M_{\rm max}/M_s = 1.054$	$M_{\rm max}/M_s = 1.295$

$\mu = 10$, $\tau_i = 0.0001$		
$f = 0.07$	$f = 0.25$	$f = 0.5$
$M_s = 0.642$	$M_s = 0.84513$	$M_s = 0.913$
$M_{\rm ave} = 0.703$	$M_{\rm ave} = 0.84524$	$M_{\rm ave} = 0.935$
$M_{\rm max} = 0.765$	$M_{\rm max} = 0.84535$	$M_{\rm max} = 0.956$
$M_{\rm ave}/M_s = 1.096$	$M_{\rm ave}/M_s = 1.00013$	$M_{\rm ave}/M_s = 1.024$
$M_{\rm max}/M_s = 1.191$	$M_{\rm max}/M_s = 1.00026$	$M_{\rm max}/M_s = 1.047$

$\mu = 10$, $\tau_i = 0.02$		
$f = 0.07$	$f = 0.25$	$f = 0.5$
$M_s = 0.728$	$M_s = 0.87816$	$M_s = 0.931$
$M_{\rm ave} = 0.750$	$M_{\rm ave} = 0.878715$	$M_{\rm ave} = 0.951$
$M_{\rm max} = 0.772$	$M_{\rm max} = 0.87927$	$M_{\rm max} = 0.972$
$M_{\rm ave}/M_s = 1.030$	$M_{\rm ave}/M_s = 1.00063$	$M_{\rm ave}/M_s = 1.022$
$M_{\rm max}/M_s = 1.060$	$M_{\rm max}/M_s = 1.00126$	$M_{\rm max}/M_s = 1.044$

Table 3.1: In this table, we present the data for the acoustic speeds, maximum soliton speeds/double layer speeds, "average"soliton speeds calculated using Eq. (3.94), as well as the ratios $M_{\rm ave}/M_s$ and $M_{\rm max}/M_s$, for given values of μ, τ_i, and f. The values of the "average" and maximum speeds presented in this table have been used to obtain the Sagdeev potential plots presented in Fig. 3.16. The value of $\tau_e = 0.0001$ has been used.

Figure 3.16 shows the Sagdeev potential plots of the slow mode for $\mu = 0.1$ (left panels) and $\mu = 10$ (right panels). Various values of f that are appropriate for each value of μ are considered. For $\mu = 0.1$, we show the results obtained for $f = 0.2$ (upper left panel), $f = 1$ (middle left panel), and $f = 7$ (lower left panel). For $\mu = 10$, we show the results for $f = 0.07$ (upper right panel), $f = 0.25$ (middle right panel), and $f = 0.5$ (lower right panel).

In the upper panels, left and right, we show two plots of the Sagdeev potential, viz. (a) a plot for a soliton with "average" Mach number calculated using Eq. (3.94), and (b) a plot for a soliton with maximal Mach number due to the occurrence of the cooler ion sonic point. The black dotted lines represent the results obtained for $\tau_i = 0.0001$, and the red solid lines indicate the results obtained for $\tau_i = 0.02$. For each value of τ_i, the curve showing the larger amplitude is for the maximal Mach number.

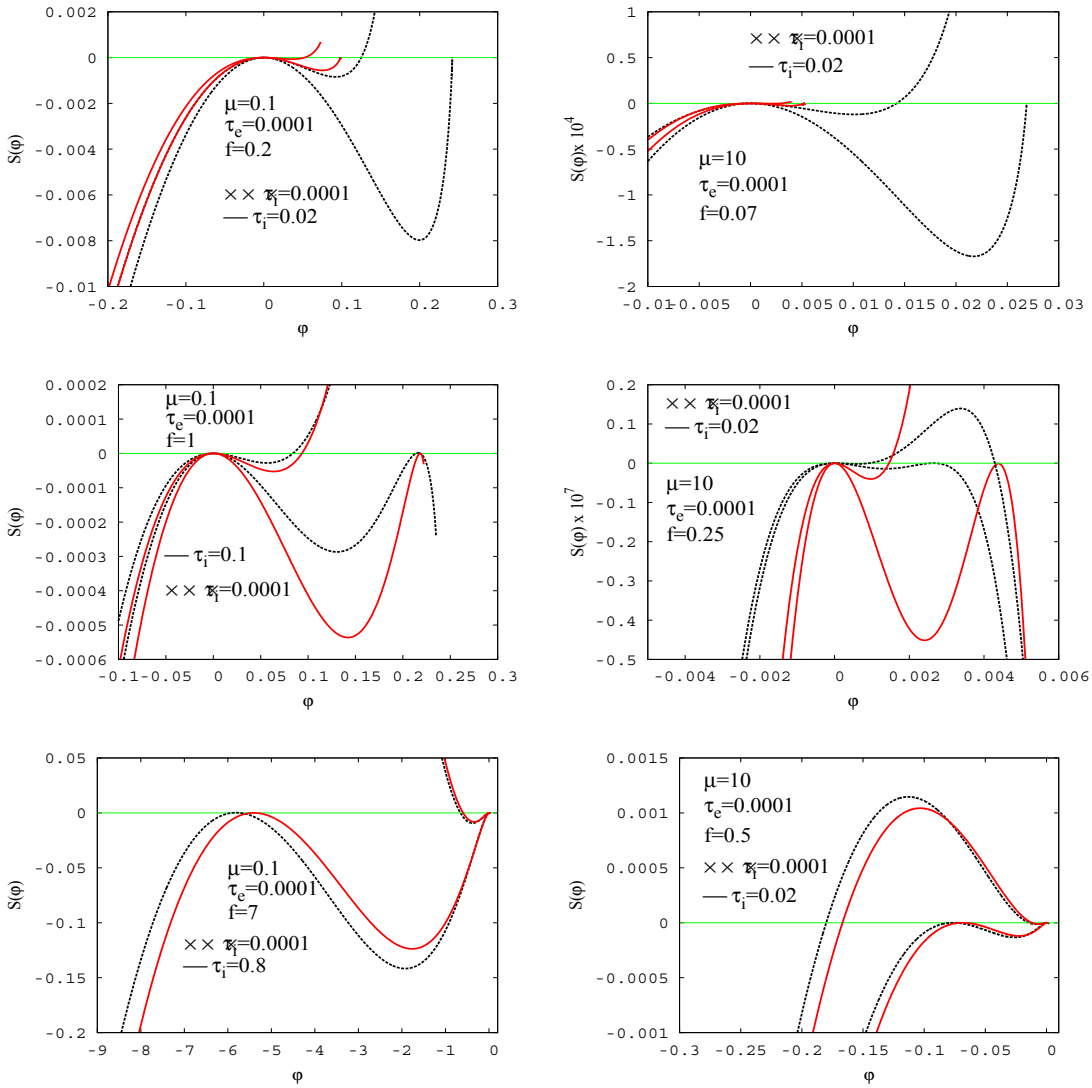

Figure 3.16: The Sagdeev potentials of the slow mode for $\mu = 0.1$ (left panels) and $\mu = 10$ (right panels). In each panel, the "average" and maximum Mach numbers presented in Table 3.1 have been used. Various values of f that are appropriate for each value of μ are considered. In the left panels, we show the results obtained for $f = 0.2$ (upper left panel), $f = 1$ (middle left panel), and $f = 7$ (lower left panel). In the right panels, we show the results for $f = 0.07$ (upper right panel), $f = 0.25$ (middle right panel), and $f = 0.5$ (lower right panel). The value of $\tau_i = 0.0001$ means that the cooler ions are cold and the effect of increasing the value of τ_i is shown. The line styles are as shown in the figure, and are described in detail in the text.

In the middle panels, left and right, we show two plots of the Sagdeev potential: (a) a plot for a soliton with "average" Mach number calculated using Eq. (3.94), and (b) a plot for a positive double layer. The black dotted lines show the results obtained for $\tau_i = 0.0001$, and the results obtained for a higher value of τ_i, shown in each panel, are illustrated by the red solid lines.

In the lower panels, left and right, the two plots of the Sagdeev potential are for: (a) a soliton with "average" Mach number calculated using Eq. (3.94), and (b) a negative double layer. The black dotted lines represent the results obtained for $\tau_i = 0.0001$, and the results obtained for a higher value of τ_i, shown in each panel, are indicated by the red solid lines.

For each case described above, the values of the Mach numbers used to plot the Sagdeev potentials are presented in Table 3.1.

We discuss our results proceeding as we did for Fig. 3.14, that is, we consider the results obtained for a given value of μ and discuss the effects of τ_i on the amplitudes and peak profile steepness of solitons and double layers as we vary f. We start with the case $\mu = 0.1$ presented in the left panels of Fig. 3.16.

In the upper left panel, for $f = 0.2$, we have increased the value of τ_i from 0.0001 to 0.02. Although this increase in τ_i is small, it has a significant effect on the soliton amplitude and profile steepness. It is seen that, for both solitons with "average" and maximum Mach numbers, the soliton amplitude and the pseudopotential well depth decrease significantly, as a result of this small increase in τ_i. The decrease in the pseudopotential well implies a decrease in the maximum steepness of the soliton profile, and hence an increase in the soliton width.

When the value of f is increased to 1, we observe a different effect of τ_i on the amplitudes and profile steepness of the nonlinear structures shown in the middle left panel of Fig. 3.16. In this case, we recall that there are positive solitons limited by positive double layers. It is seen that an increase in τ_i leads to an increase in the amplitude and the profile steepness, for both solitons and double layers. However, the increase in the amplitude is very small, particularly for double layers.

We recall from the soliton existence domains (see Figs. C.1, C.2, C.3, and 3.7) that the range in f over which solitons are limited by positive double layers decreases significantly and is shifted to higher values by an

increase in τ_i. Thus, studying the effect of τ_i on these solitons and double layers, for a fixed value of f, requires a small increment in τ_i. This explains the reason why we could not consider a value of τ_i greater than 0.1, for the case $\mu = 0.1$ and $f = 1$.

Negative solitons and negative double layers are shown in the lower left panel of Fig. 3.16, for $f = 7$. It is observed that increasing the value of τ_i results in a decrease in the amplitude and the peak profile steepness, for both solitons and double layers. However, as can be seen from the figure, this decrease in the amplitude and the profile steepness is small, even for the values of τ_i as large as 0.8.

We now consider the case $\mu = 10$ (see right panels of Fig. 3.16). A general observation from the results presented in the three right panels is that, for both solitons and double layers, the amplitudes and the profile steepness are smaller than for the case $\mu = 0.1$, for a given value of τ_i (consider $\tau_i = 0.0001$, for illustration).

Starting from the case $f = 0.07$, shown in the upper right panel, we see that increasing the value of τ_i from 0.0001 to 0.02 decreases significantly both the amplitudes and the peak profile steepness of solitons. Furthermore, we see that the amplitudes and the profile steepness of these solitons are very small, for $\tau_i = 0.02$. For this value of τ_i, we have demonstrated that these solitons are reasonably well described by KdV theory (see upper panel of Fig. 3.15).

For the case $f = 0.25$, shown in the middle right panel of Fig. 3.16, solitons are limited by positive double layers. In this case, it is seen that, as a result of an increase in τ_i, the amplitudes and the profile steepness increase, for both solitons and double layers. A plot of double layers obtained for this value of f has also been presented in the lower panel of Fig. 3.13, where we showed that the effect of τ_i on the amplitude of a positive double layer depends on the value of f. In that figure (i.e. Fig. 3.13), we showed that the amplitude of a positive double layer increases for $f = 0.25$, but decreases for $f = 0.21$ (see upper panel of Fig. 3.13), as a result of an increase in τ_i.

For completeness, we also consider the case $f = 0.21$, but in order not to overload Fig. 3.16, the results for this case have been presented in Fig. 3.17. We see that, for both $f = 0.21$ and $f = 0.25$, the amplitudes of solitons with "average" speeds increase, when the value of τ_i is increased. However, the observed increase in the soliton amplitude is small. Furthermore, in

both cases, the peak profile steepness increases for both solitons and double layers, due to an increase in τ_i.

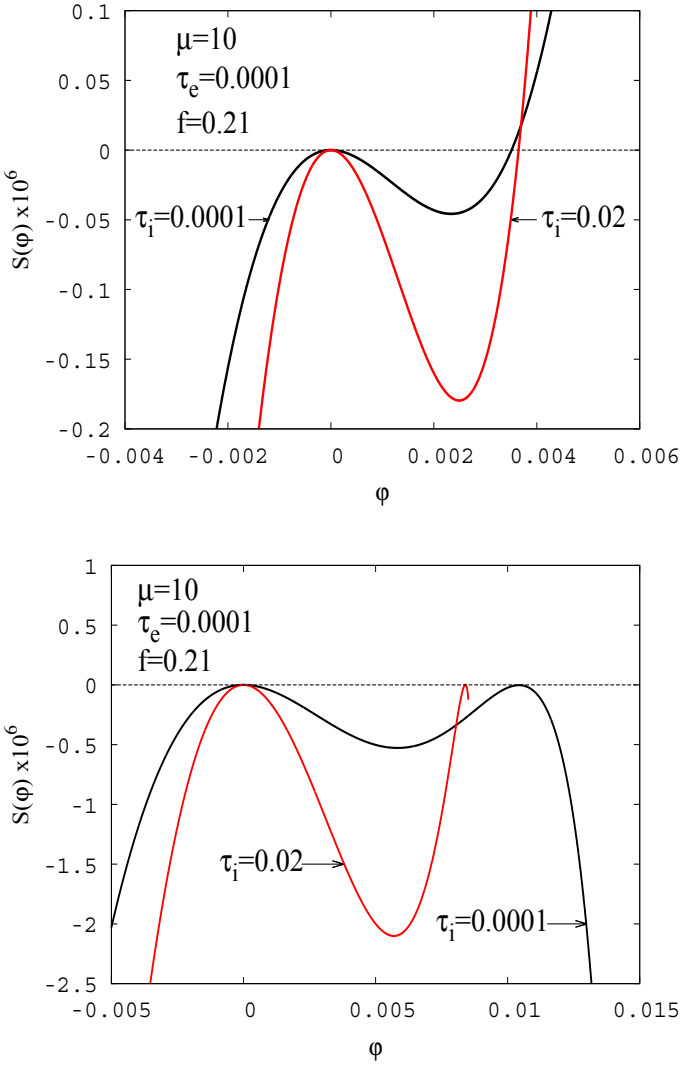

Figure 3.17: Positive solitons (upper panel) and positive double layers (lower panel) for $\mu = 10$ and $f = 0.21$, showing the effect of increasing τ_i from 0.0001 (black curves) to 0.02 (red curves). The Mach numbers of solitons are $M = 0.825$ and $M = 0.865$ for $\tau_i = 0.0001$ and $\tau_i = 0.02$, respectively. The double layer Mach numbers are $M_{dl} = 0.827$ and $M_{dl} = 0.869$ for $\tau_i = 0.0001$ and $\tau_i = 0.02$, respectively.

For negative solitons and negative double layers shown in the lower right panel of Fig. 3.16, for $f = 0.5$, increasing the value of τ_i from 0.0001 to 0.02 leads to a small decrease in the soliton and double layer amplitude and profile steepness. We recall that the values of μ and τ_i must satisfy the constraint $\mu\tau_i < 1$. Thus, for $\mu = 10$, we could, in principle, have also considered an increase in τ_i up to values as large as 0.09.

However, from the soliton existence domains presented in Figs. C.6, C.7, and 3.9, we see that both the acoustic speed and the double layer Mach numbers are close to 1, for all values of f that support negative double layers, even for values of τ_i as large as 0.02. This means that, for $\mu = 10$ and particularly for large values of τ_i, the phase speeds of the waves under study are close to the thermal speeds of the hotter ion species, suggesting that, in that case, these waves are subject to hotter ion Landau damping. We note that, in some of our discussions (see e.g. Figs. 3.14 and 3.15), we considered the case $\mu = 10$, $f = 0.5$, and $\tau_i = 0.05$, for quantitative illustration, but, in fact, this case involving such a high value of τ_i might not be realistic, for the above-mentioned reason.

Although we have used the Sagdeev potential plots to investigate the effects of τ_i on the amplitudes and maximum profile steepness of solitons and double layers, we could also have reached the same conclusions by plotting the soliton and double layer profiles, for given values of μ, f, M, τ_e, and τ_i. However, we note that whereas for the weakly nonlinear (KdV) theory a soliton profile is a straightforward plot of the well-known "sech^2" function, for the fully nonlinear Sagdeev potential theory one needs to integrate numerically Eq. (3.95), using the appropriate expression for the Sagdeev potential, and using the boundary condition: $\varphi \to 0$ as $x \to \pm\infty$. Carrying out such a numerical integration is not as simple as a straightforward Sagdeev potential plot.

Nevertheless, we present in Fig. 3.18 one plot of a soliton profile to show that we would have reached the same conclusions, had we considered the soliton/double layer profiles for the cases presented in Figs. 3.16, 3.17.

In Fig. 3.18, we show a profile of a soliton with a maximum Mach number (see Table 3.1) for $\mu = 0.1$, $f = 0.2$, $\tau_e = 0.0001$, for values of τ_i of 0.0001 and 0.02. From this figure, we see that, as a result of this increase in τ_i, the soliton profile steepness decreases, while the width increases. The soliton amplitude decreases from about 0.24 to about 0.1. Clearly, this conclusion

is the same as that reached from the Sagdeev potential plot presented in the upper left panel of Fig. 3.16.

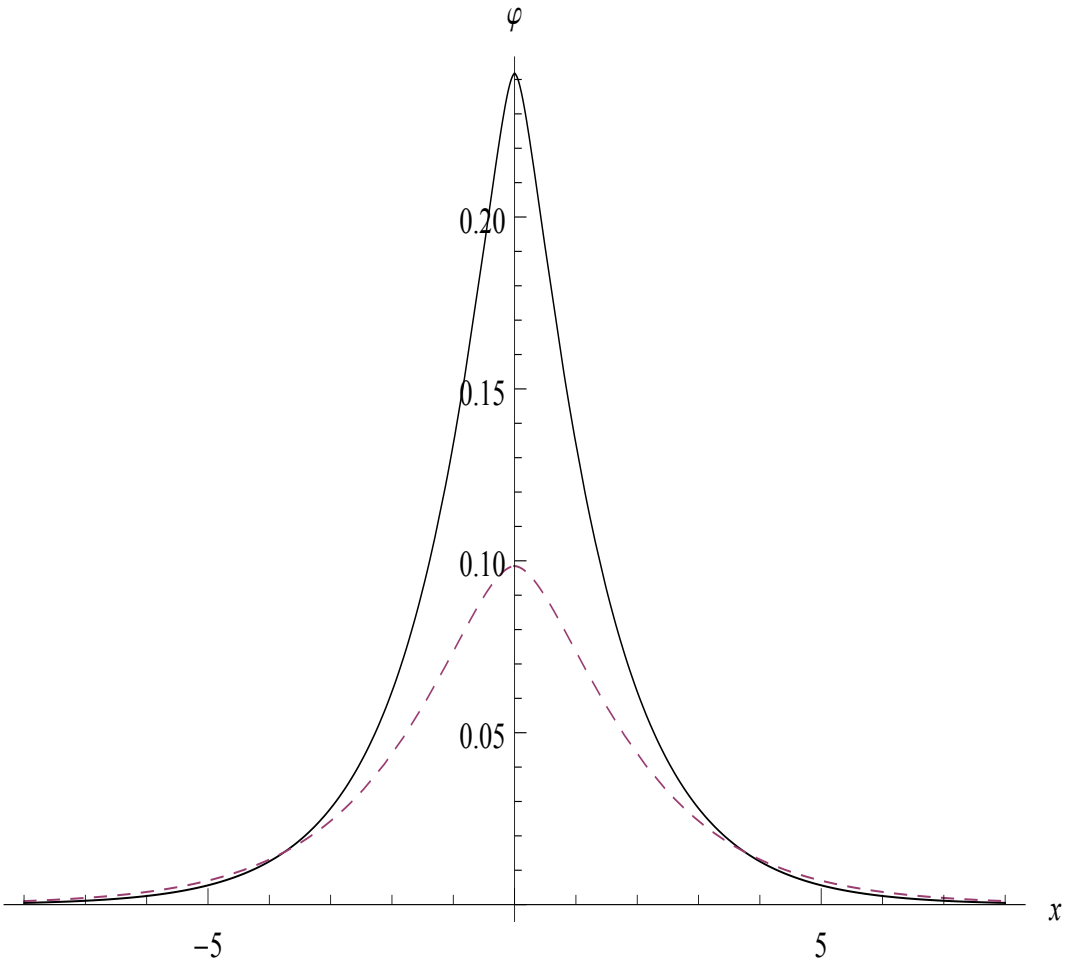

Figure 3.18: Profiles of the slow mode ion acoustic solitons with maximum Mach numbers for $\mu = 0.1$, $f = 0.2$, $\tau_e = 0.0001$, and $\tau_i = 0.0001$ (solid line), $\tau_i = 0.02$ (dashed line). For the values of the Mach numbers, see Table 3.1.

Summary

In summary, we have investigated the thermal effects of the cooler ion species, expressed through $\tau_i = T_c/T_h$, on the amplitudes and profile steepness of the slow mode ion acoustic solitons and double layers supported by the plasma model under consideration. Our investigation was carried out considering various values of the mass of the cooler ions, expressed through $\mu = m_h/m_c$, and various values of the density of the cooler ions, expressed through $f = n_{c0}/n_{h0}$. The electrons have been assumed to be much hotter than the hotter ion species, and this has been expressed through $\tau_e \equiv T_h/T_e = 0.0001$.

From small to large values of f, the slow mode ion acoustic solitons supported by the plasma model under consideration are limited, successively, by the occurrence of the cooler ion sonic point, the hotter ion sonic point, positive double layers, and negative double layers (Verheest et al., 2008, 2011).

A systematic investigation of the effect of τ_i on the maximal amplitudes of solitons limited by the sonic points and on the double layer amplitudes has been carried out, considering the cases $\mu = 0.1$, $\mu = 1$, and $\mu = 10$. We found that the effect of τ_i on the maximal amplitudes depends on the value of f. The magnitude of the maximal amplitudes due to the occurrence of the sonic points and that of the negative double layer amplitudes decreases, as a result of an increase in τ_i. However, it has been found that the magnitude of the positive double layer amplitudes may either increase or decrease, depending on the value of f.

Considering the case $\mu = 0.1$, we studied, in detail, the effect of τ_i on the amplitudes and peak profile steepness of solitons. In our investigation, we considered the values f=0.2, 1, and 7. These values of f support, respectively, positive solitons limited by the cooler ion sonic point, positive solitons limited by positive double layers, and negative solitons limited by negative double layers.

We found that a small increase in τ_i decreases significantly the amplitudes and peak profile steepness of positive solitons limited by the cooler ion sonic point. On the other hand, an increase in τ_i leads to a very small decrease in the amplitudes and maximum profile steepness of negative solitons limited by negative double layers. This is so even for values of τ_i as large as 0.8. However, an increase in τ_i results in a small increase in the amplitudes

and profile steepness of positive solitons limited by positive double layers.

Increasing the value of μ, for a fixed value of τ_i, decreases the amplitudes and profile steepness of solitons. In particular, for $\mu = 10$ and $\tau_i = 0.02$, we showed that the arbitrary amplitude positive solitons limited by the cooler ion sonic point and by positive double layers are reasonably well described by KdV theory for all Mach numbers within the soliton existence domain.

A systematic study of the effect of τ_i on double layers has been carried out. We found that an increase in τ_i results in a very small decrease in the magnitude of the negative double layer amplitudes and peak steepness of the profile. Whereas an increase in τ_i results in a decrease or an increase in the amplitudes of positive double layers, depending on the value of f, the same increase in τ_i leads to an increase in the profile steepness of positive double layers, for all values of f that we considered.

By studying the relationship between the amplitudes and the true Mach numbers of solitons and double layers, we found that all solitons are "KdV-like", that is, their amplitudes tend to zero as their speeds approach the acoustic speed, and this is so irrespective of the values of μ, f, and τ_i. This conclusion was reached by Verheest et al. (2011) when they considered the cooler ions to be cold.

3.5.4 Thermal effects on ion acoustic solitons: The fast mode

a. General features of the fast mode ion acoustic solitons

In this subsection, we discuss the fast mode ion acoustic solitons of arbitrary amplitude. After a discussion of the general features of the fast mode ion acoustic solitons, we investigate the effects of the electron and ion temperatures on the wave propagation characteristics. We recall that the fast mode has a phase speed that lies between the thermal speeds of the hotter ion species and the electrons, so that the Mach number of fast mode ion acoustic solitons satisfies $M > 1$ (see the ordering 3.16). We note, again, that M is not the true Mach number, as discussed in Sec. 3.4.

We start from the expression of the Sagdeev potential given by $S(\varphi)_+$ in Eq. (3.69), recalling that the term associated with the "$\mp$" signs becomes $[(M-1)^2 - 2\varphi]^{3/2}$ when the "+" sign is considered (Verheest et al., 2008). Throughout this subsection, the "+" sign associated with various quantities

means that the hotter ions are treated as supersonic, leaving the electrons as the only subsonic species. To study the fast mode ion acoustic solitons, one needs to treat the hotter ions as supersonic.

As mentioned earlier for the case of the slow mode, it is important to determine the soliton existence domain before proceeding for further wave study. In the case of the fast mode, under study here, we did not find any double layers, and therefore there are only positive solitons limited by the occurrence of the sonic points. As a result of the occurrence of the sonic points, there are critical values of the electrostatic potential (φ_l) beyond which the densities of the hotter (h) and the cooler (c) ion species, and hence $S(\varphi)_+$, become complex. They are

$$\varphi_{lh+} = \frac{1}{2}\bigg(M_l - 1\bigg)^2, \tag{3.96}$$

and

$$\varphi_{lc} = \frac{1}{2}\bigg(\frac{M_l}{\sqrt{\mu}} - \sqrt{\tau_i}\bigg)^2, \tag{3.97}$$

respectively, where M_l is the limiting/maximum speed of a fast soliton.

Differentiating φ_{lh+} and φ_{lc} with respect to M_l yields the slopes of the curves $\varphi_{lh+}\ (M_l)$ and $\varphi_{lc}\ (M_l)$ as

$$\frac{d\varphi_{lh+}}{dM_l} = M_l - 1, \tag{3.98}$$

and

$$\frac{d\varphi_{lc}}{dM_l} = \frac{1}{\mu}(M_l - \sqrt{\mu\tau_i}), \tag{3.99}$$

respectively.

Since $\mu\tau_i < 1$, and for the fast mode $M > 1$ (see the ordering (3.16)), it follows that both $\varphi_{lh+}\ (M_l)$ and $\varphi_{lc}\ (M_l)$ have positive slopes, irrespective of the choice of the values of μ and τ_i. As the value of μ is increased, the slope of $\varphi_{lc}\ (M_l)$ decreases and tends to zero for sufficiently large values of μ.

For cases in which the two curves intersect, $\varphi_{lh+}\ (M_l) = \varphi_{lc}\ (M_l)$ at a value of $M_l = M_{co+}$ given by

$$M_{co+} = \frac{(1 - \sqrt{\tau_i})\sqrt{\mu}}{\sqrt{\mu} - 1}, \tag{3.100}$$

where the subscript "$co+$" associated with M has been used to emphasise that at that value of the Mach number, there is a crossover from one limiting potential to the other (following the idea of Verheest et al. (2008)).

Since $0 < \tau_i < 1$, in principle, it is seen from Eq. (3.100) that M_{co+} is positive if $\mu > 1$, negative for $\mu < 1$, and infinite when $\mu = 1$. This means that, for physically meaningful Mach numbers, $\varphi_{lh+}\ (M_l)$ and $\varphi_{lc}\ (M_l)$ do not cross over for

$$\mu \leq 1. \tag{3.101}$$

In fact, we will show numerically that $\varphi_{lh+}\ (M_l)$ and $\varphi_{lc}\ (M_l)$ do not cross over for

$$\mu \lesssim 1, \tag{3.102}$$

to include also the values of μ slightly greater than 1, for Mach numbers that are not too large (e.g. $1 < M_l \lesssim 5$).

From Eq. (3.100), we see that, for a fixed value of μ satisfying the constraint (3.101), the value of M_{co+} decreases with increasing τ_i. We will show that this observation has a significant impact on the soliton existence domain.

Figure 3.19 shows the two limiting potentials, in the range $0 < \varphi_{\text{limit}} \leq 6$, plotted against the limiting Mach numbers in the range $1 < M_l \leq 5$, for various values of μ. We have omitted the thermal effects of the cooler ions, for simplicity, by using the value $\tau_i = 0.0001$. However, as we have mentioned above, for a fixed value of μ satisfying the condition (3.101), the effect of increasing the value of τ_i is to decrease M_{co+}.

We see that, for the maximum Mach numbers in the range shown in Fig. 3.19, $\varphi_{lh+}\ (M_l)$ and $\varphi_{lc}\ (M_l)$ do not intersect for values of $\mu \lesssim 1$. In this range of the values of μ, and for the range of Mach numbers shown in the figure, $\varphi_{lh+} < \varphi_{lc}$, implying that solitons are only limited by the hotter ion sonic point.

For the values of μ for which the two curves intersect, as shown in the figure, we see that $\varphi_{lh+} < \varphi_{lc}$ when $M_l < M_{co+}$, but $\varphi_{lh+} > \varphi_{lc}$ if $M_l > M_{co+}$. This means that solitons with $M_l < M_{co+}$ are limited by the occurrence of the hotter ion sonic point, whereas those with $M_l > M_{co+}$ are limited by the occurrence of the cooler ion sonic point.

Furthermore, one can see from Fig. 3.19, as well as from Eq. (3.100), that the Mach number at which the two limiting potentials cross over, i.e.

M_{co+}, decreases as the value of μ is increased. This implies that the range in maximum Mach numbers due to the occurrence of the cooler ion sonic point increases, while the range in maximum Mach numbers due to the occurrence of the hotter ion sonic point decreases.

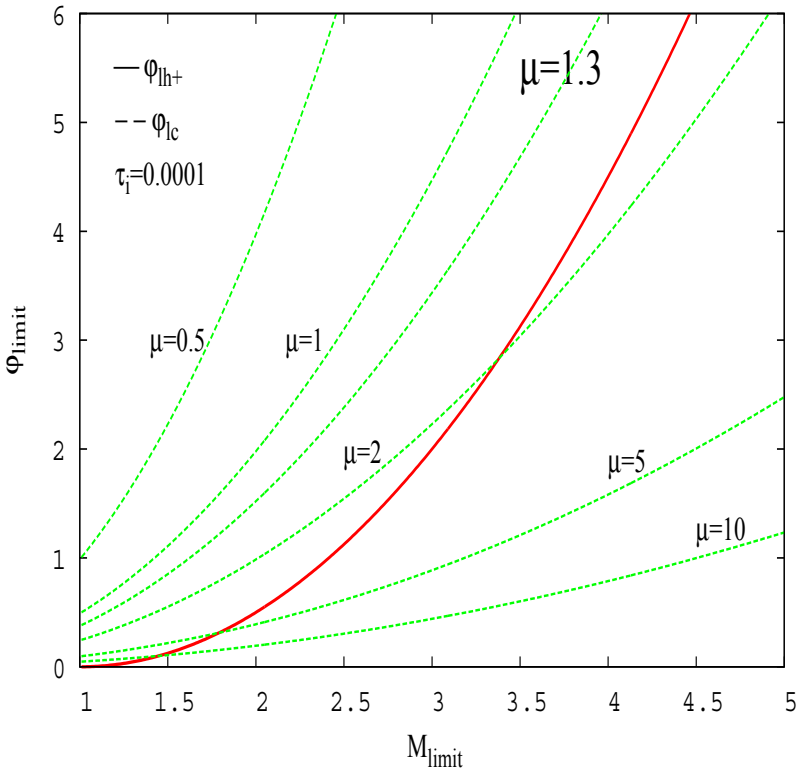

Figure 3.19: The limiting potentials of the fast mode ion acoustic solitons, i.e. Eqs. (3.96) and (3.97), plotted against the limiting Mach numbers for $\tau_i = 0.0001$ and μ=0.5, 1, 1.3, 2, 5, 10. The red solid line shows the limitation due to the occurrence of the hotter ion sonic point, whereas, for each value of μ, the green-dashed line illustrates the limitation due to the occurrence of the cooler ion sonic point. Where, for a given value of μ, a crossover occurs, the actual limiting potential is the lower of the two curves.

We proceed as for the slow mode to determine the soliton existence domain in $\{f, M\}$ parameter space. For numerical purposes, the expression for M_{s+} (f) given by Eq. (3.11) will be used to obtain the lower limit in Mach numbers for the existence of solitons, whereas the upper limit will be obtained from the conditions on the Sagdeev potential, Eq. (3.69), at the limiting potentials, Eqs. (3.96) and (3.97), in a way similar to that discussed for the slow mode, that is,

$$\left.\begin{aligned} S(\varphi_{lc})_+ &= 0 \\ S(\varphi_{lh+})_+ &= 0 \end{aligned}\right\}. \tag{3.103}$$

From Eq. (3.69) and the condition $S(\varphi_{lh+})_+ = 0$, we obtain

$$\alpha_{h+} f + \beta_{h+} = 0, \tag{3.104}$$

where

$$\alpha_{h+} = \frac{1}{\tau_e}\left\{1 - \exp\left[\frac{\tau_e}{2}\left(M_l - 1\right)^2\right]\right\} + \frac{1}{6\sqrt{\tau_i}}\left\{2\tau_i\sqrt{\tau_i} + \frac{6M_l^2\sqrt{\tau_i}}{\mu} - \left[\left(\frac{M_l}{\sqrt{\mu}} + \sqrt{\tau_i}\right)^2 - (M_l - 1)^2\right]^{3/2} + \left[\left(\frac{M_l}{\sqrt{\mu}} - \sqrt{\tau_i}\right)^2 - (M_l - 1)^2\right]^{3/2}\right\}, \tag{3.105}$$

and

$$\beta_{h+} = \frac{1}{\tau_e}\left\{1 - \exp\left[\frac{\tau_e}{2}\left(M_l - 1\right)^2\right]\right\} + \frac{1}{6}(2 + 6M_l^2 - 8M_l^{3/2}), \tag{3.106}$$

provided

$$\left(\frac{M_l}{\sqrt{\mu}} - \sqrt{\tau_i}\right)^2 - (M_l - 1)^2 \geq 0. \tag{3.107}$$

We recall that the subscript "+" associated with various quantities refers to the fast mode.

Recalling that $0 < \tau_i < 1$ and $M_l > 1$, in principle, it is seen that, for $0 < \mu \leq 1$, the constraint on M_l, μ, and τ_i given by Eq. (3.107) is satisfied irrespective of the values of M_l and τ_i. This implies that, in that range of μ values, solitons of all allowed Mach numbers are limited by the hotter ion sonic point. In fact, we have shown in Fig. 3.19 that solitons are only limited by the hotter ion sonic point for $0 < \mu \lesssim 1$, where we have used a

cutoff of $\varphi_{\rm limit} = 6$. That is, the range $0 < \mu \lesssim 1$ includes also the values of μ slightly greater than 1 (see Fig. 3.19), if one considers solitons with amplitudes less than or equal to 6. For $\mu \gtrsim 1$, the soliton limitation may result from the hotter or the cooler ion sonic point, depending on the value of M_l. In that case, the constraint (3.107) is equivalent to

$$1 < M_l \leq \frac{(1-\tau_i)\sqrt{\mu}}{\sqrt{\mu}-1} = M_{co+}. \tag{3.108}$$

Similarly from Eq. (3.69) and the condition $S(\varphi_{lc})_+ = 0$, we get

$$\alpha_{c+} f + \beta_{c+} = 0, \tag{3.109}$$

where

$$\alpha_{c+} = \frac{1}{\tau_e}\left\{1 - \exp\left[\frac{\tau_e}{2}\left(\frac{M_l}{\sqrt{\mu}} - \sqrt{\tau_i}\right)^2\right]\right\} + \frac{1}{6\sqrt{\tau_i}}\left\{2\tau_i\sqrt{\tau_i} + \frac{6M_l^2\sqrt{\tau_i}}{\mu} - \left[\left(\frac{M_l}{\sqrt{\mu}} + \sqrt{\tau_i}\right)^2 - \left(\frac{M_l}{\sqrt{\mu}} - \sqrt{\tau_i}\right)^2\right]^{3/2}\right\}, \tag{3.110}$$

and

$$\beta_{c+} = \frac{1}{\tau_e}\left\{1 - \exp\left[\frac{\tau_e}{2}\left(\frac{M_l}{\sqrt{\mu}} - \sqrt{\tau_i}\right)^2\right]\right\} + \frac{1}{6}\left\{2 + 6M_l^2 + \left[(M_l-1)^2 - \left(\frac{M_l}{\sqrt{\mu}} - \sqrt{\tau_i}\right)^2\right]^{3/2} - \left[(M_l+1)^2 - \left(\frac{M_l}{\sqrt{\mu}} - \sqrt{\tau_i}\right)^2\right]^{3/2}\right\}, \tag{3.111}$$

provided

$$(M_l - 1)^2 - \left(\frac{M_l}{\sqrt{\mu}} - \sqrt{\tau_i}\right)^2 \geq 0. \tag{3.112}$$

In principle, it is seen that the LHS of (3.112) is negative for $0 < \mu \leq 1$, irrespective of the value of M_l, implying that solitons limited by the cooler ion sonic point certainly do not exist in this case, as discussed above. In fact, we have shown in Fig. 3.19 that this is so even for the values of μ slightly greater than 1, for limiting potentials that are not too large (e.g. $0 < \varphi_l \leq 6$). In principle, for $\mu > 1$, the constraint (3.112) is the same as

$$M_l \geq \frac{(1-\tau_i)\sqrt{\mu}}{\sqrt{\mu}-1} = M_{co+}, \tag{3.113}$$

for given values of μ and τ_i satisfying the condition $\mu\tau_i < 1$.

b. The effects of the electron temperature on the fast mode ion acoustic solitons

i. The effects of the electron temperature on the existence domain of the fast mode ion acoustic solitons

Here, we carry out a numerical investigation of the effects of the electron temperature, expressed through the ratio $\tau_e = T_h/T_e$, on the existence domain of the fast mode ion acoustic solitons. During our investigation, the thermal effects of the cooler ions, expressed through the ratio $\tau_i = T_c/T_h$, will be neglected by using $\tau_i = 0.0001$.

We will assume that the electrons are hotter than the hotter ion species. However, we recall from Sec. 3.3, see Eq. (3.24), that when the electron temperature is very high in comparison with the temperature of the hotter ions, the Mach number has a very high value. Such values of the electron temperature will be avoided. Only values of the electron temperature in the range $T_h < T_e \leq 10T_h$ (i.e. $0.1 \leq \tau_e < 1$) will be considered.

As for the case of the slow mode, discussed earlier, we present the existence domain in $\{f, M\}$ parameter space, recalling that f is the density of the cooler ions expressed through the ratio $f = n_{c0}/n_{h0}$. The numerical work has been carried out considering Eq. (3.11) to obtain the lower limit in Mach numbers for the existence of the fast mode ion acoustic solitons, and Eqs. (3.104), (3.109) to obtain the upper limit, for given values of μ, τ_i, and τ_e.

The analysis of the structure of the limiting potentials of the fast mode ion acoustic solitons (i.e. Eqs. (3.96) and (3.97)), as shown in Fig. 3.19, leads one to expect a strong dependence of the soliton existence domain on the mass ratio μ. In what follows, we study the soliton existence domain in a systematic manner, considering various ranges of μ, as shown in Fig. 3.19. We then show that the structure of the soliton existence domain depends strongly on the values of μ and τ_e, and that for some cases a stopband exists in the existence domain. By a stopband, we mean values of the Mach number, between two passbands of an existence domain, for which wave propagation does not occur.

Figure 3.20 shows the existence domains of the fast mode ion acoustic solitons for $\mu = 0.5$ (upper panels), $\mu = 10$ (middle panels), and $\mu = 1.3$ (lower panels). For each value of μ, the results obtained for $\tau_e = 0.1$ are presented in the left panel, and those obtained for $\tau_e = 0.5$ are presented in the right panel. The lower black solid line represents the lower limit in Mach numbers for the existence of the fast mode ion acoustic solitons, the upper red thick solid line illustrates the upper limit in Mach numbers due to the occurrence of the hotter ion sonic point, and the upper green thin solid line shows the upper limit due to the occurrence of the cooler ion sonic point.

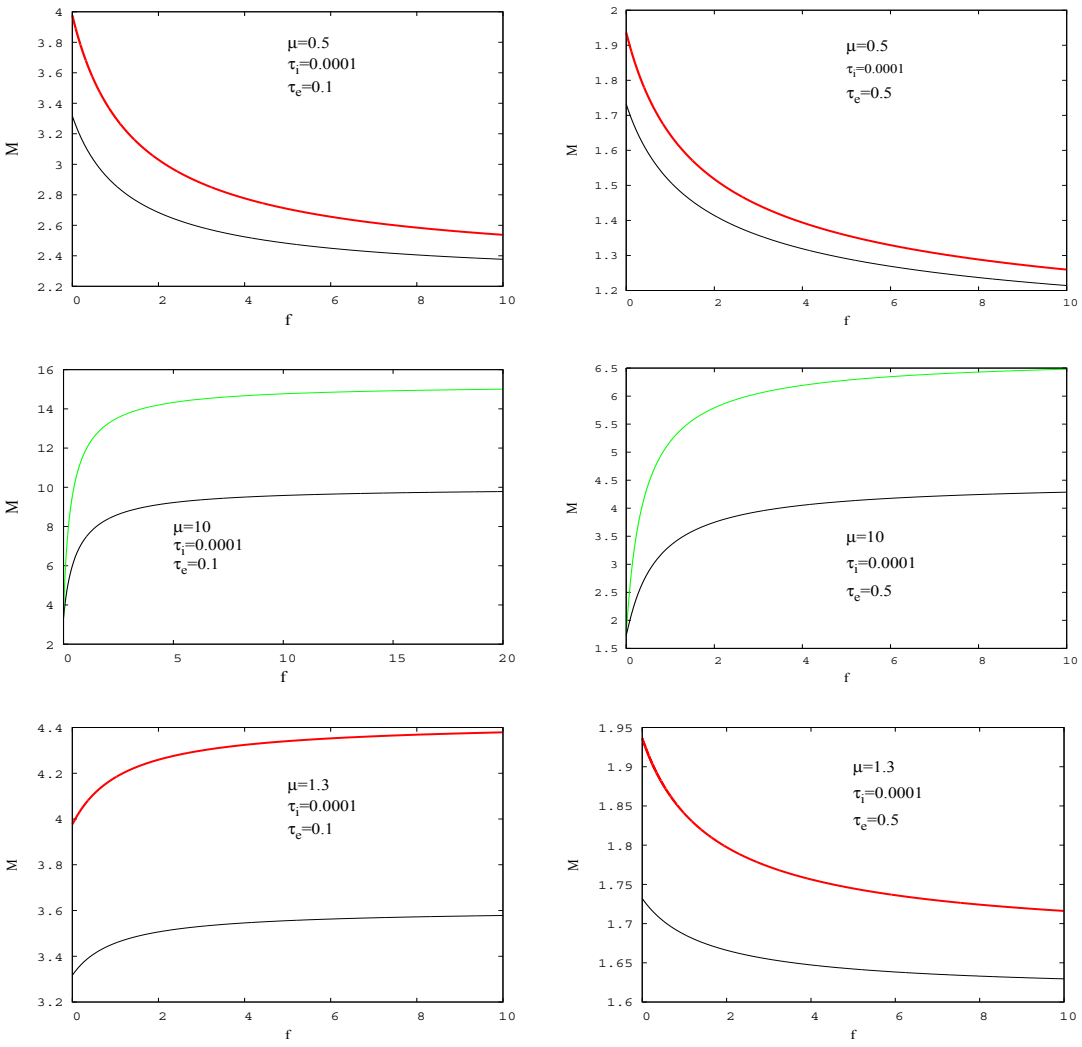

Figure 3.20: The existence domains of the fast mode ion acoustic solitons for $\mu = 0.5$ (upper panels), $\mu = 10$ (middle panels), and $\mu = 1.3$ (lower panels). For each value of μ, the results obtained for $\tau_e = 0.1$ are presented in the left panel, and those obtained for $\tau_e = 0.5$ are presented in the right panel. The lower black solid line represents the lower limit in Mach numbers for the existence of the fast mode ion acoustic solitons, the upper red thick solid line, in the upper and lower panels, illustrates the upper limit in Mach number due to the occurrence of the hotter ion sonic point, and the upper green thin solid line, in the middle panels, shows the upper limit in Mach number due to the occurrence of the cooler ion sonic point. The value of $\tau_i = 0.0001$ used in each panel means that the cooler ions are cold.

For $\mu = 0.5$, the upper limit in Mach numbers results from the occurrence of the hotter ion sonic point only, as can be seen also from Fig. 3.19. In this case, the results obtained for a fixed value of τ_e show that both the acoustic speed and the maximum Mach number have their highest value at $f \sim 0$, from which they decrease monotonically with increasing f. Increasing the value of τ_e from 0.1 (upper left panel) to 0.5 (upper right panel), i.e. decreasing T_e from $10T_h$ to $2T_h$, leads to a decrease in both the acoustic speed and the maximum Mach number as well as a decrease in the range in M. It is worth mentioning that the existence domains obtained for other values of μ in the range $0 < \mu \leq 1$ (not shown here) are qualitatively similar to that obtained for $\mu = 0.5$, with the same qualitative effect of τ_e.

The variation of M with f observed in the case $0 < \mu \leq 1$ changes drastically when $\mu \gg 1$. From the results presented in the middle panels, for $\mu = 10$, we see that, for a fixed value of τ_e, both the acoustic speed and the maximum Mach number have their lowest value at $f \sim 0$, from which they increase monotonically with increasing f, unlike the case $0 < \mu \leq 1$. When the value of τ_e is increased from 0.1 (middle left panel) to 0.5 (middle right panel), we see that the acoustic speed, the maximum Mach number and the range in M decrease. The existence domain obtained for $\mu = 10$ is typical for values of $\mu \gtrsim 3$. In this range of μ values, our numerical evaluation shows that the maximum Mach number is due to the cooler ion sonic point only, as confirmed by Fig. 3.19.

For values of μ slightly greater than 1, namely, $1 \lesssim \mu \lesssim 1.5$, we obtain an existence domain whose shape may be qualitatively similar to that for either the case $0 < \mu \leq 1$ or $\mu \gtrsim 3$, depending on the value of τ_e, but in all cases the maximum Mach number is due to the occurrence of the hotter ion sonic point only, as one would expect from Fig. 3.19. From the results obtained for the case $\mu = 1.3$ and $\tau_e = 0.1$ (see lower left panel), we see that the variation of the acoustic speed and the maximum Mach number with f is qualitatively similar to that observed for the case $\mu = 10$ (middle panels). However, when the value of τ_e is increased to 0.5 (see lower right panel), the variation of M with f changes, with a decrease in both the acoustic speed and the maximum Mach number, and the trend is like that for the case $\mu = 0.5$ (upper panels).

A useful point to remember from our discussion of the linear waves in Sec. 3.3 is that, for values of μ in the approximate range $1 \lesssim \mu \lesssim 1.5$, there exist values of τ_e and τ_i for which the acoustic speed does not vary with f, see Eq. (3.31) and upper left panels of Figs. 3.3 and 3.4. In Fig. 3.21, we show that, for this range of μ values, there also exist values of τ_e and τ_i for which the maximum Mach number does not vary with f.

From this figure, i.e. Fig. 3.21, it is seen that, for the case $\mu = 1.3$, $\tau_i = 0.0001$, and $\tau_e = 0.2$, presented in the upper panel, the variation of the maximum Mach number with f is very small. This suggests that a more careful numerical investigation would yield a case in which the maximum Mach number is exactly constant, irrespective of f. In the lower panel of this figure, we show that, for the case $\mu = 1.3$, $\tau_i = 0.0001$, and $\tau_e = 0.3$, the acoustic speed is indeed constant, irrespective of f. In this case, the value of the acoustic speed is $M_{s+} = 2.082$, for all values of f.

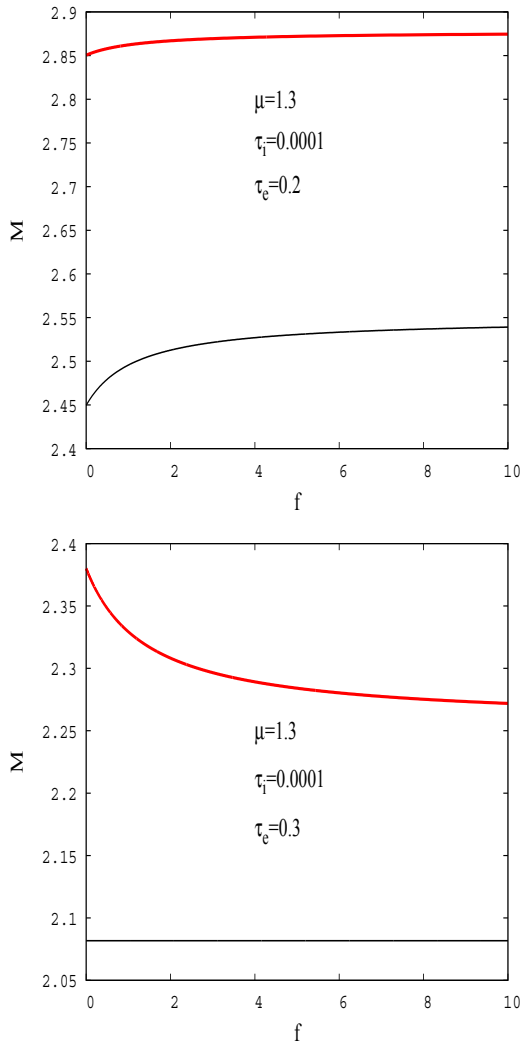

Figure 3.21: The existence domain of the fast mode ion acoustic solitons for $\mu = 1.3$, and $\tau_e = 0.2$ (upper panel), $\tau_e = 0.3$ (lower panel). In each panel, the lower curve represents the lower limit in Mach numbers for the existence of solitons, and the upper curve is for the upper limit due to the occurrence of the hotter ion sonic point. The value of $\tau_i = 0.0001$ used in each panel means that the cooler ions are cold.

A general observation from all cases presented in Figs. 3.20 and 3.21 is that both the acoustic speed and the maximum Mach number are single-valued functions of f, irrespective of the value of f. This agrees with reports in the literature (e.g. Hellberg et al. (2006); Verheest et al. (2008); Maharaj et al. (2012)).

In what follows, we show that, for values of μ in the approximate range $1.5 \lesssim \mu \lesssim 3$, there exist values of f and τ_e for which the maximum Mach number has more than one value.

Figure 3.22 illustrates the existence domains of the fast mode ion acoustic solitons for $\mu = 1.7$. The upper panel is for $\tau_e = 0.1$, the middle panel is for $\tau_e = 0.2$, and the lower panel is for $\tau_e = 0.3$. The upper limit due to the occurrence of the hotter ion sonic point is shown by the thick red solid line, whereas that due to the occurrence of the cooler ion sonic point is represented by the thin green solid line.

For the case $\tau_e = 0.1$, presented in the upper panel, the maximum Mach numbers are due to the hotter ion sonic point for small values of f up to about $f \approx 0.08$, corresponding to a value of $M \equiv M_{co+} \approx 4.2$. For higher values of f, the limit is due to the cooler ion sonic point. Over the whole range of f, the maximum Mach number is observed to be single-valued in f.

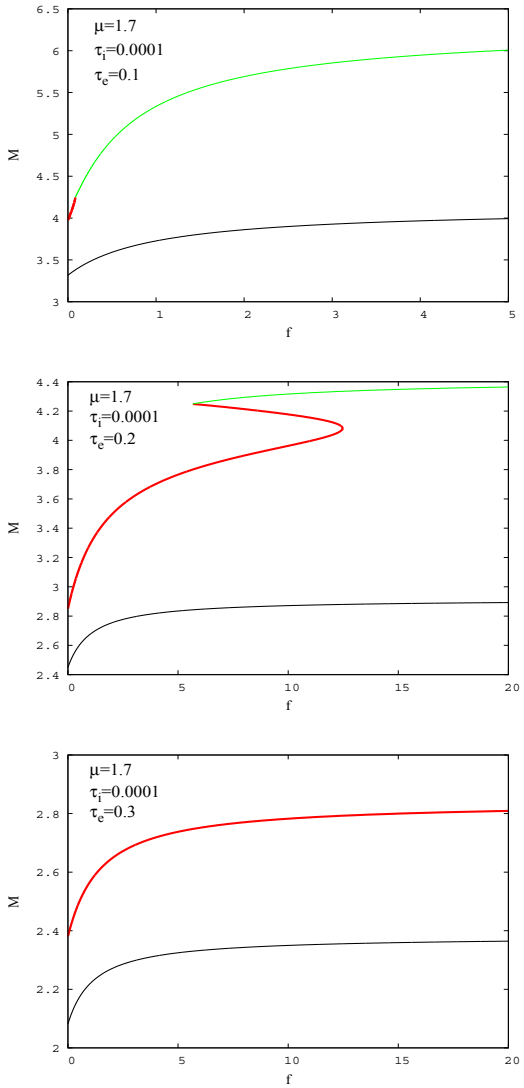

Figure 3.22: The existence domains of the fast mode ion acoustic solitons for $\mu = 1.7$, and $\tau_e = 0.1$ (upper panel), $\tau_e = 0.2$ (middle panel), $\tau_e = 0.3$ (lower panel). The lower black solid line represents the lower limit in Mach numbers for the existence of solitons, the upper thick red solid line illustrates the upper limit due to the hotter ion sonic point, and the upper thin green solid line corresponds to the upper limit due to the cooler ion sonic point. The value of $\tau_i = 0.0001$ used in each panel means that the cooler ions are cold.

Increasing the value of τ_e to 0.2 (i.e. decreasing T_e from $10T_h$ to $5T_h$), as shown in the middle panel, results in an increase in the range in f values over which solitons are limited by the hotter ion sonic point and in a decrease in the range in f values over which the soliton limitation is due to the cooler ion sonic point. Most importantly, and perhaps surprisingly, in this case, there are values of f in the approximate range $6 \lesssim f \lesssim 12$ within which the limiting Mach number, M_l, due to the hotter ion sonic point is double-valued for fixed f, giving rise to an "overhang" structure. Hence, it follows that for $\mu = 1.7$ and $\tau_e = 0.2$, there is a stopband, i.e. a range of M values for which solitary wave propagation does not occur, in the approximate range $6 \lesssim f \lesssim 12$. At $f \sim 6$, the stopband has its maximum width, lying in the approximate range $3.9 \lesssim M \lesssim 4.2$. We note that the range $6 \lesssim f \lesssim 12$ represents $0.14 \lesssim n_{h0}/n_{e0} \lesssim 0.08$. We also recall that $\tau_i = 0.0001$. That is, one is dealing with a predominantly cold ion plasma, with a weak admixture of hot ions whose temperature approaches that of the electrons (factor 0.2) and whose mass exceeds that of the cold ions by a factor 1.7.

When we increase τ_e from 0.2 to 0.3 (see lower panel), i.e. decreasing T_e from $5T_h$ to about $3T_h$, we only find solitons whose maximum Mach numbers are due to the occurrence of the hotter ion sonic point, regardless of the value of f. Furthermore, we find that the maximum Mach number is single-valued, for all values of f, i.e. no stopband is found. In passing, we note that although we have used T_e as low as $3T_h$, the typical minimum Mach numbers, which represent the phase velocity/hotter ion thermal speed, are greater than 2. Thus, ion Landau damping should not be a problem.

To check whether the above-mentioned stopband is not a numerical artefact, we have plotted Sagdeev potentials for $\mu = 1.7$, $\tau_i = 0.0001$, $\tau_e = 0.2$, $f = 8$ and for various values of M ranging from the acoustic speed to higher values. The results are shown in Fig. 3.23. Considering $M_{lh} = 3.896 < M = 4.074 < M_{lh} = 4.213$, it is clearly observed that while $M_{lh} = 3.896$ and $M_{lh} = 4.213$ correspond to solitons with maximal amplitudes, $M = 4.074$ is not for a soliton. For the value of f considered in Fig. 3.23, i.e. $f = 8$, the first passband is observed between $M = M_s = 2.862$ and $M_{lh} = 3.896$, while the second passband is observed between $M_{lh} = 4.213$ and $M_{lc} = 4.294$. Between the two passbands there is a range in Mach numbers over which solitons do not exist (i.e. a stopband), namely, $M_{lh} = 3.896 < M < M_{lh} = 4.213$.

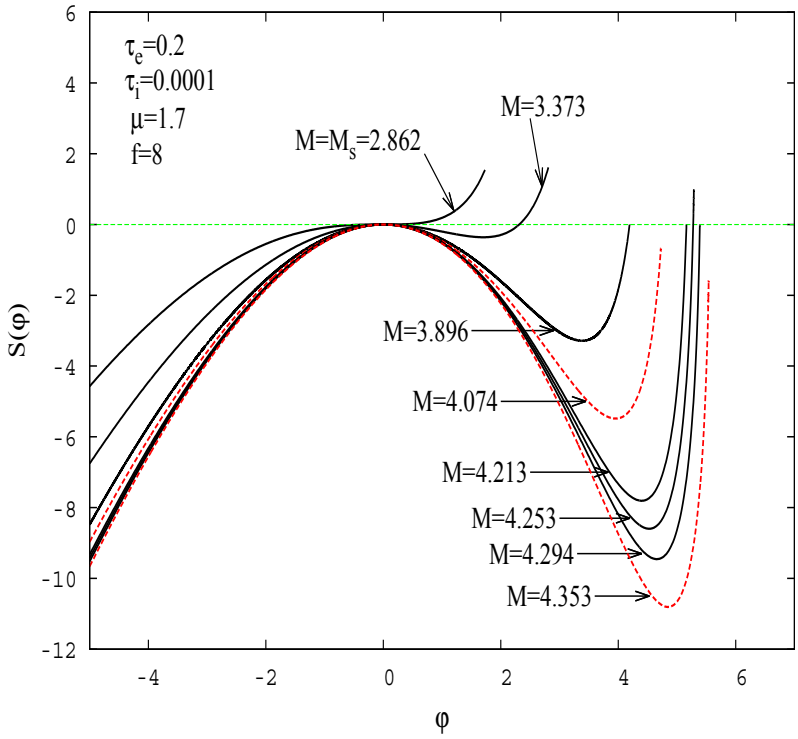

Figure 3.23: The Sagdeev potentials of the fast mode ion acoustic solitons for $\mu = 1.7$, $f = 8$, $\tau_i = 0.0001$, $\tau_e = 0.2$, and various values of M shown in the figure.

Our numerical investigation has shown that the stopband phenomenon also exists for other values of μ in the approximate range $1.5 \lesssim \mu \lesssim 3$. The value of τ_e required for the stopband to occur depends on the value of μ that is considered. For example, for the case $\mu = 1.7$ illustrated in Fig. 3.22 and discussed above, we found the stopband for values of τ_e in the approximate range $0.1 \lesssim \tau_e \lesssim 0.3$.

Increasing the value of μ to 2.2, as shown in Fig. 3.24, we find that the stopband now occurs for higher values of τ_e. In this case, our numerical investigation has shown that it occurs for $0.2 \lesssim \tau_e \lesssim 0.5$. It appears that the higher the value of μ, in the approximate range $1.5 \lesssim \mu \lesssim 3$, the greater the value of τ_e is required for the occurrence of a stopband.

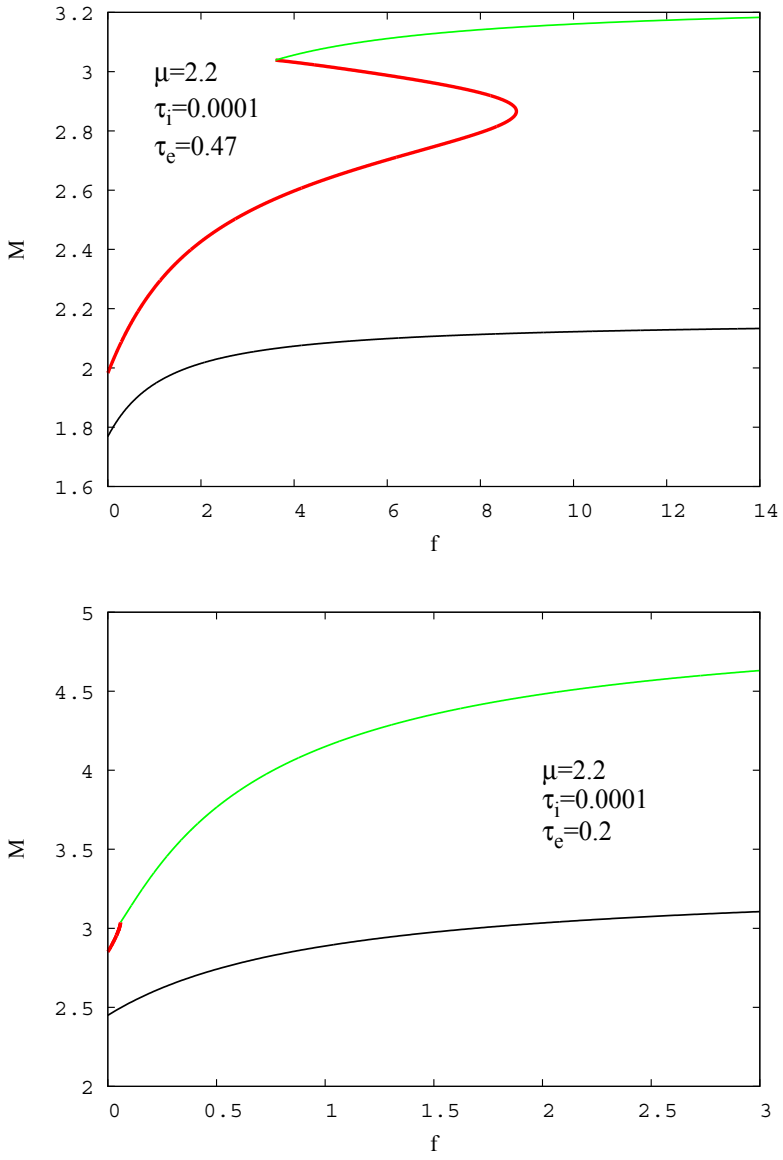

Figure 3.24: The existence domains of the fast mode ion acoustic solitons for $\mu = 2.2$, and $\tau_e = 0.47$ (upper panel), $\tau_e = 0.2$ (lower panel). In each panel, the lower curve represents the lower limit in Mach numbers for the existence of solitons, whereas the upper curve corresponds to the upper limit due to the occurrence of the hotter ion sonic point (thick red solid line) and that due to the occurrence of the cooler ion sonic point (thin green solid line).

As a result of the observed stopband, an important question arises. Under what conditions on the soliton maximum speed, expressed through M_l,

the mass of the cooler ions, expressed through μ, the density of the cooler ions, expressed through f, the electron temperature, expressed through τ_e, and the temperature of the cooler ions, expressed through τ_i, does the stopband occur in an $\{f, M\}$ existence domain?

To answer this question, we note that there are a couple of important characteristics associated with stopbands, some of which have already been commented on above. From Figs. 3.22 and 3.24, it is clear that a prerequisite is that the limitation by both the hotter and the cooler ion sonic points needs to occur. Furthermore, one notes that there exists a point on the upper limiting curve due to the hotter ion sonic point at which one may define a vertical tangent line. At that point, the slope of the curve, i.e. dM_l/df, is infinite.

Recalling that the points on the upper limiting curve due to the occurrence of the hotter ion sonic point are given by f and M_l related by Eq. (3.104) with α_{h+} and β_{h+} given by, respectively, Eqs. (3.105) and (3.106), and differentiating both sides of Eq. (3.104) with respect to M_l, we obtain

$$f\frac{d\alpha_{h+}}{dM_l} + \alpha_{h+}\frac{df}{dM_l} + \frac{d\beta_{h+}}{dM_l} = 0. \tag{3.114}$$

For the stopband to occur we require that $df/dM_l = 0$, and hence Eq. (3.114) becomes

$$f\frac{d\alpha_{h+}}{dM_l} + \frac{d\beta_{h+}}{dM_l} = 0, \tag{3.115}$$

from which we obtain

$$\begin{aligned}
&-(1+f)(M_l-1)\exp\left[\frac{\tau_e}{2}(M_l-1)^2\right] + 2\left(M_l - M_l^{1/2}\right) \\
&+\frac{f}{2\sqrt{\tau_i}}\left\{\frac{4M_l\sqrt{\tau_i}}{\mu} - \left[\frac{1}{\sqrt{\mu}}\left(\frac{M_l}{\sqrt{\mu}}+\sqrt{\tau_i}\right)-(M_l-1)\right]\left[\left(\frac{M_l}{\sqrt{\mu}}+\sqrt{\tau_i}\right)^2-(M_l-1)^2\right]^{1/2}\right. \\
&\left.+\left[\frac{1}{\sqrt{\mu}}\left(\frac{M_l}{\sqrt{\mu}}-\sqrt{\tau_i}\right)-(M_l-1)\right]\left[\left(\frac{M_l}{\sqrt{\mu}}-\sqrt{\tau_i}\right)^2-(M_l-1)^2\right]^{1/2}\right\} = 0.
\end{aligned} \tag{3.116}$$

Hence, the stopband observed in an $\{f, M\}$ existence domain occurs if the parameters μ, τ_e, τ_i, M_l, and f, related by Eq. (3.104), satisfy the condition given by Eq. (3.116).

It is easy to solve simultaneously and numerically Eqs. (3.104) and

(3.116) and check that for $\mu = 1.7$, $\tau_e = 0.2$, and $\tau_i = 0.0001$, as considered in Fig. 3.22, one obtains $f = 12.47$ and $M_l = 4.08$, whereas for $\mu = 2.2$, $\tau_e = 0.47$, and $\tau_i = 0.0001$, as used in Fig. 3.24, one gets $f = 8.77$ and $M_l = 2.86$. Clearly, the line $f = 12.47$ is tangent to the upper limiting curve obtained for the case $\mu = 1.7$ and $\tau_e = 0.2$, at the value of $M_l = 4.08$. Similarly, the line $f = 8.77$ is tangent to the upper limiting curve obtained for the case $\mu = 2.2$ and $\tau_e = 0.47$, at the value of $M_l = 2.86$. In each case, the tangent occurs at the maximum value of f for which the stopband is found. The minimum value of f coincides with the value yielding M_{co+}, Eq. (3.100).

ii. The effects of the electron temperature on the amplitudes and profile steepness of the fast mode ion acoustic solitons

Having discussed the structure of the existence domain of the fast mode ion acoustic solitons and the effects of the electron temperature on it, we now consider the parameter values from well-defined soliton existence domains and investigate the effects of the electron temperature on the soliton amplitudes and profile steepness. In this investigation, the thermal effects of the cooler ions are neglected by using $\tau_i = 0.0001$. Some of the parameter values used to obtain the necessary plots have been taken from the soliton existence domain presented in Appendix D (see Fig. D.1).

Table 3.2 contains the values of the Mach numbers that have been used to generate the necessary Sagdeev potential plots. In our investigation, we consider a soliton with an "average" speed, $M_{\rm ave}$, calculated using Eq. (3.94) and a soliton with a maximal speed, $M_{\rm max}$. In Table 3.2, we have also included the ratios $M_{\rm ave}/M_s$ and $M_{\rm max}/M_s$, as they provide useful, quantitative, information about the order of magnitude of the "average" and maximum soliton speed compared to the acoustic speed.

In our discussion of the effect of τ_e on the existence domain of the fast mode ion acoustic solitons, we observed that the acoustic speed, the maximum Mach number, and the range in Mach numbers decrease, as a result of an increase in τ_e (i.e. a decrease in T_e). This effect of the electron temperature on the soliton Mach numbers is illustrated in a more quantitative manner in Table 3.2, for the case $\mu = 0.5$ and $f = 4$, and the case $\mu = 1.7$ and $f = 15$, where we show an increase in τ_e from 0.1 to 0.2 (i.e. a decrease

in T_e from $10T_h$ to $5T_h$).

For both cases presented in Table 3.2, we see that an increase in τ_e leads to a very small decrease in $M_{\max}/M_s$. For the case $\mu = 0.5$ and $f = 4$, this ratio is close to 1, particularly for $\tau_e = 0.2$, implying that there is a very narrow range in speeds over which solitons can occur before a cutoff is reached.

$\mu = 0.5$, $f = 4$, $\tau_i = 0.0001$		$\mu = 1.7$, $f = 15$, $\tau_i = 0.0001$	
$\tau_e = 0.1$	$\tau_e = 0.2$	$\tau_e = 0.1$	$\tau_e = 0.2$
$M_s = 2.524$	$M_s = 1.848$	$M_s = 4.074$	$M_s = 2.885$
$M_{\rm ave} = 2.650$	$M_{\rm ave} = 1.922$	$M_{\rm ave} = 5.132$	$M_{\rm ave} = 3.616$
$M_{\max} = 2.777$	$M_{\max} = 1.997$	$M_{\max} = 6.190$	$M_{\max} = 4.348$
$M_{\rm ave}/M_s = 1.050$	$M_{\rm ave}/M_s = 1.040$	$M_{\rm ave}/M_s = 1.260$	$M_{\rm ave}/M_s = 1.253$
$M_{\max}/M_s = 1.100$	$M_{\max}/M_s = 1.081$	$M_{\max}/M_s = 1.520$	$M_{\max}/M_s = 1.507$

Table 3.2: In this table, we present the values of the Mach numbers needed for the Sagdeev potential plots presented in the upper panels of Fig. 3.25, for the values of μ, f, τ_i, and τ_e shown in the table. The value of $M_{\rm ave}$ has been calculated using Eq. (3.94).

The upper panels of Fig. 3.25 show the Sagdeev potentials of solitons with "average" and maximal Mach numbers. The lower panels illustrate the soliton amplitudes plotted against the true soliton Mach numbers. The left panels are for the case $\mu = 0.5$ and $f = 4$, and the right panels are for the case $\mu = 1.7$ and $f = 15$. The value of $\tau_i = 0.0001$ used in each panel means that the cooler ions are effectively cold. In each panel, we show the effect of increasing the value of τ_e from 0.1 to 0.2 (i.e. decreasing T_e from $10T_h$ to $5T_h$).

In the upper panels, the black dotted lines represent the case $\tau_e = 0.1$, and the red solid lines illustrate the case $\tau_e = 0.2$. For a given case, the larger amplitude, of course, relates to $M_{\max}$. In the lower panels, the line styles are, clearly, shown in the figure.

From the results presented in the upper left panel, i.e. for the case $\mu = 0.5$ and $f = 4$, we see that an increase in τ_e, i.e. a decrease in T_e, leads to a decrease in both the soliton amplitudes and the soliton profile peak steepness. This effect is qualitatively unchanged for the case $\mu = 1.7$ and $f = 15$, presented in the upper right panel. However, quantitatively, we note that, for a fixed value of τ_e, the soliton amplitudes and the soliton profile steepness increase, due to an increase in μ.

That the amplitudes increase due to an increase in μ can also be seen from the results presented in the lower panels. The amplitudes presented in these lower panels have been calculated for Mach numbers ranging from the maximum to the acoustic speed. Furthermore, we see that, for a given value of τ_e, the amplitude tends to zero as the speed approaches the acoustic speed. That is, for the cases presented in Fig. 3.25, the fast mode solitons are "KdV-like".

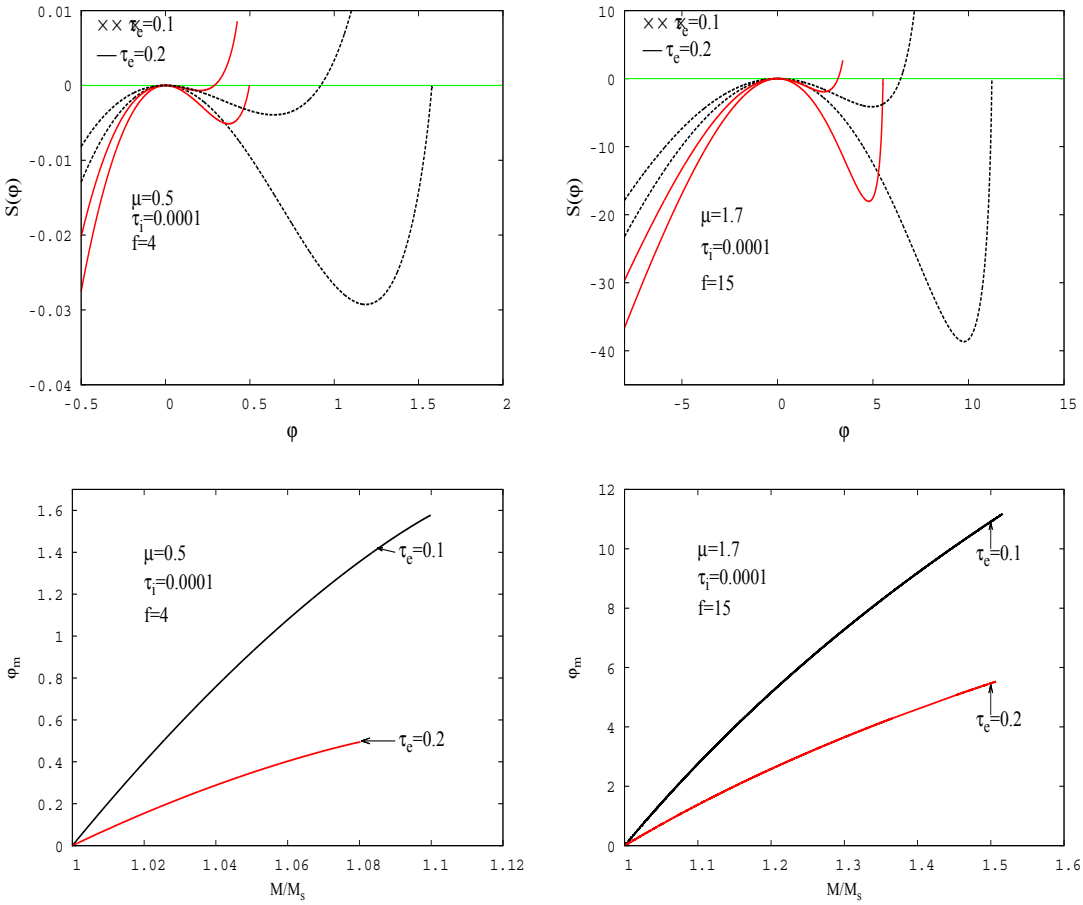

Figure 3.25: In the upper panels of this figure, we show the Sagdeev potentials of the fast mode ion acoustic solitons, and in the lower panels, we show the soliton amplitudes plotted against the true soliton Mach numbers. The left panels are for the case $\mu = 0.5$ and $f = 4$, and the right panels are for the case $\mu = 1.7$ and $f = 15$. In each panel, we show the effect of increasing the value of τ_e from 0.1 to 0.2 (i.e. decreasing T_e from $10T_h$ to $5T_h$). The value of $\tau_i = 0.0001$ used in each panel means that the cooler ions are effectively cold. The line styles are as shown in the figure, and are described in detail in the text.

Summary

In summary, we have investigated, in a systematic manner, the effects of the electron temperature, expressed through the ratio $\tau_e = T_h/T_e$, on the existence domain of the fast mode ion acoustic solitons supported by the plasma model under consideration. During our investigation, the thermal

effects of the cooler ions were ignored, and values of the electron temperature in the range $T_h < T_e \leq 10T_h$ were considered. The soliton existence domain was presented in $\{f, M\}$ parameter space, recalling that $f = n_{c0}/n_{h0}$ is the normalised density of the cooler ions, and $M = V/\sqrt{T_h/m_h}$ is the Mach number.

We have found that, for a given value of τ_e, the shape of an $\{f, M\}$ soliton existence domain depends on whether the value of the ion-mass ratio, μ, is in the following ranges: $0 < \mu \leq 1$, $1 \lesssim \mu \lesssim 1.5$, $1.5 \lesssim \mu \lesssim 3$, and $\mu \gtrsim 3$.

In the range $0 < \mu \leq 1$, the soliton limitation is due to the occurrence of the hotter ion sonic point only. Furthermore, both the minimum and maximum Mach numbers for the existence of solitons have their highest value at $f \sim 0$, from which they decrease monotonically with increasing f.

In the range $\mu \gtrsim 3$, the soliton limitation results from the occurrence of the cooler ion sonic point only. In this case, both the minimum and maximum Mach numbers have their lowest value at $f \sim 0$, from which they increase monotonically with increasing f, unlike the case $0 < \mu \leq 1$.

For values of μ slightly greater than 1, namely $1 \lesssim \mu \lesssim 1.5$, the shape of the soliton existence domain has intermediate features between those for the cases $0 < \mu \leq 1$ and $\mu \gtrsim 3$, depending on the value of τ_e.

In the range $1.5 \lesssim \mu \lesssim 3$, the soliton limitation may result from the occurrence of either the hotter ion sonic point or the cooler ion sonic point, depending on the values of f and τ_e. Most importantly, and perhaps surprisingly, we demonstrated that there exist values of f and τ_e for which the limiting Mach number due to the occurrence of the hotter ion sonic point is double-valued. Consequently, for those values of f and τ_e, there exists a range of Mach numbers between two passbands of an $\{f, M\}$ soliton existence domain over which solitary wave propagation does not occur. We have referred to this range of Mach numbers as a stopband.

For a fixed value of μ in any of the above-mentioned ranges, it has been found that an increase in τ_e (i.e. a decrease in T_e) results in a decrease in the acoustic speed, the maximum Mach number, and the range in Mach numbers over which solitons exist.

Considering the cases $\mu = 0.5$ and $f = 4$, as well as $\mu = 1.7$ and $f = 15$, it has been found that an increase in τ_e results in a decrease in the soliton amplitudes and the maximum of the soliton profile steepness. Furthermore, we have found that, for a fixed value of τ_e, the soliton amplitude tends to zero

as the soliton speed approaches the acoustic speed. That is, for the cases that we have studied, the fast mode ion acoustic solitons are "KdV-like".

c. The effects of the ion temperature on the fast mode ion acoustic solitons

i. The effects of the ion temperature on the soliton existence domain

In our discussion of the effects of τ_e on the existence domain of the fast mode ion acoustic solitons, we considered a negligible value of τ_i, i.e. the cooler ions were assumed to be effectively cold, and then showed that the variation of M with f depends on whether the value of μ is in the following ranges: $0 < \mu \leq 1$, $1 \lesssim \mu \lesssim 1.5$, $1.5 \lesssim \mu \lesssim 3$, and $\mu \gtrsim 3$. Most importantly, we showed that for the values of μ in the approximate range $1.5 \lesssim \mu \lesssim 3$, and depending on the value of τ_e, a stopband may exist in the existence domain. A detailed discussion of the observed stopband was carried out considering $\mu = 1.7$ and $\tau_e = 0.2$, as well as $\mu = 2.2$ and $\tau_e = 0.47$. Here, we consider $\tau_e = 0.2$ and various ranges of μ values, as mentioned above, and carry out a numerical investigation of the effects of τ_i on the existence domain of the fast mode ion acoustic solitons, using Eq. (3.11) to obtain the lower limit in Mach numbers and Eqs. (3.104), (3.109) to obtain the upper limit. We then show that the observed stopband exists only when the thermal effects of the cooler ions are small, i.e. when $\tau_i \to 0$.

Figures 3.26 and 3.27 illustrate the existence domains for $\mu = 0.5$ and $\mu = 10$, showing the effect of increasing the value of τ_i from 0.0001 to a higher value shown in each figure, and chosen in such a way that $\mu\tau_i < 1$. Our numerical investigation shows that for $\mu = 0.5$ solitons are limited only by the hotter ion sonic point, whereas for $\mu = 10$ solitons are limited only by the cooler ion sonic point, as expected in light of Fig. 3.19. We have overlapped the plots obtained for different values of τ_i, for the ease of comparison, but using different line styles, clearly shown in each figure. For each line style, the lower curve represents the lower limit in Mach numbers for the existence of solitons, whereas the upper curve shows the upper limit.

The results obtained for $\mu = 0.5$ show that, for a given value of τ_i, both the acoustic speed and the maximum Mach number have their highest value at $f \sim 0$, i.e. when the cooler ion density $\to 0$, and then decrease with increasing f. An increase in τ_i results in an increase in both the acoustic speed and the maximum Mach number, irrespective of the value of f.

However, for $\mu = 10$ and for a fixed value of τ_i, the results show that both the acoustic speed and the maximum Mach number have their lowest value at $f \sim 0$, and then increase with increasing f. An increase in τ_i results in a small increase in the acoustic speed and a significant decrease in the maximum Mach number, irrespective of the value of f. This implies that the range in Mach numbers over which fast solitons exist decreases as a result of an increase in the value of τ_i.

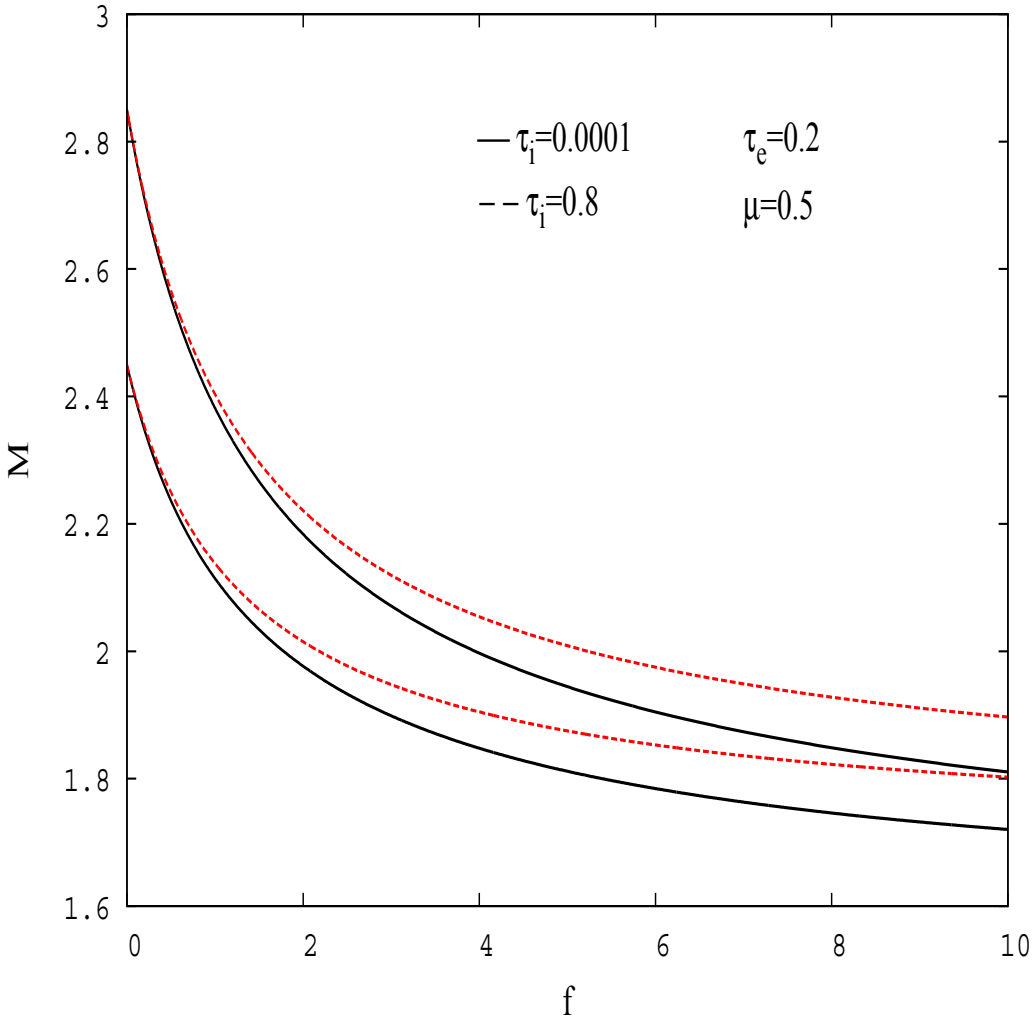

Figure 3.26: The existence domain of the fast mode ion acoustic solitons for $\mu = 0.5$ and $\tau_e = 0.2$, showing the effect of increasing the value of τ_i from 0.0001 to 0.8. The black solid lines show the results obtained for $\tau_i = 0.0001$, whereas the red dashed lines are for $\tau_i = 0.8$. For each line style, the lower curve represents the lower limit in Mach numbers for the existence of fast solitons, whereas the upper curve shows the upper limit. Here, the upper limit is due to the occurrence of the hotter ion sonic point only (see also Fig. 3.19).

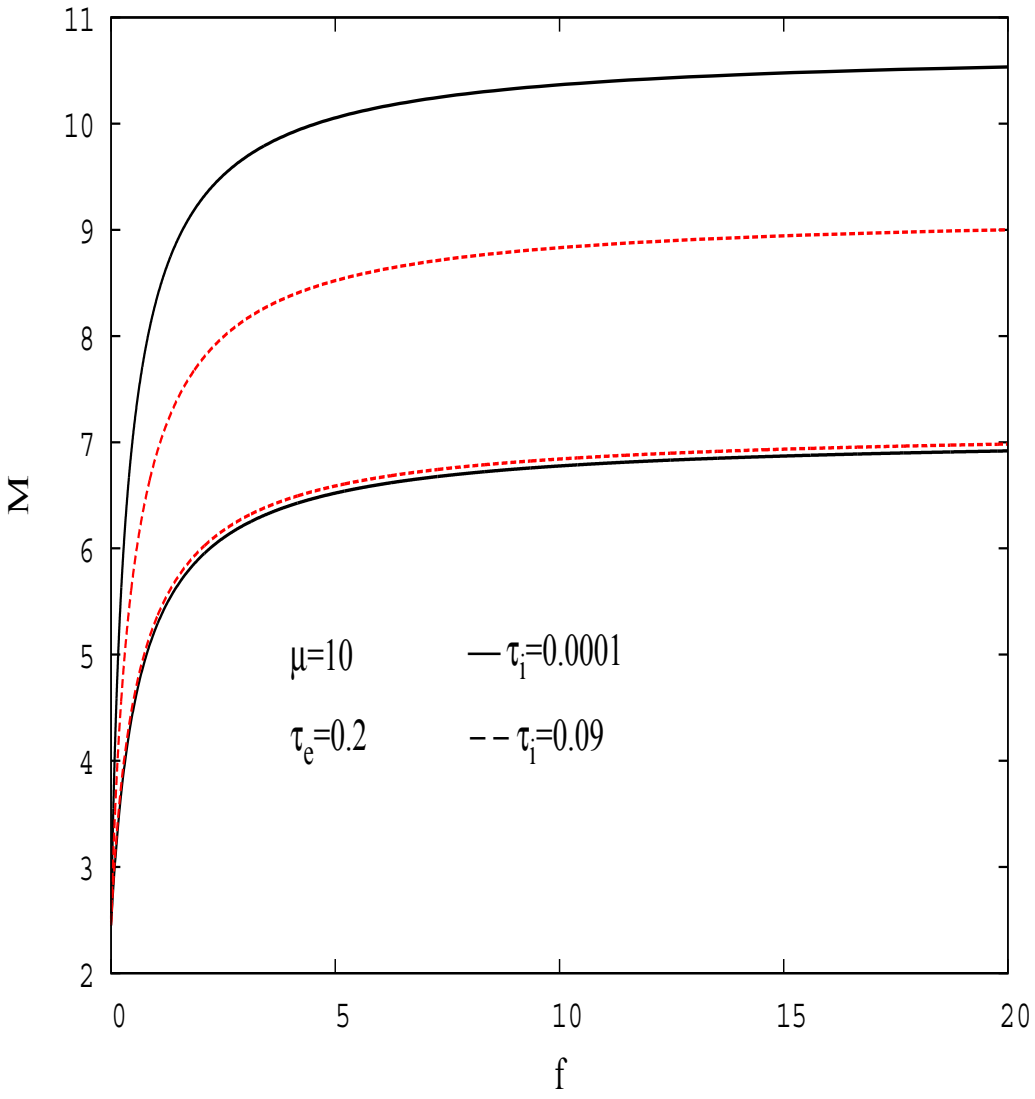

Figure 3.27: The existence domain of the fast mode ion acoustic solitons for $\mu = 10$ and $\tau_e = 0.2$, showing the effect of increasing the value of τ_i from 0.0001 to 0.09. The black solid lines show the results obtained for $\tau_i = 0.0001$, whereas the red dashed lines are for $\tau_i = 0.09$. For each line style, the lower curve represents the lower limit in Mach numbers for the existence of solitons, whereas the upper curve shows the upper limit. Here, the upper limit is due to the occurrence of the cooler ion sonic point only (see also Fig. 3.19).

Let us analyse, in a quantitative manner, the effect of τ_i on the range in Mach numbers over which fast solitons exist, for the case $\mu = 10$ and $f = 10$.

To analyse, quantitatively, the effect of τ_i on the acoustic speed of the fast mode, we also consider the case $\mu = 2$ discussed in Sec. 3.3 (see the lower panel of Fig. 3.4), for a broader picture which will be useful for our subsequent discussion.

From the results presented in the lower panel of Fig. 3.4, for the case $\mu = 2$ and $f = 10$, we find that the acoustic speed is $M_{s+} = 2.533$, when $\tau_i = 0.0001$. Increasing τ_i to 0.4, recalling that $\mu\tau_i$ must satisfy the condition $\mu\tau_i < 1$, we obtain $M_{s+} = 2.678$. Computing the ratio of the acoustic speeds obtained for the above values of τ_i, we obtain $(M_{s+})_{\tau_i=0.4}/(M_{s+})_{\tau_i=0.0001} = 1.06$. Considering the results presented in Fig. 3.27, for the case $\mu = 10$ and $f = 10$, we find that $M_{s+} = 6.776$, when $\tau_i = 0.0001$. Increasing the value of τ_i to 0.09, we get $M_{s+} = 6.842$. Computing the ratio of the acoustic speeds obtained for the above values of τ_i, we get $(M_{s+})_{\tau_i=0.09}/(M_{s+})_{\tau_i=0.0001} = 1.01$. We see that, for both cases $\mu = 2$ and $\mu = 10$, an increase in M_{s+}, due to an increase in τ_i, is small. Indeed, this is not unexpected as could be predicted from Eq. (3.32).

For the maximum Mach numbers shown in Fig. 3.27, we find $M_l = 10.37$ for $\tau_i = 0.0001$, and $M_l = 8.84$ for $\tau_i = 0.09$. The ratio of these maximum Mach numbers yields $(M_l)_{\tau_i=0.09}/(M_l)_{\tau_i=0.0001} = 0.85$.

Clearly, for $\mu = 10$ and $f = 10$, the range in Mach numbers over which fast solitons exist decreases as a result of an increase in the value of τ_i. This result holds irrespective of the value of f, as can be seen from Fig. 3.27.

Figure 3.28 shows the existence domains of the fast mode ion acoustic solitons for $\mu = 1.1$ (upper panel), and $\mu = 1.3$ (lower panel). We have considered these values of μ for a qualitative illustration of the results for values of μ in the approximate range $1 \lesssim \mu \lesssim 1.5$. For each value of τ_i, except $\tau_i = 0.45$ and $\tau_i = 0.6$, shown in each panel, the lower black solid line represents the lower limit in Mach numbers for the existence of solitons, whereas the upper line corresponds to the upper limit. The thick red solid line corresponds to the maximum Mach number due to the occurrence of the hotter ion sonic point, whereas the thin green solid line corresponds to the limitation due to the cooler ion sonic point. For both cases presented in the two panels of Fig. 3.28, it is seen that an increase in τ_i leads to an increase in both the acoustic speed and the maximum Mach number, irrespective of f.

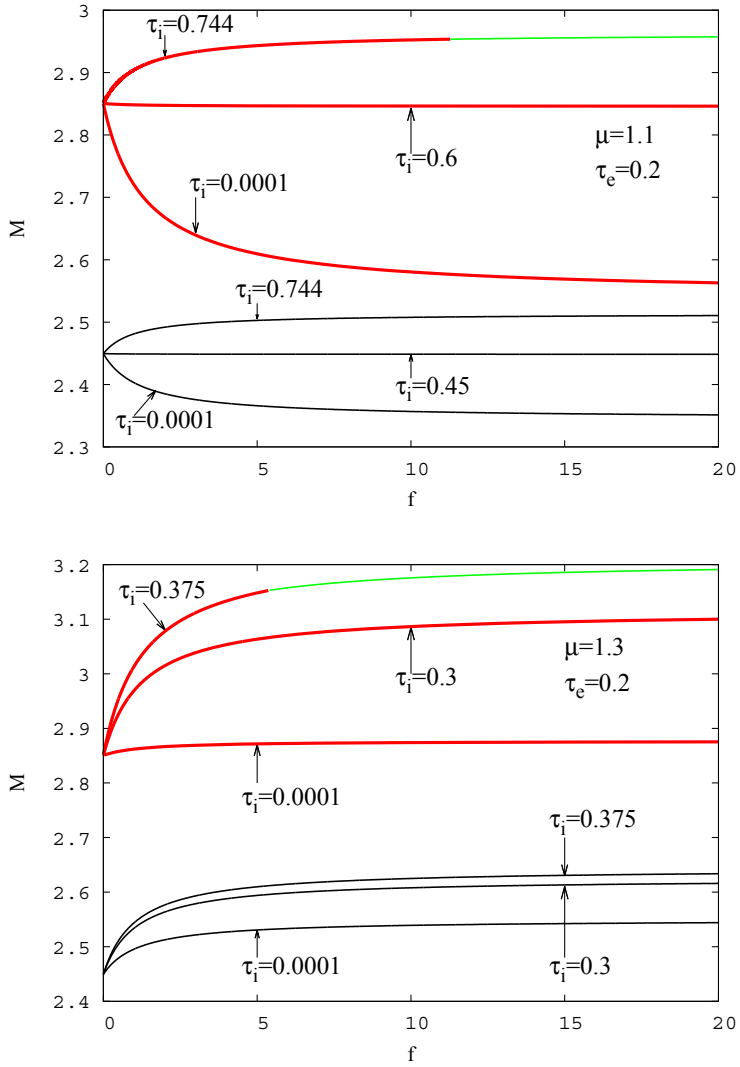

Figure 3.28: The existence domains of the fast mode ion acoustic solitons for $\mu = 1.1$ (upper panel) and $\mu = 1.3$ (lower panel). For each value of τ_i, except $\tau_i = 0.45$ and $\tau_i = 0.6$ discussed in the text, the lower line represents the lower limit in Mach numbers for the existence of solitons, whereas the upper line corresponds to the upper limit. The thick red solid line corresponds to the maximum Mach number due to the occurrence of the hotter ion sonic point, whereas the thin green solid line corresponds to the limitation due to the occurrence of the cooler ion sonic point.

For $\mu = 1.1$, we see that the variation of the acoustic speed and the maximum Mach number with f depends strongly on the value of τ_i. It is found that, for $\tau_i = 0.0001$, both the acoustic speed and the maximum Mach number have their highest values at $f \sim 0$, from which they decrease with increasing f. Importantly, it is observed that there are critical values of τ_i for which the acoustic speed and the maximum Mach number do not vary with f. Thus, for all values of f, the maximum Mach number is observed to be $M_l \approx 2.84$ for $\tau_i = 0.6$, whereas the acoustic speed is found to be $M_{s+} \approx 2.45$ for $\tau_i = 0.45$. Beyond these critical values of τ_i, the acoustic speed and the maximum Mach number have their lowest values at $f \sim 0$, from which they increase with increasing f. A value of $\tau_i = 0.744$ has been used to provide an illustration of this case. For this value of τ_i, the upper limit in Mach numbers is due to the hotter ion sonic point for values of f in the approximate range $0 \lesssim f \lesssim 11.3$, whereas for $f \gtrsim 11.3$ the soliton limitation is due to the cooler ion sonic point. For values of $\tau_i \lesssim 0.744$, the soliton limitation is due to the occurrence of the hotter ion sonic point only.

Our numerical investigation shows that, for $\mu = 1.3$, both the acoustic speed and the maximum Mach number increase with increasing f, for all values of τ_i, recalling that $0 \lesssim \tau_i < 1$. For this value of μ, the upper limit in Mach numbers results from only the occurrence of the hotter ion sonic point for the values of τ_i up to $\tau_i \sim 0.3$. For higher values of τ_i, the soliton limitation results from the occurrence of either the hotter or the cooler ion sonic point, depending on the value of f, as shown in the figure.

In our discussion of the effects of the electron temperature on the existence domain of the fast mode ion acoustic solitons, we showed that a stopband may occur in an existence domain for the values of μ in the approximate range $1.5 \lesssim \mu \lesssim 3$, depending on the value of τ_e. Such a stopband was observed assuming $\tau_i = 0.0001$, and has been discussed, in detail, considering the case $\mu = 1.7$ and $\tau_e = 0.2$ as well as the case $\mu = 2.2$ and $\tau_e = 0.47$ (see Figs. 3.22, 3.23, and 3.24).

An important question is whether the stopband observed in the existence domain of fast solitons still exists for higher values of τ_i. Here, we consider the case $\mu = 1.7$ and $\tau_e = 0.2$, and investigate the effect of increasing the value of τ_i. Our numerical results are presented in Fig. 3.29. For each value of τ_i, the lower and upper limits in Mach numbers for the existence of solitons are shown. Furthermore, for each value of τ_i, the cutoff due to

the hotter ion sonic point is shown by the red solid line, whereas that due to the cooler ion sonic point is shown by the black dashes.

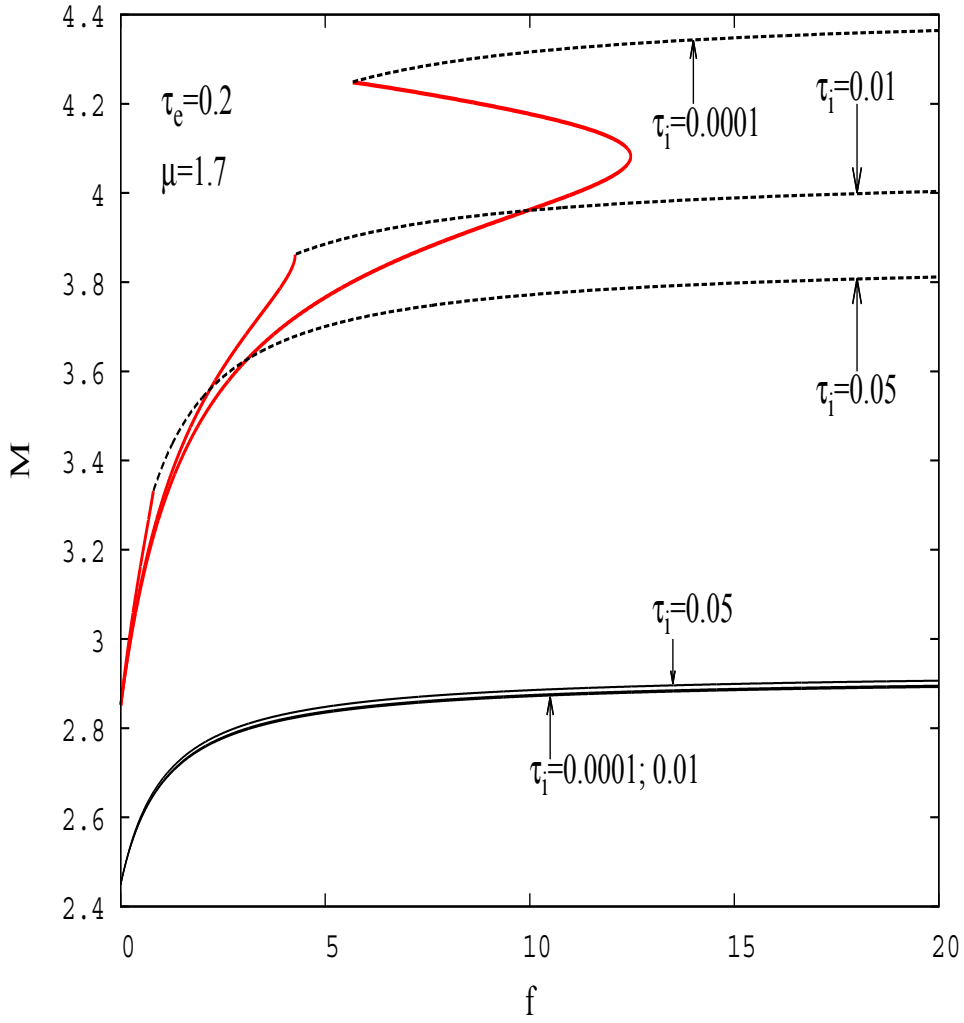

Figure 3.29: The existence domain of the fast mode ion acoustic solitons for $\mu = 1.7$ and $\tau_e = 0.2$, showing the effect of increasing the value of τ_i from 0.0001 to higher values. For each value of τ_i, the lower line represents the lower limit in Mach numbers for the existence of solitons, whereas the upper line illustrates the upper limit. The upper limit indicated by the red solid line is due to the occurrence of the hotter ion sonic point, whereas that shown by the black dashes is due to the occurrence of the cooler ion sonic point.

It is seen that increasing τ_i from 0.0001 to 0.01 has very little effect on the acoustic speed. This small effect of τ_i on the acoustic speed of the fast mode has been discussed, quantitatively, earlier (see the discussion associated with Fig. 3.27). However, it is observed that this increase in τ_i has a significant effect on the maximum Mach numbers. Most importantly, the stopband disappears as a result of this small increase in τ_i. Furthermore, it is seen that the value of the Mach number M_{co+}, Eq. (3.100), at which the limiting potentials, Eqs. (3.96) and (3.97), cross over decreases, due to an increase in τ_i. This was mentioned in our earlier discussion (see the discussion associated with Eq. (3.100). As a result of a decrease in the value of M_{co+}, the range in f over which solitons are limited by the occurrence of the hotter/cooler ion sonic point decreases/increases. For sufficiently large values of τ_i (not shown here for reasons of clarity, but the results could be predicted from Fig. 3.29), our numerical investigation shows that solitons are only limited by the occurrence of the cooler ion sonic point.

Another important point to note from Fig. 3.29 is that, for a given value of f, the limiting Mach number due to the occurrence of the cooler ion sonic point decreases while that due to the hotter ion sonic point increases, as the value of τ_i is increased.

ii. The effects of the ion temperature on the soliton amplitudes and peak profile steepness

We discuss the effects of the ion temperature on the amplitudes and profile steepness of the fast mode ion acoustic solitons. We consider the case $\mu = 0.5$ and $f = 4$, as well as the case $\mu = 1.7$ and $f = 15$. In each of these two cases, the value of $\tau_e = 0.2$ has been used in our numerical evaluation. The soliton existence domains for these cases have been presented in Figs. 3.26 and 3.29, respectively. As in our earlier discussions, we consider a soliton with an "average" speed, $M_{\rm ave}$, calculated using Eq. (3.94) and a soliton with a maximum speed.

For the cases mentioned above, the "average" and maximum Mach numbers, as well as the ratios $M_{\rm ave}/M_{s+}$ and $M_{\rm max}/M_{s+}$ are presented in Table 3.3, for two values of τ_i shown in the table.

We see from Table 3.3 that, for the two values of τ_i, the ratios $M_{\rm ave}/M_{s+}$ and $M_{\rm max}/M_{s+}$ are close to 1, in the case $\mu = 0.5$ and $f = 4$. The fact that the maximum Mach number is close to the acoustic speed implies that there is a small range in Mach numbers over which fast solitons exist before a cutoff is reached. An increase in τ_i has little effect on this range. Indeed, this is reflected in Fig. 3.26 where the lower and upper limits in Mach numbers are seen to be changed by only a small amount in $M_{\rm max}/M_{s+}$, unlike the case $\mu = 1.7$ and $f = 15$ presented in Fig. 3.29.

$\mu = 0.5$, $f = 4$, $\tau_e = 0.2$		$\mu = 1.7$, $f = 15$, $\tau_e = 0.2$	
$\tau_i = 0.0001$	$\tau_i = 0.8$	$\tau_i = 0.0001$	$\tau_i = 0.05$
$M_{s+} = 1.848$	$M_{s+} = 1.905$	$M_{s+} = 2.885$	$M_{s+} = 2.899$
$M_{\rm ave} = 1.922$	$M_{\rm ave} = 1.980$	$M_{\rm ave} = 3.616$	$M_{\rm ave} = 3.350$
$M_{\rm max} = 1.997$	$M_{\rm max} = 2.054$	$M_{\rm max} = 4.348$	$M_{\rm max} = 3.798$
$M_{\rm ave}/M_{s+} = 1.040$	$M_{\rm ave}/M_{s+} = 1.039$	$M_{\rm ave}/M_{s+} = 1.253$	$M_{\rm ave}/M_{s+} = 1.155$
$M_{\rm max}/M_{s+} = 1.081$	$M_{\rm max}/M_{s+} = 1.080$	$M_{\rm max}/M_{s+} = 1.507$	$M_{\rm max}/M_{s+} = 1.310$

Table 3.3: This table contains the parameter values that have been used to generate the Sagdeev potential plots presented in the upper panels of Fig. 3.30. The value of $M_{\rm ave}$ has been calculated using Eq. (3.94).

The upper panels of Fig. 3.30 show the Sagdeev potential plots of a fast soliton with an "average" Mach number (the smaller amplitude) and that of a fast soliton with a maximal Mach number (the larger amplitude). The soliton Mach numbers used to plot the Sagdeev potentials are presented in Table 3.3. For both solitons, the black dotted lines show the results obtained for $\tau_i = 0.0001$, and the red solid lines illustrate the results obtained for a higher value of τ_i shown in the figure.

The lower panels of Fig. 3.30 illustrate the soliton amplitudes plotted against the soliton true Mach numbers, showing the effect of increasing the value of τ_i from 0.0001 to a higher value shown in the figure. The line styles are, clearly, shown in the figure.

The left panels are for the case $\mu = 0.5$ and $f = 4$, and the right panels are for the case $\mu = 1.7$ and $f = 15$.

We see that, for the case $\mu = 0.5$ and $f = 4$, an increase in τ_i results in an increase in the soliton amplitude and peak profile steepness, for both solitons with "average" and maximal speeds. However, for the case $\mu = 1.7$ and $f = 15$, an increase in τ_i results in a decrease in the soliton amplitude and maximum profile steepness, for both solitons with "average" and maximal speeds. In both cases, the soliton amplitude vanishes as the soliton speed approaches the acoustic speed, suggesting that these solitons are "KdV-like".

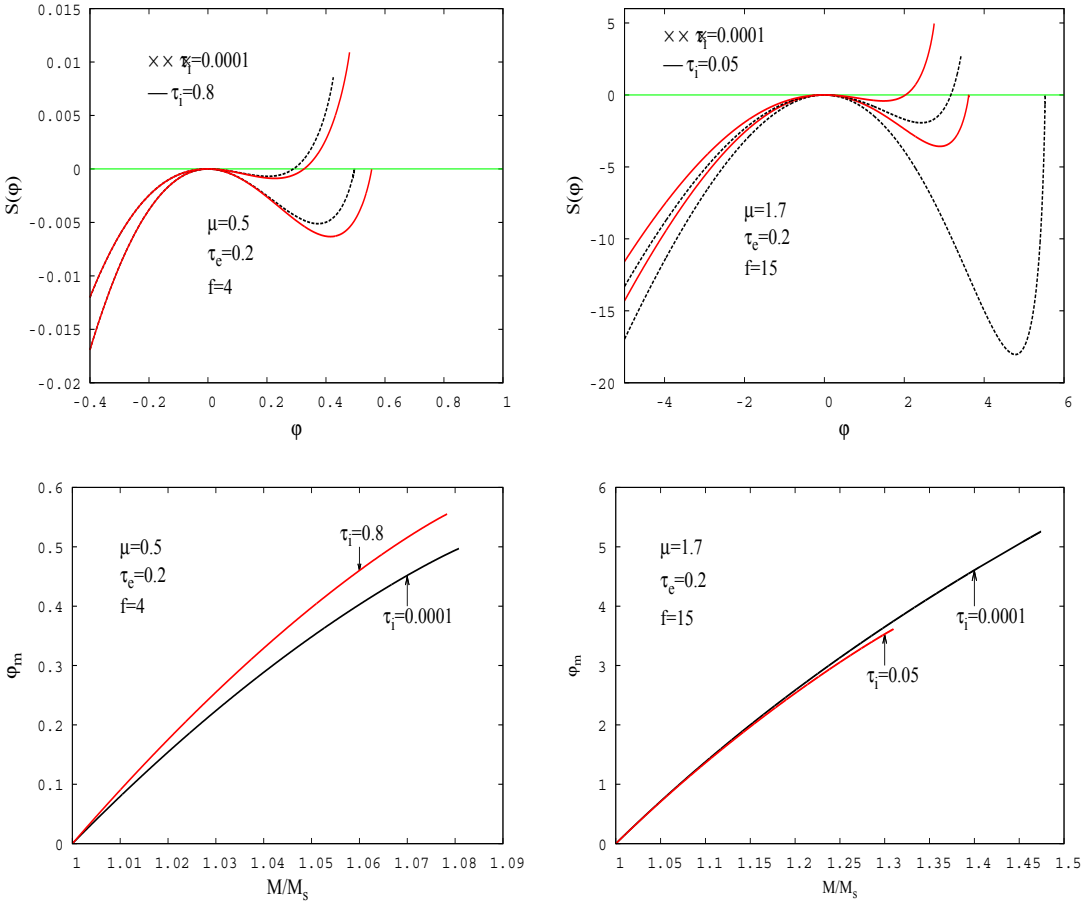

Figure 3.30: The upper panels of this figure show the Sagdeev potential plots of a fast soliton with an "average" Mach number and that of a fast soliton with a maximal Mach number. The soliton Mach numbers used to plot the Sagdeev potentials are presented in Table 3.3. For both solitons, the black dotted lines show the results obtained for $\tau_i = 0.0001$, and the red solid lines illustrate the results obtained for a higher value of τ_i shown in the figure. The lower panels illustrate the soliton amplitudes plotted against the soliton true Mach numbers, showing the effect of increasing the value of τ_i from 0.0001 to a higher value shown in the figure. The left panels are for the case $\mu = 0.5$ and $f = 4$, and the right panels are for the case $\mu = 1.7$ and $f = 15$.

3.6 Chapter summary and conclusions

In this chapter, we studied the linear and nonlinear ion acoustic waves supported by a plasma composed of Boltzmann electrons and two adiabatic, positively and singly charged, ion species. As is also well-known (e.g. Tran (1974); Verheest et al. (2008, 2011)), we showed that such a plasma model supports the propagation of two modes with different phase speeds. A comprehensive study of both the slow and the fast modes has been carried out. The main thrust was to investigate the thermal effects of the cooler ion species and the electrons on arbitrary amplitude ion acoustic solitons/double layers, using the Sagdeev potential approach.

Some of the authors who studied this plasma model before (e.g. Tran (1974); Bhattacharyya & Roychoudhury (1988)) assumed that the temperatures of the two ion species are equal and the normalisation was with respect to the electron temperature.

In this work, dimensionless quantities have been introduced following Verheest et al. (2008), that is, various quantities have been normalised with respect to the characteristics of the hotter ion species. The advantage of this normalisation is that it allows us to investigate the thermal effects of both the cooler ions and the electrons.

As a useful background, we first studied linear ion acoustic waves, using linear theory, and small amplitude ion acoustic solitons, using the KdV theory. The effects of the ion temperature on these waves have also been investigated by Tran (1974), but our work provides more details and insight. The main results obtained from this part of our study are included in those obtained using the Sagdeev potential approach, reported below. The linear dispersion relation of ion acoustic waves has also been obtained from the KdV theory, and the fully nonlinear Sagdeev potential theory.

To study arbitrary amplitude ion acoustic solitons/double layers supported by the plasma model under consideration, we derived and discussed the expression of the Sagdeev potential for both the slow and the fast modes.

i. The slow mode ion acoustic solitons and double layers

Neglecting the thermal effects of the cooler species, the slow mode ion acoustic solitons and double layers supported by the plasma model under

consideration have been studied by Verheest et al. (2008, 2011). Verheest et al. (2008) also assumed that the electrons are superhot in comparison with the adiabatic fluid species, so that the thermal effects of the electrons expressed through the ratio $\tau_e = T_h/T_e$ could be neglected. On the other hand, Verheest et al. (2011) investigated the thermal effects of the electrons on the soliton/double layer characteristics by increasing the value of τ_e from 0.1 to 1, i.e. by reducing T_e from $10T_h$ to T_h.

Perhaps the most interesting result in the work of Verheest et al. (2008, 2011) is a systematic determination of soliton existence domain in $\{f, M\}$ parameter space, where f is the normalised density of the cold/cooler plasma species, and M is the Mach number.

As reported by Verheest et al. (2008, 2011), the maximum Mach numbers of the slow mode ion acoustic solitons supported by the plasma model under consideration result, successively (i.e. from small to large values of f), from the occurrence of the cold/cooler species sonic point, the occurrence of the hotter species sonic point, the occurrence of positive double layers, and the occurrence of negative double layers. Finally, the model breaks down when the cutoff speed reaches the hotter ion thermal speed. As usual, the lower limit in Mach numbers for the existence of solitons is given by the acoustic speed.

In this work, we investigated the thermal effects of the cooler ions on the arbitrary amplitude slow mode ion acoustic solitons and double layers. In our investigation, we used $\tau_i \equiv T_c/T_h = 0.0001$ to represent the fact that the cooler ions are effectively cold, that is, we avoided $\tau_i = 0$. The value $\tau_i = 0.0001$ was chosen for numerical reasons. Furthermore, following Verheest et al. (2008), we assumed that the electrons are much hotter than the hotter ion species and used $\tau_e \equiv T_h/T_e = 0.0001$.

Considering $\tau_i = 0.0001$, we have reproduced the results of Verheest et al. (2008). By increasing the value of τ_i, we have found that the thermal effects of the cooler ions have a significant impact on the results reported by Verheest et al. (2008), particularly on the soliton existence domain.

It has been found that, when the value of τ_i is increased, both the acoustic speed and the maximum soliton speed are shifted to higher values over the whole range of the ion-density ratio, $f = n_{c0}/n_{h0}$, and this effect is enhanced as the value of the ion-mass ratio, $\mu = m_h/m_c$, is increased. For large values of f, both the acoustic speed and the maximum Mach number are close to

1, and this effect is more marked as the value of μ is increased. This means that, for large values of f, and particularly for large values of μ, the phase speed of the slow wave is close to the thermal speed of the hotter ion species and, therefore, in that case, the slow wave is subject to hotter ion Landau damping.

Furthermore, it has been found that the effect of τ_i on the maximum Mach number depends on the nature of the physical limitation on a soliton. As a result of an increase in τ_i, the range in f over which solitons are limited by the cooler ion sonic point increases significantly, whereas that for solitons associated with other physical limitations decreases. The latter decrease in the range in f is more pronounced for solitons limited by the hotter ion sonic point and by positive double layers than for solitons limited by negative double layers.

A systematic investigation of the effects of τ_i on the amplitudes and peak profile steepness of the slow mode ion acoustic solitons and double layers has been carried out, using parameter values from well-defined soliton existence domains.

We have investigated the effects of τ_i on the maximal amplitudes of solitons limited by the sonic points and on the double layer amplitudes, considering the cases $\mu = 0.1$, $\mu = 1$, and $\mu = 10$. We have found that the effect of τ_i on the maximal amplitudes depends on the value of f. The magnitude of the maximal amplitudes due to the occurrence of the sonic points and that of the negative double layer amplitudes decreases, as a result of an increase in τ_i. However, it has been found that the magnitude of the positive double layer amplitudes may either increase or decrease, depending on the value of f.

Considering the case $\mu = 0.1$, we studied, in detail, the effect of τ_i on the amplitudes and peak profile steepness of solitons. In our investigation, we considered f=0.2, 1, and 7. These values of f support, respectively, positive solitons limited by the cooler ion sonic point, positive solitons limited by positive double layers, and negative solitons limited by negative double layers.

We have found that a small increase in τ_i decreases significantly the amplitudes and maximum profile steepness of positive solitons limited by the cooler ion sonic point. On the other hand, we have found that an increase in τ_i leads to a very small decrease in the amplitudes and profile

steepness of negative solitons limited by negative double layers. This is so even for values of τ_i as large as 0.8. However, an increase in τ_i results in a small increase in the amplitudes and profile steepness of positive solitons limited by positive double layers.

Increasing the value of μ, for a fixed value of τ_i, decreases the amplitudes and profile steepness of solitons. In particular, for $\mu = 10$ and $\tau_i = 0.02$, we demonstrated that the amplitudes of positive solitons limited by the cooler ion sonic point and by positive double layers are so small that they are reasonably described by the KdV theory for all Mach numbers within the soliton existence domain.

A systematic study of the effects of τ_i on double layers has been carried out. We have found that an increase in τ_i results in a very small decrease in the magnitude of the negative double layer amplitudes and maximum profile steepness. On the other hand, increasing the value of τ_i results in a decrease or an increase in the amplitudes of positive double layers, depending on the value of f. The peak profile steepness of positive double layers are increased for all values of f that we considered, as a result of an increase in the value of τ_i.

By studying the relationship between the amplitudes and the true Mach numbers of solitons and double layers, we found that all solitons are "KdV-like", that is, their amplitudes tend to zero as their speeds approach the acoustic speed, and this is so irrespective of the values of μ, f, and τ_i. This conclusion was reached by Verheest et al. (2011) whose study was restricted to the case $\tau_i = 0$, that is, in their study the cooler ions were treated as cold.

ii. The fast mode ion acoustic solitons

Using the Sagdeev potential approach, we have studied the arbitrary amplitude fast ion acoustic solitons supported by the plasma model under consideration, considering the thermal effects of the electrons, expressed through the ratio $\tau_e = T_h/T_e$, and those of the cooler ions, expressed through the ratio $\tau_i = T_c/T_h$.

Firstly, the thermal effects of the electrons have been investigated assuming that the cooler ions are effectively cold. Secondly, we studied the thermal

effects of the cooler ions, for a given value of the electron temperature.

The conclusions reached from this part of our study are presented as follows. We first present the general conclusions reached from the study of fast solitons. Then, we present the conclusions reached considering special cases, namely, varying τ_e for fixed τ_i, and varying τ_i for fixed τ_e.

General conclusions reached from the study of fast solitons

The determination of soliton existence domain was our main interest. This is important because when the range in parameter space over which solitons exist is known, further study of solitons is straightforward. The soliton existence domain has been presented in $\{f, M\}$ parameter space, recalling that $f = n_{c0}/n_{h0}$ is the normalised density of the cooler ions, and $M = V/\sqrt{T_h/m_h}$ is the Mach number.

Unlike the slow mode, in the case of the fast mode, we did not find double layers. The maximal Mach numbers, beyond which solitons do not exist, result from the occurrence of either the hotter ion sonic point or the cooler ion sonic point.

It has been found that the shape of an $\{f, M\}$ existence domain of fast solitons depends strongly on whether the value of the ion-mass ratio, $\mu = m_h/m_c$, is in the following ranges: $0 < \mu \leq 1$, $1 \lesssim \mu \lesssim 1.5$, $1.5 \lesssim \mu \lesssim 3$, and $\mu \gtrsim 3$.

In the range $0 < \mu \leq 1$, the soliton limitation is due to the hotter ion sonic point only. Furthermore, both the minimum and maximum Mach numbers for the existence of solitons have their highest value at $f \sim 0$, from which they decrease monotonically with increasing f.

For $\mu \gtrsim 3$, the soliton limitation results from the occurrence of the cooler ion sonic point only. In this case, both the minimum and maximum Mach numbers for the existence of solitons have their lowest value at $f \sim 0$, from which they increase monotonically with increasing f, unlike the case $0 < \mu \leq 1$.

For values of μ slightly greater than 1, namely, $1 \lesssim \mu \lesssim 1.5$, the shape of the soliton existence domain has intermediate features between those for the cases $0 < \mu \leq 1$ and $\mu \gtrsim 3$. Importantly, we have found that there exist values of μ, τ_i, and τ_e for which the acoustic speed or the maximum soliton speed are constant, irrespective of the value of f.

In the range $1.5 \lesssim \mu \lesssim 3$, the soliton limitation may result from the occurrence of either the hotter ion sonic point or the cooler ion sonic point, depending on the values of f, τ_e, and τ_i. Most importantly, it has been found that there are values of f, τ_e, and τ_i for which the maximum Mach number due to the occurrence of the hotter ion sonic point is double-valued. Consequently, for those values of f, τ_e, and τ_i, there is a range of Mach numbers between two passbands of an existence domain over which solitary wave propagation does not occur. We have referred to this range of Mach numbers as a stopband. The observed stopband has been discussed in detail.

Considering the case studies $\mu = 0.5$ and $f = 4$, as well as $\mu = 1.7$ and $f = 15$, the effects of τ_e and τ_i on the soliton speed, amplitude, and peak profile steepness have been discussed in detail. In the former case, solitons are limited by the occurrence of the hotter ion sonic point, whereas for the second case, the soliton limitation is due to the occurrence of the cooler ion sonic point.

It has been found that, for a given value of μ, the soliton amplitude tends to zero as the soliton speed approaches the acoustic speed, in agreement with KdV theory.

Conclusions reached by varying τ_e, for fixed τ_i

To investigate the effects of τ_e, we assumed that $\tau_i = 0.0001$ indicating that the cooler ions are effectively cold. We considered the values of τ_e in the range $0.1 \leq \tau_e < 1$, i.e. $T_h < T_e \leq 10T_h$.

It has been found that, for fixed and arbitrary values of μ and f, an increase in τ_e (i.e. a decrease in T_e) results in a decrease in both the acoustic speed and the maximum Mach number, as well as a decrease in the range in Mach numbers over which solitons exist.

For values of μ in the approximate range $1.5 \lesssim \mu \lesssim 3$, the effect of τ_e on the observed stopband has been investigated. It has been found that the higher the value of μ the greater the value of τ_e is required for the occurrence of the observed stopband.

Conclusions reached by varying τ_i, for fixed τ_e

To investigate the effects of τ_i on fast solitons, we considered $\tau_e = 0.2$ (i.e. $T_e = 5T_h$).

It has been found that the effect of τ_i on the soliton existence domain depends on the value of μ. Considering $\mu = 0.5$, representing values of μ in the range $0 < \mu \leq 1$, we found that an increase in the value of τ_i leads to an increase in both the minimum and the maximum Mach numbers, but the range in Mach numbers over which solitons exist is almost unchanged, irrespective of the value of f.

In the range $\mu \lesssim 3$, we considered $\mu = 10$ to study the effect of τ_i on the soliton existence domain. We have found that an increase in τ_i results in a small increase in the minimum Mach number, but a significant decrease in the maximum Mach number, so that the range in Mach numbers over which solitons exist is reduced significantly, irrespective of the value of f.

Most importantly, the stopband observed in the existence domain of fast solitons, for values of μ in the approximate range $1.5 \lesssim \mu \lesssim 3$ disappears, as a result of a small increase in τ_i. In particular, for $\mu = 1.7$, the stopband disappears when the value of τ_i is increased from 0.0001 to 0.01. The effects of τ_i on the range in Mach numbers may be qualitatively similar to those observed for the cases $\mu = 0.5$ and $\mu = 10$, discussed above, depending on the value of the normalised density of the cooler ions f.

A detailed study of the effects of τ_i on the soliton amplitude, and peak profile steepness has been carried out considering the cases $\mu = 0.5$, $f = 4$, and $\mu = 1.7$, $f = 15$.

In the low ion-mass ratio case, $\mu = 0.5$ and $f = 4$, it has been found that an increase in τ_i leads to an increase in the soliton amplitude and maximum profile steepness. However, in the case $\mu = 1.7$ and $f = 15$, increasing the value of τ_i results in a decrease in the soliton amplitude and maximum profile steepness.

As discussed in detail in Sec. 3.1, the plasma model under consideration was studied by Tran (1974), using the KdV approach, and by Bhattacharyya & Roychoudhury (1988), using the Sagdeev potential approach, and the effects of the ion temperature on fast solitons were reported. We recall that both sets of authors assumed that the two ion species have equal temperatures, and the normalisation was with respect to the electron temperature.

Despite the difference in the normalisation, some of our conclusions are consistent with that reached by Bhattacharyya & Roychoudhury (1988).

Bhattacharyya & Roychoudhury (1988) reported that a finite ion temperature modifies the range in the allowed soliton Mach numbers. This conclusion of Bhattacharyya & Roychoudhury (1988) may be compared to ours regarding the effect of τ_i on the range in the allowed soliton Mach numbers, discussed above, see also Fig. 3.27, for the case $\mu = 10$, and Fig. 3.29, for the case $\mu = 1.7$. We avoid comparing our results with those of Tran (1974), as it is unclear to us how their numerical results were obtained. This has been discussed in Sec. 3.1.

Our most important finding is the presence of a stopband in the existence domain of fast solitons, i.e. a range of Mach numbers between two passbands of an existence domain for which soliton propagation does not occur. To the best of our knowledge, this result is novel. We believe that it has not been reported earlier for any plasma model that may occur in space environments.

Chapter 4

Ion acoustic solitons in a plasma with two positive ion species and kappa-distributed electrons

4.1 Introduction

In the previous chapter, we used a fluid model to study an unmagnetised plasma composed of Boltzmann electrons and two adiabatic, positively and singly charged, ion species. We showed that such a plasma supports the propagation of two modes with different phase speeds, in agreement with earlier studies (e.g. Tran (1974); Tran & Coquerand (1976); Nakamura et al. (1976); Verheest et al. (2008, 2011)).

After normalising various quantities with respect to the characteristics of the hotter ion species, a comprehensive investigation of the thermal effects of the cooler ion species and the electrons on linear and nonlinear ion acoustic waves has been carried out, for both the slow and the fast modes. We have shown that, for some parameter values, a stopband exists in the existence domain of fast solitons. We recall that by a stopband we mean a range of Mach numbers between two passbands of an existence domain over which solitary wave propagation does not occur.

Furthermore, it has been shown that the observed stopband is related to the electron temperature and exists only if the thermal effects of the cooler

ion species are small. The fact that the observed stopband is related to the electron temperature motivates us to carry out a further investigation of it, considering a non-thermal velocity distribution for the electrons.

In this chapter, we consider an unmagnetised plasma composed of two adiabatic ion species, as considered in the previous chapter, and electrons that are modelled by a kappa velocity distribution to study ion acoustic solitons. Since our aim is to carry out a further investigation of the observed stopband, we restrict our discussion to the existence domain of the fast mode ion acoustic solitons. We then show that the observed stopband does not exist for small values of the parameter kappa for which a kappa velocity distribution differs significantly from a Maxwellian-type distribution.

Although our discussion will be restricted to the existence domain of the fast mode ion acoustic solitons for the reason mentioned above, we note that the investigation of the effects of the parameter kappa of the electrons on plasma waves supported by a two-adiabatic-ion plasma is an unsolved problem. Thus, for the purpose of our future work, we derive and discuss the expression of the Sagdeev potential for both the slow and the fast modes.

4.2 Plasma densities and Sagdeev potential

The densities of the hotter and the cooler ion species have been discussed in Subsec. 3.5.2, and we recall that their dimensionless expressions are, respectively,

$$n_h = \frac{1}{2}\left[\sqrt{(1+M)^2 - 2\varphi} \pm \sqrt{(1-M)^2 - 2\varphi}\right], \tag{4.1}$$

and

$$n_c = \frac{1}{2\sqrt{\tau_i}}\left[\sqrt{\left(M/\sqrt{\mu} + \sqrt{\tau_i}\right)^2 - 2\varphi} - \sqrt{\left(M/\sqrt{\mu} - \sqrt{\tau_i}\right)^2 - 2\varphi}\right], \tag{4.2}$$

recalling that $M = V/\sqrt{T_h/m_h}$, $\tau_i = T_c/T_h$, $\mu = m_h/m_c$, and that the temperatures are expressed in energy units.

For plasma particles with mass m, charge q, moving in an electrostatic potential well, φ, with speeds v that are modelled by a kappa velocity distribution, the generalised three-dimensional form of the kappa velocity distribution function given by Eq. 1.12, see also Fig. 1.1, is (e.g. Baluku &

Hellberg (2008))

$$f_\kappa(v) = \frac{N}{\pi^{3/2}}\frac{1}{\theta^3}\frac{\Gamma(\kappa+1)}{\kappa^{3/2}\Gamma(\kappa-1/2)}\left(1+\frac{v^2+2q\varphi/m}{\kappa\theta^2}\right)^{-(\kappa+1)}. \tag{4.3}$$

The density of the kappa-distributed electrons can be obtained by integrating Eq. (4.3) over velocity space, for $q=-e$. Doing so yields (Baluku & Hellberg (2008); Baluku (2011))

$$n_e = n_{e0}\left[1-\frac{e\varphi}{(\kappa-3/2)T_e}\right]^{-(\kappa-1/2)}. \tag{4.4}$$

When $\kappa\to\infty$, the factor $[1-e\varphi/(\kappa-3/2)T_e]^{-(\kappa-1/2)}$ appearing in Eq. (4.4) can be dealt with using the usual limiting techniques to obtain $\exp(e\varphi/T_e)$, and hence the Boltzmann expression given by Eq. (3.3).

Using the normalisation presented in Subsec. 3.4.1, Eq. (4.4) can be written in dimensionless form as

$$n_e = (1+f)\left(1-\frac{\tau_e\varphi}{\kappa-3/2}\right)^{-(\kappa-1/2)}, \tag{4.5}$$

where we recall that $f=n_{c0}/n_{h0}$, and $\tau_e = T_h/T_e$.

Proceeding as in Subsec. 3.5.2 to obtain the dimensionless Poisson's equation involving the above expressions of the densities and integrating in the usual way, we obtain the expression of the Sagdeev potential as

$$\begin{aligned} S(\varphi)_\mp = {} & \left(\frac{1+f}{\tau_e}\right)\left[1-\left(1-\frac{\tau_e\varphi}{\kappa-3/2}\right)^{-\kappa+3/2}\right] + \frac{f}{6\sqrt{\tau_i}}\left\{2\tau_i\sqrt{\tau_i}+\frac{6M^2\sqrt{\tau_i}}{\mu}\right. \\ & \left. -\left[\left(\frac{M}{\sqrt{\mu}}+\sqrt{\tau_i}\right)^2-2\varphi\right]^{3/2}+\left[\left(\frac{M}{\sqrt{\mu}}-\sqrt{\tau_i}\right)^2-2\varphi\right]^{3/2}\right\} \\ & +\frac{1}{6}\{2+6M^2-[(1+M)^2-2\varphi)^{3/2}]\mp[(1-M)^2-2\varphi]^{3/2}\}, \end{aligned} \tag{4.6}$$

where we recall that the upper $(-)$ and lower $(+)$ signs refer to the slow and fast modes, respectively.

It is seen that $S(0) = S^{'}(0) = 0$, as is the usual behaviour of a Sagdeev potential. In Fig. 4.1, we show a plot of the Sagdeev potential of the slow mode obtained in this work (upper panel), i.e. $S(\varphi)_{-}$, compared to that of Verheest et al. (2008) (their Fig. 6), for parameter values described in the caption of the figure. The value of $\kappa = 100$ has been used. For this value of κ, it is seen that our Sagdeev potential reduces to that of Verheest et al. (2008). This is to be expected since a kappa distribution is already effectively Maxwellian for values of κ as large as 20, in many wave situations (see also Fig. 1.1).

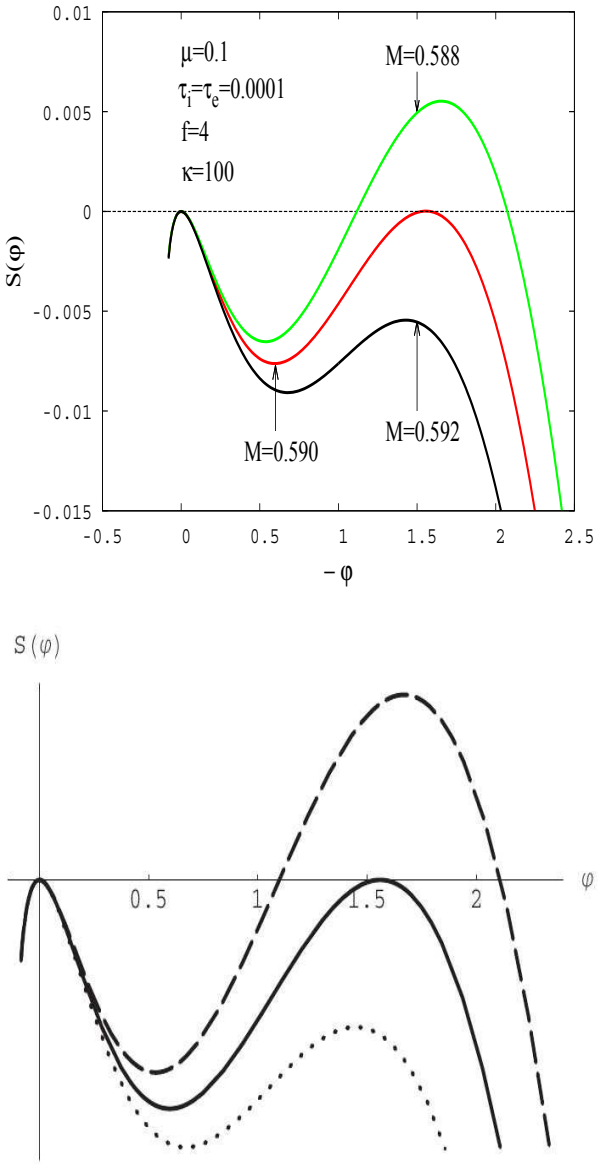

Figure 4.1: Comparison of the Sagdeev potential obtained in this work (upper panel) with that of Verheest et al. (2008) (lower panel). The Sagdeev potential presented in the upper panel corresponds to $S(\varphi)_-$ given by Eq. (4.6) for the parameter values shown in the figure, whereas that presented in the lower panel is Fig. 6 of Verheest et al. (2008). The values of μ, f, and M are as used by Verheest et al. (2008), in their Fig. 6.

As discussed in Subsec. 3.5.2, the lower limit in Mach numbers for the existence of solitons, which corresponds to the acoustic speed (M_s) for the plasma model under consideration, can be obtained from the condition

$$S^{''}(0) = 0, \tag{4.7}$$

where a prime denotes the derivative of $S(\varphi)$ with respect to φ. Evaluation of this equation for the Sagdeev potential given by Eq. (4.6) yields

$$-\tau_e(1+f)\frac{\kappa-1/2}{\kappa-3/2} \mp \frac{1}{1-M_s^2} + \frac{\mu f}{M_s^2-\mu\tau_i} = 0, \tag{4.8}$$

which is satisfied by

$$\begin{aligned} M_{s\mp}^2 = {} & \frac{1}{2(1+f)\tau_e\left(\frac{\kappa-1/2}{\kappa-3/2}\right)}\left[\tau_e(1+f)(1+\mu\tau_i)\left(\frac{\kappa-1/2}{\kappa-3/2}\right)+1+\mu f\right] \\ & \mp \frac{1}{2(1+f)\tau_e\left(\frac{\kappa-1/2}{\kappa-3/2}\right)}\left\{\left[\tau_e(1+f)(1+\mu\tau_i)\left(\frac{\kappa-1/2}{\kappa-3/2}\right)+1+\mu f\right]^2\right. \\ & \left. -4(1+f)\tau_e\left(\frac{\kappa-1/2}{\kappa-3/2}\right)[\mu\tau_i\tau_e(1+f)\frac{\kappa-1/2}{\kappa-3/2}+\mu\tau_i+\mu f]\right\}^{1/2}. \end{aligned} \tag{4.9}$$

It is seen from Eq. (4.9) that the effect of the parameter kappa on the acoustic speed of both the slow and the fast modes is introduced by the factor $(\kappa-1/2)/(\kappa-3/2)$ which is coupled with τ_e. Thus, to study the effect of the parameter kappa on either the slow or the fast mode, one must avoid values of τ_e that are close to zero as in that case the kappa effect would not be obvious. Physically, this means that the superhot approximation for the electrons is not of interest here. Furthermore, it is seen that, as $\kappa \to \infty$, M_{s-} and M_{s+} are identical to their counterparts given by Eqs. 3.10 and 3.11, as expected.

In what follows, we restrict the discussion to the existence domain of the fast mode ion acoustic solitons, leaving further study of solitary waves supported by the plasma model under consideration for future work. The "+" sign associated with various expressions will be omitted for convenience.

4.3 The effects of the parameter kappa on the existence domain of the fast mode ion acoustic solitons

In this section, we discuss the existence domain of fast solitons in $\{f, M\}$ parameter space, proceeding as in Sec. 3.5. We recall from Sec. 3.5 that, for the plasma model under study, the Sagdeev potential of the fast mode becomes complex beyond

$$\varphi_{lh} = \frac{1}{2}(M_l - 1)^2, \tag{4.10}$$

and

$$\varphi_{lc} = \frac{1}{2}\left(\frac{M_l}{\sqrt{\mu}} - \sqrt{\tau_i}\right)^2, \tag{4.11}$$

corresponding, respectively, to positions in space where the flow of the hotter and the cooler ion species reaches a sonic point (e.g. Verheest et al. (2008)), yielding a so-called choked flow (McKenzie, 2002a). In that case, the maximum Mach numbers are obtained from

$$\left.\begin{aligned} S(\varphi_{lh}) &= 0 \\ S(\varphi_{lc}) &= 0 \end{aligned}\right\}. \tag{4.12}$$

From the condition $S(\varphi_{lh}) = 0$, we obtain a relation between the normalised density of the cooler ions, f, and the maximum Mach number of solitons limited by the occurrence of the hotter ion sonic point as

$$\alpha_h f + \beta_h = 0, \tag{4.13}$$

where

$$\alpha_h = \frac{1}{\tau_e}\left\{1 - \left[1 - \frac{\tau_e}{2\kappa - 3}(M_l - 1)^2\right]^{-\kappa+3/2}\right\} + \frac{1}{6\sqrt{\tau_i}}\left\{2\tau_i\sqrt{\tau_i} + \frac{6M_l^2\sqrt{\tau_i}}{\mu}\right.$$
$$\left. - \left[\left(\frac{M_l}{\sqrt{\mu}} + \sqrt{\tau_i}\right)^2 - (M_l - 1)^2\right]^{3/2} + \left[\left(\frac{M_l}{\sqrt{\mu}} - \sqrt{\tau_i}\right)^2 - (M_l - 1)^2\right]^{3/2}\right\}, \tag{4.14}$$

and

$$\beta_h = \frac{1}{\tau_e}\left\{1-\left[1-\frac{\tau_e}{2\kappa-3}(M_l-1)^2\right]^{-\kappa+3/2}\right\}+\frac{1}{6}(2+6M_l^2-8M_l^{3/2}). \quad (4.15)$$

Similarly, from $S(\varphi_{lc}) = 0$, we obtain a relation between f and the maximum Mach number due to the occurrence of the cooler ion sonic point as

$$\alpha_c f + \beta_c = 0, \quad (4.16)$$

where

$$\alpha_c = \frac{1}{\tau_e}\left\{1-\left[1-\frac{\tau_e}{2\kappa-3}\left(\frac{M_l}{\sqrt{\mu}}-\sqrt{\tau_i}\right)^2\right]^{-\kappa+3/2}\right\}+\frac{1}{6\sqrt{\tau_i}}\left\{2\tau_i\sqrt{\tau_i}+\frac{6M_l^2\sqrt{\tau_i}}{\mu}\right.$$
$$\left.-\left[\left(\frac{M_l}{\sqrt{\mu}}+\sqrt{\tau_i}\right)^2-\left(\frac{M_l}{\sqrt{\mu}}-\sqrt{\tau_i}\right)^2\right]^{3/2}\right\}, \quad (4.17)$$

and

$$\beta_c = \frac{1}{\tau_e}\left\{1-\left[1-\frac{\tau_e}{2\kappa-3}\left(\frac{M_l}{\sqrt{\mu}}-\sqrt{\tau_i}\right)^2\right]^{-\kappa+3/2}\right\}+\frac{1}{6}\left\{2+6M_l^2-\left[(M_l+1)^2-\left(\frac{M_l}{\sqrt{\mu}}-\sqrt{\tau_i}\right)^2\right]^{3/2}\right.$$
$$\left.+\left[(M_l-1)^2-\left(\frac{M_l}{\sqrt{\mu}}-\sqrt{\tau_i}\right)^2\right]^{3/2}\right\}. \quad (4.18)$$

For given values of f, the maximum Mach numbers for the existence of solitons have been calculated numerically using the relations (4.13) and (4.16), whereas the minimum Mach numbers, i.e. the acoustic speeds, have been calculated using Eq. (4.9) (see the expression involving the "+" sign).

Figure 4.2 shows the results obtained for $\mu = 1.7$, $\tau_e = 0.2$, $\tau_i = 0.0001$, and $\kappa = 1000$ (upper left panel), $\kappa = 50$ (upper right panel), $\kappa = 10$ (lower left panel), $\kappa = 1.8$ (lower right panel). The lower line represents the lower limit in Mach numbers for the existence of solitons, the upper red thick solid line corresponds to the maximum Mach numbers due to the occurrence of the hotter ion sonic point, and the upper green thin solid line is for the Mach number limit due to the cooler ion sonic point.

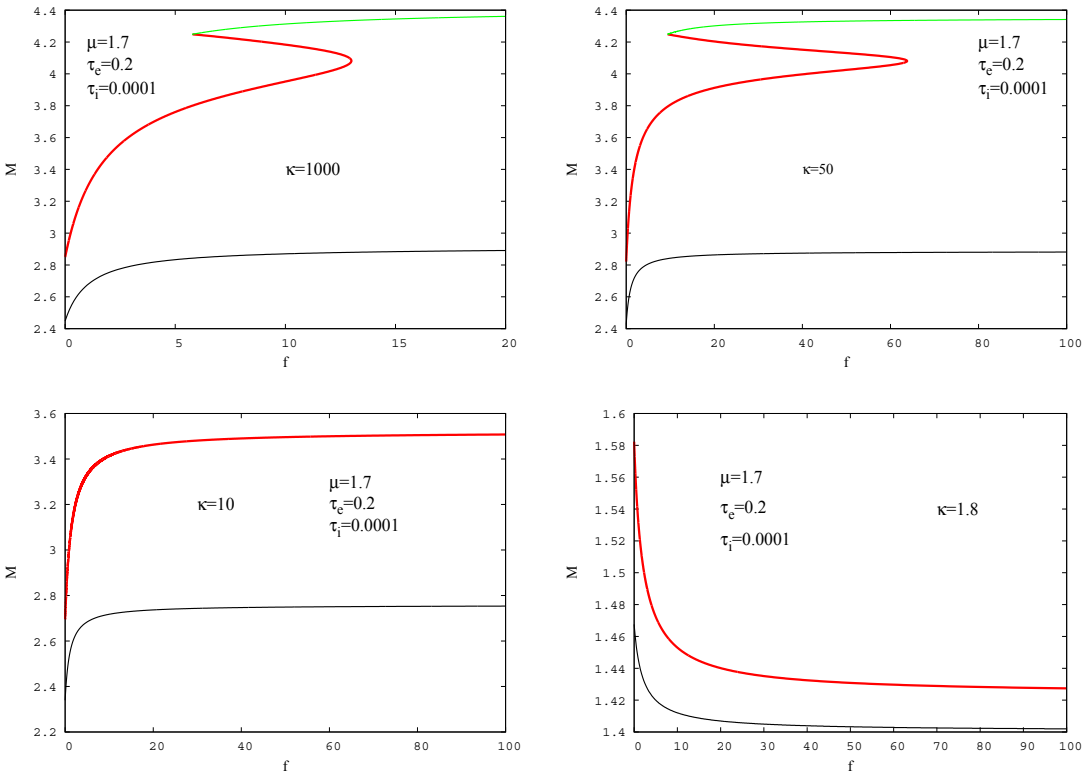

Figure 4.2: The existence domains of the fast mode ion acoustic solitons for $\mu = 1.7$, $\tau_e = 0.2$, $\tau_i = 0.0001$, and $\kappa = 1000$ (upper left panel), $\kappa = 50$ (upper right panel), $\kappa = 10$ (lower left panel), $\kappa = 1.8$ (lower right panel).

From the upper left panel of this figure, we see that the existence domain obtained for $\kappa = 1000$ is reminiscent of that obtained when the electrons are Maxwellian (see the results presented in the middle panel of Fig. 3.22). This is not unexpected as a kappa velocity distribution is already quasi-Maxwellian for values of κ as large as 20 (see Fig. 1.1).

However, whereas for the pure Maxwellian case the stopband was observed for the values of f within the range $5.7 \lesssim f \lesssim 12.5$, this range is shifted slightly to higher values for $\kappa = 1000$, and in this case we have $5.8 \lesssim f \lesssim 13$. When the value of κ is reduced to 50, as shown in the upper right panel, the range in f over which the stopband occurs is increased significantly and is shifted to much higher values, namely $9.4 \lesssim f \lesssim 63.8$.

Reducing further the value of κ to 10, as shown in the lower left panel, our numerical evaluation shows that, even for values of f as high as 100, there are only the maximum Mach numbers due to the occurrence of the hotter ion sonic point, and no stopband is observed.

Finally, we consider a case which is strongly non-thermal and use $\kappa = 1.8$. In this case, we find that the variation of the acoustic speed and the maximum Mach number with f changes, the trend is as shown in the lower right panel of the figure, and no stopband is observed. We also obtain the maximum Mach numbers due to the occurrence of the hotter ion sonic point only.

From the results shown in all panels of Fig. 4.2, we see that a decrease in the value of κ results in a decrease in both the acoustic speed and the maximum Mach number, irrespective of the value of f.

In the previous chapter, we showed that the stopband occurs in the existence domain of fast solitons for the values of μ within the approximate range $1.5 \lesssim \mu \lesssim 3$, depending on the value of τ_e. We have considered a further investigation of the effect of kappa on the existence domain of fast solitons considering other values of μ in this range. The results obtained for $\mu = 2.2$ and $\tau_e = 0.47$ are presented in Appendix E.1. Overall, what we find is that for the values of μ in the approximate range $1.5 \lesssim \mu \lesssim 3$ and for the values of τ_e for which the stopband occurs, the effect of κ on the existence domain is, qualitatively, as shown in Fig. 4.2. That is, for parameters values for which the stopband occurs when the electrons are Maxwellian, the stopband does not exist for small values of κ for which a kappa velocity distribution differs significantly from a Maxwellian.

A simple way to check whether the obtained soliton existence domains are free of numerical artefacts is to plot the Sagdeev potentials for Mach numbers ranging from the minimum to the maximum value.

Figure 4.3 shows the Sagdeev potentials obtained based on the soliton existence domains presented in Fig. 4.2. The upper panel is for $\kappa = 1000$, the middle panel is for $\kappa = 10$, and the lower panel is for $\kappa = 1.8$. Other parameter values used are shown in the figure. For each of these values of κ, we show the Sagdeev potential obtained at the acoustic speed, the maximum Mach number, and for a Mach number between the maximum one and the acoustic speed. For all cases presented in the figure, solitons have vanishing amplitudes at the acoustic speed. Clearly, for each case shown in the figure, the Mach numbers ranging from the acoustic speed to the maximum one are for real solitons. A plot of the Sagdeev potentials for a value of f for which the stopband occurs has been presented in Chap. 3, see Fig. 3.23.

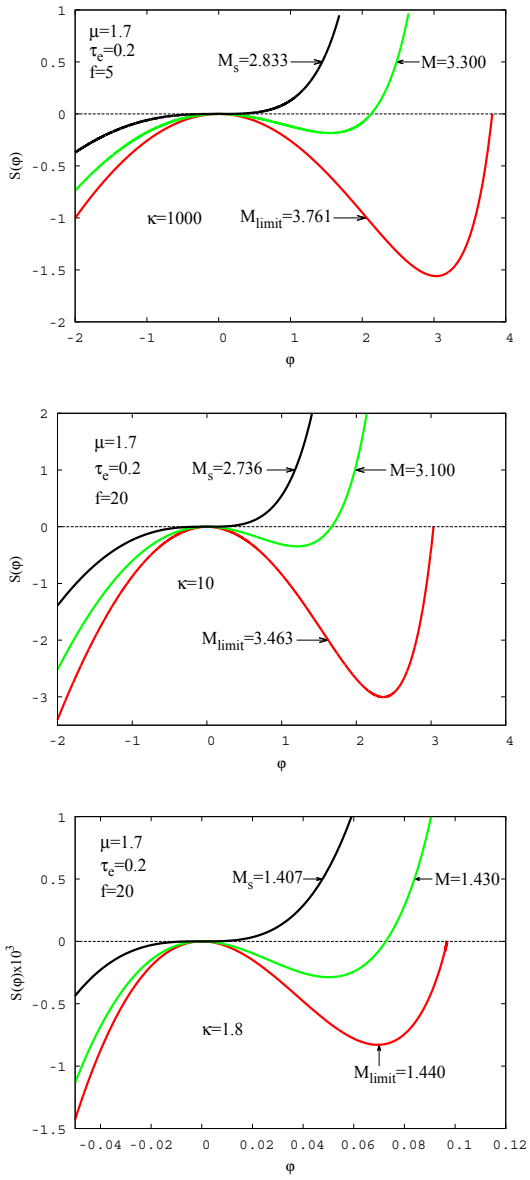

Figure 4.3: The Sagdeev potentials of the fast mode ion acoustic solitons for $\kappa = 1000$ (upper panel), $\kappa = 10$ (middle panel), $\kappa = 1.8$ (lower panel). Other parameter values considered are, clearly, shown in each panel.

From our investigation of the existence domain of fast solitons, in the previous chapter, we know that, for values of μ in the range $0 < \mu \lesssim 1$, the variation of the acoustic speed and the maximum Mach number with f is significantly different from that observed when $\mu \gg 1$. For completeness, we have also investigated the effect of the parameter κ on the existence domain of fast solitons for the values of μ in these ranges, and the results are presented in Fig. 4.4 for $\mu = 10$ (upper panels) and $\mu = 0.5$ (lower panels), showing the effect of decreasing the value of κ from 1000 (left panels) to 1.8 (right panels).

For each case shown in Fig. 4.4, it is seen that the variation of the acoustic speed and the maximum Mach number with f is as observed when the electrons are Maxwellian. A decrease in the value of κ leads to a decrease in both the acoustic speed and the maximum Mach number.

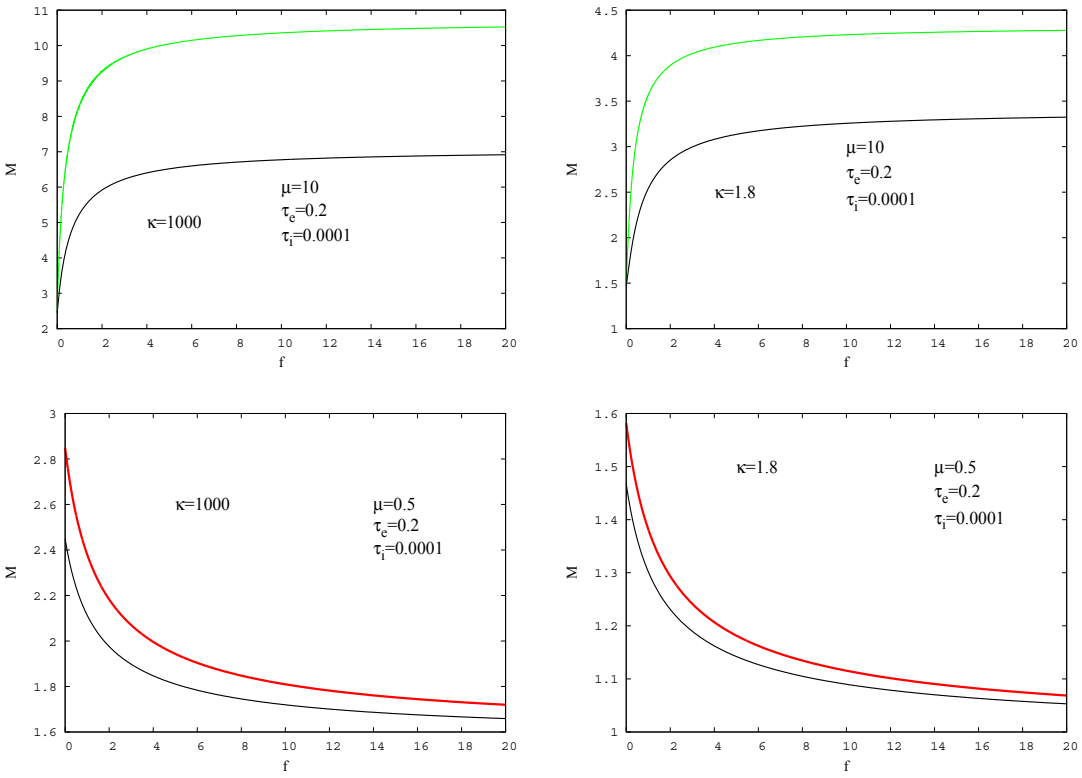

Figure 4.4: The existence domains of the fast mode ion acoustic solitons for $\mu = 10$ (upper panels) and $\mu = 0.5$ (lower panels), showing the effect of decreasing the value of κ from 1000 (left panels) to 1.8 (right panels). The lower line represents the lower limit in Mach numbers for the existence of solitons, the upper thick red solid line corresponds to the upper limit due to the occurrence of the hotter ion sonic point, and the upper thin green solid line is for the upper limit due to the occurrence of the cooler ion sonic point.

4.4 Chapter summary and future work

The stopband observed in the existence domain of fast solitons, and discussed in detail in Chap. 3, is related to the electron temperature and, therefore, further investigation of it may be carried out by modelling the electrons with velocity distributions other than a Maxwellian-type distribution.

In this chapter, we considered a two-adiabatic-ion plasma and kappa-distributed electrons to investigate the effects of the parameter kappa on the existence domain of the fast mode ion acoustic solitons. As in Chap. 3, the soliton existence domain has been presented in $\{f, M\}$ parameter space, recalling that f is the normalised density of the cooler ions and M is the Mach number. Our aim was to carry out a further investigation of the stopband observed in the existence domain of fast solitons.

It is perhaps useful to emphasise that, by a stopband, we mean a range of Mach numbers between two passbands of an existence domain over which solitary wave propagation does not occur. The observed stopband results from the fact that the maximum Mach number due to the occurrence of the hotter ion sonic point is double-valued for a range of values of f.

Using values of μ, τ_e, and τ_i for which a stopband was found for Maxwellian electrons, we have shown that the stopband exists only for large values of kappa for which a kappa velocity distribution has a Maxwellian behaviour. For values of kappa as small as 10, usually regarded as being quasi-Maxwellian in kappa plasma wave studies, the soliton limitation is only due to the occurrence of the hotter ion sonic point and the maximum Mach number is single-valued, irrespective of the value of f.

The results presented in this chapter should be regarded as preliminary. We intend to carry out a comprehensive study of plasma waves supported by a two-adiabatic-ion plasma and kappa-distributed electrons, for both the slow and the fast modes.

Two important topics are possible. On the one hand, by neglecting the thermal effects of the cooler ions, and for a given value of the electron temperature, one can carry out a survey of the parameter kappa of the electrons, for both the slow and the fast modes. On the other hand, one can consider a small value of κ for which a kappa distribution differs significantly from a Maxwellian, namely, $\kappa \sim 2$, and investigate the effect of varying the temperatures of the cooler ions and the electrons, for both the slow and the fast modes, following the approach used in Chap. 3. The results obtained can, then, be compared with those presented in Chap. 3 in which the electrons were modelled by the Boltzmann distribution.

Chapter 5

General summary and conclusions

In this chapter, we present a general overview of the content of the thesis. We do not provide details of the conclusions, as these have been presented in the appropriate chapters.

The work presented in this thesis involves a study of some linear and nonlinear plasma waves. It involves two components. One component is about a kinetic-theoretical study of ion Bernstein waves in an electron-proton plasma with a kappa velocity distribution. Another component is about a study of linear and nonlinear ion acoustic waves in a two-adiabatic-ion plasma, using fluid theory.

1. Kinetic theory of ion Bernstein waves

Regarding the kinetic-theoretical study of ion Bernstein waves, we have carried out a general numerical investigation of the effect of the parameter kappa on the dispersion relation of ion Bernstein waves, followed by an application of the results to the Earth's plasma sheet boundary layer (PSBL) in which waves propagating perpendicularly to the ambient magnetic field at frequencies between harmonics of the ion cyclotron frequency are frequently observed. The observations of these waves have been discussed in detail in Sec. 2.1.

Closed forms of the dispersion relations of Bernstein waves in kappa and in Maxwellian multi-species plasmas were obtained by Mace (2003), and an

alternative derivation was reported by Henning et al. (2011). Neglecting the ion dynamics, Mace (2003) obtained the numerical solutions of both of these dispersion relations for the electron Bernstein mode.

In this work, we considered the ion dynamics and obtained the numerical solutions of both dispersion relations reported by Mace (2003) for the ion Bernstein mode. Our aim was to investigate the effect of the parameter kappa on the dispersion relation of ion Bernstein waves. The dispersion curves of ion Bernstein waves in Maxwellian plasmas are in the literature (e.g. Fredricks (1968a); Puri et al. (1973)), but have also been obtained in this work for comparison with those obtained for the kappa case.

During our investigation, we considered a wide range of the values of the ratio of the ion plasma frequency to the ion cyclotron frequency, $\omega_{pi}/\omega_{\rm ci}$, for a broader picture that permits application of the results to various space environments. We recall that $\omega_{pi}^2/\omega_{ci}^2 \propto n_{i0}/B_0^2$, where n_{i0} is the equilibrium ion density and B_0 is the equilibrium magnetic field strength. Thus, varying $\omega_{pi}/\omega_{\rm ci}$ implies varying n_{i0} and/or B_0.

For a fixed value of $\omega_{pi}/\omega_{\rm ci}$, we have found that the dispersion relation depends significantly on the parameter kappa of the ions, κ_i, but is independent of the electron kappa. Over all cyclotron harmonics, the dispersion curves are shifted to higher wavenumbers (k) if κ_i is reduced, i.e. if there is an increased superthermal component in the distribution. We recall that $\kappa \to \infty$ yields the Maxwellian distribution. When the value of ω_{pi}/ω_{ci} is increased, the fall-off of the wave frequency, ω, at large k is smaller for lower κ_i, and curves are shifted towards larger wavenumbers.

For large values of ω_{pi}/ω_{ci}, the ion Bernstein wave dispersion curves within and above the lower hybrid frequency band exhibit coupling for the Maxwellian case, unlike the kappa case. We have suggested that this result may be a useful diagnostic for determining whether the ion velocity distribution possesses a power law tail.

Using the values of the ion density and the magnetic field strength that have been observed in the PSBL, and neighbouring environments, we have found that the derived value of ω_{pi}/ω_{ci} is very large, and that the corresponding lower hybrid frequency has a value that is close to the upper limit given by $\sqrt{1836}\omega_{ci} \approx 42.85\omega_{ci}$, for an electron-proton plasma model. The associated ion Bernstein wave dispersion curves are typical of those found for the case of a high-density plasma immersed in a weak magnetic field.

2. Fluid theory of linear and nonlinear ion acoustic waves

A fluid model was used to study linear, weakly nonlinear, and fully nonlinear ion acoustic waves supported by an unmagnetised plasma composed of Boltzmann electrons and two adiabatic, positively and singly charged, ion species. The KdV theory was used to study small amplitude ion acoustic solitons, and the fully nonlinear Sagdeev potential theory was used to study arbitrary amplitude ion acoustic solitons and double layers. The dispersion relation of linear ion acoustic waves has been obtained from linear theory, the KdV theory, and the fully nonlinear Sagdeev potential theory.

As is also well-known from earlier studies (e.g. Tran (1974); Tran & Coquerand (1976); Nakamura et al. (1976); Verheest et al. (2008, 2011)), we have shown that the plasma model under consideration supports the propagation of two modes with different phase speeds. The phase speed of the slow mode lies between the thermal speeds of the two ion species, whereas that of the fast mode lies between the thermal speeds of the hotter ion species and the electrons. A comprehensive study of both the slow and the fast modes has been carried out, using mainly the Sagdeev potential theory.

One advantage of the Sagdeev potential theory is that it permits a study of all solitons, irrespective of their amplitudes, based on a well-determined soliton existence domain, unlike the KdV theory which is restricted to weakly nonlinear effects.

Nevertheless, we have also considered small amplitude solitons using the KdV approach, for completeness. This has also been a useful background to our study of arbitrary amplitude solitons and double layers, using the fully nonlinear Sagdeev approach. The effects of the ion temperature on small amplitude solitons supported by the plasma model under study have been investigated by Tran (1974), but our work provides more details and insight. Tran (1974) assumed that the temperatures of the two ion species are equal and the normalisation was with respect to the electron temperature.

Our present work is built on the work of Verheest et al. (2008), and is very closely related to that of Verheest et al. (2011). Following Verheest et al. (2008), we assumed that the two ion species have different temperatures, and normalised variables with respect to the characteristics of the hotter ion

species. Such normalisation allows us to carry out a survey of parameters characterising both the cooler ion species and the electrons. We recall that Verheest et al. (2008, 2011) studied the slow mode, but did not consider the fast mode. Furthermore, they neglected completely the thermal effects of the cooler species.

a. The thermal effects of the cooler ion species on the arbitrary amplitude slow mode ion acoustic solitons and double layers

A comprehensive investigation of the thermal effects of the cooler ion species on arbitrary amplitude slow mode ion acoustic solitons and double layers has been carried out. Neglecting the thermal effects of the cooler ion species, expressed through the ion temperature ratio as $\tau_i = T_c/T_h$, we have reproduced the results of Verheest et al. (2008). By increasing the value of τ_i, we have found that the thermal effects of the cooler ions have a significant impact on the results reported by Verheest et al. (2008), particularly the soliton existence domains.

We have carried out an extensive survey of parameters characterising the cooler ions, emphasising the thermal effects of the cooler ions on the soliton existence domain and on the soliton/double layer speed, amplitude, and maximum profile steepness. In this way, our present work should be regarded as an extension of the work of Verheest et al. (2008) who ignored completely the thermal effects of the cooler species. The thermal effects of the electrons on solitons and double layers have not been considered in this work, as they were investigated by Verheest et al. (2011).

b. The thermal effects of the electrons and the cooler ions on the arbitrary amplitude fast mode ion acoustic solitons

The arbitrary amplitude fast mode ion acoustic solitons supported by the plasma model under consideration have been studied by Bhattacharyya & Roychoudhury (1988). A point that we have noted from the work of Bhattacharyya & Roychoudhury (1988) is that the authors never mentioned the existence of two modes in an adiabatic-two-ion plasma. Like Tran (1974), Bhattacharyya & Roychoudhury (1988) assumed that the temperatures of

the two ion species are equal and the normalisation was with respect to the electron temperature. The authors carried out an investigation of the effect of the ion temperature, and reported that a finite ion temperature modifies the range in the allowed soliton Mach numbers.

In this work, we have carried out a systematic and extensive survey of the parameters characterising both the cooler ions and the electrons, emphasising the thermal effects of the two species on the soliton existence domain, speed, amplitude, and peak profile steepness. In this way, we have shown that, while some of our conclusions are consistent with that of Bhattacharyya & Roychoudhury (1988), there are many new results which have not been reported previously.

These new results include the existence of a novel, and perhaps surprising, stopband that has been observed in the soliton existence domain. By a stopband, we mean a range of Mach numbers between two passbands of an existence domain over which solitary wave propagation does not occur. The observed stopband is related to the ion-ion mass ratio and the hotter ion to electron temperature ratio and exists only when the thermal effects of the cooler ion species are small.

We have carried out a preliminary study of the fast mode in a plasma in which the electrons are kappa-distributed, considering plasma parameters for which a stopband was found for Boltzmann electrons, and found that the stopband, although present for large κ, disappears when κ is reduced to 10 or lower.

Appendix A

Derivation of the dispersion relation of ion acoustic waves in a plasma with two positive ion species and Boltzmann electrons

In this appendix, the dispersion relation of ion acoustic waves in a plasma composed of Boltzmann electrons and two adiabatic, positively and singly charged, ion species is derived, showing the details. The basic equations given in Sec. 3.3 are considered.

Using the adiabatic-pressure-density relation, i.e. Eq. (3.5), we can express the pressure gradient in terms of the density gradient as

$$\frac{\partial p_j}{\partial x} = 3\frac{p_j}{n_j}\frac{\partial n_j}{\partial x}, \tag{A.1}$$

and hence re-write the momentum equation, i.e. Eq. (3.1), as

$$m_j n_j \left(\frac{\partial v_j}{\partial t} + v_j \frac{\partial v_j}{\partial x}\right) = -e n_j \frac{\partial \varphi}{\partial x} - 3\frac{p_j}{n_j}\frac{\partial n_j}{\partial x}. \tag{A.2}$$

To linearise the basic equations, we separate the dependent variables into an equilibrium part indicated by a subscript 0 and an oscillating part

indicated by a subscript 1 as

$$n_j = n_{j0} + n_{j1}, \tag{A.3}$$

$$p_j = p_{j0} + p_{j1}, \tag{A.4}$$

$$v_j = v_{j1}, \tag{A.5}$$

$$\varphi = \varphi_1, \tag{A.6}$$

$$n_e = n_{e0} + n_{e1}, \tag{A.7}$$

where we recall that the subscript $j = c, h$ refers to the cooler and the hotter ion species, respectively.

Assuming plane waves varying as $\exp[i(kx - \omega t)]$, we can replace the time derivative $\partial/\partial t$ by $-i\omega$ and the gradient $\partial/\partial x$ by ik. With this information and using (A.3) – (A.6), the momentum equation in the form given by Eq. (A.2) can be linearised to obtain

$$\omega m_j n_{j0} v_{j1} = e n_{j0} k \varphi_1 + T_j k n_{j1}. \tag{A.8}$$

Here, we have introduced a temperature of the j^{th} adiabatic species, expressed in energy units, as (e.g. Verheest & Hellberg (2010b), p. 279)

$$T_j = \frac{3 p_{j0}}{n_{j0}}. \tag{A.9}$$

Similarly, the continuity equation, Eq. (3.2), the density of the inertialess electrons, Eq. (3.3), and Poisson's equation, Eq. (3.4), can be linearised using the appropriate variable expressions in (A.3)-(A.7) to get, respectively

$$\omega n_{j1} = n_{j0} k v_{j1}, \tag{A.10}$$

$$n_{e1} = \frac{e n_{e0} \varphi_1}{T_e}, \tag{A.11}$$

$$\epsilon_0 k^2 \varphi_1 = e(n_{h1} + n_{c1} - n_{e1}). \tag{A.12}$$

From Eqs. (A.8) and (A.10), we obtain the density of the j^{th} ion species as

$$n_{j1} = \frac{e n_{j0} \varphi_1}{m_j \omega^2 / k^2 - T_j}. \tag{A.13}$$

Substituting (A.11) and (A.13) in (A.12), we obtain

$$\epsilon_0 k^2 \varphi_1 = e^2 \left(\frac{n_{h0}\varphi_1}{m_h\omega^2/k^2 - T_h} + \frac{n_{c0}\varphi_1}{m_c\omega^2/k^2 - T_c} - \frac{n_{e0}\varphi_1}{T_e} \right), \tag{A.14}$$

or

$$\epsilon_0 k^2 + \frac{e^2 n_{e0}}{T_e} = e^2 \left(\frac{n_{h0}}{m_h\omega^2/k^2 - T_h} + \frac{n_{c0}}{m_c\omega^2/k^2 - T_c} \right), \tag{A.15}$$

which, after rearranging, becomes

$$\begin{aligned} m_c m_h \left(\epsilon_0 k^2 + \frac{e^2 n_{e0}}{T_e} \right) \frac{\omega^4}{k^4} - \left[\left(\epsilon_0 k^2 + \frac{e^2 n_{e0}}{T_e} \right) (m_h T_c + m_c T_h) + e^2 (n_{h0} m_c + n_{c0} m_h) \right] \frac{\omega^2}{k^2} \\ + \left(\epsilon_0 k^2 + \frac{e^2 n_{e0}}{T_e} \right) T_h T_c + e^2 (n_{h0} T_c + n_{c0} T_h) = 0, \end{aligned} \tag{A.16}$$

or simply

$$\begin{aligned} \epsilon_0 m_c m_h \left(k^2 + \lambda_{De}^{-2} \right) \frac{\omega^4}{k^4} - \left[\epsilon_0 \left(k^2 + \lambda_{De}^{-2} \right) (m_h T_c + m_c T_h) + e^2 (n_{h0} m_c + n_{c0} m_h) \right] \frac{\omega^2}{k^2} \\ + \epsilon_0 \left(k^2 + \lambda_{De}^{-2} \right) T_h T_c + e^2 (n_{h0} T_c + n_{c0} T_h) = 0, \end{aligned} \tag{A.17}$$

where $\lambda_{De} = (\epsilon_0 T_e / e^2 n_{e0})^{1/2}$ is the electron Debye length.

Eq. (A.17) is the desired dispersion relation and reduces to

$$\begin{aligned} m_c m_h n_{e0} \frac{\omega^4}{k^4} - (n_{e0} m_h T_c + n_{e0} m_c T_h + n_{h0} m_c T_e + n_{c0} m_h T_e) \frac{\omega^2}{k^2} \\ + n_{e0} T_h T_c + n_{h0} T_c T_e + n_{c0} T_h T_e = 0, \end{aligned} \tag{A.18}$$

in the long wavelength limit, i.e. $k^2 \lambda_{De}^2 \to 0$.

Appendix B

Derivation of Korteweg-de Vries (KdV) equation

B.1 Expression of the basic equations in terms of a small parameter ε

In this appendix, we derive the KdV equation, and obtain its soliton solution, for a plasma composed of Boltzmann electrons and two adiabatic, positively and singly charged, ion species. The basic equations, i.e. Eqs. (3.1)−(3.4), and the adiabatic-pressure-density relation, i.e. Eq. (3.5), presented in Sec. 3.3, are considered.

Using the adiabatic-pressure-density relation, Eq. (3.5), we can express the pressure gradient of the j^{th} adiabatic species in terms of the density gradient as

$$\frac{\partial p_j}{\partial x} = \frac{T_j n_j^2}{n_{j0}^2} \frac{\partial n_j}{\partial x}, \tag{B.1}$$

and hence re-write the momentum equation, i.e. Eq. (3.1), as

$$m_j n_j \left(\frac{\partial v_j}{\partial t} + v_j \frac{\partial v_j}{\partial x} \right) = -e n_j \frac{\partial \varphi}{\partial x} - \frac{T_j n_j^2}{n_{j0}^2} \frac{\partial n_j}{\partial x}, \tag{B.2}$$

where we have introduced the undisturbed pressure of the j^{th} adiabatic species as $p_{j0} = n_{j0} T_j / 3$ (e.g. Verheest & Hellberg (2010b), p. 279).

By normalising various quantities with respect to the characteristics of the hotter ion species, dimensionless quantities, denoted by primes, are in-

troduced as follows. The electrostatic potential: $\varphi^{'} = e\varphi/T_h$; the time: $t^{'} = t\omega_{ph}$, where $\omega_{ph} = (n_{h0}e^2/\epsilon_0 m_h)^{1/2}$ is the plasma frequency for the hotter ion species; the space coordinate: $x^{'} = x/\lambda_{Dh}$, where $\lambda_{Dh} = (\epsilon_0 T_h/n_{h0}e^2)^{1/2}$ is the Debye length for the hotter ion species; the densities of the j^{th} adiabatic ion species and electrons (e): $n^{'}_{j,e} = n_{j,e}/n_{h0}$, where n_{h0} is the equilibrium density of the hotter ion species; the flow speed of the j^{th} adiabatic ion species: $v^{'}_j = v_j/v_{th}$, recalling that v_{th} is the thermal speed of the hotter ion species. Furthermore, the parameters μ, τ_i, τ_e, and f will be introduced as defined in Sec. 3.3, that is, $\mu = m_h/m_c$, $\tau_i = T_c/T_h$, $\tau_e = T_h/T_e$, and $f = n_{c0}/n_{h0}$.

With the above normalisation, and omitting primes for convenience, we can express the basic equations in dimensionless form as

$$n_c\left(\frac{\partial v_c}{\partial t} + v_c\frac{\partial v_c}{\partial x}\right) = -\mu n_c\frac{\partial \varphi}{\partial x} - \frac{\mu\tau_i}{f^2}n_c^2\frac{\partial n_c}{\partial x}, \tag{B.3}$$

$$n_h\left(\frac{\partial v_h}{\partial t} + v_h\frac{\partial v_h}{\partial x}\right) = -n_h\frac{\partial \varphi}{\partial x} - n_h^2\frac{\partial n_h}{\partial x}, \tag{B.4}$$

$$\frac{\partial n_j}{\partial t} + \frac{\partial (n_j v_j)}{\partial x} = 0, \tag{B.5}$$

$$n_e = g\exp(\tau_e\varphi), \tag{B.6}$$

and

$$\frac{\partial^2\varphi}{\partial x^2} = n_e - n_h - n_c, \tag{B.7}$$

where $g = 1 + f$.

To obtain the KdV equation (e.g. Tagare (1973); Tran (1974)), we use the usual reductive perturbation technique (e.g. Tagare (1973); Tran (1974)). From the stretched coordinates (e.g. Tagare (1973); Tran (1974))

$$\left.\begin{aligned}\xi &= \varepsilon^{1/2}(x - M_s t)\\ \tau &= \varepsilon^{3/2}t\end{aligned}\right\}, \tag{B.8}$$

one obtains

$$\left.\begin{aligned}\frac{\partial}{\partial x} &= \varepsilon^{1/2}\frac{\partial}{\partial \xi}\\ \frac{\partial}{\partial t} &= \varepsilon^{3/2}\frac{\partial}{\partial \tau} - \varepsilon^{1/2}M_s\frac{\partial}{\partial \xi}\end{aligned}\right\}, \tag{B.9}$$

where ε is a small, non-zero, expansion parameter and M_s is the normalised

phase speed of the ion acoustic waves for the plasma model under consideration.

We consider the perturbation of variable quantities as follows.

$$n_c = f + \varepsilon n_c^{(1)} + \varepsilon^2 n_c^{(2)} + \varepsilon^3 n_c^{(3)} + ..., \tag{B.10}$$

$$n_h = 1 + \varepsilon n_h^{(1)} + \varepsilon^2 n_h^{(2)} + \varepsilon^3 n_h^{(3)} + ..., \tag{B.11}$$

$$v_c = \varepsilon v_c^{(1)} + \varepsilon^2 v_c^{(2)} + \varepsilon^3 v_c^{(3)} + ..., \tag{B.12}$$

$$v_h = \varepsilon v_h^{(1)} + \varepsilon^2 v_h^{(2)} + \varepsilon^3 v_h^{(3)} + ..., \tag{B.13}$$

$$\varphi = \varepsilon \varphi^{(1)} + \varepsilon^2 \varphi^{(2)} + \varepsilon^3 \varphi^{(3)} + ..., \tag{B.14}$$

and

$$n_e = g + \varepsilon g\tau_e \varphi^{(1)} + \varepsilon^2 [g\tau_e \varphi^{(2)} + \frac{1}{2} g\tau_e^2 (\varphi^{(1)})^2] + \varepsilon^3 [g\tau_e \varphi^{(3)} + g\tau_e^2 \varphi^{(1)} \varphi^{(2)} + \frac{1}{6} g\tau_e^3 (\varphi^{(1)})^3] + ... \tag{B.15}$$

The expression for the electron density, n_e, given by Eq. (B.15) results from Taylor expansion of its form given by Eq. (B.6), in conjuction with Eq. (B.14).

Using (B.9)−(B.15), we can express the normalised basic equations in terms of the expansion parameter ε as follows.
The momentum equation for the cooler ions:

$$\begin{aligned}
&\varepsilon^{3/2}\left[-fM_s\frac{\partial v_c^{(1)}}{\partial \xi}+\mu f\frac{\partial \varphi^{(1)}}{\partial \xi}+\mu\tau_i\frac{\partial n_c^{(1)}}{\partial \xi}\right]+\varepsilon^{5/2}\left[f\frac{\partial v_c^{(1)}}{\partial \tau}+fv_c^{(1)}\frac{\partial v_c^{(1)}}{\partial \xi}-fM_s\frac{\partial v_c^{(2)}}{\partial \xi}\right.\\
&\left.-M_s n_c^{(1)}\frac{\partial v_c^{(1)}}{\partial \xi}+\mu f\frac{\partial \varphi^{(2)}}{\partial \xi}+\mu n_c^{(1)}\frac{\partial \varphi^{(1)}}{\partial \xi}+\mu\tau_i\frac{\partial n_c^{(2)}}{\partial \xi}+\frac{2\mu\tau_i}{f}n_c^{(1)}\frac{\partial n_c^{(1)}}{\partial \xi}\right]\\
&+\varepsilon^{7/2}\left\{f\frac{\partial v_c^{(2)}}{\partial \tau}-fM_s\frac{\partial v_c^{(3)}}{\partial \xi}+fv_c^{(1)}\frac{\partial v_c^{(2)}}{\partial \xi}+fv_c^{(2)}\frac{\partial v_c^{(1)}}{\partial \xi}+n_c^{(1)}\frac{\partial v_c^{(1)}}{\partial \tau}\right.\\
&+n_c^{(1)}v_c^{(1)}\frac{\partial v_c^{(1)}}{\partial \xi}-M_s n_c^{(1)}\frac{\partial v_c^{(2)}}{\partial \xi}-M_s n_c^{(2)}\frac{\partial v_c^{(1)}}{\partial \xi}+\mu f\frac{\partial \varphi^{(3)}}{\partial \xi}+\mu n_c^{(1)}\frac{\partial \varphi^{(2)}}{\partial \xi}\\
&\left.+\mu n_c^{(2)}\frac{\partial \varphi^{(1)}}{\partial \xi}+\mu\tau_i\frac{\partial n_c^{(3)}}{\partial \xi}+\frac{2\mu\tau_i}{f}n_c^{(1)}\frac{\partial n_c^{(2)}}{\partial \xi}+\frac{\mu\tau_i}{f^2}\left[2fn_c^{(2)}+\left(n_c^{(1)}\right)^2\frac{\partial n_c^{(1)}}{\partial \xi}\right]\right\}+... = 0;
\end{aligned} \tag{B.16}$$

the momentum equation for the hotter ions:

$$\varepsilon^{3/2}\left[-M_s\frac{\partial v_h^{(1)}}{\partial\xi}+\frac{\partial\varphi^{(1)}}{\partial\xi}+\frac{\partial n_h^{(1)}}{\partial\xi}\right]+\varepsilon^{5/2}\left[\frac{\partial v_h^{(1)}}{\partial\tau}+v_h^{(1)}\frac{\partial v_h^{(1)}}{\partial\xi}-M_s\frac{\partial v_h^{(2)}}{\partial\xi}-M_s n_h^{(1)}\frac{\partial v_h^{(1)}}{\partial\xi}\right.$$
$$\left.+\frac{\partial\varphi^{(2)}}{\partial\xi}+n_h^{(1)}\frac{\partial\varphi^{(1)}}{\partial\xi}+\frac{\partial n_h^{(2)}}{\partial\xi}+2n_h^{(1)}\frac{\partial n_h^{(1)}}{\partial\xi}\right]+\varepsilon^{7/2}\left\{\frac{\partial v_h^{(2)}}{\partial\tau}-M_s\frac{\partial v_h^{(3)}}{\partial\xi}+v_h^{(1)}\frac{\partial v_h^{(2)}}{\partial\xi}\right.$$
$$+v_h^{(2)}\frac{\partial v_h^{(1)}}{\partial\xi}+n_h^{(1)}\frac{\partial v_h^{(1)}}{\partial\tau}+n_h^{(1)}v_h^{(1)}\frac{\partial v_h^{(1)}}{\partial\xi}-M_s n_h^{(1)}\frac{\partial v_h^{(2)}}{\partial\xi}-M_s n_h^{(2)}\frac{\partial v_h^{(1)}}{\partial\xi}+\frac{\partial\varphi^{(3)}}{\partial\xi}$$
$$\left.+n_h^{(1)}\frac{\partial\varphi^{(2)}}{\partial\xi}+n_h^{(2)}\frac{\partial\varphi^{(1)}}{\partial\xi}+\frac{\partial n_h^{(3)}}{\partial\xi}+2n_h^{(1)}\frac{\partial n_h^{(2)}}{\partial\xi}+\left[2n_h^{(2)}+\left(n_h^{(1)}\right)^2\frac{\partial n_h^{(1)}}{\partial\xi}\right]\right\}+...=0; \tag{B.17}$$

the continuity equation for the cooler ions:

$$\varepsilon^{3/2}\left[-M_s\frac{\partial n_c^{(1)}}{\partial\xi}+f\frac{\partial v_c^{(1)}}{\partial\xi}\right]+\varepsilon^{5/2}\left\{\frac{\partial n_c^{(1)}}{\partial\tau}-M_s\frac{\partial n_c^{(2)}}{\partial\xi}+f\frac{\partial v_c^{(2)}}{\partial\xi}+\frac{\partial[n_c^{(1)}v_c^{(1)}]}{\partial\xi}\right\}$$
$$+\varepsilon^{7/2}\left\{\frac{\partial n_c^{(2)}}{\partial\tau}-M_s\frac{\partial n_c^{(3)}}{\partial\xi}+f\frac{\partial v_c^{(3)}}{\partial\xi}+\frac{\partial[n_c^{(1)}v_c^{(2)}]}{\partial\xi}+\frac{\partial[n_c^{(2)}v_c^{(1)}]}{\partial\xi}\right\}+...=0; \tag{B.18}$$

the continuity equation for the hotter ions:

$$\varepsilon^{3/2}\left[-M_s\frac{\partial n_h^{(1)}}{\partial\xi}+\frac{\partial v_h^{(1)}}{\partial\xi}\right]+\varepsilon^{5/2}\left[\frac{\partial n_h^{(1)}}{\partial\tau}-M_s\frac{\partial n_h^{(2)}}{\partial\xi}+\frac{\partial v_h^{(2)}}{\partial\xi}+\frac{\partial[n_h^{(1)}v_h^{(1)}]}{\partial\xi}\right]$$
$$+\varepsilon^{7/2}\left[\frac{\partial n_h^{(2)}}{\partial\tau}-M_s\frac{\partial n_h^{(3)}}{\partial\xi}+\frac{\partial v_h^{(3)}}{\partial\xi}+\frac{\partial[n_h^{(1)}v_h^{(2)}]}{\partial\xi}+\frac{\partial[n_h^{(2)}v_h^{(1)}]}{\partial\xi}\right]+...=0; \tag{B.19}$$

and Poisson's equation:

$$g-f-1+\varepsilon[g\tau_e\varphi^{(1)}-n_h^{(1)}-n_c^{(1)}]+\varepsilon^2\left[g\tau_e\varphi^{(2)}+\frac{1}{2}g\tau_e^2(\varphi^{(1)})^2-n_h^{(2)}-n_c^{(2)}-\frac{\partial^2\varphi^{(1)}}{\partial\xi^2}\right]$$
$$+\varepsilon^3\left[g\tau_e\varphi^{(3)}+\frac{1}{6}g\tau_e^3(\varphi^{(1)})^3+g\tau_e^2\varphi^{(1)}\varphi^{(2)}-n_h^{(3)}-n_c^{(3)}-\frac{\partial^2\varphi^{(2)}}{\partial\xi^2}\right]+...=0. \tag{B.20}$$

B.2 KdV equation

Since the parameter ε is finite, Eqs. (B.16)−(B.20)) hold if all coefficients of ε vanish. The solution of Eq. (B.20) at the zeroth order of ε yields

$$g - f - 1 = 0, \tag{B.21}$$

which is the overall charge neutrality in equilibrium.

At the first non-zero order of ε, we obtain the solutions of Eqs. $(B.16 - B.20)$, respectively, as

$$-fM_s\frac{\partial v_c^{(1)}}{\partial \xi} + \mu f\frac{\partial \varphi^{(1)}}{\partial \xi} + \mu\tau_i\frac{\partial n_c^{(1)}}{\partial \xi} = 0, \tag{B.22}$$

$$-M_s\frac{\partial v_h^{(1)}}{\partial \xi} + \frac{\partial \varphi^{(1)}}{\partial \xi} + \frac{\partial n_h^{(1)}}{\partial \xi} = 0, \tag{B.23}$$

$$-M_s\frac{\partial n_c^{(1)}}{\partial \xi} + f\frac{\partial v_c^{(1)}}{\partial \xi} = 0, \tag{B.24}$$

$$-M_s\frac{\partial n_h^{(1)}}{\partial \xi} + \frac{\partial v_h^{(1)}}{\partial \xi} = 0, \tag{B.25}$$

$$g\tau_e\varphi^{(1)} - n_h^{(1)} - n_c^{(1)} = 0, \tag{B.26}$$

from which we get

$$v_c^{(1)} = \frac{\mu M_s}{M_s^2 - \mu\tau_i}\varphi^{(1)}, \tag{B.27}$$

$$v_h^{(1)} = \frac{M_s}{M_s^2 - 1}\varphi^{(1)}, \tag{B.28}$$

$$n_c^{(1)} = \frac{\mu f}{M_s^2 - \mu\tau_i}\varphi^{(1)}, \tag{B.29}$$

$$n_h^{(1)} = \frac{1}{M_s^2 - 1}\varphi^{(1)}, \tag{B.30}$$

and

$$g\tau_e - \frac{1}{M_s^2 - 1} - \frac{\mu f}{M_s^2 - \mu\tau_i} = 0. \tag{B.31}$$

At the second non-zero order of ε, the solutions of Eqs. (B.16) − (B.20) yield, respectively

$$f\frac{\partial v_c^{(1)}}{\partial \tau} + f v_c^{(1)}\frac{\partial v_c^{(1)}}{\partial \xi} - f M_s \frac{\partial v_c^{(2)}}{\partial \xi} - M_s n_c^{(1)}\frac{\partial v_c^{(1)}}{\partial \xi} + \mu f \frac{\partial \varphi^{(2)}}{\partial \xi} + \mu n_c^{(1)}\frac{\partial \varphi^{(1)}}{\partial \xi} + \mu\tau_i \frac{\partial n_c^{(2)}}{\partial \xi} + \frac{2\mu\tau_i}{f} n_c^{(1)}\frac{\partial n_c^{(1)}}{\partial \xi} = 0, \quad \text{(B.32)}$$

$$\frac{\partial v_h^{(1)}}{\partial \tau} + v_h^{(1)}\frac{\partial v_h^{(1)}}{\partial \xi} - M_s \frac{\partial v_h^{(2)}}{\partial \xi} - M_s n_h^{(1)}\frac{\partial v_h^{(1)}}{\partial \xi} + \frac{\partial \varphi^{(2)}}{\partial \xi} + n_h^{(1)}\frac{\partial \varphi^{(1)}}{\partial \xi} + \frac{\partial n_h^{(2)}}{\partial \xi} + 2n_h^{(1)}\frac{\partial n_h^{(1)}}{\partial \xi} = 0, \quad \text{(B.33)}$$

$$\frac{\partial n_c^{(1)}}{\partial \tau} - M_s \frac{\partial n_c^{(2)}}{\partial \xi} + f\frac{\partial v_c^{(2)}}{\partial \xi} + \frac{\partial [n_c^{(1)} v_c^{(1)}]}{\partial \xi} = 0, \quad \text{(B.34)}$$

$$\frac{\partial n_h^{(1)}}{\partial \tau} - M_s \frac{\partial n_h^{(2)}}{\partial \xi} + \frac{\partial v_h^{(2)}}{\partial \xi} + \frac{\partial [n_h^{(1)} v_h^{(1)}]}{\partial \xi} = 0, \quad \text{(B.35)}$$

$$g\tau_e \varphi^{(2)} + \frac{1}{2} g\tau_e^2 (\varphi^{(1)})^2 - n_h^{(2)} - n_c^{(2)} - \frac{\partial^2 \varphi^{(1)}}{\partial \xi^2} = 0. \quad \text{(B.36)}$$

Differentiating Eq. (B.36) with respect to ξ, we get

$$g\tau_e \frac{\partial \varphi^{(2)}}{\partial \xi} + g\tau_e^2 \varphi^{(1)}\frac{\partial \varphi^{(1)}}{\partial \xi} - \frac{\partial n_h^{(2)}}{\partial \xi} - \frac{\partial n_c^{(2)}}{\partial \xi} - \frac{\partial^3 \varphi^{(1)}}{\partial \xi^3} = 0. \quad \text{(B.37)}$$

Substituting the first order speed and density of the cooler ions expressed in terms of the first order potential, i.e. Eqs. (B.27) and (B.29), respectively, in the second non-zero order solutions of the momentum and continuity equations for the cooler ions, i.e. Eqs. (B.32) and (B.34), respectively, we obtain

$$\frac{M_s \mu f}{M_s^2 - \mu\tau_i}\frac{\partial \varphi^{(1)}}{\partial \tau} - f M_s \frac{\partial v_c^{(2)}}{\partial \xi} + \mu f \frac{\partial \varphi^{(2)}}{\partial \xi} + \frac{\mu^2 f}{M_s^2 - \mu\tau_i}\varphi^{(1)}\frac{\partial \varphi^{(1)}}{\partial \xi} + \mu\tau_i \frac{\partial n_c^{(2)}}{\partial \xi} + \frac{2\mu^3 \tau_i f}{(M_s^2 - \mu\tau_i)^2}\varphi^{(1)}\frac{\partial \varphi^{(1)}}{\partial \xi} = 0, \quad \text{(B.38)}$$

and

$$\frac{\mu f}{M_s^2 - \mu\tau_i}\frac{\partial \varphi^{(1)}}{\partial \tau} - M_s \frac{\partial n_c^{(2)}}{\partial \xi} + f\frac{\partial v_c^{(2)}}{\partial \xi} + \frac{2M_s f \mu^2}{(M_s^2 - \mu\tau_i)^2}\varphi^{(1)}\frac{\partial \varphi^{(1)}}{\partial \xi} = 0. \quad \text{(B.39)}$$

Similarly, substituting the first order speed and density of the hotter ions expressed in terms of the first order potential, i.e. Eqs. (B.28) and (B.30), respectively, in the second non-zero order solutions of the momentum and continuity equations for the hotter ions, i.e. Eqs. (B.33) and (B.35), respectively, we get

$$\frac{M_s}{M_s^2-1}\frac{\partial\varphi^{(1)}}{\partial\tau}-M_s\frac{\partial v_h^{(2)}}{\partial\xi}+\frac{\partial\varphi^{(2)}}{\partial\xi}+\frac{1}{M_s^2-1}\varphi^{(1)}\frac{\partial\varphi^{(1)}}{\partial\xi} + \frac{\partial n_h^{(2)}}{\partial\xi}+\frac{2}{(M_s^2-1)^2}\varphi^{(1)}\frac{\partial\varphi^{(1)}}{\partial\xi}=0, \quad \text{(B.40)}$$

and

$$\frac{1}{M_s^2-1}\frac{\partial\varphi^{(1)}}{\partial\tau}-M_s\frac{\partial n_h^{(2)}}{\partial\xi}+\frac{\partial v_h^{(2)}}{\partial\xi}+\frac{2M_s}{(M_s^2-1)^2}\varphi^{(1)}\frac{\partial\varphi^{(1)}}{\partial\xi}=0. \quad \text{(B.41)}$$

From the second non-zero order solutions of the continuity equations for the cooler and hotter ions, i.e. Eqs. (B.39) and (B.41), the second order speeds are eliminated as

$$\frac{f\partial v_c^{(2)}}{\partial\xi}=M_s\frac{\partial n_c^{(2)}}{\partial\xi}-\frac{\mu f}{M_s^2-\mu\tau_i}\frac{\partial\varphi^{(1)}}{\partial\tau}-\frac{2M_s f\mu^2}{(M_s^2-\mu\tau_i)^2}\varphi^{(1)}\frac{\partial\varphi^{(1)}}{\partial\xi}, \quad \text{(B.42)}$$

and

$$\frac{\partial v_h^{(2)}}{\partial\xi}=M_s\frac{\partial n_h^{(2)}}{\partial\xi}-\frac{1}{M_s^2-1}\frac{\partial\varphi^{(1)}}{\partial\tau}-\frac{2M_s}{(M_s^2-1)^2}\varphi^{(1)}\frac{\partial\varphi^{(1)}}{\partial\xi}. \quad \text{(B.43)}$$

Substituting the expressions for $f\partial v_c^{(2)}/\partial\xi$ and $\partial v_h^{(2)}/\partial\xi$, given by Eqs. (B.42) and (B.43), in the second non-zero order solutions of the momentum equations for the cooler and hotter ions, i.e. Eqs. (B.38) and (B.40), we obtain, respectively

$$\frac{2M_s\mu f}{M_s^2-\mu\tau_i}\frac{\partial\varphi^{(1)}}{\partial\tau}+\left[\frac{\mu^2 f}{M_s^2-\mu\tau_i}+\frac{2\mu^3\tau_i f}{(M_s^2-\mu\tau_i)^2}+\frac{2\mu^2 f M_s^2}{(M_s^2-\mu\tau_i)^2}\right]\varphi^{(1)}\frac{\partial\varphi^{(1)}}{\partial\xi} + \left(\mu\tau_i-M_s^2\right)\frac{\partial n_c^{(2)}}{\partial\xi}+\mu f\frac{\partial\varphi^{(2)}}{\partial\xi}=0, \quad \text{(B.44)}$$

and

$$\frac{2M_s}{M_s^2-1}\frac{\partial\varphi^{(1)}}{\partial\tau}+\left[\frac{1}{M_s^2-1}+\frac{2}{(M_s^2-1)^2}+\frac{2M_s^2}{(M_s^2-1)^2}\right]\varphi^{(1)}\frac{\partial\varphi^{(1)}}{\partial\xi}$$
$$+\left(1-M_s^2\right)\frac{\partial n_h^{(2)}}{\partial\xi}+\frac{\partial\varphi^{(2)}}{\partial\xi}=0. \quad \text{(B.45)}$$

The second order densities for the cooler and hotter ions are eliminated from Eqs. (B.44) and (B.45) as

$$\frac{\partial n_c^{(2)}}{\partial\xi}=\frac{1}{M_s^2-\mu\tau_i}\left\{\frac{2M_s\mu f}{M_s^2-\mu\tau_i}\frac{\partial\varphi^{(1)}}{\partial\tau}\right.$$
$$\left.+\left[\frac{\mu^2 f}{M_s^2-\mu\tau_i}+\frac{2\mu^3\tau_i f}{(M_s^2-\mu\tau_i)^2}+\frac{2\mu^2 f M_s^2}{(M_s^2-\mu\tau_i)^2}\right]\varphi^{(1)}\frac{\partial\varphi^{(1)}}{\partial\xi}+\mu f\frac{\partial\varphi^{(2)}}{\partial\xi}\right\}=0, \quad \text{(B.46)}$$

and

$$\frac{\partial n_h^{(2)}}{\partial\xi}=\frac{1}{M_s^2-1}\left\{\frac{2M_s}{M_s^2-1}\frac{\partial\varphi^{(1)}}{\partial\tau}\right.$$
$$\left.+\left[\frac{1}{M_s^2-1}+\frac{2}{(M_s^2-1)^2}+\frac{2M_s^2}{(M_s^2-1)^2}\right]\varphi^{(1)}\frac{\partial\varphi^{(1)}}{\partial\xi}+\frac{\partial\varphi^{(2)}}{\partial\xi}\right\}=0. \quad \text{(B.47)}$$

Substituting the expressions for $\partial n_c^{(2)}/\partial\xi$ and $\partial n_h^{(2)}/\partial\xi$ given by Eqs. (B.46) and (B.47), respectively, in the second non-zero order solution of Poisson's equation obtained after differentiation with respect to ξ, i.e. Eq. (B.37), and rearranging, we obtain

$$\left[\frac{2M_s}{(M_s^2-1)^2}+\frac{2\mu f M_s}{(M_s^2-\mu\tau_i)^2}\right]\frac{\partial\varphi^{(1)}}{\partial\tau}+\left[\frac{\mu^2 f}{(M_s^2-\mu\tau_i)^2}+\frac{2\mu^3\tau_i f}{(M_s^2-\mu\tau_i)^3}+\frac{2\mu^2 f M_s^2}{(M_s^2-\mu\tau_i)^3}\right.$$
$$\left.+\frac{1}{(M_s^2-1)^2}+\frac{2}{(M_s^2-1)^3}+\frac{2M_s^2}{(M_s^2-1)^3}-g\tau_e^2\right]\varphi^{(1)}\frac{\partial\varphi^{(1)}}{\partial\xi}+\frac{\partial^3\varphi^{(1)}}{\partial\xi^3}$$
$$-\left(g\tau_e-\frac{1}{M_s^2-1}-\frac{\mu f}{M_s^2-\mu\tau_i}\right)\frac{\partial\varphi^{(2)}}{\partial\xi}=0. \quad \text{(B.48)}$$

Since the coefficient of $\frac{\partial\varphi^{(2)}}{\partial\xi}$ vanishes in light of (B.31), Eq. (B.48) reduces to

$$\frac{\partial\varphi^{(1)}}{\partial\tau}+a\varphi^{(1)}\frac{\partial\varphi^{(1)}}{\partial\xi}+b\frac{\partial^3\varphi^{(1)}}{\partial\xi^3}=0, \quad \text{(B.49)}$$

where

$$a = \frac{A}{B}, \tag{B.50}$$

$$b = \frac{1}{B}, \tag{B.51}$$

$$A = \frac{\mu^2 f(3M_s^2 + \mu\tau_i)}{(M_s^2 - \mu\tau_i)^3} + \frac{3M_s^2 + 1}{(M_s^2 - 1)^3} - (1 + f)\tau_e^2, \tag{B.52}$$

$$B = \frac{2M_s}{(M_s^2 - 1)^2} + \frac{2\mu f M_s}{(M_s^2 - \mu\tau_i)^2}, \tag{B.53}$$

and recalling that $g = n_{e0}/n_{h0} = 1 + f$.

Equation (B.49), written in terms of the first order electrostatic potential and with the coefficients a and b given by Eqs. (B.50) and (B.51), is the desired KdV equation for a plasma composed of Boltzmann electrons and two adiabatic, positively and singly charged, ion species.

B.3 Soliton solution of the KdV equation

The KdV equation has a well-known "sech^2"-type soliton solution (see e.g. Zabusky & Kruskal (1965); Tagare (1973); Tran (1974); Mace et al. (1991)). However, in this appendix, the details of obtaining a soliton solution of the KdV equation are presented, for completeness. To obtain a soliton solution of the KdV equation, one seeks a stationary solution by using the transformation

$$\eta = \xi - M_0\tau, \tag{B.54}$$

from which one gets

$$\frac{\partial}{\partial\xi} = \frac{\partial\eta}{\partial\xi}\frac{d}{d\eta} \equiv \frac{d}{d\eta}, \tag{B.55}$$

$$\frac{\partial}{d\tau} = \frac{\partial\eta}{\partial\tau}\frac{d}{d\eta} \equiv -M_0\frac{d}{d\eta}, \tag{B.56}$$

where M_0 is the normalised soliton speed in a co-moving frame. Substituting the expressions for $\partial/\partial\xi$ and $\partial/\partial\tau$ given by Eqs. (B.55) and (B.56), respectively, in the KdV equation, i.e. Eq. (B.49), one obtains

$$-M_0\frac{d\varphi^{(1)}}{d\eta} + a\varphi^{(1)}\frac{d\varphi^{(1)}}{d\eta} + b\frac{d^3\varphi^{(1)}}{d\eta^3} = 0, \tag{B.57}$$

or

$$\frac{d}{d\eta}\left[-M_0\varphi^{(1)}+\frac{a}{2}\left(\varphi^{(1)}\right)^2+b\frac{d^2\varphi^{(1)}}{d\eta^2}\right]=0. \tag{B.58}$$

Integrating (B.58) and using the boundary conditions

$$\eta\to\pm\infty,\varphi^{(1)}\to 0,\frac{d\varphi^{(1)}}{d\eta}\to 0,\frac{d^2\varphi^{(1)}}{d\eta^2}\to 0, \tag{B.59}$$

one gets

$$-\frac{M_0}{b}\varphi^{(1)}+\frac{a}{2b}\left(\varphi^{(1)}\right)^2+\frac{d^2\varphi^{(1)}}{d\eta^2}=0. \tag{B.60}$$

Multiplying (B.60) by $d\varphi^{(1)}/d\eta$, one has

$$-\frac{d}{d\eta}\left[\frac{M_0}{2b}\left(\varphi^{(1)}\right)^2\right]+\frac{d}{d\eta}\left[\frac{a}{6b}\left(\varphi^{(1)}\right)^3\right]+\frac{d}{d\eta}\left[\frac{1}{2}\left(\frac{d\varphi^{(1)}}{d\eta}\right)^2\right]=0, \tag{B.61}$$

or

$$\frac{d}{d\eta}\left[-\frac{M_0}{2b}\left(\varphi^{(1)}\right)^2+\frac{a}{6b}\left(\varphi^{(1)}\right)^3+\frac{1}{2}\left(\frac{d\varphi^{(1)}}{d\eta}\right)^2\right]=0. \tag{B.62}$$

Integrating (B.62) and using the boundary conditions

$$\eta\to\pm\infty,\varphi^{(1)}\to 0,\frac{d\varphi^{(1)}}{d\eta}\to 0, \tag{B.63}$$

one gets

$$\frac{1}{2}\left(\frac{d\varphi^{(1)}}{d\eta}\right)^2+S(\varphi^{(1)})=0, \tag{B.64}$$

where

$$S(\varphi^{(1)})=\frac{a}{6b}\left(\varphi^{(1)}\right)^3-\frac{M_0}{2b}\left(\varphi^{(1)}\right)^2, \tag{B.65}$$

is the approximate Sagdeev potential. A discussion about the Sagdeev potential is provided in detail in Sec. 3.5 where its full expression is presented.

It is well-known from the Sagdeev potential theory (e.g. Verheest et al. (2008)) that a requirement for the existence of a soliton is

$$S(\varphi_m)=0, \tag{B.66}$$

where φ_m is the soliton amplitude. From Eqs. (B.65) and (B.66), one has

the relation between the soliton amplitude and the soliton speed as

$$\varphi_m = \frac{3M_0}{a}. \tag{B.67}$$

Equation (B.67) suggests that $\varphi_m \propto M_0$, that is, in a frame moving with a soliton, the amplitude and the speed of a KdV soliton are linearly proportional.

Substituting the expression for M_0 given by (B.67) in (B.64) one gets

$$\left(\frac{d\varphi^{(1)}}{d\eta}\right)^2 + \frac{a}{3b}\left(\varphi^{(1)}\right)^2\left(\varphi^{(1)} - \varphi_m\right) = 0. \tag{B.68}$$

Equation (B.68) can, alternatively, be written as

$$\frac{d\varphi^{(1)}}{d\eta} = \sigma\sqrt{\frac{a}{3b}}\varphi^{(1)}\sqrt{\varphi_m - \varphi^{(1)}}, \tag{B.69}$$

or

$$\eta = \sigma\sqrt{\frac{3b}{a}}\int \frac{d\varphi}{\varphi\sqrt{\varphi_m - \varphi}} + c, \tag{B.70}$$

where $\sigma = \pm 1$ and c is a constant of integration.

Evaluating the integral in (B.70), using the boundary condition $\eta \to 0, \varphi^{(1)} \to \varphi_m$, one obtains

$$\eta = -\sigma\sqrt{\frac{3b}{a\varphi_m}}\ln\left|\frac{\sqrt{\varphi_m} + \sqrt{\varphi_m - \varphi^{(1)}}}{\sqrt{\varphi_m} - \sqrt{\varphi_m - \varphi^{(1)}}}\right|, \tag{B.71}$$

or

$$\frac{\sqrt{\varphi_m} + \sqrt{\varphi_m - \varphi^{(1)}}}{\sqrt{\varphi_m} - \sqrt{\varphi_m - \varphi^{(1)}}} = e^{-\sigma\sqrt{\frac{a\varphi_m}{3b}}\eta}, \tag{B.72}$$

or

$$\sqrt{\varphi_m - \varphi^{(1)}} = \frac{\sqrt{\varphi_m}\left(e^{-\sigma\sqrt{\frac{a\varphi_m}{12b}}\eta} - e^{\sigma\sqrt{\frac{a\varphi_m}{12b}}\eta}\right)}{\left(e^{-\sigma\sqrt{\frac{a\varphi_m}{12b}}\eta} + e^{\sigma\sqrt{\frac{a\varphi_m}{12b}}\eta}\right)}, \tag{B.73}$$

or

$$\sqrt{\varphi_m - \varphi^{(1)}} = \sqrt{\varphi_m}\tanh\left(\sigma\sqrt{\frac{a\varphi_m}{12b}}\eta\right), \tag{B.74}$$

or

$$\varphi^{(1)} = \varphi_m\left[1 - \tanh^2\left(\sqrt{\frac{a\varphi_m}{12b}}\eta\right)\right], \tag{B.75}$$

or simply

$$\varphi^{(1)} = \frac{3M_0}{a}\mathrm{sech}^2\left(\sqrt{\frac{M_0}{4b}}\eta\right). \tag{B.76}$$

Equation (B.76) is the form of the well-known solution (e.g. Tagare (1973); Tran (1974)) of the KdV equation in a frame moving with a solitary wave. It can be transformed to the laboratory frame as follows (see also e.g. Mace et al. (1991)).

Using the stretched coordinates given by Eq. (B.8) in the transformation given by Eq. (B.54), one obtains

$$\eta = \varepsilon^{1/2}(x - Mt), \tag{B.77}$$

where $M = M_s + \delta M$ is the normalised speed of a solitary wave in the laboratory frame, and we have defined the small quantity δM as

$$\delta M = M_0\varepsilon \equiv M - M_s. \tag{B.78}$$

Furthermore, from Eq. (B.14) one gets the approximate electrostatic potential as

$$\varphi \approx \varepsilon\varphi^{(1)}. \tag{B.79}$$

Using (B.77) − (B.79) in (B.76), one obtains the soliton solution of the KdV equation in the laboratory frame as (e.g. Mace et al. (1991))

$$\varphi(x,t) = \frac{3\delta M}{a}\mathrm{sech}^2\left[\sqrt{\frac{\delta M}{4b}}(x - Mt)\right]. \tag{B.80}$$

Appendix C

The effects of the ion temperature on the existence domain of the slow mode ion acoustic solitons: other values of τ_i

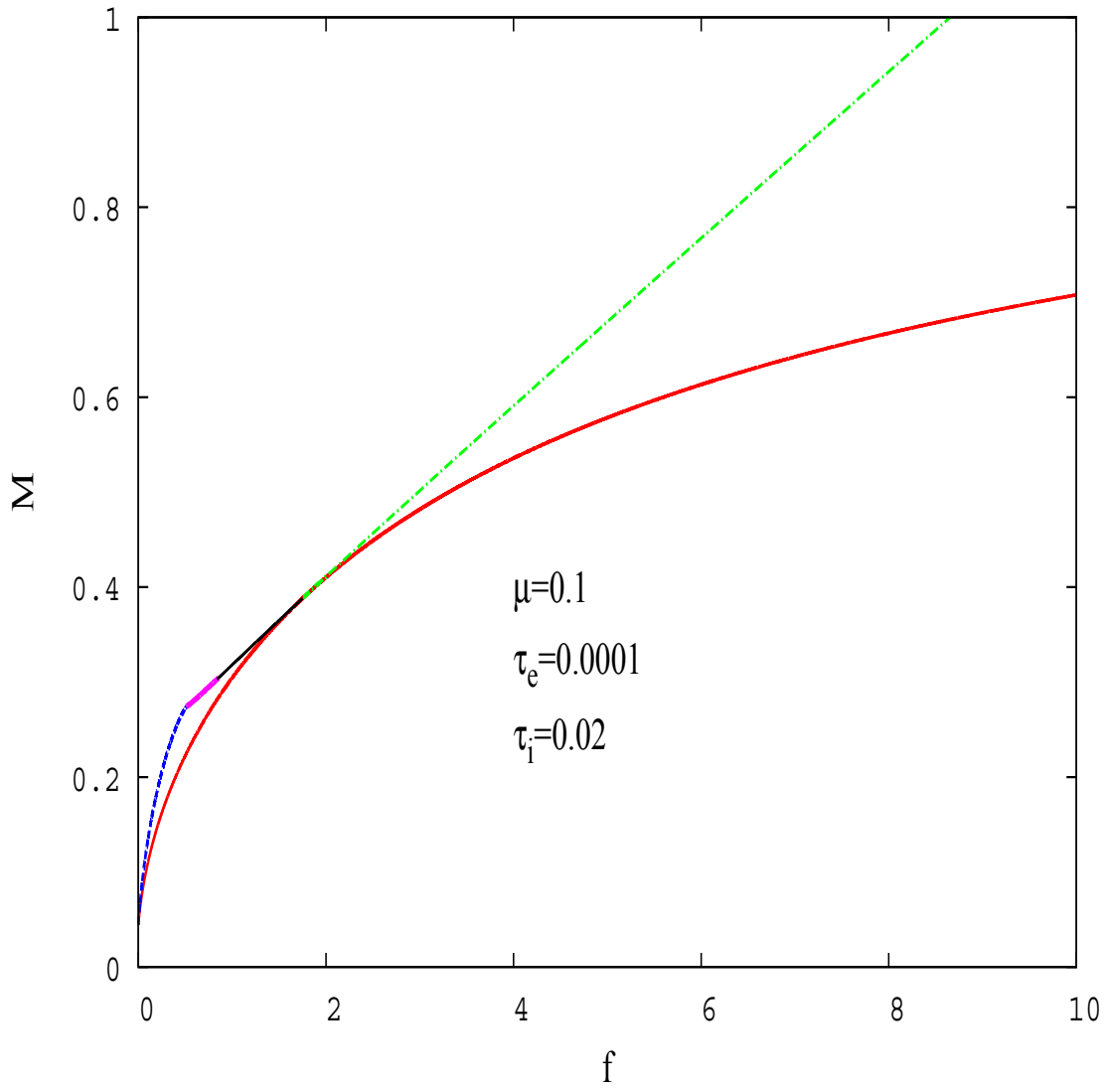

Figure C.1: The existence domain of the slow mode ion acoustic solitons for $\mu = 0.1$, $\tau_e = 0.0001$, and $\tau_i = 0.02$. The line styles are as in Fig. 3.7. The cutoff observed for $M = 1$ is imposed by the model (see the ordering (3.16)).

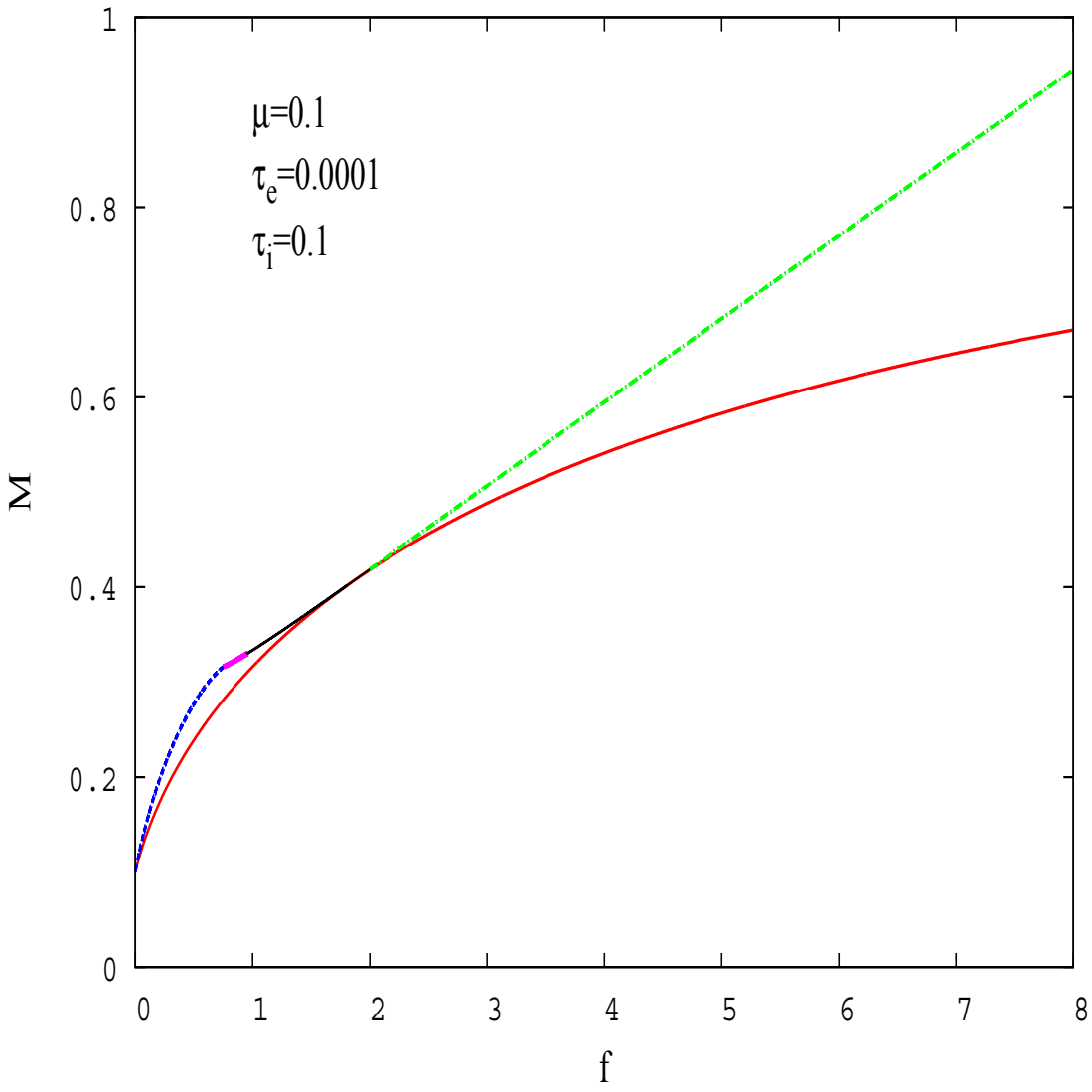

Figure C.2: The existence domain of the slow mode ion acoustic solitons for $\mu = 0.1$, $\tau_e = 0.0001$, and $\tau_i = 0.1$. The line styles are as in Fig. 3.7. The cutoff observed for $M = 1$ is imposed by the model (see the ordering (3.16)).

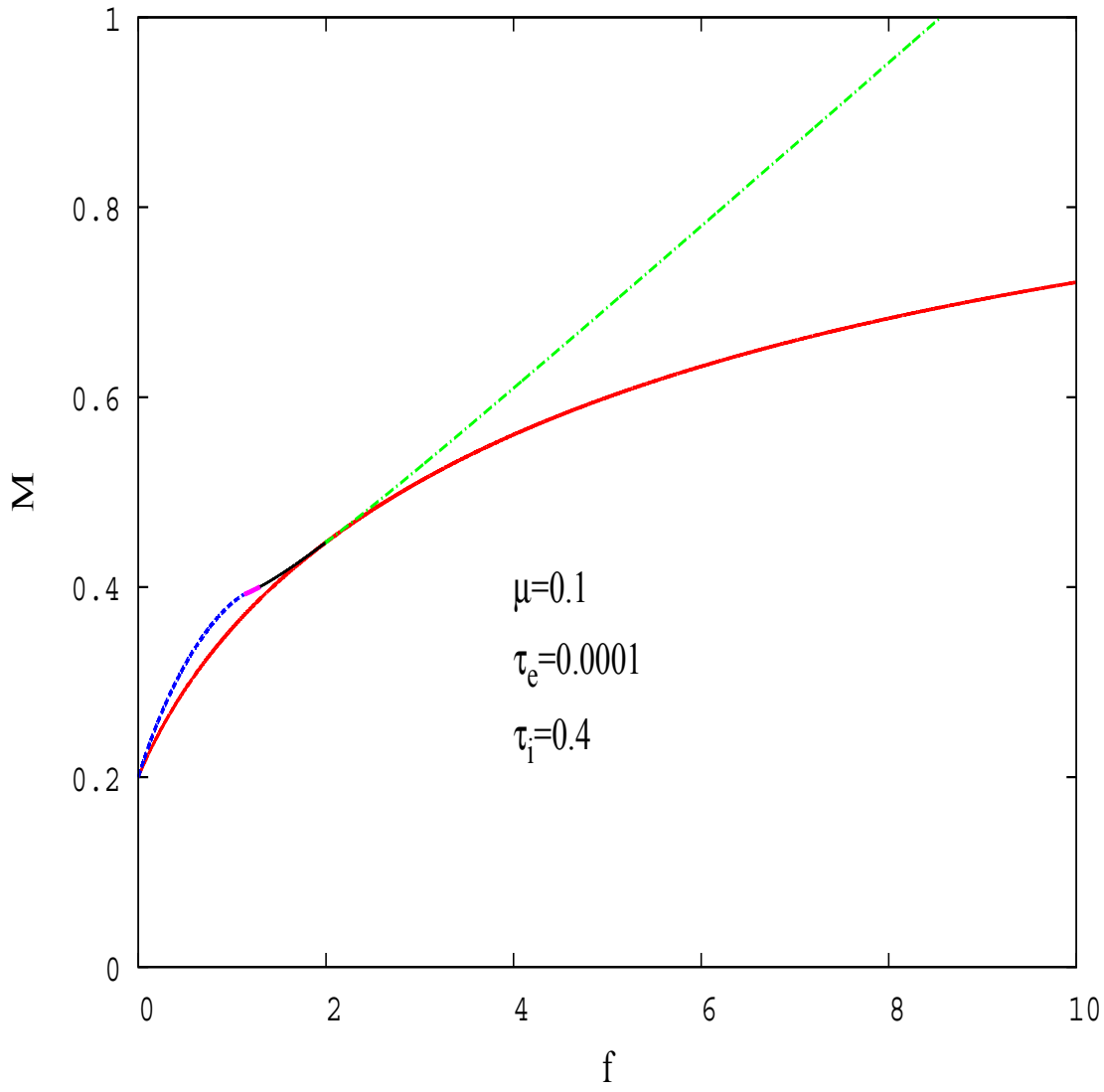

Figure C.3: The existence domain of the slow mode ion acoustic solitons for $\mu = 0.1$, $\tau_e = 0.0001$, and $\tau_i = 0.4$. The line styles are as in Fig. 3.7. The cutoff observed for $M = 1$ is imposed by the model (see the ordering (3.16)).

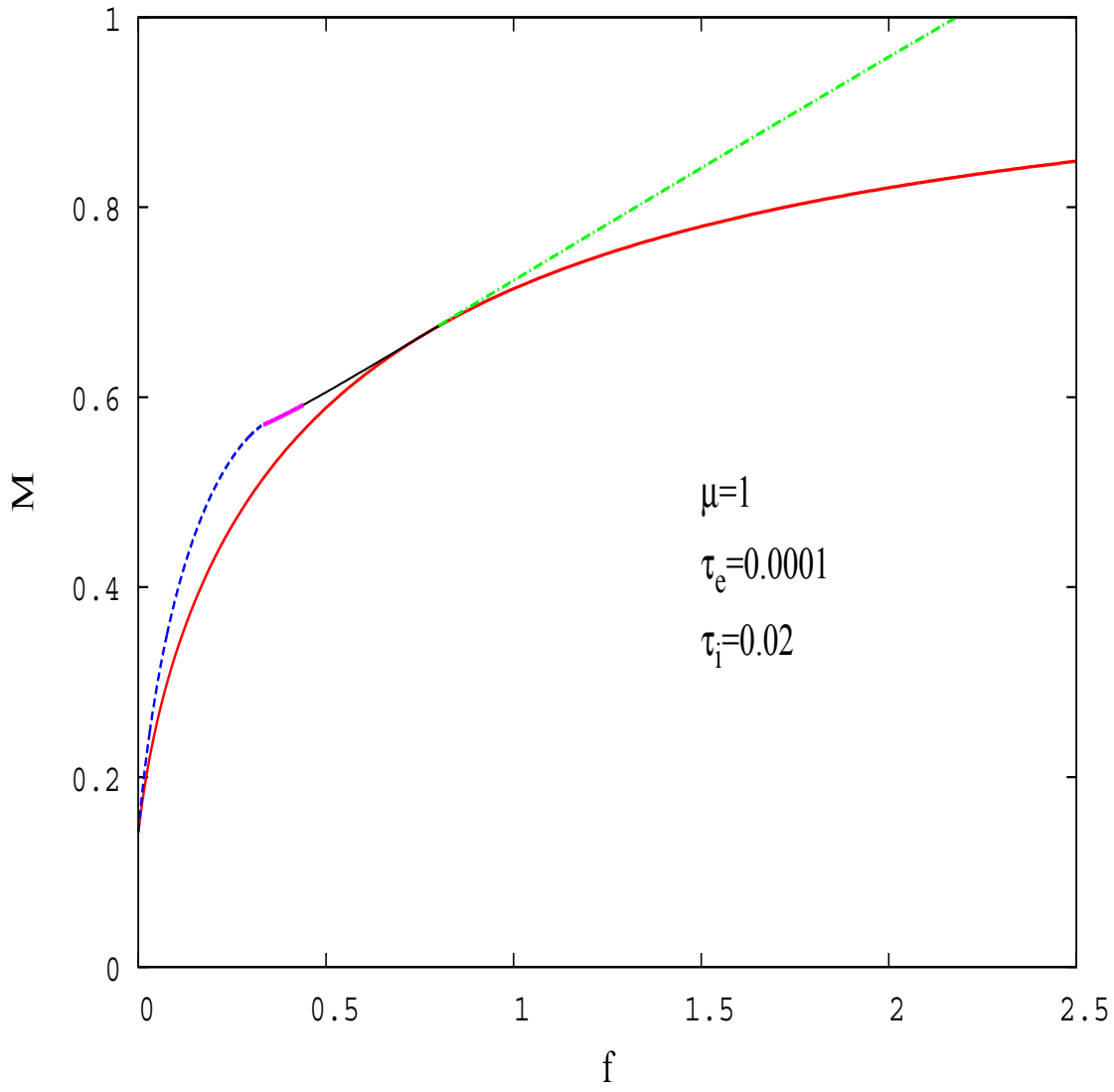

Figure C.4: The existence domain of the slow mode ion acoustic solitons for $\mu = 1$, $\tau_e = 0.0001$, and $\tau_i = 0.02$. The line styles are as in Fig. 3.7. The cutoff observed for $M = 1$ is imposed by the model (see the ordering (3.16)).

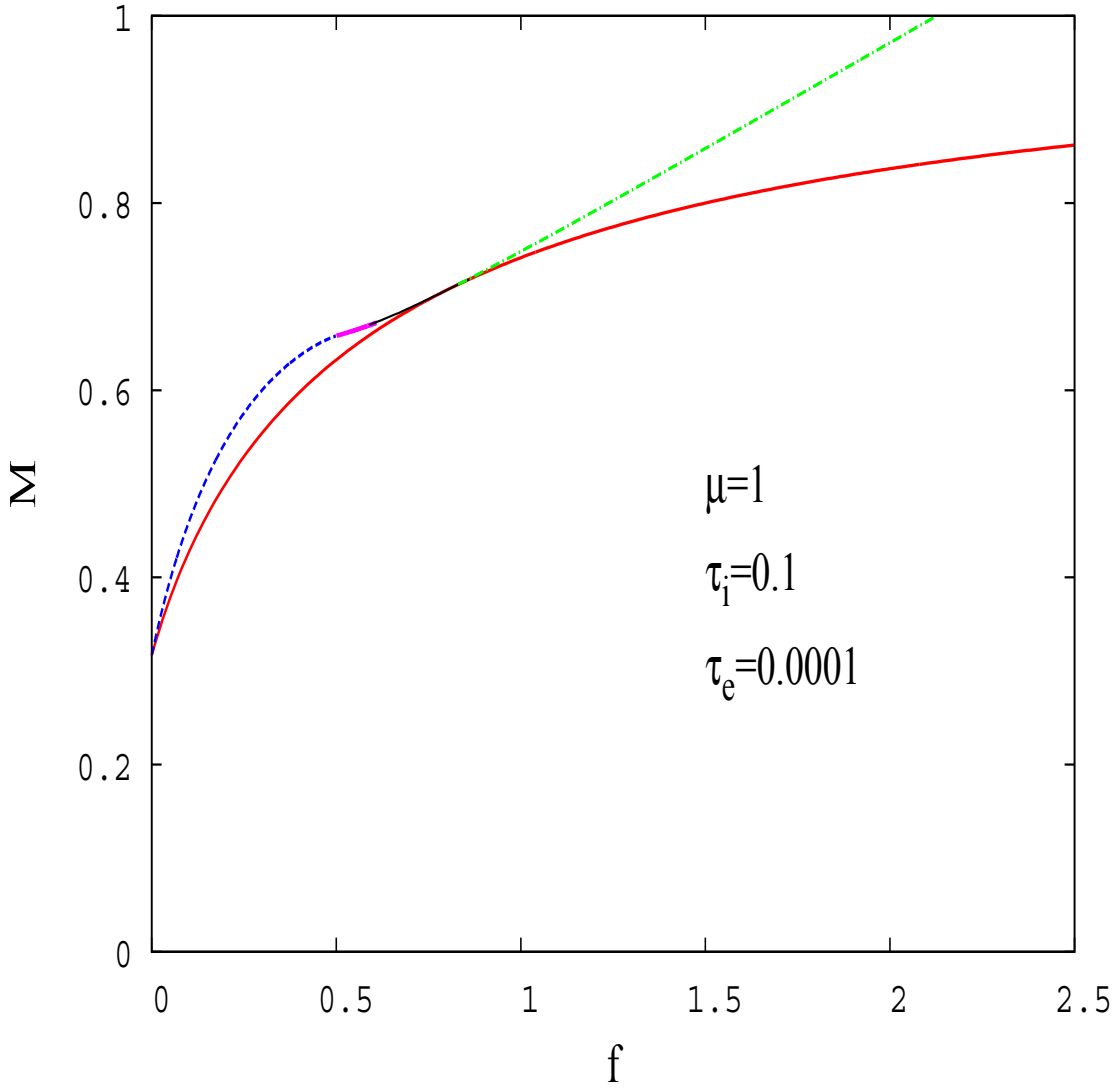

Figure C.5: The existence domain of the slow mode ion acoustic solitons for $\mu = 1$, $\tau_e = 0.0001$, and $\tau_i = 0.1$. The line styles are as in Fig. 3.7. The cutoff observed for $M = 1$ is imposed by the model (see the ordering (3.16)).

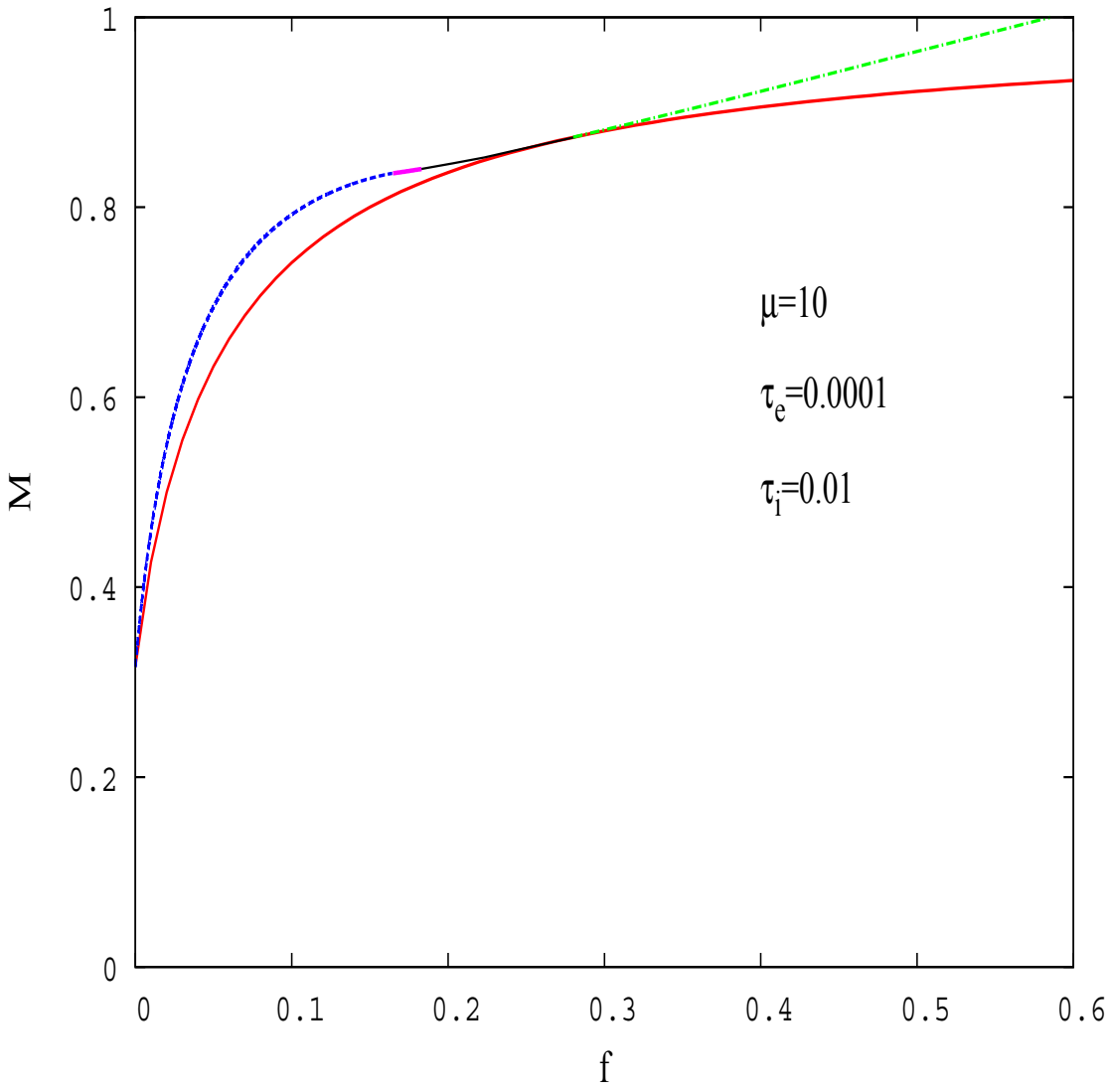

Figure C.6: The existence domain of the slow mode ion acoustic solitons for $\mu = 10$, $\tau_e = 0.0001$, and $\tau_i = 0.01$. The line styles are as in Fig. 3.7. The cutoff observed for $M = 1$ is imposed by the model (see the ordering (3.16)).

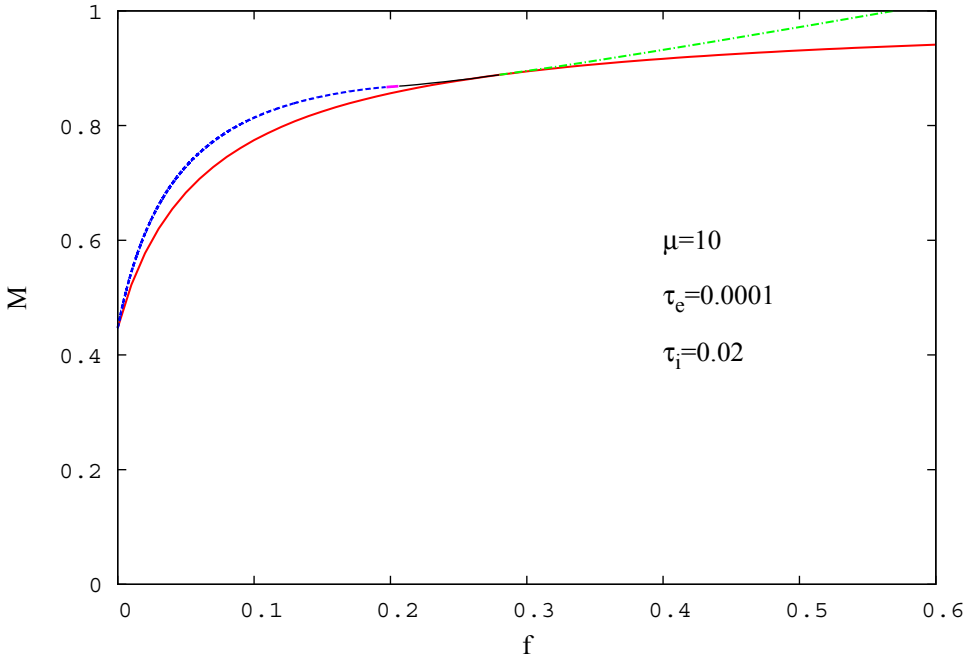

Figure C.7: The existence domain of the slow mode ion acoustic solitons for $\mu = 10$, $\tau_e = 0.0001$, and $\tau_i = 0.02$. The line styles are as in Fig. 3.7. The cutoff observed for $M = 1$ is imposed by the model (see the ordering (3.16)).

Appendix D

The existence domain of the fast mode ion acoustic solitons in a two-adiabatic-ion plasma and Boltzmann electrons for $\mu = 0.5$, $\tau_i = 0.0001$, and $\tau_e = 0.2$

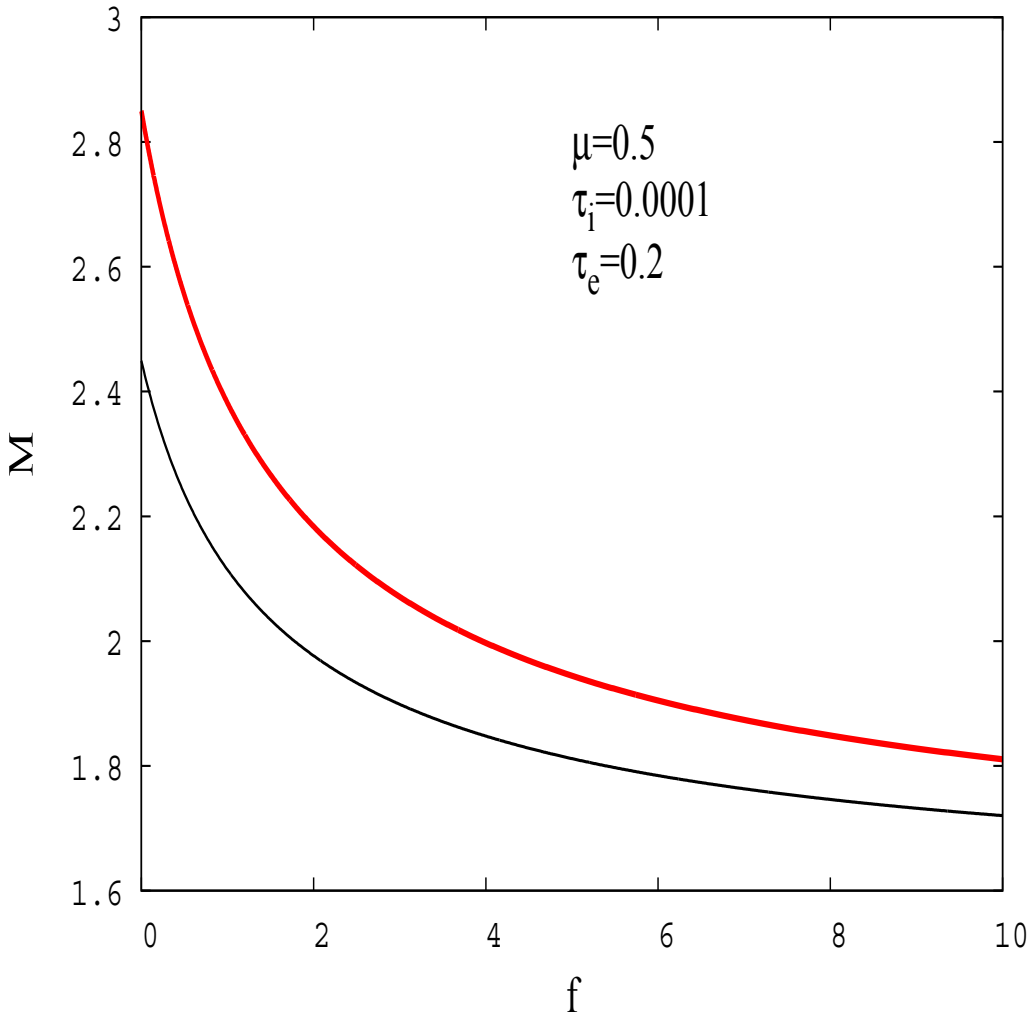

Figure D.1: The existence domain of the fast mode ion acoustic solitons for $\mu = 0.5$, $\tau_i = 0.0001$, and $\tau_e = 0.2$. The lower curve represents the lower limit in Mach numbers for the existence of solitons, whereas the upper curve is for the upper limit.

Appendix E

The existence domains of the fast mode ion acoustic solitons in a two-adiabatic-ion plasma and kappa-distributed electrons for $\mu = 2.2$, $\tau_i = 0.0001$, $\tau_e = 0.47$, and various values of κ

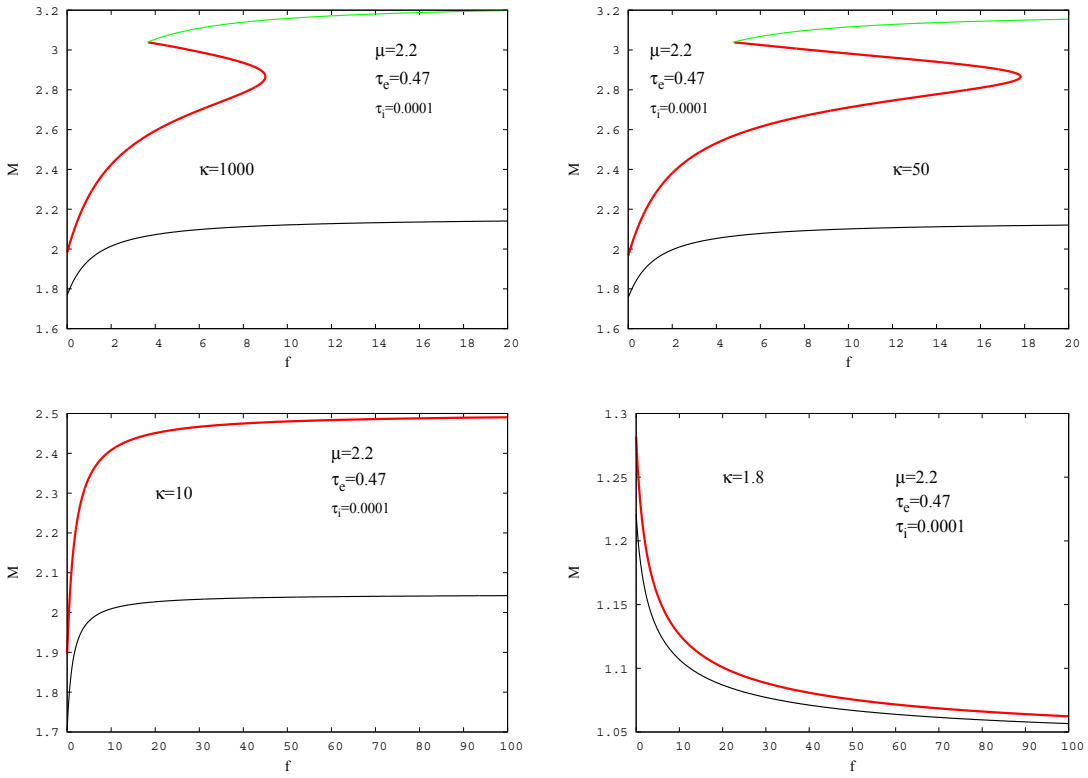

Figure E.1: The existence domains of the fast mode ion acoustic solitons for $\mu = 2.2$, $\tau_i = 0.0001$, and $\tau_e = 0.47$, showing the effect of decreasing the value of κ.

Bibliography

Baboolal, S., Bharuthram, R., & Hellberg, M. A. 1988, Journal of Plasma Physics, 40, 163.

—. 1989, Journal of Plasma Physics, 41, 341.

—. 1990, Journal of Plasma Physics, 44, 1.

Baluku, T. K. 2011, Studies of Linear and Nonlinear Acoustic Waves in Space Plasmas, PhD thesis, University of KwaZulu-Natal, Durban, South Africa.

Baluku, T. K. & Hellberg, M. A. 2008, Physics of Plasmas, 15, 123705.

—. 2011, Plasma Physics and Controlled Fusion, 53, 095007.

—. 2012, Physics of Plasmas, 19, 012106.

Baluku, T. K., Hellberg, M. A., Kourakis, I., & Saini, N. S. 2010a, Physics of Plasmas, 17, 053702.

Baluku, T. K., Hellberg, M. A., & Mace, R. L. 2008, Physics of Plasmas, 15, 033701.

—. 2011, Journal of Geophysical Research, 116, 4227.

Baluku, T. K., Hellberg, M. A., & Verheest, F. 2010b, Europhysics Letters, 91, 15001.

Bandyopadhyay, A. & Das, K. P. 2002, Physics of Plasmas, 9, 465.

Baumjohann, W., Paschmann, G., & Cattell, C. A. 1989, Journal of Geophysical Research, 94, 6597.

Baumjohann, W., Paschmann, G., Sckopke, N., Cattell, C. A., & Carlson, C. W. 1988, Journal of Geophysical Research, 93, 11507.

Baumjohann, W. & Treumann, R. A. 1997, Basic Space Plasma Physics, Imperial College Press, London, pp. 6-7.

Benson, R. F., Viñas, A. F., Osherovich, V. A., Fainberg, J., Purser, C. M., Adrian, M. L., Galkin, I. A., & Reinisch, B. W. 2013, Journal of Geophysical Research, 118, 5039.

Bernstein, I. B. 1958, Physical Review, 109, 10.

Bharuthram, R. & Shukla, P. K. 1992, Planetary and Space Science, 40, 465.

Bhattacharyya, S. & Roychoudhury, R. K. 1988, Canadian Journal of Physics, 66, 467.

Block, L. P. 1978, Astrophysics and Space Science, 55, 59.

Brodin, G. 1997, American Journal of Physics, 65, 66.

Broughton, M. C., Engebretson, M. J., Glassmeier, K.-H., Narita, Y., Keiling, A., Fornaçon, K.-H., Parks, G. K., & Rème, H. 2008, Journal of Geophysical Research, 113, 12217.

Bryant, D. A. 1996, Journal of Plasma Physics, 56, 87.

Cairns, R. A., Mamun, A. A., Bingham, R., Boström, R., Dendy, R. O., Nairn, C. M. C., & Shukla, P. K. 1995, Geophysical Research Letters, 22, 2709.

Cattell, C., Johnson, L., Bergmann, R., Klumpar, D., Carlson, C., McFadden, J., Strangeway, R., Ergun, R., Sigsbee, K., & Pfaff, R. 2002, Journal of Geophysical Research, 107, 1238.

Chen, F. 1984, Introduction to Plasma Physics and Controlled Fusion, 2nd edition, Plenum Press, New York.

Christon, S. P., Mitchell, D. G., Williams, D. J., Frank, L. A., Huang, C. Y., & Eastman, T. E. 1988, Journal of Geophysical Research, 93, 2562.

Christon, S. P., Williams, D. J., Mitchell, D. G., Frank, L. A., & Huang, C. Y. 1989, Journal of Geophysical Research, 941, 13409.

Cottrell, G. A., Bhatnagar, V. P., Da Costa, O., Dendy, R. O., Jacquinot, J., McClements, K. G., McCune, D. C., Nave, M. F. F., Smeulders, P., & Start, D. F. H. 1993, Nuclear Fusion, 33, 1365.

Crary, F. J., Goldman, M. V., Ergun, R. E., & Newman, D. L. 2001, Geophysical Research Letters, 28, 3059.

Dawson, J. 1961, Physics of Fluids, 4, 869.

Deeba, F., Ahmad, Z., & Murtaza, G. 2011, Physics of Plasmas, 18, 072104.

Denton, R. E., Engebretson, M. J., Keiling, A., Walsh, A. P., Gary, S. P., Décréau, P. M. E., Cattell, C. A., & Rème, H. 2010, Journal of Geophysical Research, 115, 12224.

Divine, N. & Garrett, H. B. 1983, Journal of Geophysical Research, 88, 6889.

Dubinov, A. E. 2009, Plasma Physics Reports, 35, 991.

Dubinov, A. E. & Kolotkov, D. Y. 2012, IEEE Transactions on Plasma Science, 40, 1429.

Eastman, T. E., Frank, L. A., Peterson, W. K., & Lennartsson, W. 1984, Journal of Geophysical Research, 89, 1553.

Engebretson, M. J., Kahlstorf, C. R. G., Posch, J. L., Keiling, A., Walsh, A. P., Denton, R. E., Broughton, M. C., Owen, C. J., Fornaçon, K.-H., & Rème, H. 2010, Journal of Geophysical Research, 115, 12225.

Fredricks, R. W. 1968a, Journal of Plasma Physics, 2, 197.

—. 1968b, Journal of Plasma Physics, 2, 365.

Fried, B. D. & Conte, S. D. 1961, The Plasma Dispersion Function, Academic Press, New York.

Fried, B. D., White, R. B., & Samec, T. K. 1971, Physics of Fluids, 14, 2388.

Gary, S. P., Liu, K., Winske, D., & Denton, R. E. 2010, Journal of Geophysical Research, 115, 12209.

Ghosh, S. & Bharuthram, R. 2011, Astrophysics and Space Science, 331, 163.

Ghosh, S. S., Ghosh, K. K., & Sekar Iyengar, A. N. 1996, Physics of Plasmas, 3, 3939.

Glassmeier, K. H., Motschmann, U., Dunlop, M., Balogh, A., Acuña, M. H., Carr, C., Musmann, G., Fornaçon, K.-H., Schweda, K., Vogt, J., Georgescu, E., & Buchert, S. 2001, Annales Geophysicae, 19, 1439.

Gledhill, I. M. A. & Hellberg, M. A. 1986, Journal of Plasma Physics, 36, 75.

Hall, L. S., Heckrotte, W., & Kammash, T. 1965, Physical Review, 139, 1117.

Harris, E. G. 1953, Physical Review Letters, 2, 34.

Harris, E. G. 1970, in Physics of Hot Plasmas, edited by Rye, B. J., and Taylor, J. C., pp. 145–201.

Hellberg, M. A., Baluku, T. K., & Verheest, F. 2010, in American Institute of Physics Conference Series, edited by Eliasson, B., and Shukla, P. K., pp. 50–60.

Hellberg, M. A. & Mace, R. L. 2002, Physics of Plasmas, 9, 1495.

Hellberg, M. A., Mace, R. L., Armstrong, R. J., & Karlstad, G. 2000, Journal of Plasma Physics, 64, 433.

Hellberg, M. A., Mace, R. L., Baluku, T. K., Kourakis, I., & Saini, N. S. 2009, Physics of Plasmas, 16, 094701.

Hellberg, M. A., Raadu, M. A., & Mace, R. L. 1997, in Double Layers-Potential Formation and related Nonlinear Phenomena in Plasmas, edited by Sendai "Plasma Forum", pp. 1–13.

Hellberg, M. A. & Verheest, F. 2008, Physics of Plasmas, 15, 062307.

Hellberg, M. A., Verheest, F., & Cattaert, T. 2006, Journal of Physics A: Mathematical and General, 39, 3137.

Henning, F. D., Mace, R. L., & Pillay, S. R. 2011, Journal of Geophysical Research, 116, 12203.

Infeld, E. & Rowlands, G. 1990, Nonlinear waves, Solitons and Chaos, Cambridge University Press, Cambridge.

Korteweg, D. J. & De Vries, G. 1895, Philosophical Magazine, 39, 422.

Krimigis, S. M., Carbary, J. F., Keath, E. P., Armstrong, T. P., Lanzerotti, L. J., & Gloeckler, G. 1983, Journal of Geophysical Research, 88, 8633.

Landau, L. D. 1946, Journal of Physics (USSR), 10, 25.

Leubner, M. P. 1982, Journal of Geophysical Research, 87, 6335.

Mace, R. L. 2003, Physics of Plasmas, 10, 2181.

—. 2004, Physics of Plasmas, 11, 507.

Mace, R. L., Baboolal, S., Bharuthram, R., & Hellberg, M. A. 1991, Journal of Plasma Physics, 45, 323.

Mace, R. L. & Hellberg, M. A. 1995, Physics of Plasmas, 2, 2098.

—. 2009, Physics of Plasmas, 16, 072113.

Mace, R. L., Hellberg, M. A., & Treumann, R. A. 1998, Journal of Plasma Physics, 59, 393.

Maharaj, S. K., Bharuthram, R., Singh, S. V., & Lakhina, G. S. 2012, Physics of Plasmas, 19, 072320.

—. 2013, Physics of Plasmas, 20, 083705.

Mamun, A. A. 1997, Physical Review E, 55, 1852.

—. 2008, Physics Letters A, 372, 1490.

Mamun, A. A., Jahan, N., & Shukla, P. K. 2008, Journal of Plasma Physics, 75, 413.

Mamun, A. A. & Shukla, P. K. 2002, Geophysical Research Letters, 29, 1870.

McKenzie, J. F. 2002a, Physics of Plasmas, 9, 800.

—. 2002b, Journal of Plasma Physics, 67, 353.

—. 2003, Journal of Plasma Physics, 69, 199.

McKenzie, J. F. & Doyle, T. B. 2003, New Journal of Physics, 5, 26.

McKenzie, J. F., Doyle, T. B., Hellberg, M. A., & Verheest, F. 2005, Journal of Plasma Physics, 71, 163.

McKenzie, J. F., Verheest, F., Doyle, T. B., & Hellberg, M. A. 2004, Physics of Plasmas, 11, 1762.

Motschmann, U., Woodward, T. I., Glassmeier, K. H., Southwood, D. J., & Pinçon, J. L. 1996, Journal of Geophysical Research, 101, 4961.

Mukai, T., Hirahara, M., Machida, S., Saito, Y., Terasawa, T., & A., N. 1994, Geophysical Research Letters, 21, 1023.

Nakamura, Y., Nakamura, M., & Itoh, T. 1976, Physical Review Letters, 37, 209.

Perraut, S., Roux, A., Robert, P., Gendrin, R., Sauvaud, J.-A., Bosqued, J.-M., Kremser, G., & Korth, A. 1982, Journal of Geophysical Research, 87, 6219.

Puri, S., Leuterer, F., & Tutter, M. 1973, Journal of Plasma Physics, 9, 89.

Raadu, M. A. & Carlqvist, P. 1981, Astrophysics and Space Science, 74, 189.

Raadu, M. A. & Rasmussen, J. J. 1988, Astrophysics and Space Science, 144, 43.

Roy, K., Saha, T., & Chatterjee, P. 2012, Astrophysics and Space Science, 342, 125.

Russell, C. T., Holzer, R. E., & Smith, E. J. 1970, Journal of Geophysical Research, 75, 755.

Sagdeev, R. Z. 1966, Reviews of Plasma Physics, 4, 23.

Saini, N. S., Chahal, B. S., & Bains, A. S. 2013, Astrophysics and Space Science, 347, 129.

Saini, N. S., Kourakis, I., & Hellberg, M. A. 2009, Physics of Plasmas, 16, 062903.

Sarris, E. T., Krimigis, S. M., Lui, A. T. Y., Ackerson, K. L., Frank, L. A., & Williams, D. J. 1981, Geophysical Research Letters, 8, 349.

Schippers, P., Blanc, M., André, N., Dandouras, I., Lewis, G. R., Gilbert, L. K., Persoon, A. M., Krupp, N., Gurnett, D. A., Coates, A. J., Krimigis, S. M., Young, D. T., & Dougherty, M. K. 2008, Journal of Geophysical Research, 113, A07208.

Sittler, Jr., E. C., Ogilvie, K. W., & Scudder, J. D. 1983, Journal of Geophysical Research, 88, 8847.

Stix, T. H. 1992, Waves in plasmas, Springer-Verlang, New York.

Summers, D. & Thorne, R. M. 1991, Physics of Fluids B, 3, 1835.

Tagare, S. G. 1973, Plasma Physics, 15, 1247.

—. 1986, Journal of Plasma Physics, 36, 301.

Tataronis, J. A. & Crawford, F. W. 1970, Journal of Plasma Physics, 4, 231.

Tran, M. Q. 1974, Plasma Physics, 16, 1167.

Tran, M. Q. & Coquerand, S. 1976, Physical Review A, 14, 2301.

Tran, M. Q. & Hirt, P. J. 1974, Plasma Physics, 16, 617.

Vasyliunas, V. M. 1968, Journal of Geophysical Research, 73, 2839.

Verheest, F. 2008, in New Aspects of Plasma Physics, edited by Schukla, P. K., Stenflo, L., and Eliasson, B., pp. 316–354.

Verheest, F. 2009, Physics of Plasmas, 16, 013704.

—. 2010, Physics of Plasmas, 17, 062302.

—. 2013, Physics of Plasmas, 16, 013704.

Verheest, F., Cattaert, T., & Hellberg, M. A. 2005, Physics of Plasmas, 12, 082308.

Verheest, F., Cattaert, T., Lakhina, G. S., & Singh, S. V. 2004, Journal of Plasma Physics, 70, 237.

Verheest, F. & Hellberg, M. A. 2010a, Physics of Plasmas, 17, 102312.

—. 2010b, Journal of Plasma Physics, 76, 277.

—. 2010c, Physics of Plasmas, 17, 023701.

Verheest, F., Hellberg, M. A., & Kourakis, I. 2008, Physics of Plasmas, 15, 112309.

—. 2013a, Physics of Plasmas, 20, 012302.

—. 2013b, Physical Review E, 87, 043107.

—. 2013c, Physics of Plasmas, 20, 082309.

Verheest, F., Hellberg, M. A., & Lakhina, G. S. 2007, Astrophysics and Space Sciences Transactions, 3, 15.

Verheest, F., Hellberg, M. A., Saini, N. S., & Kourakis, I. 2011, Physics of Plasmas, 18, 042309.

Viñas, A. F., Mace, R. L., & Benson, R. F. 2005, Journal of Geophysical Research, 110, A06202.

Washimi, H. & Taniuti, T. 1966, Physical Review Letters, 17, 996.

Yadav, L. L. & Sharma, S. R. 1990, Physics Letters A, 150, 397.

Yaroshenko, V. V., Nosenko, V., Hellbeg, M. A., Verheest, F., Thomas, H. M., & Morfill, G. E. 2010, New Journal of Physics, 12, 073038.

Zabusky, N. J. & Kruskal, M. D. 1965, Physical Review Letters, 15, 240.